REINFORCEMENT OF CLAY SOILS USING WASTE CARPET FIBRES

MEHDI MIRZABABAEI

A thesis submitted in partial fulfilment of the

requirements of the University of Bolton

for the degree of Doctor of Philosophy

MAY 2012

Dedicated to my parents

Acknowledgement

First and foremost, I would like to thank God for giving me this opportunity to increase the boundaries of my knowledge.

I wish to express my sincerest and genuine gratitude to my supervisors Dr. Mohsen Miraftab, Dr. Mostafa Mohamed and Dr Paul McMahon for their support and patience throughout my thesis. I am indebted to Dr. Miraftab for his great scientific knowledge and also for facilitating this study from the very first day by giving many helpful advice and support.

It is with immense gratitude that I acknowledge the supports of Dr. Mohamed for permitting me to use the facilities at the University of Bradford and also for involving me in teaching activity at the University of Bradford. His valuable advice and knowledge in geotechnical engineering gave me the opportunity to conduct a successful research. I am really thankful to Professor Simon Tait from University of Bradford for providing the DynamicStudio software and also for his guidance for carrying out particle image velocimetry (PIV) studies.

I would like to acknowledge helps received from my fellow PhD student, Mr. Andy Nichols for his assistance and guidance in PIV analysis. Special thanks to my fellow MSc. students Miss Nour Ammari and Mr. Equere Inibong who helped me through part of the experimental work. I acknowledge the help and expertise of Mr Saeed Hamzeh in assisting me to design and produce the pressure distribution panel and staff of university of Bradford especially Mr. Lee Thomas and God blessed Mr. Dij Chavda for their assistance in manufacturing suction probes and accessories. I would also thank engineering technicians of university of Bolton, Mr. Martin Webster, Mr. Dave Barnes, Mr. Jason Bolton and Mr. Melvyn Collier for their continuous help and support during my study. I appreciate kind help of my friend Miss Diana Reichl for final proofreading of my thesis.

During my study, receiving passionate affection, love and moral support from my family helped me through various stages and I owe my parents the deepest gratitude.

Finally, I would like to express appreciation and acknowledgement of the full scholarship received for this valuable investigation from University of Bolton and Envirolink, Northwest.

Abstract

It is reported that about 500,000 tonnes (i.e. 2% of the total waste) of waste carpet fibres are plunged into landfills annually in the UK. Municipalities and environmental authorities are increasingly concerned about the growing amount of carpet waste produced by household, commercial and industrial sectors.

The notion of reusing such waste in industry has therefore attracted substantial attention in recent years by researchers and environmentalists.

There have been a large number of studies in utilisation of virgin fibres in soils and other civil engineering applications. However, by contrast there have been relatively few studies of waste fibres especially waste carpet fibres in this context and in particular in cohesionless soils. In this study, the mechanical behaviour of composite cohesive soils (i.e. clay soils) with proportionate concentration of two types of waste carpet fibre is investigated.

A series of consolidated undrained triaxial shear tests, Oedometer tests, swelling pressure tests and unconfined compression tests have been carried out to evaluate the effectiveness of the waste carpet fibres in improving the mechanical properties of cohesive clay soils including; shear strength and compression strength as well as reducing swelling pressure and consolidation settlement of such soils.

The results have shown that waste carpet fibres do increase the shear strength and unconfined compression strength of clay soils proportional to fibre content. It was found that relative increase in unconfined compression strength or reduction in swelling pressure of the fibre reinforced clay soils is dependent on the initial dry unit weight and moisture content of the clay.

A neural network analysis was conducted on the results of the triaxial shear tests to construct a predictive model for estimating the maximum deviator stress in consolidated undrained triaxial tests as a function of fibre type, fibre content, dry unit weight and consolidation pressure. The modelled behaviour was shown to be a perfect fit with the experimental data.

Model slope tests were also carried out using a large scale laboratory test tank (L:800mm x W:300mm x H:500mm) to investigate the load bearing pressure of the slope made of fibre reinforced clay soil under strip footing load. The results confirmed that bearing pressure of the model slopes increased significantly with increased fibre content.

Particle image velocimetry (PIV) method was used to track the displacement of the soil particles in the exposed front view of the model slope and contours of displacement and slip surfaces of the model slopes were determined and compared.

Content

List of Figures

List of Tables

Chapter 1 Introduction

1.1 Background and motivation of the study

Carpet manufacturing produces a large quantity of processing waste due to end of line leftovers, stop-start wastage, yarn breakages due to faults and quality control rejects of end products. As consumer demand for new carpets increases, the old and post-consumer carpet waste which account for the biggest quantity of carpet waste also increase. These waste are currently dumped into landfills. However, pressures to stop such actions are growing due to shortages of landfill sites and environmental concerns of local communities and governmental agencies.

Fibres used in carpet may include a variety of natural and synthetic fibres. Synthetic fibres are particularly problematic as they do not degrade with time and have the tendency to release colour pigments and additives in the landfills which can subsequently penetrate the ground and potentially pollute surrounding land and underground water reservoirs. Hence the concern for reduction and elimination of this type of waste is growing. Therefore, the topic of reusing such waste in industry has gained substantial attraction by researches in recent years.

Moreover, annual increase in tax levied on landfilling waste has also played a large part in engaging carpet manufacturers in finding alternative ways of reusing their waste rather than dumping them in to landfills.

An extensive range of study has been reported in the literature on investigation of potential effectiveness of fibre reinforcement of soils. Majority of the conducted studies have been focused on the use of virgin synthetic fibres for improving the mechanical behaviour soils with great concentration on granular soils.

Reinforcing soils with waste carpet fibres has been recently appreciated by two researchers (Murray et al., 2000 and Ghiassian et al., 2004) who focused their

study on the utilisation of recycled carpet fibres for improving the shear strength properties of granular soils. However, the effectiveness of waste carpet fibres for improving the mechanical behaviour of clay soils has not yet been studied.

1.2 The aim and objectives of study

The primary aim of current study is to investigate the effect of waste carpet fibres on mechanical behaviour of clay soils. In order to fulfil this objective, a comprehensive experimental programme is designed to evaluate the influence of waste carpet fibres on shear strength, compression strength and consolidation behaviour of clay soils.

Since the current study is aimed to find novel solutions for the application of waste carpet fibres in geotechnical engineering practice, it is necessary to evaluate the possible findings of this study in larger scales than laboratory experiments. Therefore, the effectiveness of waste carpet fibres in enhancing the load bearing pressure of clay slopes is investigated using a large scale laboratory model.

The observed mechanical behaviour of such fibre reinforcement is modelled to construct a predictive model for estimating the shear strength of the reinforced clay soils with waste carpet fibres.

Therefore, in this study the following experiments and investigations are conducted:

1) *Consolidated undrained triaxial test*

   In order to investigate the effect of waste carpet fibres on shear strength of clay soils a series of consolidated triaxial tests in undrained condition is undertaken to discuss the relative gain in shear strength parameters and pore-water pressure behaviour of clay soils with increased fibre content.

2) *Modelling the mechanical behaviour*

   Neural network analysis is employed to model the shear strength of the fibre reinforced clay soil statistically. In this model it is anticipated to

evaluate the effect of type of fibre, fibre content, confining stress and dry unit weight on the obtained strength

3) *Unconfined compression strength test*

A series of unconfined compression strength tests is carried out on clay soil specimens with the motivation of investigating the effect of waste carpet fibres on the compression strength of clay soil specimens prepared at different initial conditions of dry unit weight and moisture content

4) *Swelling pressure test*

Swelling pressure of clay soils with different plasticity indices are being investigated to determine the improving effect of waste carpet fibres for suppressing the swelling pressure of such soils. Moreover, in order to fill the gap in the previous studies (reported in the literature), the effect of initial dry unit weight and moisture content on swelling pressure of reinforced clay soils with different fibre contents is investigated.

5) One-dimensional consolidation

A series of one-dimensional consolidation tests is conducted on clay soils with different swelling properties to study the effect of waste carpet fibres on one-dimensional settlement of clay soils.

6) *Laboratory large scale model*

To extend the findings of the experimental programme on a larger scale, the effect of waste carpet fibres on load bearing pressure of clay soils is investigated using a laboratory model slope.

1.3 Structure of the thesis

In this study a comprehensive investigation on the influence of waste carpet fibres on mechanical behaviour of clay soils has been carried out. The thesis has been prepared in 9 chapters. Following the introduction chapter, history of fibre

reinforcement of soil in geotechnical engineering is reviewed in Chapter 2. This includes studies since early 1980s till 2011.

Chapter 3 introduces the properties of the soils and fibres used in this study. A summary of the methods and procedures pertaining to the experiments carried out in the current study has also been given in this chapter.

Chapter 4 describes the methods utilised for calibrating the sensors used in triaxial test apparatus and model slope test. Detailed design of the suction probe which was developed in this study and equipment used for saturating suction probes are explained in this chapter.

Chapter 5 to Chapter 8 discuss the results of the experimental programme. In Chapter 5, the results of unconfined compression tests, swelling pressure tests and Oedometer consolidation tests are explained. Chapter 6 discusses the results of consolidated triaxial tests. In Chapter 7, a neural network analysis is conducted on the results of triaxial shear tests.

In chapter 8, results of the model slope tests are discussed. In this chapter particle image velocimetry method is introduced and used for the analysis of the displacements incurred in model slope under footing load.

Conclusions of the entire testing programme conducted in this study are explained in Chapter 9 and further recommendation for building on and extending the results of the current thesis are given.

Appendix A, comprises the manual of the in-house developed pressure control panel for triaxial test apparatus and Appendix B, describes the manual of DAQ 32 (a professional data logging software developed by the author).

This research work has been supported partly by Envirolink North West[1] and partly by University of Bolton set up to examine the effect of waste carpet fibres on improving the characteristics of low grade clayey soils.

[1] http://www.envirolinknorthwest.co.uk/

Chapter 2 Literature Review

Summary

This chapter covers a brief introduction to the different soil improvement practices including soil replacement, water table lowering, ground freezing, Electro-Osmosis, compaction control, chemical stabilisation and soil reinforcement.

In proceeding parts of this chapter, a comprehensive history of soil fibre reinforcement is reported to build an understanding of the fibre reinforcement impact on strength and swelling properties of soils.

2.1 Soil improvement techniques

The soil available on a project site might not meet all the engineering requirements for the intended purpose. In some cases, the soil might not even be desirable for simple engineering construction. Engineers can avoid problematic soils by either changing the project site or replacing the undesirable soil with suitable soils from a nearby site. In early days of constructions of highways, bridges and buildings, soil replacement methods were widely employed. However, with increasing use of land and growth of cities, highways and industrial zones, decisions to avoid use of poor grounds are less frequently made and ground improvement methods have been developed extensively (Lambe and Whitman, 1979).

About 3000 years ago, soil improvement technique were employed by Babylonians to build Babylon temples, In the same period Chinese utilised wood and straw to reinforce the soil (Van Impe, 1989).

Hence since those early years, soil improvement methods have attracted growing attention and to date several methods have been introduced to improve the quality of poor grounds. There are two major types of ground improvement method:

1. Temporary soil improvement which is applied for a short period of time
2. Permanent soil improvement which is designed for long term functionality

In this chapter a few temporary ground improvement methods such as dewatering, freezing and electro-osmosis and some permanent methods (such as; soil replacement, compaction control, thermal treatment, stabilisation by admixtures, lime/stone columns, grouting, drainage by vertical drains and soil reinforcement) are described briefly. Of course, there are a plethora of ground treatment methods that fall into these two major categories which are beyond the scope of the current thesis and readers can find related materials elsewhere (‘A Guide to Ground Treatment’, Mitchell and Jardine, 2002a).

As a part of site investigation, after assessing the possible hazards, which could be because of poor soil, a suitable ground improvement method must be chosen. Wisely engineered selection of the ground improvement method depends mainly on the degree of importance of the project. Mitchell and Jardine (2002b) recommended consideration of the following factors for ground improvement projects:

1. The aim of soil treatment method in order to establish the level of required improvement based on soil properties such as strength, stiffness, compressibility and permeability
2. Total area, depth and volume of the soil to be treated
3. Soil type
4. Available machinery and skilled workforce
5. Time
6. Cost

2.1.1 Water table lowering

Water table lowering is one of the primary temporary soil improvement methods that can be accomplished by inserting a drainage system and removing the extra water through drainage wells. Drop in pore-water pressure is the direct effect of water table lowering and therefore, effective stress as the difference between total stress and pore-water pressure increases. Increased effective stress leads to more confinement and hence increases in shear strength of the soil. Application of this method depends largely on permeability of the soil. The permeability of drained soil should normally be greater than $1x10^{-7}$ m/sec (Van Impe, 1989).

However, dewatering may cause settlement in surrounding areas in several ways (Powers, 1992):

1. By removing fine soils from the soil through poorly built wells
2. By misusing dewatering solution or open pumping from excavation in an improper way
3. By consolidation of silts or clays or elastic settlement of loose sands due to increase in effective stresses

If there is compressible clay or silt layer adjacent to dewatering system, settlement can occur even if dewatering is carried out properly. Therefore, a proper dewatering system considering all consequences in short term and long term must be designed in advance.

2.1.2 Artificial ground freezing

Ground freezing as a temporary ground improvement method was first used in mine shaft excavations in South Wales in 1862. This method was patented in Germany by Poetsch in 1883 under title of “Poetsch Process” (Xanthakos, et al., 1994). Subsequently ground freezing was used in Stockholm during construction of Brunkeberg tunnel in 1884 (Van Impe, 1989).

The ground freezing method comprises circulation of refrigerated coolant into a series of subsurface tubes, close enough together to freeze the soil moisture to form an ice wall. The frozen moisture provides a cementing agent, which binds the soil particles together and provides a structural support network in the soil profile. In other words, this process creates a strong watertight material, which prevents water to flow in excavated area. Upon freezing, water volume may increase by 9% when it is transformed to solid ice state. Assuming moisture content of 30% for the available soil in the site, the direct soil heave may be about 3%. Therefore volume expansion during soil freezing is not a significant matter and does not impose any extra stress unless the spotting area is confined. Ground freezing has wide application in mine excavation but it is also associated with civil engineering operations at shallow depths such as shafts and tunnels in bad or poorly treated grounds (Mitchell and Jardine, 2002a).

Although ground freezing is perhaps the most appropriate method of groundwater exclusion and can be used wherever the soil is moist, there are some limitations to use of this method (Mitchell and Jardine, 2002a):

1. Dissolved salts can affect freezing point of water.
2. Clayey soils may not freeze.
3. Petroleum products prevent ground freezing at regular temperatures.

It is also necessary to protect the soil in neighbouring ground containing steel sheet piles or piles from cold zones using insulating shields (Van Impe, 1989).

2.1.3 Electro-Osmosis

Electro-osmosis is a technique used for consolidating and strengthening of soft, saturated clay soils (Rowe, 2000). In this method two electrodes are placed in the soil and DC electricity is conducted between them. Water in the soil moves from anode (positive pole electrode) to cathode (negative pole electrode) due to the interaction between the electric field and the ions in the pore-water and the soil particles. This phenomenon induces a negative pore-water pressure in the soil which increases the effective stress and expedites the consolidation of the soil layers. This phenomenon is called electro-osmosis. If collected water in cathode is drained, the moisture content and compressibility of the soil are reduced with increase in shear strength. Casagrande first applied this method for stabilising soft silty clay in 1939. Since then electro-osmosis method has been utilised in ground improvement projects involving stabilising earth slopes, reinforcing piles installed in clay soils and rapid improvement in properties of soft clay soils (Row, 2000).

2.1.4 Compaction control

Historically, one of the earliest methods for compacting soil was herding sheep back and forth across newly placed ground which nowadays has been developed as a device called sheep's foot roller (Xanthakos, et al., 1994).

One of the most common permanent ground improvement methods is to increase the density of the soil. This includes a variety of methods such as light surface compaction, dynamic compaction, compaction by explosives, compaction grouting, preloading and so forth.

Surface compaction is applicable in small scale projects for cohesionless soils using a heavy or light smooth roller or sheep's foot rollers. When it comes to less permeable soils, the efficiency of this method depends upon saturation ratio of the soil and possibility of removing trapped air by compaction. At a given compaction

energy for achieving the most dense soil, the number of layers, thickness of layers, amount of water to be mixed with the soil and vibration frequency of dynamic rollers and number of passes can be designed according to the value of maximum dry unit weight and optimum moisture content.

In 1957, the Road Research Laboratory in England analysed dynamic compaction as a deep compaction method following the concepts of the laboratory Proctor compaction test (Van Impe, 1989). This method consists of dropping heavy weights (in scale of tens of tonnes) from a height of almost 10 to 40 meters using a sufficient capacity crawler crane. For an efficient dynamic compaction practice a number of factors such as weight and height of the falling weight, number of drops, specific tamping space over spot area and recovery time are required. Recovery time is described as required time between tamping passes to allow excess pore-water pressure to be dissipated to a low enough value for the next pass. The most common approach to perform a suitable dynamic compaction is to consider the ground in three layers with the first layer receiving the highest number of tamps from a certain height (according to design approach), narrowing the number of tamps and falling height gradually to the third layer.

Another type of dynamic compaction method for the saturated loose granular soils is to transfer a sudden shock to the soil layer by generating blast using explosive materials in depth of the layer. This method is more suitable for saturated granular soils due to uniform transmission of shock waves through water (Bell, 1993). The released energy induces a liquefaction effect in the adjacent soil layer close to the explosion point. Therefore, pore-water pressure increases temporarily to the level of effective vertical overburden stress in the soil layer and a heavy fluid is created. The induced liquefaction in the soil layer is followed by time-dependent dissipation of the pore-water pressure, which leads to re-consolidating of the soil layer for a while depending on permeability of the sub soil layers and drainage boundary conditions.

Once the spot area of the ground is treated and pore-water pressures are largely dissipated, controlled blasting sequences result in additional settlement depending on the soil density and stiffness. The first blast is responsible for breaking the bond between granular particles, which have been formed due to aging. Subsequent

blasts cause additional settlements by cyclic straining and the ground will be resistant to cyclic loading (Gohl, 2005)

Compaction grouting as another technique of ground improvement via compaction control, improves the strength, and/or stiffness of ground by controlled process of injection of low mobility grout, which resembles very stiff mortar. Upon expansion of grout, the soil is compacted. The purpose of this method is to increase the density of the sub surface soil prior to construction to compensate post-construction settlement. A controlled and gradual injection of grout provides a consistent densification around the expanding grout mass. This technique is most suitable in loose soils with a suitable drainage to prevent excess pore-water pressure build up. Compaction grouting was first established in 1952 by a small contractor in Los Angeles called James Warner for filling small voids underneath a structure (ASCE standard/G-153-10, 2010).

Preloading in brief is applying an external load to the soil layer for a long duration to allow most of the post-construction displacements to happen. In low permeable soils, inserting vertical drains can expedite the preloading process. Preloading can be carried out prior to construction or even after construction like liquid storage tanks. Preloading leads to increase in the pore-water pressure, quick consolidation, increase in effective stress and increase in surface settlement of the soil. The preloading materials which are placed over the ground produce a stress in the soil equal to the final anticipated (Raj, 1999).

2.1.5 Chemical stabilisation

The principle of this method relies on chemical reactions between soil particles, pore-water and admixture agent to create stronger bond between soil particles. Chemical stabilisation comprises mixing soil with one or several combination of admixtures in the form of powder, slurry or liquid for improving or controlling its volume, stability, strength, permeability and durability. A wide variety of chemical admixtures such as lime, cement, fly ash, asphalt, silicates, resins, acids have been studied over the years (Mirzababaei, et al., 2008). The most commonly used admixtures are Portland cement, lime, fly ash and bitumen (Fang, 1990).

When clay soils are stabilised with lime, lime reacts with the clay minerals and calcium silicate is produced. As a result, moisture content of the soil decreases. Calcium silicate with the properties of non-solubility in water acts as a binding agent between soil particles. Comparing to cement stabilisation, lime stabilisation gives soil a much more immediate improvement in strength than cement. However, in long term, cement stabilised soils gain more strength than lime stabilised soils.

The required amount of stabilisers for soil improvement lies between 2 to 6 percent by dry weight of the soil. Effectiveness of the chemical stabilisation depends on the interaction between stabiliser agents and soil particles and also on the properties of the agent like water affinity, water retention capacity, ion exchange capacity. Clay content, grain size distribution, permeability of the soil also play and important role in the efficiency of stabilisers (Smoltczyk, 2003).

2.1.6 Soil reinforcement

Soil can be reinforced by inserting reinforcing elements such as metallic strips or bars, geotextile layers, grouted needle piles, micro piles, or fibres into the soil.

Reinforced earth was first introduced by a French engineer, Henry Vidal, in 1963. He placed flexible, 5mm thick strips of galvanised steel in the layers of the fill with one end bolted to the retaining wall and the other end extended into the soil (Van Impe, 1989). For an efficient reinforcement, a high quality clean sand and gravel backfill are required for strip reinforcement to generate required frictional forces between back fill soil and reinforcement elements. Grid form reinforcements have shown better reinforcing effects due to their more pull out resistance in comparison to strip reinforcements. Moreover, grid reinforcement does not necessarily require high quality granular back fill.

Subsequently, developed forms of reinforced earth technique such as steel grids, welded wire mats or welded steel bars (patented by Bill Hilfiker in 1970s), strong polymer grids, woven or non-woven geotextiles have been proposed (Bergado, et al., 1996) in recent years.

The principle of any type of soil reinforcement method is to introduce materials having tensile restraining strength to the soil to limit the induced lateral stresses for maintaining the equilibrium of a loaded soil mass. When a reinforced soil layer receives vertical stress and tends to strain laterally, tensile strength of reinforcement elements contributes to resists outward movement and to lower the induced horizontal stresses. This technique has extensively been used to construct retaining walls, steep slopes, embankment on soft soils and repair partly failed slopes.

There are also other traditional forms of soil reinforcement methods such as:

- Soil nailing: insertion of steel or glass fibre rods into the front face of an excavation followed by shotcrete protection
- Micro-pile: piles with diameter of less than 300mm
- Lime, lime/cement columns: introduction of quick lime and/or cement by hollow stem auger into the depth of the soil
- Stone column: as a multi aspect reinforcing element for increasing bearing capacity and ease of drainage in granular soils with 10% to 25% fines or cohesive soils

Since the introduction of geosynthetics as planar soil reinforcing materials, the geotechnical engineering society has reviewed growing applications of such materials in construction of retaining walls, steep slopes, embankments, road construction and drainage systems in order to reduce consolidation time, increase shear strength and bearing capacity of soils. Successful application of different types of geosynthetics materials such as geotextiles and geogrids in recent decades has proved to be just as good if not better than traditional techniques with an enormous cost saving advantages.

2.2 Fibre Reinforcement

One of the most recent methods for improving the properties of problematic soils is to include randomly arranged discrete fibres in such soils. The roots of fibre reinforcement can be found in the history of humans too long time ago.

Early civilisations used different masonry materials such as sun dried clay bricks or thatch which has been used in Europe since Neolithic period for covering roofs and often making walls (Evans, et al., 2002). Somewhere in their experience it became commonly accepted practice to increase the strength of masonry material with adding straw or other available natural fibres such as rice husks. However, they may have not fully understood the mechanism involved in such material.

“Cob”, which is an English term for mud buildings using no forms of bricks and wooden structures, has been seen in ancient buildings since prehistoric times. Cob is a mixture of clay, sand, straw and water and has a long history of use as building material (Wood, et al., 1999). Other forms of historical building materials include Chirpici (a Romanian term for baked adobe bricks made of clay and straw in the sun), mud brick (an unfired, sun dried brick made of clay, or mud mixed with a binding materials such as rice husks or straw).

Remainder of the houses built with thatch and straw denotes use of such strengthening composite masonry as building material by human beings in the early ages. Soil fibre reinforcement is a modern form of ancient methods used for strengthening masonry and building materials. Gray (1970), Waldron (1977), Wu et al. (1988) and Abe and Ziemer (1991) as pioneers of investigation of soil fibre reinforcement topic in geotechnical engineering reported on the beneficial application of plant roots to increase the shear strength of the soil and consequently, the stability of natural slopes.

Since the 1980s, synthetic fibres have also been introduced to improve the mechanical behaviour of soil in geotechnical engineering practice. Therefore, the beneficial effect of fibres in geotechnical and construction engineering has become a known fact to all engineers.

Studies on the fibre reinforced soil have been mainly consisted of conducting laboratory experimental research such as using triaxial compression tests, unconfined compression tests, direct shear tests and Oedometer tests to investigate the mechanical behaviour of fibre reinforced soils. A few large scale application of fibre reinforced soil has also been reported in the literature.

2.2.1 Influence of fibres on soil strength and stress strain behaviour

2.2.1.1 Reinforcement of embankments with plant roots

Reinforcement of soil slopes with plant roots has been studied extensively by Wu (1976), Waldron (1977) and Waldron and Dakessian (1981) who proposed the following model describing the shear strength of rooted soil.

$$\Delta S_R = a_R Tn(\sin\beta + \cos\beta \tan\varphi) \quad (2.1)$$

Where:

ΔS_R Contribution of roots to soil shear strength

a_R Cross section area of the root

φ Angle of internal friction of soil

Tn Maximum tensile stress in the root (i.e. $\sqrt{\frac{4\tau' EZ}{D}}$)

τ' Maximum tangential friction between root and soil

z Thickness of shear zone

E Young's modulus

D Diameter of root

β Angle of root deformation

They reported increased shear strength of root reinforced soil. In the proposed model, root tensile strength considered as add on strength to shear strength of pure soil.

Burroughs and Thomas (1977), Ziemer and Swanston (1977) and Tsukamoto and Kusabe (1984) reported increased stability of the slopes with vegetation and afforestation. Abe and Ziemer (1991a) stated that after afforestation, increase in shear strength of slope would increase quickly for 20 years and then it remains nearly constant.

2.2.1.2 Reinforcement of sand with discrete fibres

Since 1980s a plethora of investigations has been conducted on reinforcement of granular soils with synthetic discrete fibres (i.e. polypropylene, nylon fibres and fibre glass). Consensus conclusions such as significant increase in the peak shear

and compression strengths and reduction in the post peak shear/compression strength loss have been reported frequently in the literature.

Gray and Ohashi (1983) studied the mechanical behaviour of fibre reinforced dry sand with natural, synthetic and metal fibres (copper wire). Orientations of fibres relative to the shear plane were defined in a controlled manner. They also modified the shear strength model proposed by Wu (1976), Waldron (1977) (equation (2.1)) to account for the initial orientation of the fibres and reported that initial orientation of 60 degree to the shearing plane resulted in highest shear strength of fibre reinforced soil within a pool of different orientations such as 30, 60, 90, 120 and 150 degree to the shear plane.

Fibre area ratio[2], fibre modulus, initial fibre orientation and the friction angle of the sand were found to influence the contribution of fibres in shear strength of the sand. Fibre modulus was found to have direct effect on shear strength of fibre reinforced sand. The initial stiffness of sand was remained unchanged due to fibre reinforcement. A limiting fibre length was found beyond which the shear strength was constant. Therefore, they concluded that making fibres longer does not assure full mobilisation of the tensile strength of the fibres.

Maher and Gray (1990) developed a mechanical model based on the statistical theory of strength for composite material to describe the interaction between fibre and sand under static loads. They proposed equation (2.2) which was similar to the model described by earlier researchers (Wu (1976), Waldron (1977) and Waldron and Dakessian (1981)) for the contribution of fibre's tensile strength to shear strength of the sand.

$$\Delta S_R = t_R(\sin\omega + \cos\omega \tan\varphi) \quad (2.2)$$

Where:

ΔS_R	Shear-strength increase resulting from fibre inclusion
t_R	Mobilised tensile strength of fibres per unit area of soil
φ	Angle of internal friction of sand
ω	Angle of shear distortion ($= \tan^{-1}(x/z)$)
x	Shear displacement parallel to the shear zone
z	Thickness of shear zone

[2] total cross section of fibres over cross section of specimen

They validated the proposed model, by carrying out several triaxial tests on different types of sand reinforced with rubber fibre, glass fibre and natural fibres. Uniform and rounded sand exhibited curved-linear principal stress against confining stress while well-graded or angular sand exhibited bilinear one. The transition from curved section to linear section or break in bilinear envelope happened at a certain confining stress acknowledged as critical confining stress. At high confining stresses a linear increase in shear strength with increased fibre content was observed. However, at lower confining stresses, increase in shear strength with increased fibre content soon reached an upper asymptote.

Al-Refeai (1991), studied the behaviour of sand reinforced with 0.5% of different types of fibre (i.e. glass fibre, polypropylene pulp and mesh element) by conducting a series of triaxial tests on fine and medium sands. Fibre inclusion was found to influence the shear strength of fine sand with sub-rounded particles significantly compared to that of medium sand with sub-angular particles. Ultimate strength and ductility of the sands irrespective of type of sand increased with increased fibre content. Increased fibre length was also found to improve the strength of fibre reinforced sand significantly especially in fine sand. Mesh elements were reported to be superior for increasing the shear strength of the sand.

Heineck et al. (2005) studied the behaviour of fibre reinforced silty sand, uniform sand and bottom ash reinforced with 0.5% polypropylene fibre. Results of their study showed increased shear strength and residual strength with fibre reinforcement. Moreover, strain hardening behaviour was observed for fibre reinforced silty sand and uniform sand at all confining stresses. However, bottom ash specimens showed plastic strain behaviour at lower confining stresses (i.e. 100 kPa). The effect of fibres on stiffness and elastic shear moduli at very small strains was found to be insignificant.

Chen and Loehr (2008) studied the consolidated drained and consolidated undrained shear strength of reinforced loose and medium dense sand with 0.4% polypropylene fibre. They reported that lower strain is required for mobilising the fibre resistance in drained tests compared to that of undrained tests. This was attributed to the volume change of the soil specimen in drained tests. Fibre

reinforcement increased the effective internal friction angle and effective cohesion intercept of the sands.

As contradictory to the previous studies, Yetimoglu and Salbas (2003) reported insignificant change of initial stiffness and peak shear strength of clean sand reinforced with polypropylene fibre. They attributed the observed results to relatively smaller horizontal failure strain of fibre reinforced sand than required strain to mobilise the tensile strength of the fibres. However, similar to previous findings by other researchers, they confirmed increased ductility of fibre reinforced sand compared to brittle behaviour of non-reinforced sand.

2.2.1.3 Critical confining stress

The influence of fibre inclusion on shear strength of granular soils has been reported to be dependent on the confining stress. Gray and Ohashi (1983), Al-Refeai (1991) and Zornberg and Li (2003) investigated the effect of confining stress on failure mechanism of fibre reinforced sand.

Therefore, a critical confining pressure was reported bellow which, fibres tend to pull out. Beyond the critical confining stress, fibres were found to be stretched or broken at failure of the soil specimen. Maher and Gray (1990) claimed that the critical confining pressure is sensitive to fibre aspect ratio, grain shape and gradation of soil and it is not related to the fibre content and medium grain size of the soil. Increase in coefficient of uniformity and fibre aspect ratio and reduction in particle sphericity was found to reduce the critical confining stress and hence higher degree of contribution of fibres to shear strength. They obtained the highest strength at confining stresses less than the critical confining stress.

Consoli et al. (2007) conducted an investigation into the drained stress path behaviour of polypropylene fibre reinforced uniform fine sand at different ranges of confining stress. It was found that the stress-strain behaviour of neither non-reinforced nor fibre reinforced sand was dependent of applied stress path. Fibre reinforced sand showed a bilinear strength stress path envelope with higher slope at lower effective stresses and lower slope with significant cohesion intercept at higher stresses. However, at all effective stresses, non-reinforced soil revealed similar stress path envelope to that of fibre reinforced soil at lower

effective stresses. The failure mechanism at lower effective stresses was justified as combined slippage and yielding of fibres while at higher effective stresses stretching with no breakage was observed.

2.2.1.4 Fibre reinforcement with natural fibres

Discrete natural fibres have also been proved to enhance the mechanical properties of the soils. However, due to bio degradable properties of such fibres, they might not last for long time and hence might be considered as temporary reinforcement. The durability of natural fibres as reinforcement elements has not yet been investigated. Prabakar and Sridhar (2002) reported limiting fibre content for increasing the peak cohesion intercept of sisal fibre reinforced soil. There was slight increase in cohesion intercept with increase in fibre length. Internal friction angle of reinforced soil was almost the same as non-reinforced soil. They also reported increased effect of fibre length and fibre content on measured deviator stress of fibre reinforced sand. On the contrary, Ghavami, et al. (1998), reported insignificant increase in strength of fibre reinforced soil with natural sisal and coconut fibres. However, natural fibres changed the brittle behaviour of non-reinforced soil to ductile behaviour.

Huat, et al. (2005) studied the effect of three types of grass and a legume on shear strength of residual shale. They concluded that shear strength of the soil increased with increase in root density and decreased with increase in depth of which the sample was taken.

Marandi et al. (2008) studied the strength properties of palm fibre reinforced sand at different fibre contents and fibre lengths. They reported increase in unconfined compression peak strength, secant modulus, residual strength and failure strain with increased fibre content and fibre length. Chauhan et al. (2008) investigated the effect of natural and synthetic fibres (Coir and polypropylene) on unconfined compression strength of sand-fly ash mixture. Optimum fly ash content was determined using compaction and unconfined compression strength tests on different mixtures of sand and fly ash. They concluded that there was an upper limit of fibre content at which the unconfined compression strength of natural and synthetic fibre reinforced sand-fly ash mixture yields a peak.

2.2.1.5 Fibre reinforcement of clay soils

Strength properties of fibre reinforced clay soils have also been studied to some extent. However, compared to granular soils, research on the use of fibre reinforcement with cohesive soils has been more limited.

Andersland and Khattak (1979) studied the behaviour of kaolinite specimens prepared from slurry and reinforced with 40% cellulose fibre. They reported increased shear strength of fibre reinforced kaolinite at consolidated drained and consolidated undrained conditions. They described the load transfer mechanism at the interface of soil and fibre as an attraction and bonding between soil particles. Fibre inclusion was also found to increase the ductility of the kaolinite.

Freitag (1986) investigated the unconfined compression strength behaviour of fibre reinforced silty clay with 1% spun nylon string, polypropylene rope fibre and polypropylene concrete reinforcement fibre (commercially called fibre mesh). He reported increased compression strength of fibre reinforced clay at near and wet side of optimum moisture content. However, at dry side of optimum no benefit was observed from presence of fibres in soil. There was also no significant change in strength of fibre reinforced specimens with different fibre types.

Maher and Ho (1994) reported the effect of fibre reinforcement on compression strength, tensile strength and hydraulic conductivity of fibre reinforced kaolinite specimens with 0.5% to 4% fibre (i.e. polypropylene, glass and softwood pulp fibres). All specimens were prepared from slurry. It was found that increased fibre content and fibre length result in increased peak compression strength, ductility and absorbed energy (area underneath stress-strain curve up to strain level of 15%) of fibre reinforced soil. They postulated the observed improvement due to higher probability of crossing potential slip surfaces by short fibres, and therefore, better contribution of fibres to increase the peak strength of cohesive soils (assuming no friction angle). At post peak strength condition, short fibres were pulled out easier and long fibres performed better to reduce the post peak strength loss. Split tensile strength was improved with increased fibre content and defected with increase in fibre length. Hydraulic conductivity also increased with increase in fibre content.

Nataraj, et al. (1997), carried out a series of unconfined compression tests, direct shear tests and California bearing ratio (CBR) tests on polypropylene fibre reinforced clay and sand soil specimens with 0.1 to 0.4% fibre content. Peak and post peak compression strength, initial tangent modulus, secant and tangent modulus at peak compression strength and peak frictional angle and cohesion intercept of the studied soils increased with fibre inclusion. They reported bulging under compression as the failure mechanism of fibre reinforced soil compared to development of shear planes as failure mechanism of non-reinforced clay soils. The strength of both clay and sand soil specimens increased with increasing moisture content up to optimum value. Beyond the optimum moisture content, strength of specimens decreased. Post peak strength loss of fibre reinforced specimens prepared at wet side of optimum was less than that of specimens prepared at optimum moisture content.

Kumar and Tabor (2003) studied the effect of nylon fibres on compression strength of compacted silty clays at different compaction efforts. Significant increase in peak and residual strength was observed by increasing the fibre content from 0.05% to 0.30%. It was found that the degree of improvement was highly dependent on compaction density of the specimens. Fibre reinforced specimens compacted at density of 93% of maximum dry unit weight (compared to specimens compacted at 96% and 99% of maximum dry unit weight) showed highest increase in peak and residual strength.

Falorca et al. (2006) studied the effectiveness of polypropylene fibres on shear strength of medium plasticity clay soil under normal stresses ranging from 35 kPa to 295 kPa. It was found that effect of fibre addition (to 0.25% and 0.50%) on shear strength of composite specimens was more significant at lower normal stresses. They stated that increase in the shear strength of the fibre reinforced specimens was dependent on fibre orientation and amount of shear displacement. Whereas, maximum shear strength was observed when horizontal displacement was about fibre's length. Unlike other studies they reported that post peak shear strength of fibre reinforced soil approached that of non-reinforced soil.

Tang et al. (2008) studied the effect of specimen size, moisture content and compaction density on unconfined compression strength of fibre reinforced clay

soils with 0.2%, 0.5% and 1% polypropylene monofilament fibres. They reported significant increase in the strength of fibre reinforced clay soil with increased fibre content. It was observed that unconfined compression strength of the clay soil increased with increasing the compaction density at constant moisture content or with reducing the moisture content at the same compaction density. However, fibre reinforcement did not change the sensitivity of the soil strength to moisture content. It was also reported that specimen size influenced the improved compression strength. Smaller specimens showed higher compression strength.

On onset of failure of fibre reinforced specimen, tiny cracks developed around main cracks. Unlike non-reinforced specimens, appeared main cracks on fibre reinforced specimens did not develop more. Therefore, fibre reinforcement transformed the brittle behaviour of non-reinforced specimen to ductile behaviour.

2.2.1.6 Fibre reinforcement of high plastic clays and soft soils

High plastic clays are always categorised as problematic soils due to their high volume change properties and low shear strength. Effect of synthetic fibre inclusion has been investigated in an attempt to increase the shear strength of such problematic soils.

Casagrande et al. (2006) studied the behaviour of fibre reinforced bentonite with 170% moisture content at large strains. The results of ring shear tests showed insignificant impact of fibre addition (i.e. 1.5% and 3%) on the peak shear strength of bentonite. At large shear displacement values (i.e. 50mm), residual strength of fibre reinforced soil was gradually reduced and reached that of non-reinforced bentonite at higher shear displacement (i.e. 180mm). Recovered fibres from sheared zone after terminating the test showed that most of fibres underwent extension or breakage during shearing.

Kumar et al. (2006) reported the results of unconfined compression strength tests on fibre reinforced mixture of soft clay and sand with 0.5% to 2% plain and crimped polyester fibres. They reported increased compression strength of fibre reinforced soil with increase in fibre content and length of fibres. Moreover, plain fibres were found more effective to increase the strength of the soft clay soil. For

example, inclusion of 2% of 6mm plain fibres or 1% of 12mm plain fibres or 1.5% of 6mm crimped fibres increased the strength of clay soil by almost 100%.

Freilich et al. (2010) studied the effect of 0.5% polypropylene short fibres on drained and undrained strength of high plastic clay soils. They reported increased shear strength of fibre reinforced clay at undrained condition.

Although non-reinforced clay soils showed the same strength in drained and undrained condition, the strength of fibre reinforced clay soils reduced in drained condition. They attributed the observed reduction in strength to creep deformation and clay particle rearrangement during drainage as well as influence of time on the behaviour of fibre reinforced clay soils.

It was reported that, ductility of the fibre reinforced specimens was increased compared to brittle behaviour of non-reinforced specimen. Similar to the results of work carried out by Nataraj, et al. (1997), they reported shear plane failure and bulging at failure for non-reinforced and fibre reinforced clay soil specimens respectively.

Estabragh et al. (2011) studied the mechanical behaviour of reinforced soft clay soil with nylon fibres. Specimens with high percentages of fibre (i.e. 10%, 20% and 30%) were prepared from slurry in similar way as Andersland and Khattak (1979) and Maher and Ho (1994) prepared their test specimens. They reported increased internal friction angle and initial stiffness of the fibre reinforced clay soil with increase in fibre content under undrained condition. Volumetric dilation of the reinforced clay soil was limited with increased fibre content resulting in increase in pore-water pressure during undrained shear.

Estabragh et al. (2011) and Freilich et al. (2010) confirmed increased pore-water pressure during undrained shear test of clay soils. They hypothesised that fibres increased the stress distribution rate in the soil specimen and hence caused more contraction during shear stage resulting in increased pore-water pressure.

Freilich et al. (2010) claimed that consolidated undrained triaxial test on fibre reinforced soil might result in higher estimation of effective strength due to effect of fibres on pore-water pressure.

2.2.1.7 Fibre reinforcement of treated soils

The coupled effect of addition of fibres and other additives such as fly ash, lime or cement on strength properties of granular and cohesive soils has been studied by several researchers.

Consoli et al. (1998) conducted a series of drained triaxial tests on fibre reinforced cemented sand with 3% chopped fibre glass. Cement addition increased the peak strength, cohesion intercept, internal friction angle, rigidity and brittleness of the sand soil. However, residual strength of cemented sand was not changed significantly. In return, fibre addition increased peak and residual strength, internal friction angle of the fibre reinforced sand followed by reduction in its rigidity. Combination of cement and fibre addition improved the mechanical behaviour of the sand significantly. They concluded that, cement addition increased the cohesion intercept of sand while internal friction angle of fibre reinforced cemented sand was more influenced by fibre addition.

Makiuchi and Minegishi (2001) reported on the results of a series of unconfined compression strength tests and direct shear tests of fibre reinforced mixture of sand and 10% of high plastic clay with 1% nylon and polypropylene fibres. They reported increase in peak and residual shear strength of fibre reinforced sand. This was described by interface friction, interlocking and intertwining between fibres' surfaces and sand soil particles.

Increase in diameter of fibres at constant fibre content had adverse effect on strength of the sand soil. They attributed this to decreased number of fibres in the soil specimen at constant fibre content. Marked improvement effect on peak and residual strength of fibre reinforced mixture of sand and clay was observed compared to degree of improvement in fibre reinforced sand soil.

Cai, et al. (2006) studied the strength properties and volume change behaviour of fibre reinforced lime-treated clay with 0.05% to 0.25% polypropylene fibres. They reported increase in peak unconfined compression strength, shear strength, cohesion intercept and internal friction angle of the fibre reinforced lime-treated clay soil with increase in fibre content and curing time. The swelling/shrinkage potential of clay soil specimens decreased with addition of lime while fibres tended

to increase the shrinkage potential and reduce the swelling potential. Fibres also changed the brittle behaviour of lime-treated clay soil to a ductile one.

Micro fabric of lime-treated clay soils showed cementation gel between aggregated particles. However, that of fibre reinforced soil contained big packets of soil particles spaced with large pores. Furthermore, micrograph of sheared zones of failed specimens proved that fibres increased the soil strength by imparting friction property to the soil particles. They reported that Inclusion of 5% lime and 0.25% fibre increased the unconfined compression strength, cohesion intercept and shearing angle of the treated soil by 730%, 330% and 240% respectively compared to those of untreated specimens.

Tang et al. (2007) reported increased unconfined compression strength and shear strength of fibre reinforced uncemented/cemented low plastic clay soils with 0.05% to 0.25% short polypropylene fibres. Unconfined compression strength of the fibre reinforced cemented soil was found to be more than the sum of unconfined compression strength of fibre reinforced uncemented soil and that of cemented soil. Unlike cement addition, fibres decreased the stiffness of the treated specimens. Axial strain at failure was increased with fibre addition posing a ductile behaviour compared to brittle behaviour of non-reinforced specimen. In a similar study, Park (2011) also reported increased compression strength and failure strain of fibre reinforced cemented sand.

They reported similar SEM analysis results to the findings of Cai, et al. (2006). And stated that interaction between surface of fibres and clay particles controlled the mechanical behaviour of the fibre reinforced uncemented soil. However, in fibre reinforced cemented soil interactions between hydrated products and fibres' surface made contribution to strength at the interface between fibres and soil particles.

Kumar et al. (2007) studied the influence of lime, fly ash and plane and crimped polyester fibres on unconfined compression strength of clay soils. Based on a series of preliminary tests a mixture of 15% fly ash and 8% lime was used for preparing polyester fibre reinforced clay soil specimens. They reported continuous increase in compression strength of lime-fly ash treated clay soils with increasing

the fibre content from 0% to 2% in fractions of 0.5%. Lime and fibre addition were also found to improve the tensile strength of the clay soil specimens.

Bhardwaj and Mandal (2008) extended the study of composite soils with the intension of investigating the shear strength and compression strength of reinforced fly ash with 1% polypropylene fibre. The results of their study confirmed increased peak compression strength of the reinforced fly ash. Moreover, the apparent cohesion intercept and internal friction angle of the fly ash specimen increased with fibre addition.

They also conducted a centrifuge test on fibre reinforced fly ash model slope with slope of 78.6 degree and reported reduced displacement and increased factor of safety of fibre reinforced fly ash model slope. Results of the analysis of the reinforced slope using geotechnical finite element software (Plaxis) showed consistency between experimental work and model analysis.

Park (2009) prepared different specimens with variable number of reinforced layers with poly vinyl alcohol (PVA) fibres. He reported increased unconfined compression strength of fibre reinforced cemented sand specimens.

2.2.1.8 Field trial of fibre reinforced soils

Gregory and Chill (1998) reinforced a failed clay slope in a highway located in Beaumont, Texas, USA using polypropylene geo-fibres. Prior to fibre reinforcement of the slope, the repeated failure of embankment slopes on Northeast and Northwest quadrant of this highway was locally being improved using normal compaction methods. They identified the failure mechanism of local slopes as degradation of shear strength of over consolidated as-compacted clay soil due to desiccation, swell-shrinkage, water infiltration and downhill creep, which resulted in formation of a non-cohesive normally consolidated clay layer prone to failure. They carried out a series of experimental works including consolidated drained shear box tests and consolidated undrained triaxial tests on fibre reinforced soil. The results showed increased cohesion intercept and internal friction angle of fibre reinforced local clay soil. They repaired the failed slope on the basis of laboratory experiment results and analysis using a computer code programme. They reported increased safety factor of fibre reinforced slope to 1.5.

Consoli et al. (2003) studied the bearing capacity of layered soils formed by two top layers of sand-cement and sand-cement-fibre overlain by homogeneous residual soil layer. Plate load test on improved layers showed that at displacement of about 8mm, the bearing capacity of the sand-cement layer was 5 times of that of residual soil. However, when it reached peak strength there was an abrupt loss in strength in a way that the ultimate strength reached that of residual soil.

Addition of fibres to sand-cement layer did not change the maximum bearing capacity of the soil significantly but it improved the soil ultimate bearing capacity. This made the soil-foundation system more ductile, which was more reliable than sand-cement soil foundation system. They also investigated the failure mechanism of foundation by excavating boreholes close to the plate load test point. It was reported that formation of tension cracks from bottom to the top of the layer, especially under the border of the plate was the failure mechanism of sand-cement layer. However, the failure mechanism of fibre reinforced sand-cement layer was formation of a thick shear band around the plate.

2.2.1.9 Soil reinforcement with recycled and waste fibres

Majority of the studies on fibre reinforcement of soils have been conducted using virgin or natural fibres. However, just a few studies have been carried out to use the waste fibres including tyre rubber fibres or waste carpet fibres for improving the strength properties of soils.

Özkul and Baykal (2006) studied the behaviour of reinforced clay soil with 10% rubber fibre. They reported that improvement in shear strength of fibre reinforced soil was dependent on compaction energy of the soil. At standard compaction energy, the quick undrained shear strength and stress-strain behaviour of both non-reinforced and fibre reinforced soils were the same. However, with increase in compaction energy, shear strength of fibre reinforced soil approached that of non-reinforced soil at higher confinements. Similar to the results reported by Freilich et al. (2010), they confirmed reduction in shear strength of fibre reinforced clay soils under drained condition.

Cetin, et al. (2006) reported increased undrained shear strength and permeability of composite specimens of clay and tyre chips. Addition of 10% to 50% tyre chip to

clay soil changed the compression behaviour of the pure clay soil to dilative behaviour. Permeability tests were carried out under different normal stresses of 46, 93, 185, 287 and 370 kPa to simulate various possible overburden pressures. Although the permeability of composite specimens was increased in comparison with pure clay soil specimens, the resulted permeability was still as low as 10^{-7} to 10^{-8} cm/sec.

Özkul and Baykal (2007) reported increased deviator stress and cohesion intercept and reduction in internal friction angle of fibre reinforced kaolinite with 10% tyre buffing. In drained test, volume change of fibre reinforced specimen was more than that of non-reinforced specimen. However, final volume change at 20% axial strain was almost the same for both non-reinforced and fibre reinforced specimens. Evolution of pore-water pressure in fibre reinforced specimen was dependent on the compactive effort. At standard compactive effort, similar to the findings by Freilich et al. (2010) and Estabragh et al. (2011), the pore-water pressure developed in fibre reinforced specimen during shear was more than that in non-reinforced specimen. However, for specimens prepared at modified compactive effort, pore-water pressure of fibre reinforced specimen at lower confining stresses was lower than that in non-reinforced specimen. This was reversed at high levels of confinements. Adding rubber fibres resulted in reduction in internal friction angle (1 to 3 degree) and increase in apparent cohesion of fibre reinforced soil specimen (20 kPa to 40 kPa).

Akbulut et al. (2007) investigated the reinforcing effect of rubber tyre fibres (i.e. at concentrations of 1% to 5%) and polypropylene fibres (i.e. at concentrations of 0.1% to 0.5%) on strength properties of high plastic clays. The results showed that unconfined compression strength of fibre reinforced clay soils with natural rubber and polypropylene fibres increased up to an optimum fibre content of 2% and 0.2% respectively. Furthermore, they reported improving effect of fibre content and fibre length on increasing the cohesion intercept of fibre reinforced clay soils.

Esna-Ashari and Asadi (2008) reported that tyre cord waste (i.e. made of nylon fibres) enhanced the unconfined compression strength and peak shear strength of sand. The observed improvement was found to be dependent on fibre content and length of fibres. Whereas, increase in length of fibres at constant fibre content

reduced the stiffness of the fibre reinforced sand while increased fibre content (from 0.2% to 1%) at constant fibre length showed increased peak compression strength and no change in initial stiffness of the specimen. Fibre reinforcement increased the internal friction angle of the soil without any significant improvement in its apparent cohesion intercept.

On a similar study by Naeini and Sadjadi (2008) on shear strength of high plastic clays, they reported insignificant change in initial stiffness and increase in shear strength parameters of tyre rubber fibre reinforced soil (with fibre content ranging from 1% to 4%). They concluded that fibre reinforcement with rubber tyre fibres was more effective in clay soils with lower plasticity indices. Edincliler et al. (2010) also reported increased apparent cohesion and internal friction angle of sand reinforced with tyre waste.

Study of the fibre reinforced soil with recycled carpet fibres has been limited to a few recent studies on sand soils. These include the investigations of Murray et al. (2000) and Ghiassian et al. (2004) who studied the shear strength behaviour of fibre reinforced sand with recycled carpet fibres.

Murray et al. (2000) concluded on the results of a series of consolidated undrained triaxial tests on sandy silt soil reinforced with recycled carpet fibres and fibrillated polypropylene fibres that fibre reinforcement with recycled carpet fibres up to 3% and virgin polypropylene fibres up to 1% offered increase in peak shear strength, reduction in post peak strength loss. Fibre addition transformed the behaviour of the specimen form brittle to ductile state, and sometimes changed the stress-strain behaviour from strain softening to strain hardening. No asymptotic upper limit in shear strength of specimens reinforced with recycled carpet fibres was observed. However, an upper limit of 1% fibre content was found for specimens reinforced with fibrillated polypropylene fibres.

Ghiassian et al. (2004) carried out a series of drained triaxial tests on sand reinforced with carpet waste strips. They reported increased peak and residual strength, decreased maximum modulus and increased volume change with either increasing strip content at constant aspect ratio or increasing aspect ratio at

constant strip content. Moreover, behaviour of specimens after failure changed from brittle (for non-reinforced specimen) to ductile one (for reinforced specimens).

2.2.2 Influence of fibres on volume change behaviour of cohesive soils

Fibre reinforcement has been appreciated by several researchers for its potential to limit the volume change behaviour (i.e. free swell potential and shrinkage behaviour) and swelling pressure of expansive clay soils.

Loehr et al. (2000) reported reduction in vertical free swell potential of fibre reinforced clay soils with increased fibre content (from 0% to 0.2% and 0.4%). However, they stated that the free swell potential of fibre reinforced clay soils is dependent on the specimen size. Whereas, reinforced specimens with 102mm diameter showed significant reduction in free swell potential while 64mm diameter specimens did not show any reduction in free swell potential.

On the contrary, Puppala and Musenda (2000) reported increase in free swell potential of fibre reinforced clay soils with increase in fibre content to 0.9% (with increments of 0.3%). However, shrinkage and swelling pressure of fibre reinforced clays were decreased with increased fibre content. They attributed the increase in free swell potential to increase in distribution of water in soil mass due to paths created by fibres. They also attributed reduction in swelling pressure to better pore-water pressure dissipation due to drainage paths created by fibres and restraining effect of fibres due to their tensile strength.

A comprehensive study on the free swell potential and swelling pressure of expansive clay soils reinforced with 1% to 5% natural Palmyra and synthetic nylon fibres was reported by Al-Akhras et al. (2008). They found that fibres improved the free swell potential and swelling pressure of reinforced soils significantly. However, fibre length had an adverse effect on reducing the swelling pressure. They reported that performance of natural Palmyra fibres outperformed synthetic nylon fibres.

Ikizler et al. (2009) reported that addition of multifilament polypropylene fibres to highly expansive bentonite at percentages of 0% to 0.5%, suppressed its swelling

pressure significantly. However, fibrillated fibres did not change the swelling pressure of bentonite significantly due to increase in void ratio of the compacted bentonite at higher fibre contents and difficulties in effective compaction.

Punthutaecha et al. (2006) conducted research on improvement of problematic volume change behaviour of expansive clay soils using class F fly ash, bottom ash, and synthetic fibres (nylon and polypropylene fibres). Maximum ash content was limited to 20% and 0% to 0.6% fibre was used to prepare fibre reinforced specimens. The results showed that free swell potential decreased with increased ash content or nylon fibre content. However, it increased with increase in polypropylene fibre content. They postulated the latter effect as difficulty in compacting polypropylene fibres in clay soil and hence increasing the void ratio of the soil.

They also reported that although fibre inclusion (i.e. nylon fibres) led to low reduction in swelling pressure of clay soils, the combined effect of stabilisers and fibres reduced the swelling pressure, free swell potential and shrinkage potential significantly.

Investigation of one-dimensional consolidation behaviour of fibre reinforced clay soils has also been reported in the literature. Abdi et al. (2008) reported substantial reduction in consolidation settlement of reinforced clay soils with 1%, 2%, 4% and 8% polypropylene fibre. Increased fibre content led to increase in shrinkage limit and significant resistance to extension of desiccation cracks. Fibre length was reported to have no significant effect on swelling potential, consolidation settlement and hydraulic conductivity of the reinforced clay soils

Viswanadham et al. (2009) also investigated the one-dimensional consolidation behaviour and swelling pressure of reinforced expansive clay soils with 0.25% and 0.50% polypropylene fibre. They reported reduction in one-dimensional heave and swelling pressure with increase in fibre content. However, increase in aspect ratio reduced the performance of fibre reinforced soil.

Estabragh et al. (2011) also reported reduction in one-dimensional settlement of clay soil reinforced with 10% to 30% nylon fibre. Pre-consolidation stress of fibre reinforced clay soil reduced with increase in fibre content.

2.2.2.1 Effect of fibre reinforcement on tensile strength and desiccation cracks of expansive soils

Soil structures constructed using clay soils such as embankments, may exhibit desiccation cracks under seasonal changes when subjected to wet-dry cycles. Fibres were found effective to mitigate such unwanted phenomenon by reducing the extent and number of desiccation cracks. Fibre reinforcement can also reduce potential cracking induced by differential settlements of the soil structures due to ductile behaviour of fibre reinforced soil mass. Therefore, fibre reinforcement has been investigated in the literature for such application.

Miller and Al-Refeai (2004) reported significant crack reduction in clay soil reinforced with 0.2% to 2% polypropylene fibres.

Harianto et al. (2008) investigated the impact of fibres to suppress the desiccation cracks of highly plastic clay. They reported reduction in volumetric shrinkage strain and extent of tension cracks of fibre reinforced clay with adding 0.2% to 1.2% polypropylene fibre.

Soils usually do not pose any tensile strength. However, with fibre reinforcement clay soils may exhibit tensile strength due to add-up tensile strength of fibres. Ziegler et al. (1998) reported on the results of a series of tensile strength tests and wetting/drying cycles to evaluate the development of tensile strength and crack extension of fibre reinforced expansive clay soils with 0% to 0.3% polypropylene fibres. Increased fibre content resulted in increase in tensile strength of the fibre reinforced clay soils. Visual inspection of the fibre reinforced specimens after wetting/drying cycles showed reduction in width and length of the cracks however, the number of cracks increased.

2.2.3 Potential application and merits of fibre reinforcement

Fibre reinforced soils can be extensively used in different geotechnical and civil engineering projects involving slope stabilisation, road construction, construction of embankments, repairing or construction of landfill covers and crack controlling.

The merits of such reinforcement method can be considered as:

1) Since fibre reinforcement method may be used for stabilising shallow layers or constructing an embankment from scratch, mixing fibres with local soils can be fulfilled using conventional construction equipment such as rotary mixer in separate lifts. The mixed fibre-soil lift can then be compacted using conventional compactors. In such reinforcement method due to random placement of fibres in the soil, no extra considerations are required for maintaining the arrangement and direction of reinforcing elements.

2) Conventional stabilisers such as lime, cement, fly ash or other chemical agents used in soil stabilisation practice require careful considerations against weather conditions. However, fibres due to their neutral compositions are not significantly sensitive to changes in weather condition.

3) Fibres are relatively cheaper material compared to other reinforcing material such as geotextiles and geogrids or stabilising agents like lime and cement. Variety of different types of fibre including natural fibres, virgin fibres, recycled fibres and waste fibres which are abundantly available at economical costs may be used for fibre reinforced soil application.

One of the potential applications of fibre reinforcement method is to repair the localised failure zones of slopes especially in steep slopes. Since the shape and direction of the failed zone and its extent may not be suitable enough for application of continuous planar reinforcement methods such as use of geotextiles and geogrids, fibre reinforcement is a viable alternative. Planar reinforcement material requires considerations for suitable anchorage at boundaries. However, fibres due to their simple application do not need such considerations

Application of fibre reinforcement method does not require any special design for their application other than finding optimum fibre content based on the experimental work. However, planar reinforcement must be designed precisely

Potential application of fibres for mitigating the volume change behaviour of expansive clays has been cited frequently in the literature (Ziegler et al., 1998, Miller and Al-Refeai, 2004, Harianto et al., 2008). Fibres have been proved to

reduce the swelling pressure, free swell potential and control the cracking in swelling soils.

Fibre reinforcement can also be used to control soil surface erosion in landfills as it increases the permeability of the soil and hence facilitate vegetation on cover system used in landfills.

2.2.4 Summary of the literature review of fibre reinforcement

Review of the literature of soil fibre reinforcement shows that there is a general consensus that fibre reinforcement of soils (with either natural or synthetic fibres) can improve the mechanical behaviour of granular and cohesive soils. This may include improvement in stress-strain behaviour properties such as increase in peak shear/compression strength, residual strength, cohesion intercept and internal friction angle. Moreover, it has been appreciably accepted that, fibre inclusion would reduce the post peak loss of strength and would increase the failure strain and ductility of the soil. However, there is no agreement on the amount and type of fibre for improving the properties of different soils.

Volume change behaviour of the expansive clay soils may be improved by fibre inclusion with prospects of reduction in free swell potential, swelling pressure, shrinkage limit and one-dimensional consolidation. Fibre inclusion also adds tensile strength to cohesive soils which manifests itself in reduction of desiccation cracks.

However, the degree of improvement yielded by fibre reinforcement will depend on several aspects such as type of soil, type of fibre, fibre content, length of fibre, water content and compaction density of the soil.

Strength and volume change properties of soils especially cohesive soils are highly sensitive to their initial dry unit weight and moisture content. Therefore, any improvement in such soils by fibre inclusion is a function of its initial conditions (i.e. dry unit weight and moisture content).

Critical review of the literature implies that in some of the conducted studies, unfair conclusions and comparisons may have been casted based on fibre reinforced

specimens prepared with unequal initial dry unit weight and moisture content conditions. And a comprehensive study of the effect of initial conditions of soil on the performance of fibre reinforced soils has not yet been undertaken.

Of course a few researchers may have sought the individual effect of initial conditions of soils on effectiveness of fibre reinforcement. Examples of such studies would be the investigation on impact of moisture content (Nataraj, 1997) or compaction density (Özkul and Baykal, 2006 and Kumar and Tabor, 2003) on fibre reinforcement performance. Tang et al. (2008) also investigated the individual effect of compaction density and moisture content on unconfined compression strength of fibre reinforced clay soils. However, the individual and coupled effect of dry unit weight and moisture content on different mechanical properties of fibre reinforced clay soils has not yet been investigated. In this study it aimed to fill the observed gap by investigating the effect moisture content and dry unit weight on shear strength, unconfined compression strength and swelling pressure of clay soils.

Majority of investigations on fibre reinforced soil topic has been appreciated with natural or synthetic virgin fibres for improving the shear strength of soils. In fact, only a few numbers of published studies have been conducted on utilisation of recycled carpet fibres in order to enhance the strength properties of soils. To the date there has been no published research to investigate the performance of waste carpet fibres on mechanical properties of cohesive soils.

Therefore, the primary aim of this study has been set to conduct a comprehensive investigation on mechanical behaviour of fibre reinforced clay soils with waste carpet fibres. This includes investigating the effect of proportionate amount of waste carpet fibres on shear strength, compression strength and swelling pressure of clay soils.

Chapter 3 Materials and experimental methods

Summary

This chapter is divided into three sections. In the first section, materials used in the current research including soils and fibres are characterised. In the second section, a summary of sampling methods including: recovering undisturbed samples, reconstitution and remoulding is described. The next section presents a comprehensive coverage for all testing procedures which are carried out to achieve the objectives of the current research programme. Therefore, a summary of triaxial tests, one-dimensional consolidation tests, swelling pressure tests, and unconfined compression strength tests is given.

3.1 Scope of the testing programme

In foundation engineering; shear strength and compressibility properties (i.e. consolidation settlement, swelling pressure and free swell) are the two important factors that characterise the soil behaviour under foundation loadings. Shear strength, in particular, plays a fundamental role in displacement of soil particles when they are subjected to axial or lateral loading. These factors are commonly considered when analysing bearing capacity of a shallow or deep foundation, stability of a slopes and retaining walls.

It has been addressed frequently in the literature that fibres (mostly virgin fibres) can improve the shear strength of the soils to some extent depending on the type of fibres, type of soil and extent of applied stresses. In order to evaluate the impact of waste carpet fibres used in the current research on short term shear strength parameters of clay soils, a series of consolidated undrained triaxial tests were carried out on non-reinforced and fibre reinforced clay soil specimens.

Furthermore, one-dimensional consolidation and swelling pressure tests were carried out to evaluate compressibility characterisation of the fibre reinforced clay soils. Unconfined compression strength tests were also carried out to evaluate the compression strength of fibre reinforced clay soils.

In this study, all fibre reinforced clay soil specimens were prepared at fibre contents of 0%, 1%, 3% and 5% of dry mass of soil and different moisture content and dry unit weight conditions.

3.2 Materials

3.2.1 Fibres

Tufted carpets are the most common types of carpet and are made up of a complex multi-component system, typically consisting of two layers of backing (usually polypropylene fabrics), joined by $CaCO_3$ filled styrene-butadiene latex rubber (SBR), and face fibres that are tufted into the primary backing.

Figure 3.1 shows the basic structure of tufted carpets. SBR is a thermoset[3] material and cannot be melted down to reshape (Wang et al., 2003).

Two different types of waste tufted carpet fibre from shearing and/or edge trimming were supplied by Carpet Recycling UK[4] and Milliken Industries[5]. These fibres will be referred to as ABF and GBF throughout this thesis. Table 3.1 depicts general specifications of ABF and GBF fibres. Given that the used fibres are waste-based, no definite fibre size or diameters are defined.

ABF fibres were supplied as 100% nylon 6 sheared piles from tufted carpets. The average length of these fibres was measured using optical microscopy and they ranged from 2 to 5 millimetres. Scanning electron microscopy (SEM) examination of these fibres showed thickness range of between 60 to 100µm.

GBF fibres were supplied as chopped up carpet waste where face fibres, backings and other additives were included in the batch. The average length of these fibres ranged from 2 to 20 millimetre and diversity of their thicknesses was between 80 to 1500µm. GBF waste carpet fibres consisted of 20% SBR latex, 5% wool, 15% nylon and 60% polypropylene. Figure 3.2 and Figure 3.3 show the optical and SEM images of ABF and GBF fibres.

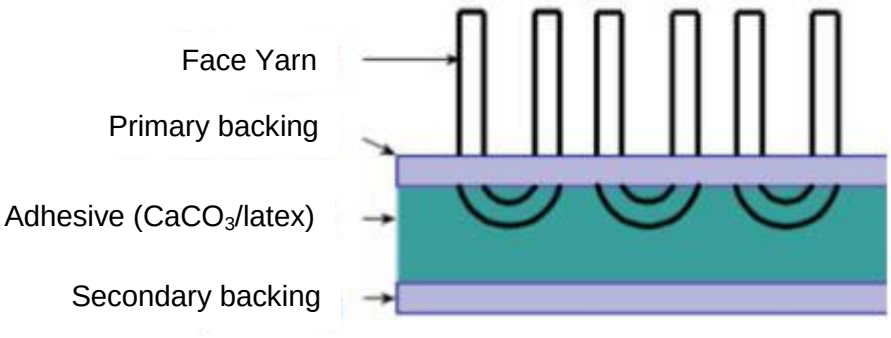

Figure 3.1 Structure of tufted carpets (Wang, et al., 2003)

[3] Type of plastic that remains rigid when set, and does not soften with heating
[4] www.carpetrecyclinguk.com
[5] http://www.millikencarpeteurope.com

Table 3.1 Properties of the waste carpet fibres

GBF Fibres	Synthetic carpet shred 60% polypropylene (Almost no water absorption, Specific gravity: 0.90) 20% SBR latex 15% nylon (water absorption: 4.1% to 4.5%, Specific gravity: 1.14) 5% wool (water absorption: 13% to 15%, Specific gravity: 1.32) Length : 2 to 20mm Diameter: 80 to 1500µm
ABF Fibres	Short fibres from shearing process 100% nylon (water absorption: 4.1% to 4.5%, Specific gravity: 1.14) Length : 2 to 5mm Diameter: 60 to 100µm

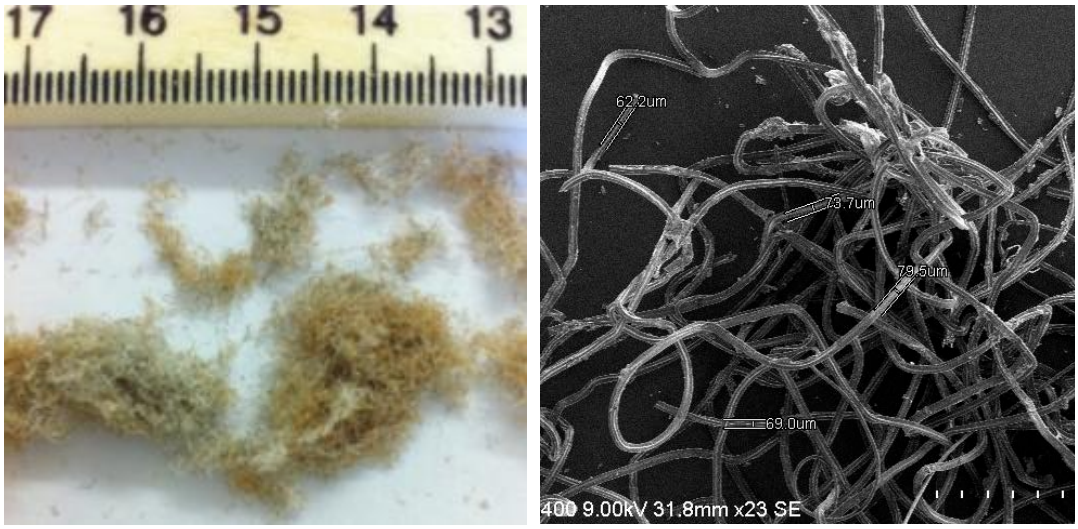

Figure 3.2 Optical and SEM images of ABF fibres

Figure 3.3 Optical and SEM images of GBF fibres

Nominal physical properties of individual fibres used in this study supplied by manufacturers included water absorption of 4.1% to 4.5%, nil and 13% to 15% for nylon, polypropylene and wool fibres respectively. Specific gravity of 0.9, 1.14 and 1.32 were also reported for polypropylene, nylon and wool fibres respectively.

3.2.2 Soils

For evaluating the effect of fibre reinforcement on clay soils, about 4 tonnes of natural clay soil from a local site in Northwest region of the UK was acquired in the form of wet-bulk material. In order to prepare a uniform and reproducible clay soil, it was decided to create a fine dry clay soil powder from the bulk.

Based upon non-quantitative categorisation of the wet-bulk clay soils (i.e. natural colour and tactile qualification), they were divided into two different batches. To prepare the clay powder, each batch of soil was crushed into smaller pieces and air dried for few days. Air-dried small lumps were transferred to an oven and dried at 105°C for 24 to 48 hours. Dried clay lumps were ground in an electromechanical mill (grinder) until a soft powder was achieved. The ground clay soils were separated out and placed in sealed plastic bags and stored for gradual use. Figure 3.4 shows the milling equipment and ground clay soils in the laboratory.

Therefore, two different clay soils were identified from the bulk clay soils and sealed in separate plastic bags. The clay soils were designated as C1 and C2 throughout this study. Due to visual observation C1 soil was more plastic than C2 soil. Sieve analysis on both C1 and C2 clay soils was undertaken according to BS1377-2:1990.

Figure 3.4 Clay crushing, milling equipment

Due to recent evolution of the practice standards in Europe to Eurocode 7, BSI group (which develops standards within the UK and worldwide) has issued the EU7 compatible version of BS codes (i.e. BS EN 1997-2:2007).
However, in National Annex to BS EN 1997-2:2007, it has been mentioned that: “In the UK, laboratory tests should continue to be carried out using parts of BS 1377. DD CEN ISO/TS 17892-6 is the only laboratory test to be used in the UK; the other CEN ISO/TS 17892 parts are not implemented in the UK.”

To the date only the test procedure of ‘fall cone test’ has been implemented in BS code to meet the requirements of CEN ISO/TS 17892-6: Fall cone test. Therefore, all the testing procedures and methods mentioned in BS1377 are still

valid except the fall cone test. Hence, BS 1377 has been considered as test procedure and method for all geotechnical experiments throughout the research.

Figure 3.5 shows particle size distribution curves for C1 and C2 soils. Consistency limits of C1 and C2 soils were also determined using the standard procedure outlined in BS1377-2:1990. Specific gravity of the soil was determined for both soils according to BS1377-2:1990 standard procedure.

Table 3.2 shows details of soil classification of both C1 and C2 soils. For soil classification and identification as it is recommended in BS EN 1997-2:2007, the contents of EN ISO 14688-1 and EN ISO 14688-2 have been used. Therefore, C1 and C2 soils were classified as low plasticity clay and clayey silt respectively.

Based upon the results of a series of preliminary experiments (including the Proctor compaction tests and quick undrained triaxial tests) it was found that increase in fibre content results in reduction in mixing efficiency of fibres and clay soils. Whereas mixing more than 5% fibre with current clay soils was very difficult. Therefore, the upper limit for fibre content in this study was set at 5%. In order to examine an even distribution of fibre contents, three fibre contents of 1%, 3% and 5% were chosen.

In order to evaluate the effect of fibres on different clay soils, a number of laboratory-made clay soils were also prepared by mixing proportionate amounts of sodium bentonite with the C1 and C2 soils. Physical and chemical properties of sodium bentonite used in this study, as given by the manufacturer[6], have been depicted in Table 3.3. Therefore, to produce moderate to high plasticity clays for testing, consistency limits of C1 and C2 soils with 5% up to 50% sodium bentonite were determined. Results of consistency limits of C1 and C2 soils with different bentonite contents are given in Table 3.4.

To prepare a second clay soil with predefined plasticity index, a mixture of 10% sodium bentonite and the C1 soil was selected based on the data depicted in Table 3.4. Moreover mixtures of C2 soil with 10% bentonite and 20% bentonite were also chosen.

[6] RS Minerals Ltd., www.RSMinerals.co.uk

A simplified coding system is used to refer to different combinations of soils and fibres throughout this study. For example 3A-C1 is used to refer to C1 soil specimen with 3% of ABF fibre, or 3G-C1-10B is the abbreviated name for soil specimen composed of C1 soil, 10% Bentonite and 3% GBF fibre.

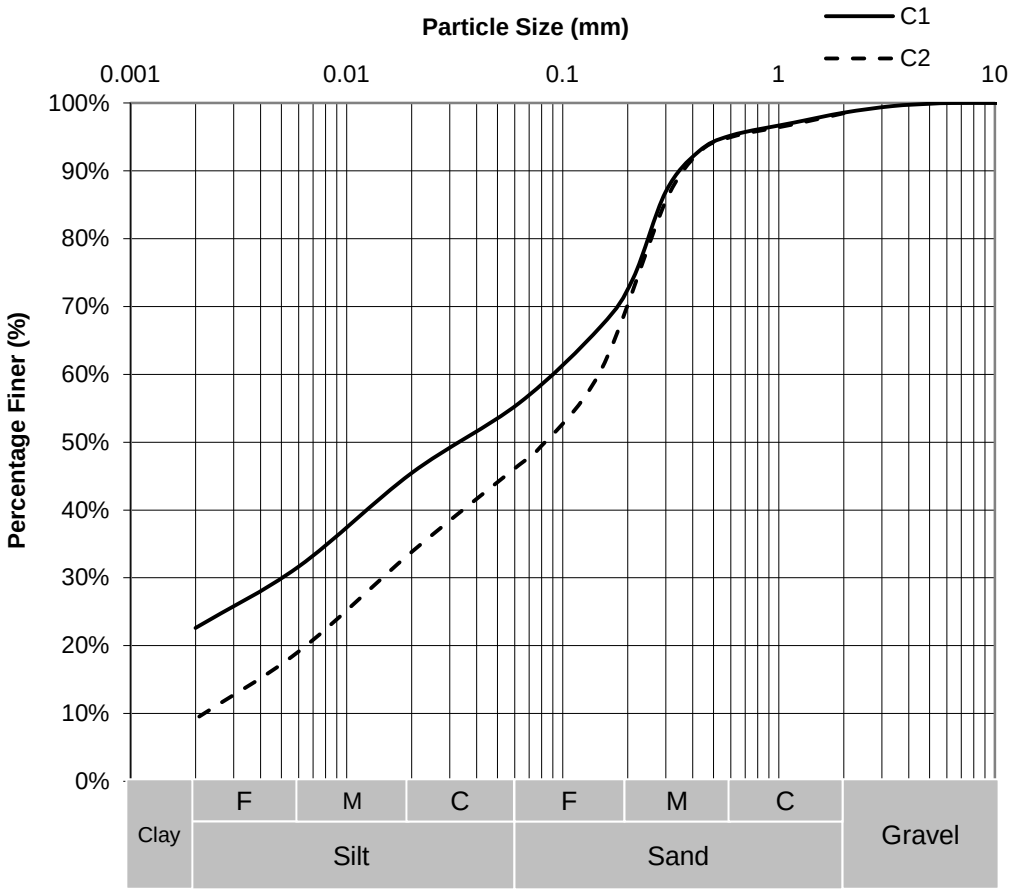

Figure 3.5 Particle size analysis of C1 and C2 soil

Table 3.2 Details of particle size distribution analysis

	C1 soil	C2 soil
Clay fraction (%)	22.6	9.2
Silt Fraction (%)	33.2	37.5
Fine sand fraction (%)	18.4	25.3
Medium sand fraction (%)	21.1	23
Coarse sand fraction (%)	3.4	3.5
Gravel fraction (%)	1.4	1.5
Specific gravity	2.68	2.68
Liquid limit (%)	29.0	21.1
Plastic limit (%)	12.0	10.4
Plasticity index (%)	17.0	10.7
Maximum dry unit weight (kN/m^3)	20.1	20.7
Optimum moisture content (%)	11.0	9.2
Soil classification	Low plastic clay	Clayey Silt

Table 3.3 Physical and chemical properties of sodium bentonite

Physical properties		Chemical properties	
Bulk density (kN/m^3)	8-9	SiO_2	%54.7
pH	10.8	Al_2O_3	%17.6
Swelling volume (mls/2g)	20-40	Fe_2O_3	%5.2
Moisture content (%)	10-14	CaO	%4.5
Retained on 150 µm	5% Max	MgO	%3.8
		K_2O	%0.8
		Na_2O	%3.1
		LoI	%8.9

Table 3.4 Consistency limits of laboratory made clay soils

Bentonite content (%)	Liquid limit (%)	Plastic limit (%)	Plasticity index (%)	Liquid limit (%)	Plastic limit (%)	Plasticity index (%)
	C1 soil			**C2 soil**		
5	-	-	-	27.9	15.8	12.1
10	48.3	16.8	31.5	42.6	17.2	25.4
15	-	-	-	51.4	17.7	33.7
20	66.5	21.5	45.0	72.2	21.4	50.8
30	97.5	23.8	73.7	-	-	-
40	125.8	27.5	98.3	-	-	-
50	168.5	31.4	137.1	-	-	-

Standard Proctor compaction tests were carried out following the procedure outlined in BS1377-4:1990 on both pure C1 and C2 soils as well as on fibre reinforced soil combinations. Table 3.5 shows the results of Proctor compaction tests on C1 and C1-10B soils. Figure 3.6 and Figure 3.7 show the effect of ABF and GBF fibres on compaction properties of C1 soil respectively. Figure 3.6 and Figure 3.7 show that maximum dry unit weight of C1 soil drops with increase in ABF/GBF fibre content. Optimum moisture content of C1 soil increases with increase in fibre content of both fibre types. This is attributed to replacement of soil grains with fibres, which have less specific gravity compared to that of soil grains and lubricating effect of absorbed water by fibres, which lessens the compaction impact.

Figure 3.8 and Figure 3.9 show the Proctor compaction curves of fibre reinforced C1-10B soils. These figures show that C1-10B soil possesses lower maximum dry unit weight and higher optimum moisture content compared to C1 soil. This is mainly due to presence of fine bentonite particles which increase the specific surface of the soil. Increase in specific surface results directly in increase in the amount of water required for reaching the maximum dry unit weight state. Moreover, the C1-10B soil reaches the maximum dry unit weight at higher moisture content than C1 soil does. Therefore, the maximum dry unit weight of C1-10B drops compared to C1 soil.

Table 3.5 Proctor compaction test results of C1 soil

Specimen	Dry unit weight (kN/m^3)	Moisture content (%)	Specimen	Dry unit weight (kN/m^3)	Moisture content (%)
C1	20.1	11.0	C1-10B	19.0	13.9
1A-C1	19.6	11.0	1A-C1-10B	18.3	14.0
3A-C1	18.8	12.0	3A-C1-10B	17.5	15.0
5A-C1	18.0	13.0	5A-C1-10B	15.7	19.5
1G-C1	19.2	11.0	1G-C1-10B	18.4	14.0
3G-C1	18.9	12.2	3G-C1-10B	17.9	14.5
5G-C1	17.8	12.4	5G-C1-10B	17.2	15.0

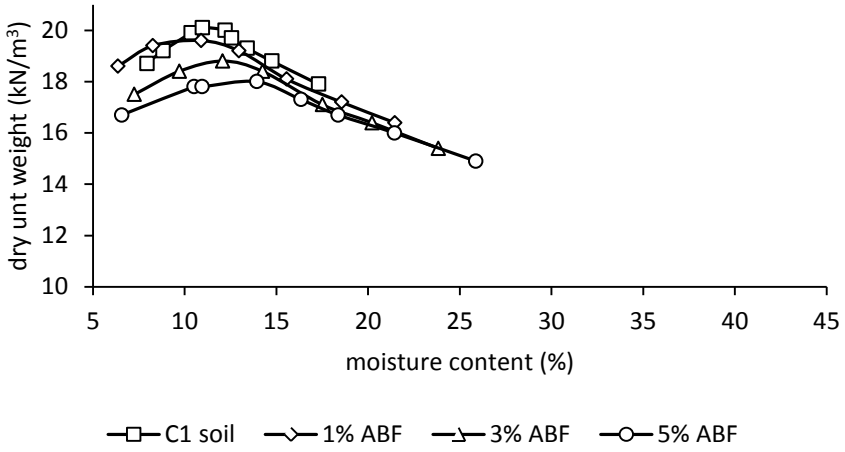

Figure 3.6 Proctor compaction curves of ABF fibre reinforced C1 soil

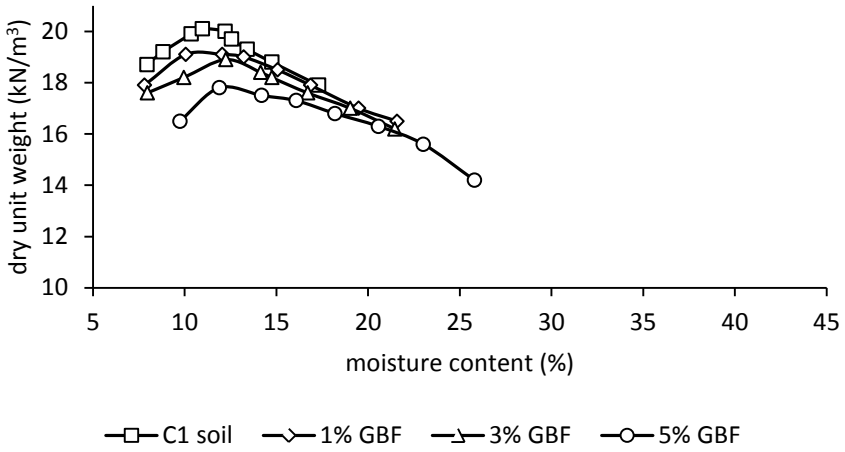

Figure 3.7 Proctor compaction curves of GBF fibre reinforced C1 soil

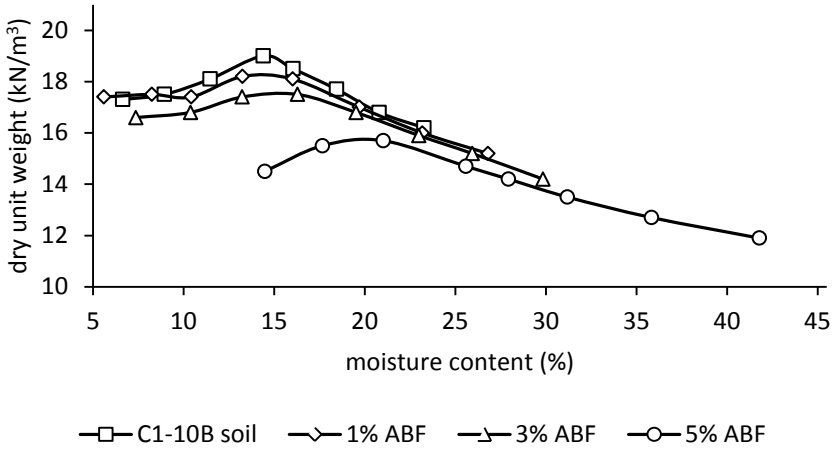

Figure 3.8 Proctor compaction curves of ABF fibre reinforced C1-10B soil

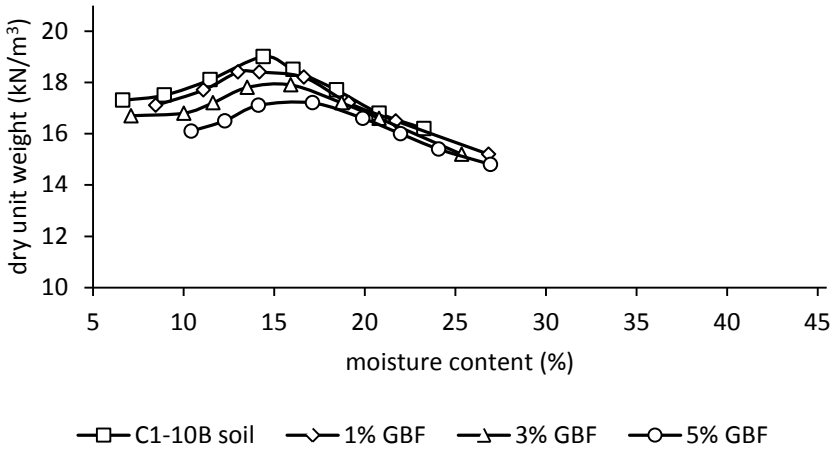

Figure 3.9 Proctor compaction curves of GBF fibre reinforced C1-10B soil

Table 3.6 shows the results of Proctor compaction tests on C2, C2-10B and C2-20B soils. Figure 3.10, Figure 3.11 and Figure 3.12 show the effect of GBF fibre on compaction curves of C2, C2-10B and C2-20B soil respectively. Maximum dry unit weight of C2 soil is slightly more than C1 soil. This can be attributed to the slight difference between the particle size distributions of C1 and C2 soils. The coarse content of C2 soil (i.e. 53.3%) is more than that of C1 soil (i.e. 44.3%). The optimum moisture content of C2 soil is less than that of C1 soil. This is related to lower fine contents of C2 soil (i.e. 46.7%) than fine contents of C1 soil (i.e. 55.8%). Table 3.6 also confirms that increase in bentonite content of C2 soil in C2-10B and C2-20B soils results in reduction in maximum dry unit weight and increase in optimum moisture content.

Figure 3.10, Figure 3.11 and Figure 3.12 show that adding GBF fibre to C2, C2-10B and C2-20B soils results in reduction in maximum dry unit weight and optimum moisture content. There was almost slight reduction in optimum moisture content of fibre reinforced C2-10B soil with 1% GBF fibre content.

Table 3.6 Proctor compaction test results of C2 soil

Specimen	Dry unit weight (kN/m^3)	Moisture content (%)	Specimen	Dry unit weight (kN/m^3)	Moisture content (%)
C2	20.7	9.2	C2-10B	20.0	12.2
1G-C2	20.5	9.5	1G-C2-10B	19.5	11.5
3G-C2	19.9	10.0	3G-C2-10B	18.9	13.5
5G-C2	18.4	11.2	5G-C2-10B	18.2	13.8
			C2-20B	18.4	15.0
			1G-C2-20B	18.6	15.4
			3G-C2-20B	17.2	16.3
			5G-C2-20B	17.1	17.6

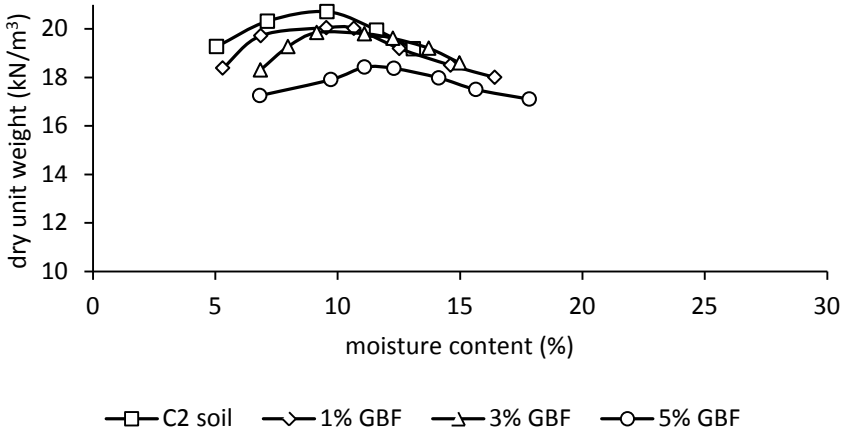

Figure 3.10 Proctor compaction curve for GBF fibre reinforced C2 soil

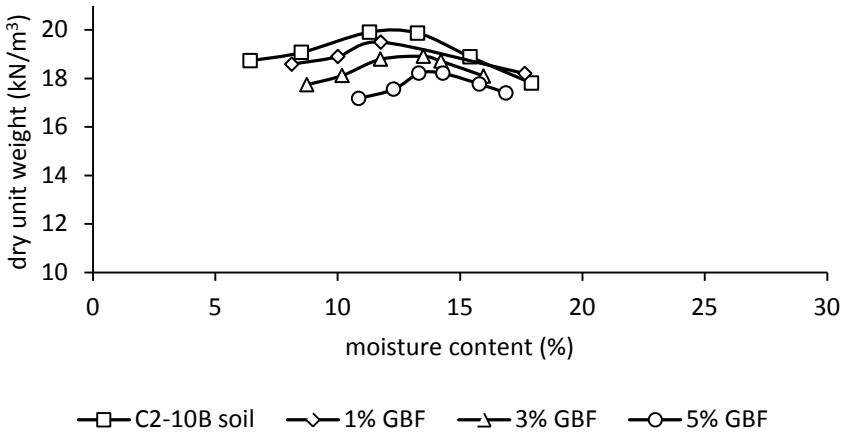

Figure 3.11 Proctor compaction curve for GBF fibre reinforced C2-10B soil

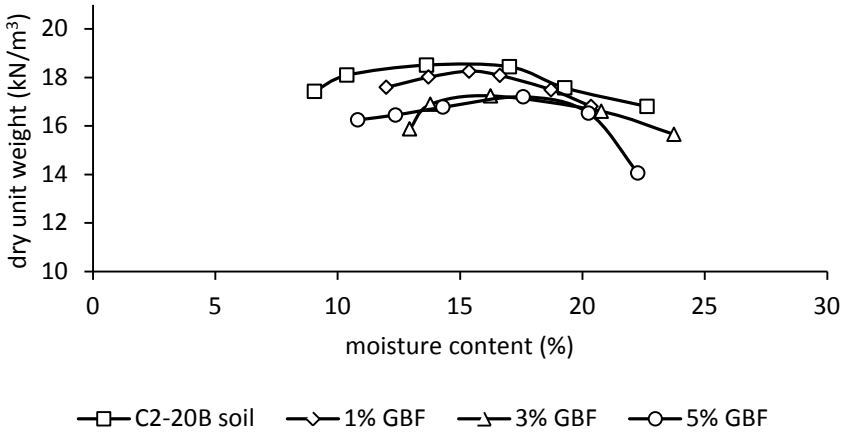

Figure 3.12 Proctor compaction curve for GBF fibre reinforced C2-20B soil

3.3 Sample preparation methods

The engineering characteristics of clay soils required for geotechnical analysis and design are obtained either from in-situ testing or laboratory experiments. In-situ testing has a number of disadvantages including; poorly defined boundary conditions (in terms of stresses and deformations), and uncertain drainage conditions of the soil under investigation (Bjerrum, 1973). Therefore, preparing reproducible clay soil specimens for different experiments such as triaxial test, unconfined compression strength test, swelling pressure and consolidation test is not readily achieved from in-situ soils for comprehensive works. Laboratory testing has the advantage of readily defining and precisely controlling stresses, deformations and boundary conditions. However, the inherent problem with the sampling approach is that it disturbs the soil (Rahman and Siddique, 2010).

Soil specimen preparation for laboratory testing ranges from undisturbed and remoulded samples to reconstituted samples prepared from slurry. In the following sections, these methods will be described briefly.

3.3.1 Undisturbed samples

Undisturbed soil samples include samples which are cut, removed, and packed carefully with the least possible disturbance. In undisturbed samples natural structure, void ratio, and moisture content are preserved as carefully as possible. Any loss of moisture from these samples during transportation, preparation and storage must be prevented. Wrapping samples in both cling film/plastic and aluminium foil creates short term prevention of moisture content loss. If the gap time between soil sampling and testing is prolonged, samples must be preserved and stored in temperature controlled room avoiding vibration and jolting. Thin-walled tubes are best suited to take undisturbed samples from field. Figure 3.13 shows some of the regular devices for sampling.

Figure 3.13 Soil sampling devices[7]

3.3.2 Remoulded specimens

Remoulded soil specimens might be used for shear strength, compressibility or permeability tests. A remoulded specimen is prepared at a specified moisture content and dry unit weight using static compaction or dynamic compaction. There are two criteria for preparing remoulded specimens:

a) to compact the soil to a specified void ratio or dry unit weight
b) to apply a known compactive effort to the soil

With the first criterion, due to the known volume of the mould, calculated mass of dry soil is mixed evenly with required water to reach the target moisture content and dry unit weight and compacted in the mould. Compaction can be done either by hand tamping with a steel rod or automatic compaction equipment (dynamic compaction), or by using a stress/strain controlled compression machine (static compaction). The main equipment for static compaction consists of a suitable mould with piston and a compression loading frame. Soil specimens can be prepared in appropriate moulds with the same size as test specimen in single layer or multi-layer fashion using compression machine. With the strain controlled compression machine, compression can be carried out at a specified rate of compression (i.e. vertical displacement rate). For preparing soil specimens in multi-layer fashion using static compression, the available soil is divided in several equal portions and every portion is compacted in equal volume at a constant volumetric strain rate.

[7] http://www.humboldtmfg.com/c-1-p-25-id-1.html

To prepare soil specimens at constant compactive effort, either the Proctor compaction mould or the Harvard miniature compaction device might be employed to prepare a specimen with target dimensions. In both methods, the specimen is compacted dynamically in several layers using equal number of blows per layer to transfer constant compaction energy to each layer. Figure 3.14 shows the Harvard miniature compaction device.

Figure 3.14 Harvard miniature compaction device[8]

3.3.3 Reconstituted samples

Reconstituted samples are those prepared from slurry at fully saturated condition to simulate the condition of naturally consolidated deposits in the field. In this method, clay soil powder is mixed with distilled or de-ionised water to form slurry at moisture content equal to or twice the liquid limit of the soil. At such high moisture content, the viscosity of the soil is low enough to remove air discontinuities in the slurry by application of vacuum (BS1377-6:1990). Then the prepared slurry is consolidated at a specific consolidation stress to mimic the field overburden pressure. Because the soil specimen prepared with this method has no stress history other than the imposed consolidation pressure, under successive loading increments greater than consolidation pressure the clay soil specimen behaves as normally consolidated clay (NC) and under unloading steps, it behaves as an over consolidated clay (OC).

[8] http://www.humboldtmfg.com/c-2-p-60-id-2.html#266

In the current study, to investigate the effect of fibres on strength properties of clay soils at different dry unit weights and moisture contents, remoulding method was employed as the soil specimen preparation method. All specimens prepared in this study were compacted statically using strain controlled compression machine.

3.4 Saturated triaxial test

Triaxial test data in general, include evolution of axial and volumetric strains, deviator and isotropic stresses and induced pore-water pressures. The results of this test can be used for deducing the shear strength parameters, namely; internal friction angle, cohesion intercept, dilatancy angle and the other dependent parameters. In a normal saturated triaxial test, a cylindrical soil specimen of height to diameter ratio of 2 to 2.5 is subjected to stress controlled or strain controlled axial load and confining stress. The specimen is isolated from confining fluid using natural rubber membrane(s) and placed in a Perspex chamber. Confining pressure is applied to the isolated soil specimen using pressurised water or oil and a loading plunger axially pushes the specimen in axial direction. In triaxial compression tests confining pressure is less than axial load and specimens is compressed vertically and in inverse, when confining pressure is more than axial load, specimen is compressed laterally and test is called triaxial extension test. Figure 3.15 shows a simple schematic of triaxial test apparatus.

Triaxial tests can be carried out under variety of stress paths in the triaxial apparatus. To replicate the real conditions arising in typical geotechnical problems, only a few stress paths are used including unconsolidated undrained test, consolidated undrained test and consolidated drained test.

3.4.1 Unconsolidated undrained (UU) test

The main purpose of unconsolidated undrained triaxial test (quick undrained) is to measure the undrained shear strength of a saturated soil quickly in terms of total stresses (undrained cohesion, c_u). The test procedure includes applying a cell pressure to a soil specimen without allowing the dissipation of the excess

pore-water pressure. Axial load is applied at a constant rate of displacement of usually 1 mm/min.

In triaxial test, given the soil specimen is fully saturated, any increase in confining stress without allowing the soil specimen to drain, leads to the same amount of increase in pore-water pressure and therefore, the effective stress remains constant. The strength of a soil specimen depends entirely on the applied effective stress. And hence the measured strength remains the same regardless of the applied confining stress. Therefore, the envelope tangent to the generated Mohr circles would be a horizontal line with intercept equal to C_u (i.e. undrained cohesion,$\varphi_u = 0$). Progressive development of negative pore-water pressure during testing heavily over consolidated clays or silts especially at high shear strains may cause large values of negative pore-water pressure during application of the deviator stress. This induces cavitations in the pore-water and therefore, the first drawn Mohr circles might not hold the case of $\varphi_u = 0$. This case usually happens when the initial applied cell pressure is far less than consolidation pressure in the field.

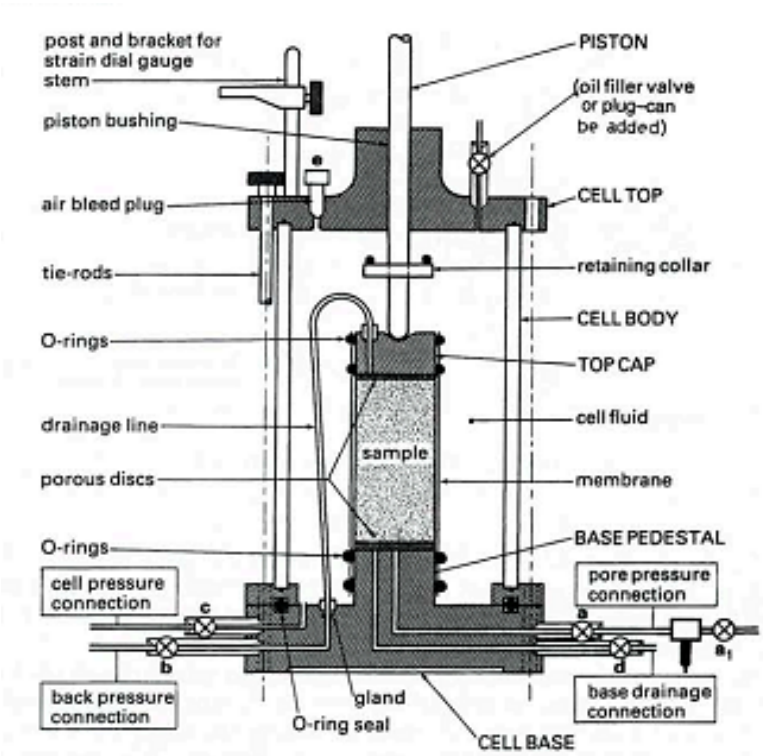

Figure 3.15 Schematic of triaxial cell apparatus (Head, 1998)

Quick undrained tests can be done without pore-water pressure measurement or with measurement of pore-water pressure. In the latter, the state of effective stress is known. The state of stresses during quick undrained test without pore-water pressure measurement is shown in Figure 3.16 (a). One of the most important matters concerning quick undrained triaxial test with pore-water pressure measurement which sometimes is ignored is that, the soil specimen should be fully saturated prior to shear test otherwise the measured pore-water pressure and hence calculated effective stresses are erratic. Achieving full saturation, forces pore air into solution and hence uniform pore-water pressure distribution is achieved all over a specimen.

Figure 3.17 shows the Mohr circles during quick undrained test. In a quick undrained triaxial test, undrained shear strength of soil specimen is defined in terms of undrained cohesion, which equals to $\frac{\sigma_{1f}-\sigma_3}{2}$.

3.4.2 Consolidated undrained (CU) test

In a consolidated undrained triaxial test, a minimum of three fully saturated cylindrical soil specimens are consolidated to different confining pressures whilst allowing dissipation of induced pore-water pressure (consolidation). Following consolidation, soil specimens are loaded axially at a lower strain rate than that used in the unconsolidated undrained test to allow uniform distribution of pore-water pressure throughout the soil specimen. The purpose of this test is to measure the shear strength of soil based on an effective stress analysis of failure envelopes (effective cohesion, c' and effective internal frictional angle, φ'). Figure 3.16 (b) shows the state of stresses in triaxial CU test. Typical total stress and effective stress Mohr circles for triaxial CU test on a clay soil is shown in Figure 3.18.

3.4.3 Consolidated drained (CD) test

In standard consolidated drained test, the specimen is first consolidated under a confining pressure, and then is brought to failure by increasing axial stress under condition of full drainage. The rate of applying axial load is much lower than that

used in consolidated undrained test in a way that negligible excess pore-water pressure is present in the specimen at any time during the shearing stage until failure. Therefore, minor stress (cell pressure) and major stress (sum of cell pressure and axial stress) are always effective stresses due to absence of pore-water pressure in specimen. Figure 3.16 (c) shows the state of stresses during triaxial CD test.

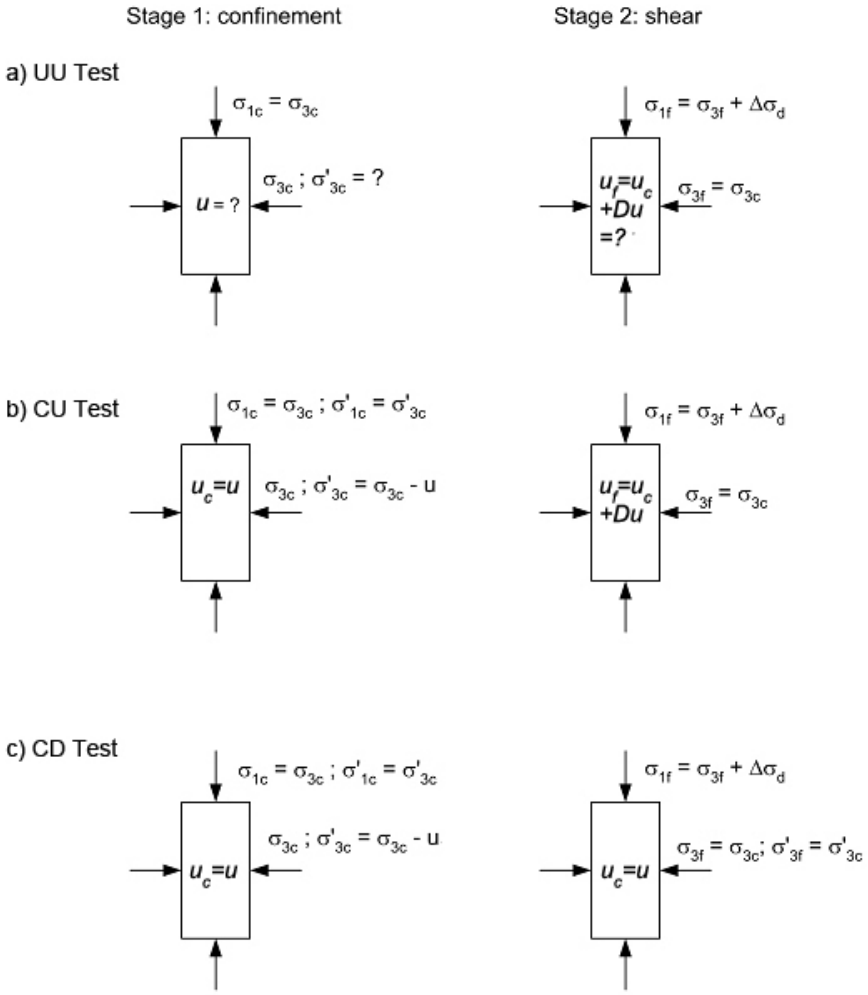

Figure 3.16 State of stresses during different types of triaxial test (US Army Corps of Engineers, 2003)

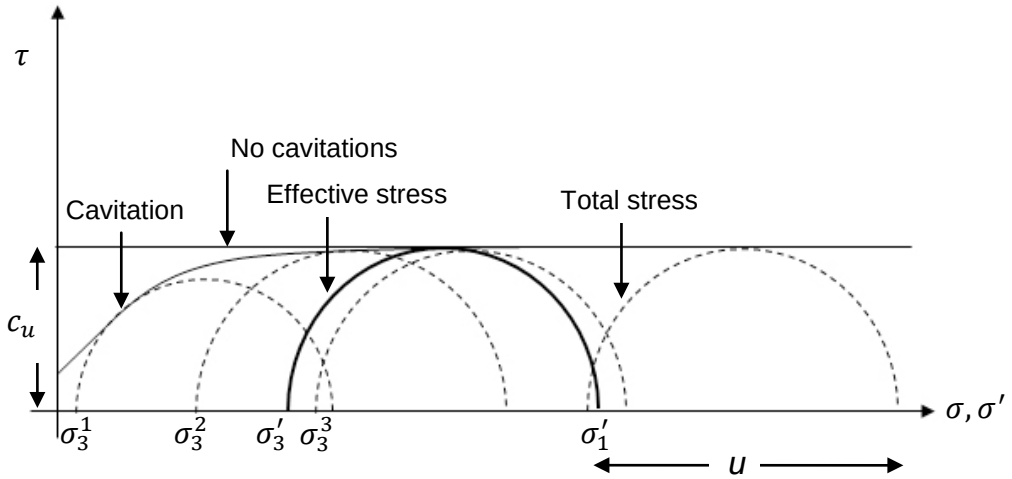

Figure 3.17 Failure envelopes of unconsolidated undrained test (quick undrained test)

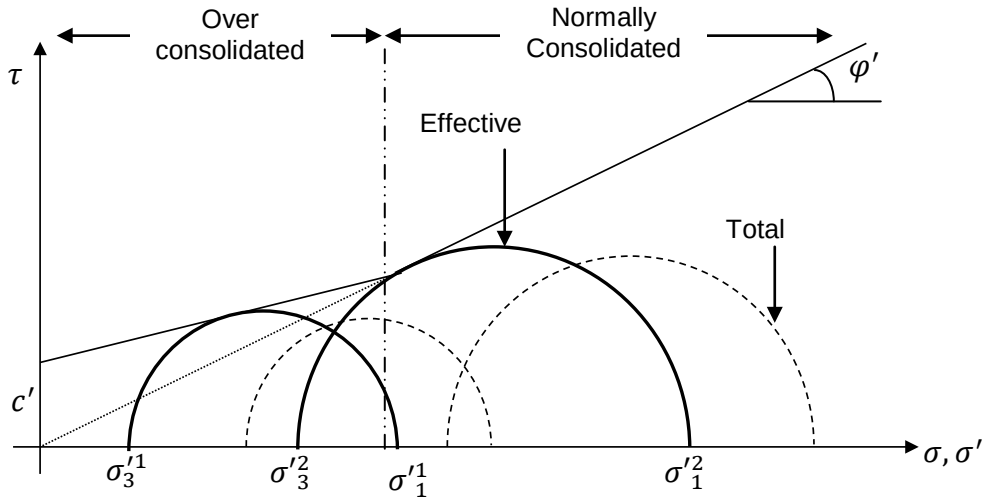

Figure 3.18 Failure envelopes of consolidated undrained test (CU test)

3.4.4 Saturation procedure during triaxial test

Air voids are inevitable during the preparation of the soil specimen by the remoulding method. Therefore, to achieve reliable measurement of pore-water pressure during the consolidation stage or shearing stage, full saturation of the soil specimen is an essential requisite. The saturation ratio of a soil specimen can be examined periodically using Skempton B-value which shows generated excess pore-water pressure due to application of increased confining pressure. Achieving B-value of more than 0.97 virtually ensures 100% saturation of the soil specimen.

The purpose of the saturation stage is to increase the pore-water pressure in the soil specimen to force pore air phase into solution. The time required for saturation depends mainly on the type, size, density and initial water content of the soil specimen.
BS 1377-8:1990 has addressed five different methods for saturating soil specimen inside the triaxial cell including:

1) Application of back pressure increments
2) One-stage elevation of back pressure
3) Use of initial effective stress
4) Saturation at constant water content
5) Automatic saturation

Description of the above mentioned methods and procedures for achieving a highly saturated soil specimen is beyond the scope of the thesis and readers can find related materials elsewhere (Head, 1998).

The method undertaken in the current research for saturating soil specimens in triaxial cell is slightly modified application of increments of back pressure (first method).

Before initiating a triaxial test, all the water lines connected to the chamber must be air drained. In order to remove air bubbles out of water pressure lines (including back pressure, pore-water pressure and cell pressure lines), application of a small water pressure (i.e. 5 kPa) prior to setting up the specimen followed by deaerating the water tubes is helpful. For cell pressure and back pressure line applying 5 kPa pressure would move bubbles from water pressurising system (air/water bladder system, automatic volume change/pressure controller system or oil/water pressurising system) towards cell connections. Usually in modern triaxial test apparatus, cell pressure, back pressure and pore-water pressure are measured with pressure sensors which are connected to the chamber body using solid aluminium blocks. In this case the solid blocks must be deaerated using the bleed valve on upper side of the block whilst deaerating the related pressure lines.

Deaerating the pressure lines prior to setting up the soil specimen on lower pedestal makes sure that:

a) No air bubble is introduced to the soil specimen through back pressure line
b) Reliable cell pressure, back pressure and pore-water pressure values are recorded
c) Time required for saturation is reduced

Following from deaerating pressure lines, the soil specimen is set up and saturation stage is initiated. In this research the following method (based on experience) was adopted to saturate the soil specimens:

1) Let the specimen be drained from top end to atmospheric pressure by opening appropriate valves.
2) Apply initial scheduled cell pressure.
3) Apply initial scheduled back pressure to the bottom of specimen.
4) Wait until water comes out from top of the specimen
   This stage might take few hours for clay soils, depending on permeability of the soil.
5) If in few hours, no water comes out from top of the specimen proceed to apply the next cell pressure and back pressure leaving the top of the specimen to drain under atmospheric pressure.
6) Repeat step 5 for few times to see enough flow rate from top of the specimen. Proceed to step 7 once enough flow rate is seen from top drainage line.
7) Connect the top drainage line to back pressure system and apply the same back pressure to top and bottom of specimen for few hours.
8) Close the back pressure line to top and bottom of specimen and wait until pore-water pressure measurement from bottom of specimen shows stabilised readings. A graph of pore-water pressure against square root of time is helpful to monitor equalisation of pore-water pressure.
9) Once pore-water pressure is stabilised record it and increase the cell pressure by 50 kPa
10) Monitor pore-water pressure readings from bottom of specimen using graph of pore-water pressure against square root of time.
11) Once the pore-water pressure is equalised, record it and calculate the Skempton B-value (3.1).

12) Achieving a B-value of more than 97% maintains full saturation of the specimen. Otherwise open back pressure line to top and bottom of specimen and apply the next pair of cell pressure and back pressure for increasing the saturation ratio of the specimen
13) Repeat steps 8 to 12 until calculated B-value is more than 0.97.

$$B = \frac{\Delta u}{\Delta \sigma_3} \qquad \text{Skempton B-value} \qquad (3.1)$$

Where:

Δu Change in pore-water pressure

$\Delta \sigma_3$ Change in cell pressure

Applying back pressure steps should be done over sufficient time to distribute the applied back pressure all over the specimen rather than stressing just the ends of the specimen. Quick application of increments of back pressure may result in formation of localised stresses at specimen's ends and therefore, non-uniform pore-water pressure distribution in specimen.

The above mentioned method for saturating clay soils showed satisfactory results in the current study. This method is almost as the same methodology as that is described in BS1377 with extra stage including percolation of water from top of specimen at small back pressures. This ensures wetting of specimen before applying back pressure at both ends of the specimen. Therefore, some of air bubbles trapped in the pores of the specimen are forced out of specimen to make the saturation procedure easier. A complete saturation stage for 38mm diameter clay soil specimen takes place from 3 to 10 days depending on the density, moisture content and type of clay. The required back pressure for full saturation of a clay soil specimen ranges from 300 kPa to 600 kPa.

3.4.5 Consolidation procedure during triaxial test

In the consolidation stage, the specimen is consolidated by allowing pore-water pressure to dissipate through back pressure line under a certain confining pressure and back pressure.

Positions of back pressure line and pore-water pressure line on lower pedestal of triaxial apparatus are close together and applying back pressure to bottom end of specimen might prevent reliable measurement of pore-water pressure from the vicinity of back pressure line. Therefore, for recording reliable readings of pore-water pressure during consolidation stage, it is better to apply the back pressure to the top end of the specimen and measure the pore-water pressure from the bottom end of the specimen. During consolidation stage, water from specimen is drained into volume change measuring device through back pressure line. Therefore, pore-water pressure drops gradually to back pressure value. Hence, by dissipating pore-water pressure, soil volume change occurs. Volume change measurement at suitable intervals (according to BS 1377-8:1990) up to the end of consolidation stage enables calculating updated height and diameter of specimen and also suitable strain rate for shear stage. For this reason, a graph of change in volume change against square root of time is drawn. Information such as time for 100% consolidation can be extracted graphically from the graph of volume change against square root of time. On onset of completion of consolidation, this curve flattens out and calculated consolidation ratio reaches a value more than 95%.

Once consolidation is completed, t_{100} (time for 100% consolidation) is extracted from the curve of volume change against square root of time. Required time for failure of specimen, t_f, can be calculated from the following formulae (Head, 1998):

Consolidated Undrained test (CU test)

$t_f = 0.53 \times t_{100}\ (minutes)$ Without side drains (3.2)

$t_f = 1.80 \times t_{100}\ (minutes)$ With side drains (3.3)

Consolidated Drained test (CD test)

$t_f = 8.5 \times t_{100}\ (minutes)$ Without side drains (3.4)

$t_f = 14 \times t_{100}\ (minutes)$ With side drains (3.5)

The maximum strain rate for shear stage can be calculated as follows:

$$\varepsilon = \frac{\varepsilon_f \times H}{100 \times t_f}\ mm/min \tag{3.6}$$

where;

H Height of specimen at the end of consolidation stage (millimetre)

ε_f Failure strain (minute)

Table 3.7 shows typical suggested values of failure strain (ε_f) for different soils. For more details about carrying out different stages of soil triaxial test, reader is referred to BS 1377-8:1990.

Table 3.7 Suggested failure strain for different soil (Head, 1998)

Soil type	CU test (%)	CD test (%)
Undisturbed clay (Normally consolidated)	15-20	15-20
Undisturbed clay (Over consolidated)	20 or more	4-15
Remoulded clay	20-30	20-25
Brittle soil	1-5	1-5
Compacted 'boulder clay' dry of optimum	3-10	4-6
Compacted 'boulder clay' wet of optimum	15-20	6-10
Compacted sandy silt	8-15	1-15
Saturated dense sand	25 or more	5-7
Saturated loose sand	12-18	15-20

3.5 Oedometer test

In one-dimensional consolidation of saturated cohesive soils, a gradual reduction in volume takes place in the direction of applied axial load due to dissipation of pore-water pressure. Oedometer test is used to simulate this process in laboratory to extract compressibility properties and the coefficient of consolidation of saturated cohesive soils. The test apparatus consists of a lever-loading frame and Oedometer cell. Oedometer cell itself consists of consolidation ring, two porous discs, lateral restraint and loading cap. Figure 3.19 and Figure 3.20 show different parts of the Oedometer test apparatus. The test can be carried out in two types of Oedometer cells including fixed-ring cell and floating-ring cell.

In the floating-ring cell, the ring including the soil specimen is used to hold the specimen during the test and it is only supported by the friction interface between soil specimen and the ring. The porous discs at top and bottom of consolidation ring are slightly smaller than diameter of soil specimen and therefore, specimen can be compressed from top and bottom. In fixed-ring cell, consolidation ring including the soil specimen is clamped into the cell between two porous discs with the lower one larger than the specimen's diameter. Therefore, the top porous disc can only enter the ring as the specimen is consolidated. Although floating-ring cell has less side friction, due to less support of the ring, only light rings can be used to hold the specimen. Hence, the ring might experience some lateral deformation under high vertical stresses. Moreover, setting up the floating-ring cells is more difficult because it must be located accurately to allow both top and bottom porous discs to enter the ring easily during the consolidation. Due to the mentioned shortcomings of the floating-ring cell, usually fixed-ring cell is preferred for one-dimensional consolidation test. The test is initiated by installing the soil specimen in the cell, fitting the cell on the load frame and setting up the loading yoke on top of the loading cap. Then the Oedometer cell is filled with water followed by the application of the first consolidation stress by adding appropriate weight on the weight hanger. At suitable time intervals such as what is recommended in BS1377-5:1990 (0, 10, 20, 30, 40, 50 seconds, 1, 2, 4, 8, 15, 30 minutes and 1, 2, 4, 8, 24 hours and then once a day), vertical displacement of the soil specimen is recorded using a displacement dial gauge. When primary consolidation is finished the vertical stress is doubled and the same procedure is repeated. Usually it is assumed that at each loading stage, the primary consolidation is completed within 24 hours. Therefore, each loading is kept for 24 hours and is doubled after 24 hours. In cases where in-situ stresses is not simulated in Oedometer test, suitable range of stresses for conventional consolidation test includes 12 kPa, 25 kPa, 50 kPa, 100 kPa, 200 kPa, 400 kPa, 800 kPa, 1600 kPa and 3200 kPa. Usually four to six stress ranges for loading and two to three stress ranges for unloading are enough for extracting consolidation characteristics of a clay soil.

3.6 Swelling pressure

Expansive clays and heavily over consolidated clays tend to swell when allowed access to water. Swelling properties of these soils including swelling pressure, free swell and swell potential can be measured in laboratory, using the same apparatus for one-dimensional consolidation test. The swelling pressure, P_s, is defined as the required vertical stress to prevent the soil that is confined in the consolidation ring from swelling. In swelling pressure test after setting up the soil specimen in the Oedometer cell, a small seating load is applied to the hanger beam to maintain good contact between loading yoke and soil specimen. Then water is added to the Oedometer compartment and induced vertical displacement is monitored using a displacement dial gauge. Upon observing any increase in the height of the specimen through dial gauge, appropriate weights must be added to the hanger to maintain the displacement gauge reading within the 0.01 mm. Adjustment of the beam hanger weights must continue until equilibrium is achieved and specimen has no further tendency to swell.

With highly over consolidated clays, enough time should be allowed to maintain equilibrium. Approaching equilibrium state under applied load can be realised by plotting cumulative weights against time. At equilibrium condition, the plotted curve flats out. Upon achieving equilibrium condition, swelling pressure can be calculated as the sum of stresses caused by weights times lever ratio plus stress caused by weight of seating pressure. Average time for the swelling pressure tests carried out in this study was in a range of 3 to 5 days.

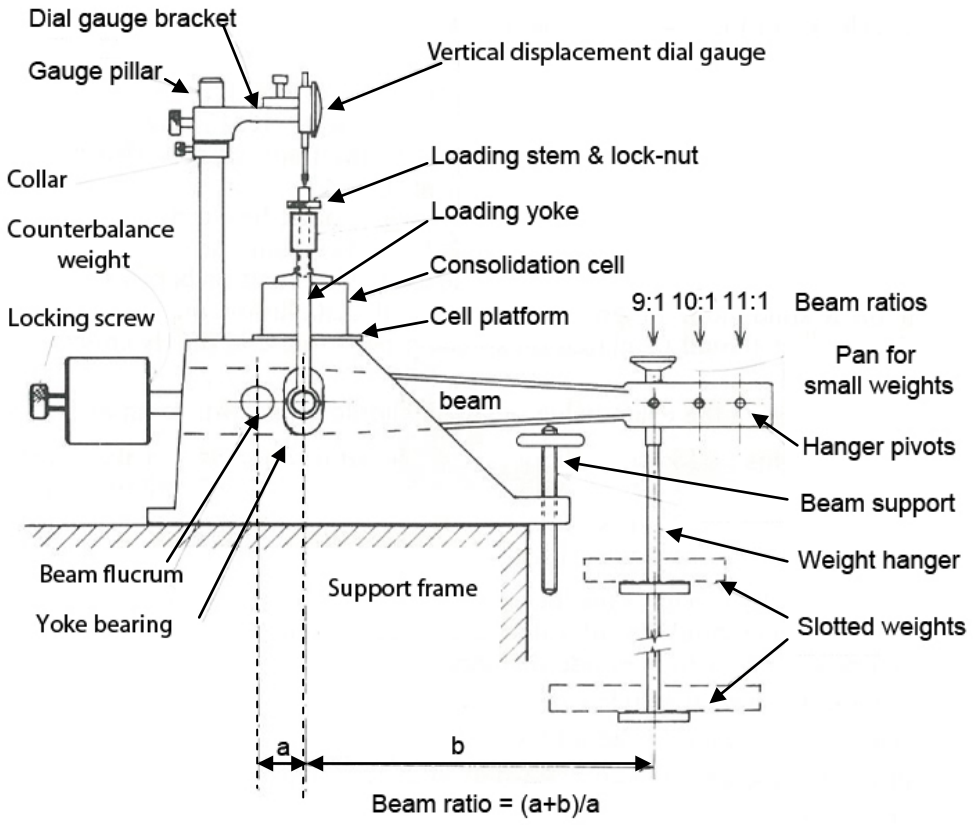

Figure 3.19 Oedometer test loading frame 9 (Head, 1998)

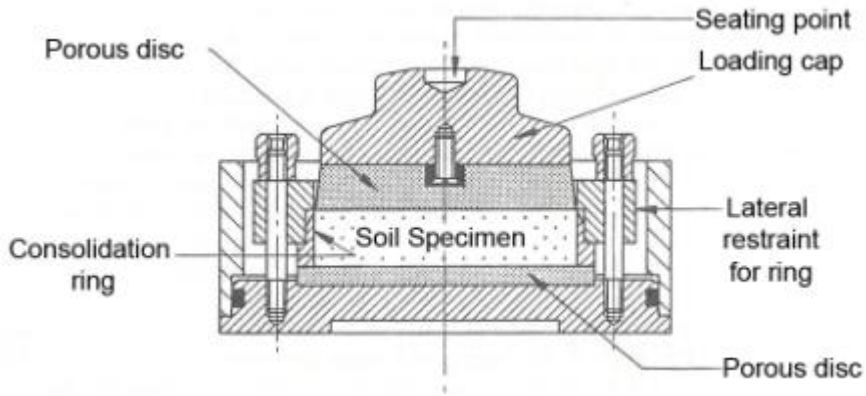

Figure 3.20 Oedometer cell (Head, 1998)

3.7 Unconfined compression test

The primary purpose of unconfined compression strength test is to determine unconsolidated undrained shear strength of cohesive soils (clay soils) under the unconfined condition.

A cylindrical clay soil specimen is subjected to axial compression in a strain controlled loading frame until failure occurs. Usually, soil specimens with 38mm to 100mm in diameter and height to diameter ratio of 2:1 are suitable for unconfined compression test.

Due to the completion of the test in short time an immediate approximate value of the compression strength of the soil assuming no drainage condition is achieved. According to BS 1377-7:1990, unconfined compression strength test (UCS test) is accomplished when three or more consecutive readings of load ring dial gauge show reducing or constant values.

A suitable range of strain rate falls into region of $0.5\%/min$ and $2\%/min$ to complete the test in less than 15 minutes. In the current study, a displacement rate of $1.4\ mm/min$ was used to carry out unconfined compression tests on clay soil specimens of 38mm in diameter and 76mm in height. Failure strain was also limited to 15%. Reading intervals of every 0.2mm of vertical displacement have been recommended by B.S. code to maintain continuity in plotted graphs however, in this study readings were taken at intervals of 0.1mm vertical displacement.

3.8 Soil/Fibre mixing procedure

To prepare a homogeneous mixture of clay soil and fibre, several trial methods were undertaken. Table 3.8 shows different methods used for mixing the clay soil, fibre and water and their disadvantages. To compare the results of strength and compressibility experiments, all soil specimens for triaxial consolidated undrained, consolidation, swelling pressure and unconfined compression strength tests were prepared using remoulding method.

The following procedure was adopted to prepare reproducible and fairly uniform soil/fibre mixture. In order to reach the target dry unit weight, sufficient amount of oven-dried soil and required amount of dry fibre were mixed inside a sealed container by shaking for few minutes. In case of soil specimens including bentonite, first oven dried soil and bentonite were mixed evenly, followed by adding fibres and remixing in sealed container by shaking. Then dry mixture was transferred into a pan and water sprayed on the mixture in several steps to reach

the target moisture content. The mixture was then mixed thoroughly by hand to reach evenly distributed moisture content. Latex gloves seemed to be very useful during hand mixing of soil, fibre and water to avoid losing soil particles and water. The prepared mixture was kept in a sealed container for 3 to 4 days to achieve uniform moisture content. After the moisture content curing period, on the day of the test, moisture content was re-measured and any loss in moisture content (which was in the region of 1% or less) was compensated. The outlined procedure for preparing soil/fibre mixtures was found to be reproducible and consistent enough to prepare uniformly distributed fibre and moisture content thorough the soil specimen. Therefore, drawbacks such as creating twisted fibres, non-uniform moist pockets of soil/fibre and porous structure due to addition of soap foam were avoided. Figure 3.21 shows different stages of soil preparation method.

3.9 Soil specimen preparation method

Conventional method of remoulding the soil specimen for soil strength or compressibility testing experiments consists of pushing a tube or consolidation ring into the compaction mould which is filled by soil. However, for the case of fibre reinforced specimen, this method was found to be unsuccessful in producing satisfactory specimens due to the following drawbacks:

a) During pushing the tube (or ring) into the compacted fibre reinforced soil, fibres which intersect with the cutting edges of the tube are dragged along the exterior side of the specimen. Therefore, longitudinal dents/voids might be formed on the circumference of the specimen
b) Once a small soil specimen is taken by pushing a tube into the compaction mould, due to random presence of fibres in the mould, the soil specimen might not include the target fibre content.

Therefore, the conventional method of remoulding the soil specimen was found to be unsuitable for the preparation of fibre reinforced soil specimens. To overcome the outlined drawbacks and also to prepare reproducible soil specimens, special moulds for both triaxial and consolidation test specimens were developed.

Figure 3.22 shows the components of the new moulds for preparing soil specimens for triaxial test and Oedometer test. In order to compress the soil in the

mould to the target volume, load was applied using a stress/strain controlled compression machine (DMG Retrofit model, Figure 3.23). The rate of loading was set at 4 mm/min at the beginning and was reduced to 0.5 mm/min once the height of the specimen was close to the target height.

During specimen preparation, when the soil/fibre mixture was compressed in the mould, pore-water pressure in the specimen was increased. The excess pore-water pressure could be dissipated slowly through the small hole manufactured at the bottom of the mould. For the case of fibre reinforced soil specimen, induced pore-water pressure was dissipated through the paths produced by the fibres towards the bottom hole. Therefore, induced pore-water pressure in fibre reinforced specimens could be dissipated earlier due to presence of fibre paths.

Upon releasing the axial force from top of the specimen after reaching the target height, the specimen started swelling due to combined influence of unbalanced generated pore-water pressure and rebounding forces of fibre lumps.

A few experiments were undertaken to determine the maximum amount of swelling after releasing the load from top for specimens with different fibre contents. The maximum swelling of about 5% (i.e. 3.8mm) was observed for triaxial soil specimen with 5% fibre content. To prevent post preparation free swell of specimens, all specimens were compressed to corrected target height. Corrected target height was defined as standard height (i.e. 76 mm) minus observed free swell after spontaneous release of load from the top of specimen.

Once a 76mm high specimen was prepared in the mould, the loading system was locked at this position and maximum stress was recorded. Therefore, no volume change was induced and the fibres and soil particles were rearranged due to dissipation of generated pore-water pressure in the specimen. Dissipation of pore-water pressure resulted in reduction in the total stress on the specimen (which could be read from compression machine’s software). Once the total stress was reduced by 40% to 50% of the maximum stress, the axial load on the specimen was released to remove the specimen from mould using manual soil sample extruder.

After removing the specimen from the mould, physical specifications such as average height (measured at 6 points) and mass of specimen were recorded and the specimen was wrapped in a cling film. The specimen was sealed in a container and kept for a day or two to allow stabilisation of pore-water pressure. Following this procedure reproducible cylindrical specimens (containing target fibre content) with smooth exterior surface were obtained. On the day of the test, the average height of the specimen from 6 measurements and the mass of specimen were again recorded to monitor any swelling or contraction during the relaxation period.

Another mould was also made for preparing Oedometer test specimens (Figure 3.22 (b)). In this mould, the consolidation ring is placed on a base plate and a metal cylinder lies on top of the ring. The soil is compressed in the cylinder using a steel cap and a plunger (shown in Figure 3.22 (b)). The height of the components was designed in such way that, once the top end of the rammer was reached the edge of the cylinder, the soil was completely compressed into the consolidation ring and an appropriate test specimen (with 19mm height) for Oedometer was achieved.

Table 3.8 Advantages and disadvantages of trial soil-fibre reinforced preparation methods

Spraying water on non-mixed fibre and soil
Disadvantage: Fibres become twisted together and non-uniform mixture of soil and fibre is created **Advantage:** Rapid and easy mixing process
Adding dry soil and appropriate amount of water to water saturated fibres followed by air drying to reach the desired moisture content
Disadvantage: Thick GBF fibres tend to form moist pockets of soil-fibre which store high moisture content. Therefore, a non-uniform distribution of moisture content is achieved **Advantage:** fibres are completely wet
Mixing fibres with small amount of soap foam and adding to previously moisten soil
Disadvantage: Soap foam might increase porosity of the specimen during compaction and therefore, strength characteristics are affected **Advantage:** Fibres may distribute uniformly by dispersing effect of soap foam
Mixing dry soil and fibres by shaking in a sealed container followed by spraying water on the mixture
Disadvantage: The procedure is time consuming **Advantage:** A fairly uniform mixture is produced

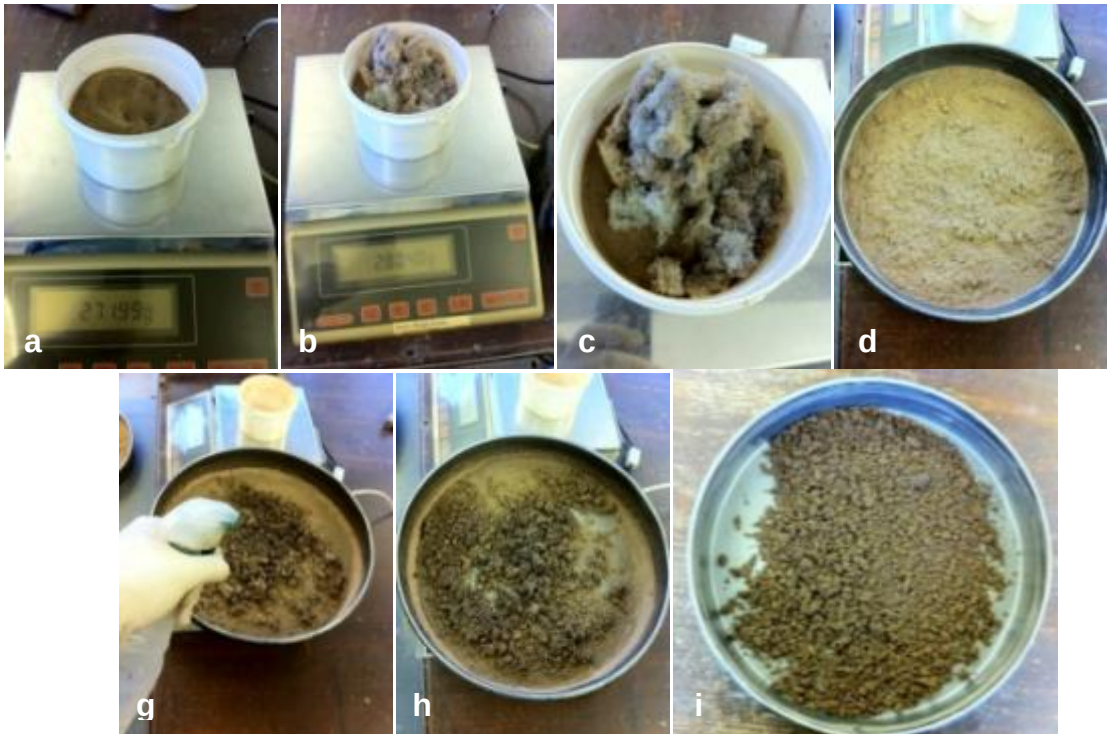

Figure 3.21 Soil/Fibre efficient mixing method

a)

b)

Figure 3.22 Components of soil specimen preparation mould for a) Triaxial test b) Oedometer test

Figure 3.23 Denison Mayer universal compression machine

Chapter 4 Calibration procedure and other equipment

Summary

In this chapter, the calibration procedure of different sensors used in the study is described.

A suction probe was developed to measure the negative pore-water pressure in the soil. Furthermore, the detail of the developed saturation cup which was used for saturating the ceramic disc of suction probe is presented. The method of calibration of developed suction probes and pressure cells used in the study is described accordingly.

4.1 Introduction

Calibration of sensors is a critical step in experimental techniques. The calibration of a sensor correlates A/D (Analogue to Digital) signals (i.e., numbers displayed on computer screen) and physical quantities (e.g., displacements).

With modern data acquisition systems and electronic sensors, only mere numbers are obtained on the computer screen. These numbers become meaningful only after they have been related to physical quantities by means of a calibration. Calibrations process is always carried out before starting a series of experiments. It does not need to be repeated for each experiment. It is however a good experimental practice to check that the sensors are properly calibrated before starting any experiment.

To compare the results of the tests together, all sensors must be calibrated against a master sensor or measuring device. Moreover, to compare the results of the same tests on the same material elsewhere, sensors must be calibrated to a nationally certified master device. The following sections describe the methods used for calibrating sensors used in the current research.

4.2 Calibrating procedure of sensors

In the current study totally three load cells, three LVDTs and nine pressure sensors were utilised to electronically sense the physical phenomena such as vertical displacement, applied load and applied/induced pore-water pressure during triaxial test. The following methodologies for calibration were found to satisfy the accuracy required for measuring load, displacement and pressure for the level of the research.

4.2.1 Calibrating load cell sensor

Force measuring sensors, also called load cells, are used to measure the applied axial loads in the unconfined compression test, direct shear test, and triaxial tests. The setup of data logging system used in the current research had three load cell sensors for measuring applied load on the soil specimen in the triaxial test.

To calibrate load cells used in the setup, a master load ring was calibrated against UKAS certificated universal compression machine (Denison Universal Compression Machine). Therefore, the master load ring was calibrated carefully in compression at 20 points from zero to 19 kN with steps of 1 kN.

Figure 4.1 shows the calibration chart for the master load ring. Calibrated load ring had a linear compression within the tested range with regression squared value of 0.9997 which showed the high degree of linearity of the load ring compression behaviour. Data shown in Figure 4.1 are the average of three compression trials.

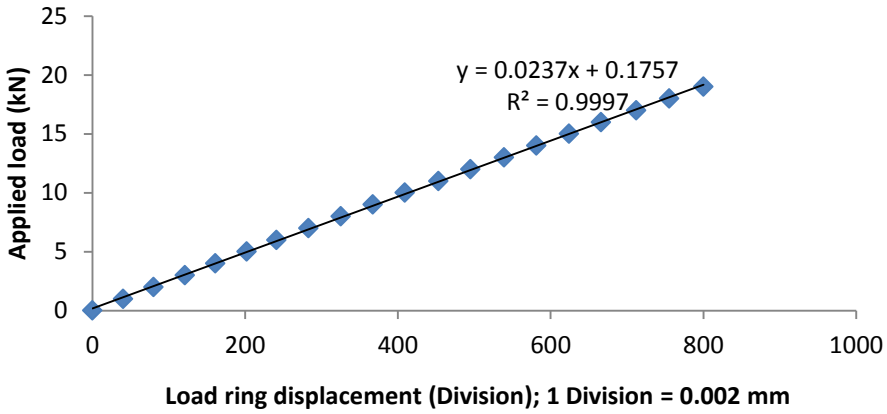

Figure 4.1 Calibration chart of master load ring

The next step was calibrating the load cells against the master load ring. Therefore, master load ring was set up in the triaxial loading frame underneath the load cell and load was applied by driving up the loading frame and compressing the load ring. The corresponding output was read from the data logging software and the load cell was calibrated against the applied load using the calibrating patch of the software (DAQ 32). Figure 4.2 shows the setup used for calibrating the load cell. Load cells used in this study were manufactured by Bongshin[9] with capacity of 10 kN. Load cells were calibrated against the master load ring at 12 points ranging from zero to 10 kN. Calibrating charts of the load cells have been shown in Figure 4.3.

[9] www.Bongshin.com

Figure 4.2 Setup used for calibrating load cell

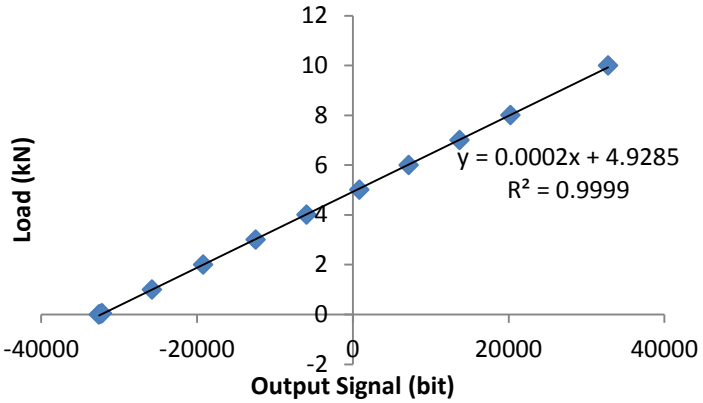

a)

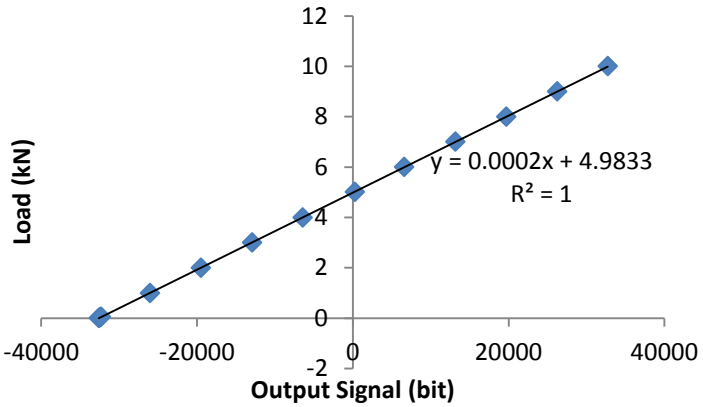

b)

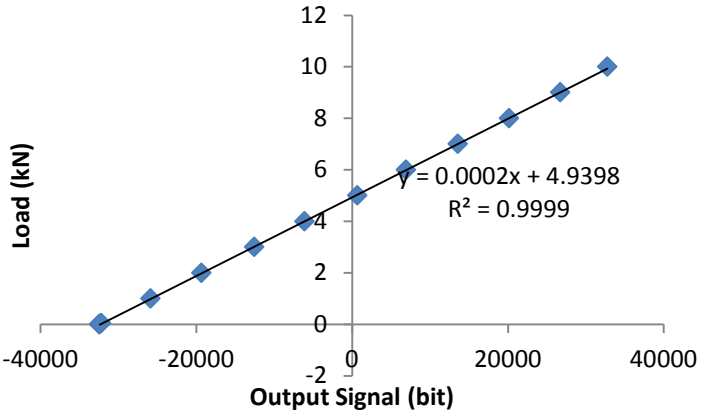

c)

Figure 4.3 Calibration charts of load cells

a) Load cell 1

b) Load cell 2

c) Load cell 3

4.2.2 Calibrating pressure sensor

Nine pressure sensors were used in this study to measure the values of cell pressure, back pressure and pore-water pressure of three triaxial apparatus. There were mixed brands of Druck and Bell & Howell pressure sensors.

GDS[10] pressure/volume change controller is a highly accurate device which can hold the pressure at a constant preset value with precision of 1 kPa. All pressure sensors were calibrated against a previously calibrated GDS digital pressure/volume change controller at 16 positions from zero to 1000 kPa. Figure 4.4, Figure 4.5 and Figure 4.6 show the calibration charts for all pressure sensors used in three triaxial test apparatus.

[10] http://www.gdsinstruments.com/

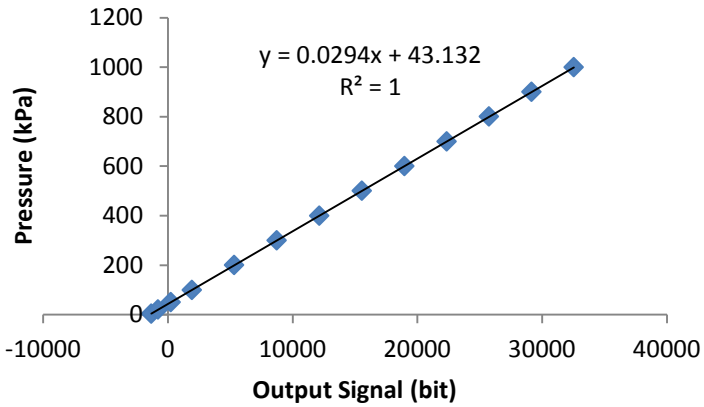

a)

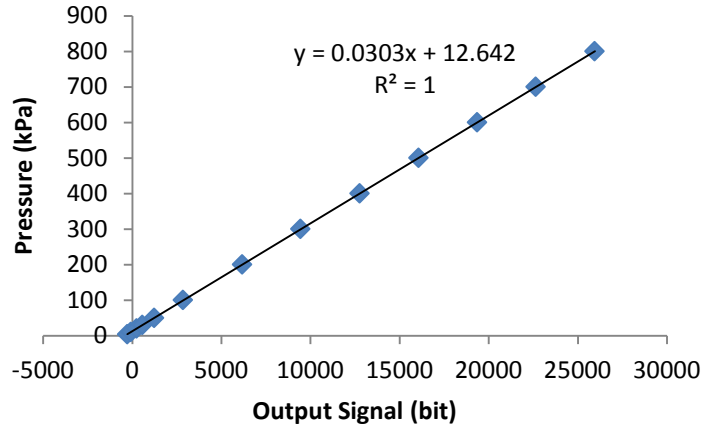

b)

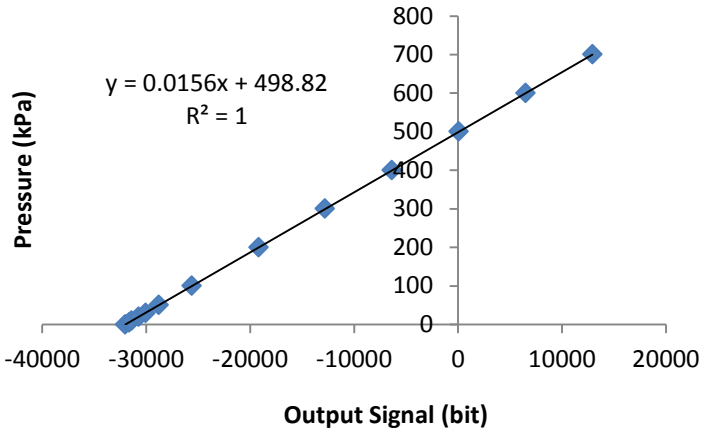

c)

Figure 4.4 Calibration charts of pressure sensors used in first triaxial apparatus

a) Back pressure sensor

b) Cell pressure sensor

c) Pore-water pressure sensor

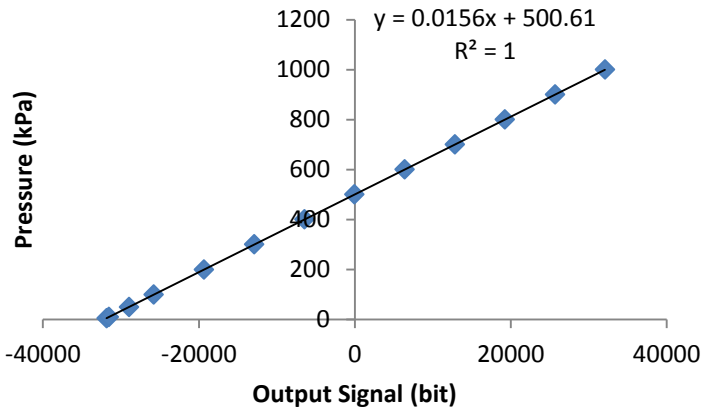

a)

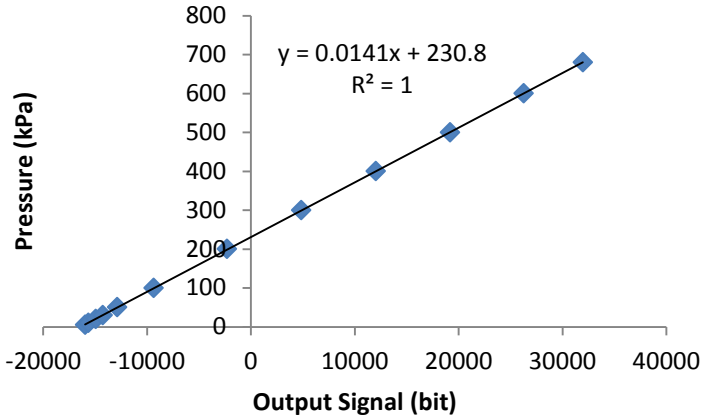

b)

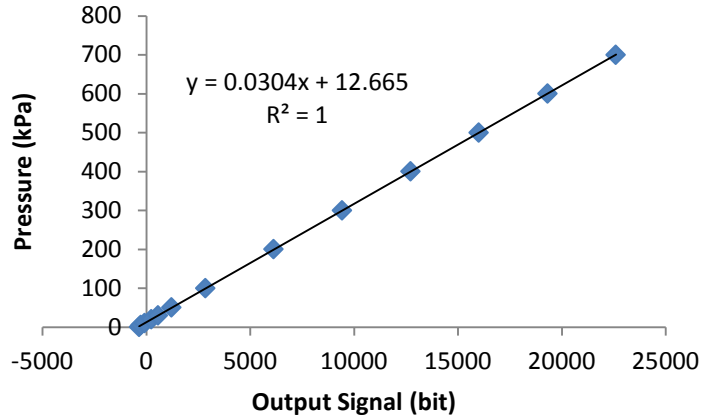

c)

Figure 4.5 Calibration charts of pressure sensors used in second triaxial apparatus

a) Back pressure sensor

b) Cell pressure sensor

c) Pore-water pressure sensor

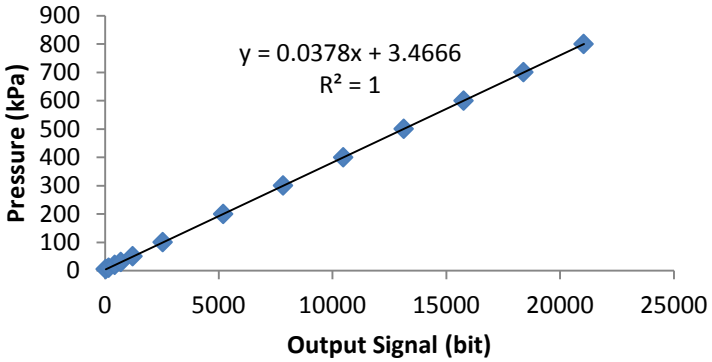

a)

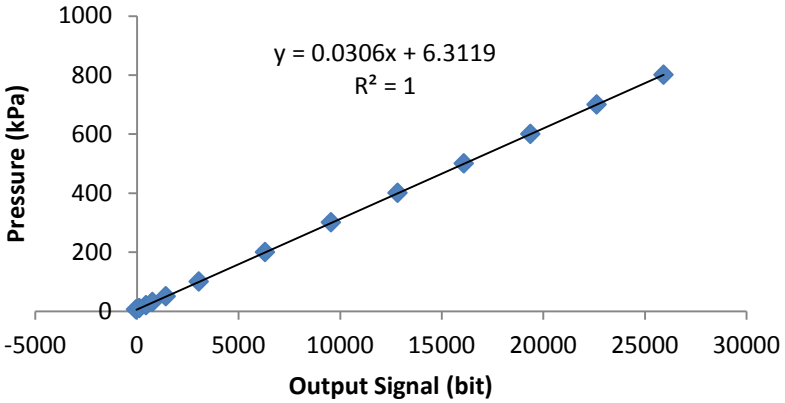

b)

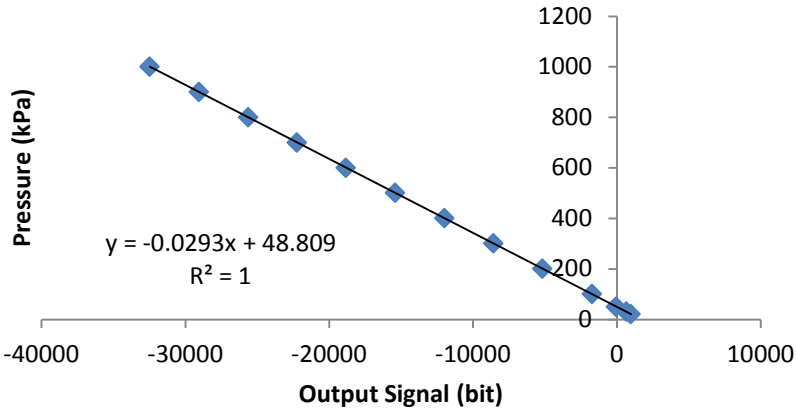

c)

Figure 4.6 Calibration charts of pressure sensors used in third triaxial apparatus

a) Back pressure sensor

b) Cell pressure sensor

c) Pore-water pressure sensor

4.2.3 Calibrating LVDT sensors

The linear variable differential transformer (LVDT) is a type of electrical transformer used for measuring linear displacement. In this study, three LVDT sensors manufactured by MPE were used for measuring the vertical displacement of the soil specimen in triaxial test apparatus. Calibrating LVDT sensors were accomplished by making in-house simple LVDT calibrator using a stand and a digital calliper. Therefore, each LVDT was subjected to known displacement and induced output voltage was measured with the data logger. All LVDT sensors were calibrated from zero to 50 mm at 15 points. Figure 4.7 and Figure 4.8 show the LVDT calibrator device and calibration charts respectively.

Figure 4.7 LVDT calibrating device

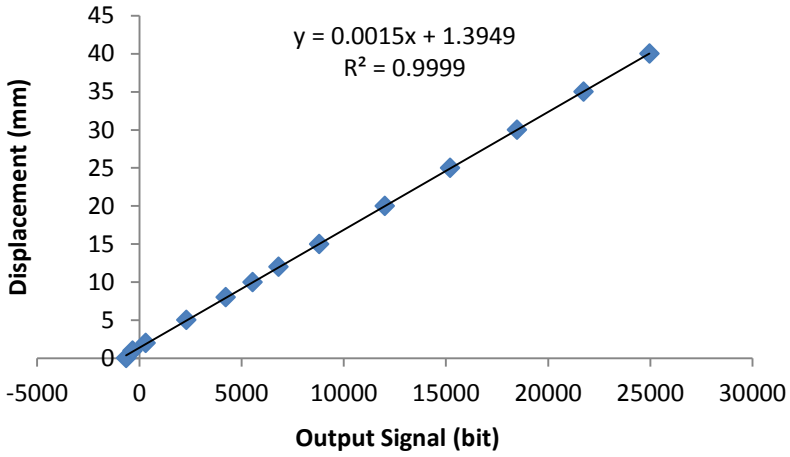

a)

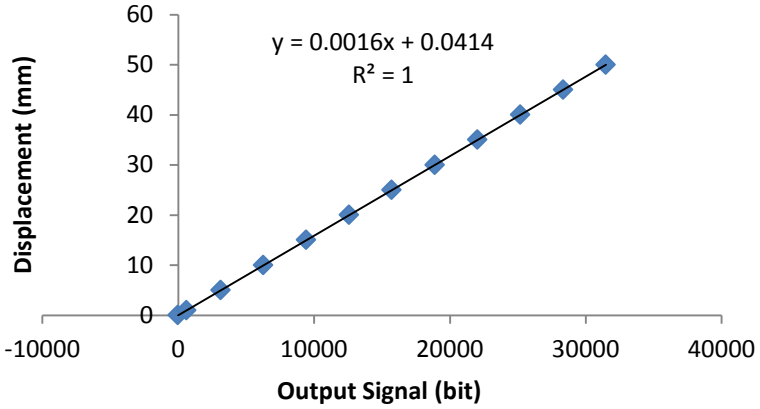

b)

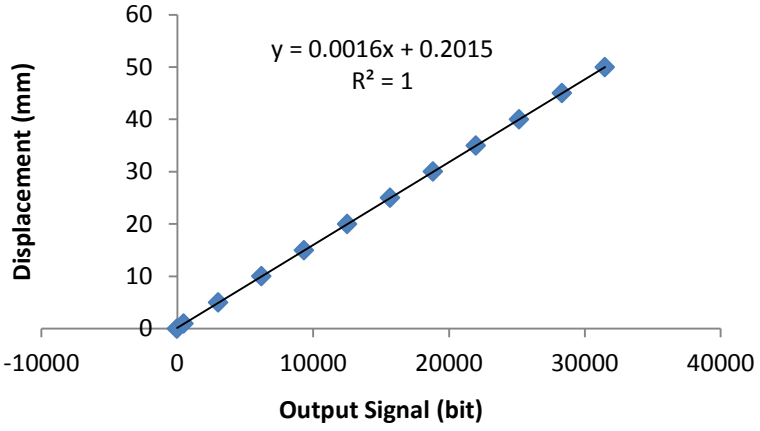

c)

Figure 4.8 Calibration charts of LVDT sensors

a) LVDT 1

b) LVDT 2

c) LVDT 3

4.3 Developing new design of mini suction probe

Ordinary pressure sensors used in engineering practice are capable of measuring positive fluid pressures. However, in geotechnical engineering sometimes it is required to determine negative pore-water pressure corresponding to water held in tension.

Recent development in unsaturated soil science has made improvement in measuring soil suction. Ridley and Burland (1993) developed soil suction probe for measuring matric suction ($u_{air} - u_{water}$). Suction probes are composed of a pressure measurement device such as pressure sensor, a high-air entry ceramic disc as the interface between the soil and the pressure measurement device and a miniature water reservoir between pressure measurement device and ceramic disc. The basic principle of measuring soil negative pore-water pressure using suction probe is explained through the equilibrium of the pressure of pore-water contained in the compartment underneath the high-air ceramic disc and the soil pore-water pressure. Therefore, as long as the water reservoir is saturated, any change in soil pore-water pressure will be reflected in the water pressure in the water compartment. Soil negative pore-water pressure force the water to flow from the water compartment into the soil however, positive pore-water pressure causes flow of water from the soil into the water compartment (Meilani et al., 2002).

Different suction probe designs have been introduced by several researchers such as those by Sjoblom (1996), Guan and Fredlund (1997), Take and Bolton (2003). The differences between the developed suction probes mainly comprise the dimensions, materials and sealing method (Lourenco et al., 2006).

A suction probe was designed by author and manufactured in the University of Bradford to measure the possible negative pore-water pressure induced in the soil. The suction probe included a ceramic disc with air entry value of 15 bar, and a 10 bar miniature pressure sensor with a rigid body made of aluminium. The unique design of this suction probe that makes it different to the former designs is the capability of changing the head of the suction probe for fitting ceramic discs with different air entry values. Therefore, several probe heads can be made with

different air entry value discs to fit the body of the suction probe. Figure 4.9 shows the design details of the developed suction probe. The overall dimensions of the suction probe were diameter of 32mm and height of 26mm. The depth of the water compartment underneath the ceramic disc was 1mm which produced a total capacity of 14.9mm^3 which is small enough to be sensitive to changes in pore-water pressure of the soil medium adjacent to the ceramic disc. The capacity of suction probe manufactured by Wykeham Farrance in association with University of Durham (Lourenço et al., 2006) was 10 mm^3. All dimensions can be reduced whilst a relatively smaller pressure sensor is used such as those manufactured by Entran[11] (Entran EPB series).

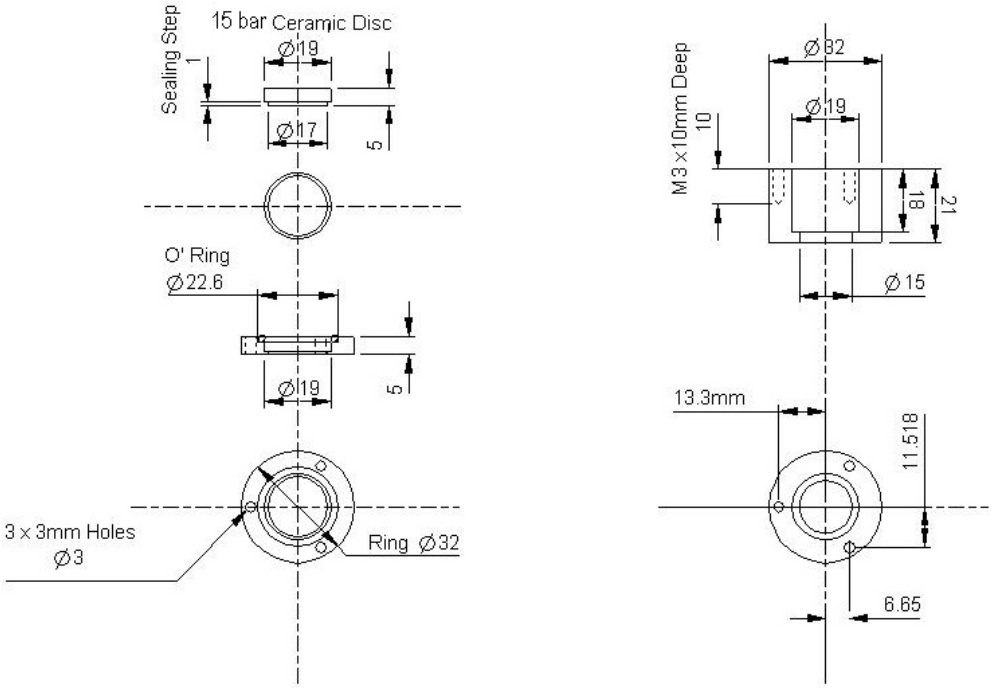

Figure 4.9 Design details of the developed suction probe

[11] http://www.entran.com/

Figure 4.10 Manufactured suction probe

4.4 Saturation cylinder and saturation cup

For precise measurement of pore-water pressure using suction probe, the water in the compartment and high-air entry value ceramic disc should be fully saturated. After a successful saturation, it is possible to measure the change in the pore-water pressure at exterior side of the suction probe using the internally fitted pressure sensor of the suction probe. The saturation process of the developed suction probe followed the method recommended by Bolton and Take (2003).

Unlike the device developed by Bolton and Take (2003), a cylinder was designed to introduce both vacuum pressures and positive pressures to the suction probe without the need to disassemble the probe from the cylinder. Figure 4.11 and Figure 4.12 show the design details and the manufactured saturation cylinder respectively.

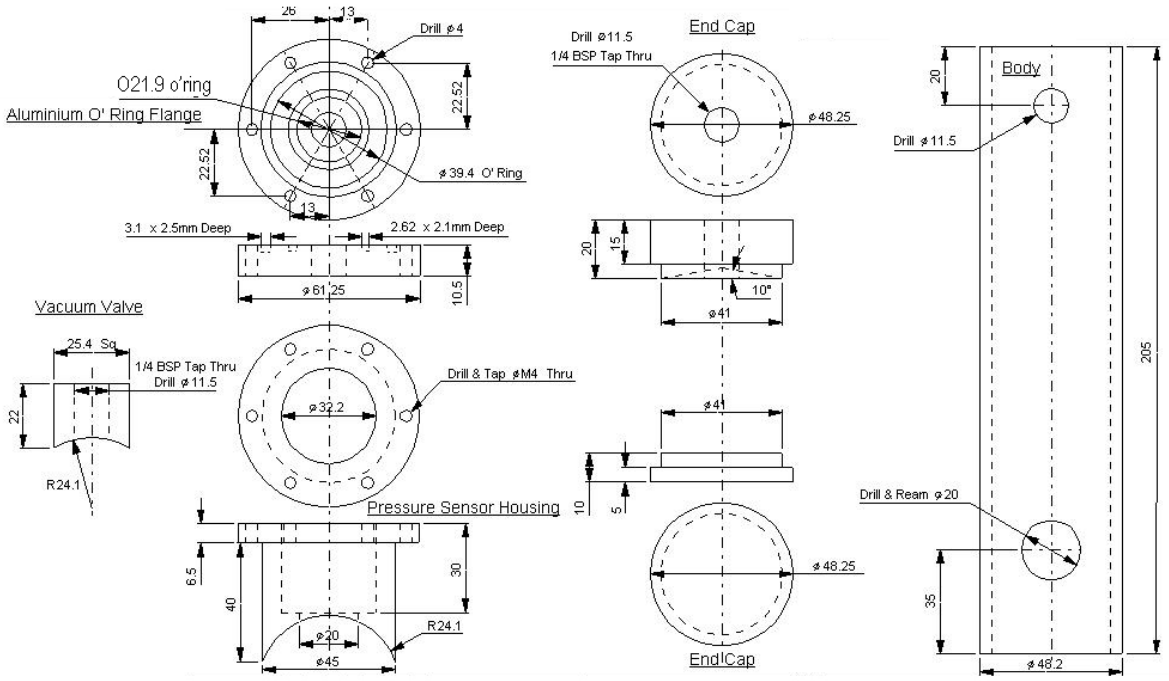

Figure 4.11 Design details of the saturation cylinder

Due to application of high pressures i.e. as much as 1800 kPa during saturation, a special sealing mechanism was designed. The mechanism included using two O-rings, one lying on the lower end of the suction probe and the other lying on the attachment for sealing the probe into the cylinder. The attachment was pushed on the suction probe using 6 screws. The device was tested under high pressures using GDS pressure controller to determine any possible leakage for few days. Very small amount of flow of water into the cylinder was observed for some period of time. This was related to the compression of water in the cylinder and occurred volume changes due to saturation of the ceramic disc and water compartment. However, the observed flow was ceased after the first day. Therefore, it was proved that the sealing mechanism worked properly.

Figure 4.12 Manufactured saturation cylinder

The suction probe was installed carefully in the saturation cylinder which was previously half filled with deaerated water. At this stage the cylinder was placed on

the bench in such way that the suction probe wires faced upward. Therefore, in this way the surface of the ceramic disc was kept above the water (dry). The cylinder was kept under a suction pressure of -90 kPa for 24 hours using a vacuum pump. After 24 hours, the cylinder was placed on the bench in such way that the suction probe submerged under water. To increase the degree of saturation of the fitted ceramic disc, cyclic pressures of +1800 kPa (using GDS pressure controller) and -90 kPa (using a vacuum pump) was applied for few hours. The changeover of the positive and negative pressure was controlled using appropriate ball valves on the cylinder.

The overburden pressure of the pressure sensors used in the suction probes was 200% of the reported measurement range by manufacturer (i.e. 2000 kPa). Therefore, applying 1800 kPa was still below the safe measurement range.

The application of positive and negative cyclic pressures to the suction probe was continued for 24 hours and once there was no volume change as observed by the GDS pressure controller, it was assumed that the suction probe had been saturated.

The described saturation cylinder was used to saturate the suction probes for the first use. However, for consecutive use of suction probes, suction probes were saturated in suction cups for a period of 24 hours before each test. Saturation cups were manufactured as smaller size of the saturation cylinder for saturating and calibrating several suction probes at the same time. Figure 4.13 shows the manufactured saturation cups.

The measured pore-water pressure by suction probe is highly sensitive to the saturation ratio of the ceramic disc and water compartment underneath the ceramic disc. Therefore, after saturation process it is recommended to calibrate the suction probe for each test to precisely measure the reflected pore-water pressures in the soil. Therefore, just before installing the suction probes in the soil, they were calibrated using GDS pressure controller for a small range of 0-200 kPa.

It was found that reducing the span of calibration, virtually increased the linearity of the calibration equation due to the higher linearity of the pressure sensors at lower

pressures. Range of 0-200 kPa was expected to be far more than the generated pore-water pressures during the test. Negative pore-water pressures were calculated by extrapolation using the calibration data for the positive range.

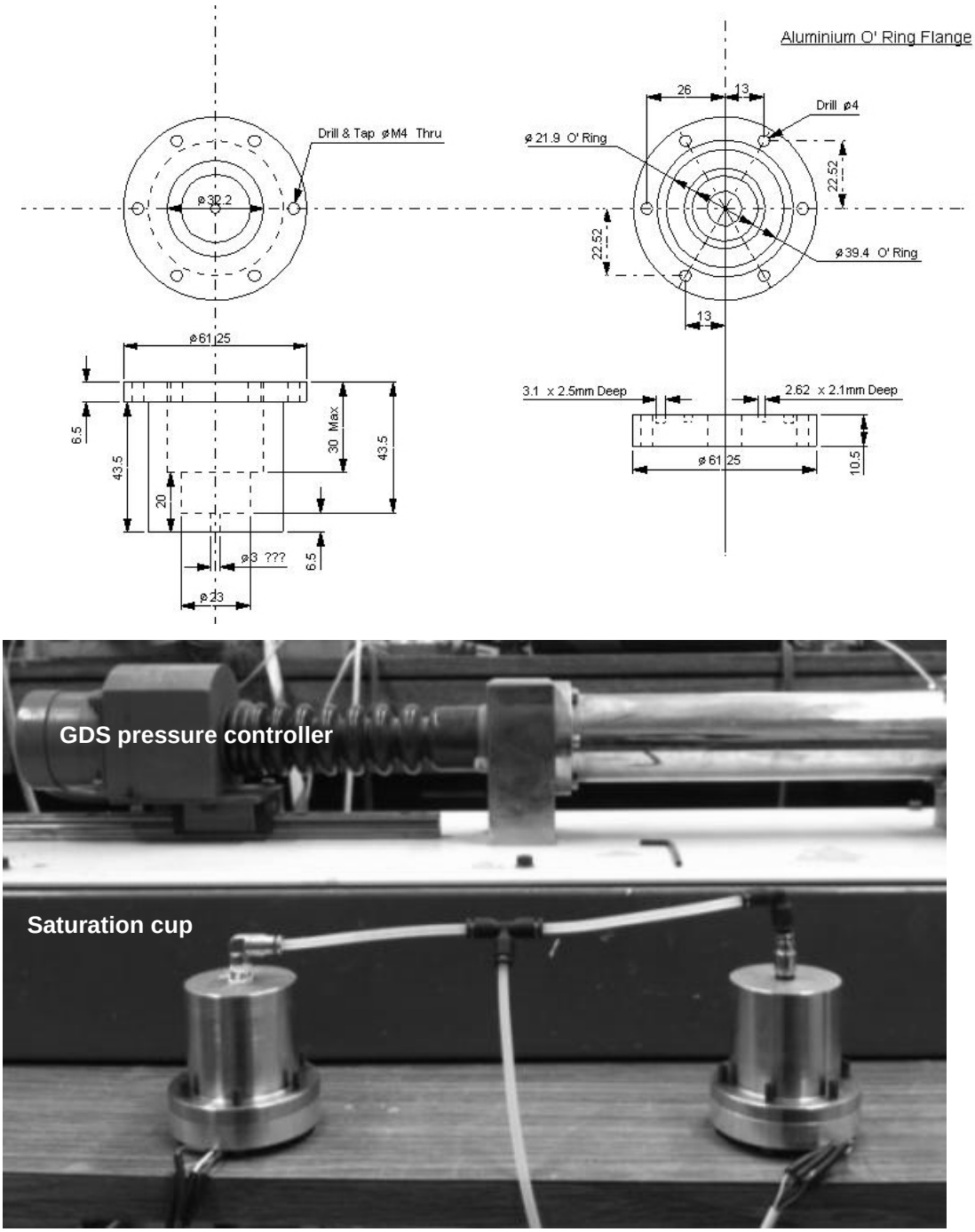

Figure 4.13 Saturation cup for saturating and calibrating suction probes

4.5 Pressure cells

Pressure cells were used in this research to measure the total stress underneath the model slope. Three soil pressure cells (Type 0234) manufactured by KULITE SENSORS LTD with capacity of 7 bar were used. This type of pressure cell is comprised of a small fluid reservoir under its exterior flexible diaphragm with a solid state silicon pressure sensor. A new attachment to the previously manufactured saturation cylinder was designed to seal the pressure cell and calibrate it using GDS pressure controller. In order to seal the pressure cell against applied water pressure in the cylinder, an O-ring was placed in a circular groove on the attachment. The O-ring was tighten to the exterior ring of the pressure cell using a set of bolts. Figure 4.14 shows the manufactured attachment. Calibration of the pressure cells was carried out in the range of 0-600 kPa using GDS pressure controller in steps of 50 kPa.

Figure 4.14 Attachment to saturation cylinder for calibrating pressure cells and its installation

Chapter 5 Results and Discussion (part one)

Summary

This chapter addresses a comprehensive study of the influence of waste carpet fibre addition on unconfined compression strength, swelling pressure and one-dimensional consolidation behaviour of different clay soils. To evaluate these parameters a series of experiments were conducted on fibre reinforced clay soil specimens with different fibre types and different fibre contents.

The results of each series of experiments have been reported followed by broad analysis and discussion on the observed behaviours.

5.1 Unconfined compression strength (UCS) test

To evaluate the influence of ABF/GBF fibres on unconfined compression strength of C1 and C1-10B soil specimens a comprehensive unconfined compression strength testing programme was conducted.

Three major parameters might affect the induced strength of a fibre reinforced soil specimen including; dry unit weight, moisture content (known as initial conditions of the specimen) and fibre content. In order to evaluate the influence of a single parameter, other parameters should ideally be kept constant.

In the current study, due to substantial differences between the dry unit weight of the non-reinforced and fibre reinforced soil specimens, it was found impractical to locate a common point on the respective compaction curves depicting the same dry unit weight and moisture content for all the specimens.

Therefore, five series of fibre reinforced soil specimens were prepared for UCS tests in order to determine the influence of initial conditions on the compression strengths:

(i) C1 soil specimens prepared at maximum dry unit weight and optimum moisture content

(ii) C1 and C1-10B soil specimens prepared at constant dry unit weight of 17.8 kN/m^3 and corresponding moisture contents from Proctor compaction data

(iii) C1-10B soil specimens prepared at constant dry unit weight of 17.2 kN/m^3 and corresponding moisture contents from Proctor compaction data

(iv) C1 soil specimens prepared at different dry unit weights and constant moisture content (i.e. 12%) and constant fibre content (i.e. 1%, 3% and 5%)

(v) C1 soil specimens prepared at different dry unit weights and moisture contents with constant fibre content

Table 5.1 presents details of the comprehensive testing programme demonstrating the fixed and variable parameters in each testing series. UCS tests were conducted according to BS1377-7 (1990).

Table 5.1 Details of unconfined compression strength testing programme

	Dry Unit weight (kN/m^3)	Moisture content (%)	Fibre content (%)	Fibre type	Soil type
Series 1	Maximum dry unit weight of each specimen	Optimum moisture content of each specimen	0, 1, 3, 5	ABF GBF	C1
Series 2	17.8	Corresponding moisture content from compaction data	0, 1, 3, 5	ABF GBF	C1 C1-10B
Series 3	17.2	Corresponding moisture content from compaction data	0, 1, 3, 5	ABF GBF	C1-10B
Series 4	15.8, 16.8, 17.8, 18.8	12	1, 3, 5	ABF	C1
Series 5	15.8, 16.8, 17.8, 18.8	7, 8, 10, 12	3	ABF	C1

In the first series, tests were carried out on non-reinforced and fibre reinforced C1 soil specimens compacted at their respective maximum dry unit weight and optimum moisture content. In order to reduce the number of affecting parameters (to exclude the influence of dry unit weight), second series of testing programme was implemented to evaluate the UCS of non-reinforced and fibre reinforced C1 soil and C1-10B soil specimens compacted at the same dry unit weight of 17.8 kN/m^3 and varying moisture contents which were extracted from their respective compaction curves. In the second series, C1-10B soil specimens with maximum dry unit weight of less than 17.8 kN/m^3 (i.e. 3A-C1-10B, 5A-C1-10B, 5G-C1-10B) were over compacted to achieve a dry unit weight of 17.8 kN/m^3. Therefore, in order to carry out UCS test on non-reinforced and fibre reinforced C1-10B soil specimens prepared at the same dry unit weight (less than their respective maximum dry unit weight), a third series of testing programme was implemented. In the third series, specimens were prepared at a dry unit weight of

17.2 kN/m^3 (dry unit weight of 5G-C1-10B, i.e. specimen composed of C1-10B soil plus 5% GBF fibre). Series 4 was undertaken at a wide range of dry unit weight while maintaining the moisture content at the same value so that the influence of dry unit weight with increasing fibre content could be evaluated. In series 5, the specimens were prepared at different dry unit weights and moisture contents while keeping the fibre content constant. Table 5.1 and Table 5.2 show the details of dry unit weight and moisture content of specimens tested in all series. All specimens in this study except specimens prepared at maximum dry unit weight and optimum moisture content were prepared at the dry side of optimum to avoid practical difficulties during preparation at higher moisture content.

Table 5.2 Dry unit weight and moisture content of specimens prepared for unconfined compression strength test

Specimen	γ[1]	ω[2]	γ	ω	γ	ω	Specimen	γ	ω	γ	ω
	1st Series		2nd Series		3rd Series			4th Series		5th Series	
0F-C1	20.1	11.0	17.8	6.1	-	-	1A-C1	15.8	12.0	-	-
1A-C1	19.6	11.0	17.8	4.9	-	-	1A-C1	16.8	12.0	-	-
3A-C1	18.8	12.0	17.8	8.0	-	-	1A-C1	17.8	12.0	-	-
5A-C1	18.0	13.0	17.8	10.7	-	-	1A-C1	18.8	12.0	-	-
1G-C1	19.2	11.0	17.8	7.6	-	-	3A-C1	15.8	12.0	15.8	7.0
3G-C1	18.9	12.2	17.8	8.9	-	-	3A-C1	16.8	12.0	16.8	8.0
5G-C1	17.8	12.4	17.8	12.4	-	-	3A-C1	17.8	12.0	17.8	10.0
0F-C1-10B	-	-	17.8	10.0	17.2	7.0	3A-C1	18.8	12.0	18.8	12.0
1A-C1-10B	-	-	17.8	10.0	17.2	5.4	5A-C1	15.8	12.0	-	-
3A-C1-10B	-	-	17.8	10.0	17.2	11.6	5A-C1	16.8	12.0	-	-
5A-C1-10B	-	-	17.8	13.0	17.2	14.0	5A-C1	17.8	12.0	-	-
1G-C1-10B	-	-	17.8	11.0	17.2	8.3	5A-C1	18.8	12.0	-	-
3G-C1-10B	-	-	17.8	11.0	17.2	11.0					
5G-C1-10B	-	-	17.8	13.0	17.2	15.0					

[1]: Dry unit weight (kN/m^3)
[2]: Moisture content (%)

5.2 Swelling pressure tests

A series of swelling pressure tests were carried out on non-reinforced and fibre reinforced C1 and C1-10B soil specimens. Swelling pressure tests were undertaken according to BS1377-5 (1990) using Oedometer apparatus on specimens with 100mm diameter and 19mm thickness. As depicted in

Figure 5.1(a), rear loaded Oedometer was used in the current study to carry out swelling pressure tests.

To be able to compare the influence of ABF/GBF fibres on swelling pressure behaviour of specimens compacted at different dry unit weights and moisture contents, three series of swelling pressure tests on C1 and C1-10B soil specimens were undertaken.

I. Fibre reinforced C1 soil specimens were prepared at maximum dry unit weight and corresponding optimum moisture content.

II. Fibre reinforced C1 and C1-10B soil specimens were compacted at the same dry unit weight (i.e. 17.8 kN/m^3) and corresponding moisture contents that are obtained from the Proctor compaction data.

III. Specimens were prepared with 3% ABF fibre content but with a range of moisture contents while keeping dry unit weight constant or a range of dry unit weights while maintaining the same moisture content or at the corresponding moisture contents from the compaction data.

Table 5.3 describes the combination of swelling pressure tests carried out in this study.

Table 5.3 Dry unit weight and moisture content of specimens prepared for swelling pressure test

Specimen	γ[1]	ω[2]	γ	ω	Specimen	γ	ω	γ	ω
	1st Series		2nd Series			3rd Series		4th Series	
0F-C1	20.1	11.0	17.8	6.1	3A-C1	17.8	8.0	-	-
1A-C1	19.6	11.0	17.8	4.9	3A-C1	17.8	12.0	-	-
3A-C1	18.8	12.0	17.8	8.0	3A-C1	17.8	12.0	-	-
5A-C1	18.0	13.0	17.8	10.7	3A-C1	17.8	12.0	-	-
1G-C1	19.2	11.0	17.8	7.6	3A-C1	15.8	12.0	15.8	7.0
3G-C1	18.9	12.2	17.8	8.9	3A-C1	16.8	12.0	16.8	8.0
5G-C1	17.8	12.4	17.8	12.4	3A-C1	17.8	12.0	17.8	10.0
0F-C1-10B	-	-	17.2	7.0	3A-C1	18.8	12.0	18.8	12.0
1A-C1-10B	-	-	17.2	5.4					
3A-C1-10B	-	-	17.2	11.6					
5A-C1-10B	-	-	17.2	14.0					
1G-C1-10B	-	-	17.2	8.3					
3G-C1-10B	-	-	17.2	11.0					
5G-C1-10B	-	-	17.8	15.0					

[1]: Dry unit weight (kN/m^3) [2]: Moisture content (%)

5.3 One-dimensional consolidation test

One-dimensional consolidation tests were undertaken on non-reinforced and GBF fibre reinforced C2, C2-10B and C2-20B soil specimens compacted at their respective maximum dry unit weights and optimum moisture contents.

One-dimensional consolidation tests were carried out according to BS1377-5 (1990) on specimens with 75mm diameter and 19.7mm height. Figure 5.1 (b) shows front loaded Oedometer which was used for carrying out one-dimensional consolidation tests in this study.

To evaluate the behaviour of non-reinforced and fibre reinforced clay soils under one-dimensional loading/unloading, specimens with different fibre contents were consolidated under normal stresses of 50, 100, 200, 400, 800 and 1600 kPa. Following consolidation at 1600 kPa, specimens were unloaded to 800, 400 and 200 kPa respectively at periods of 24 hours.

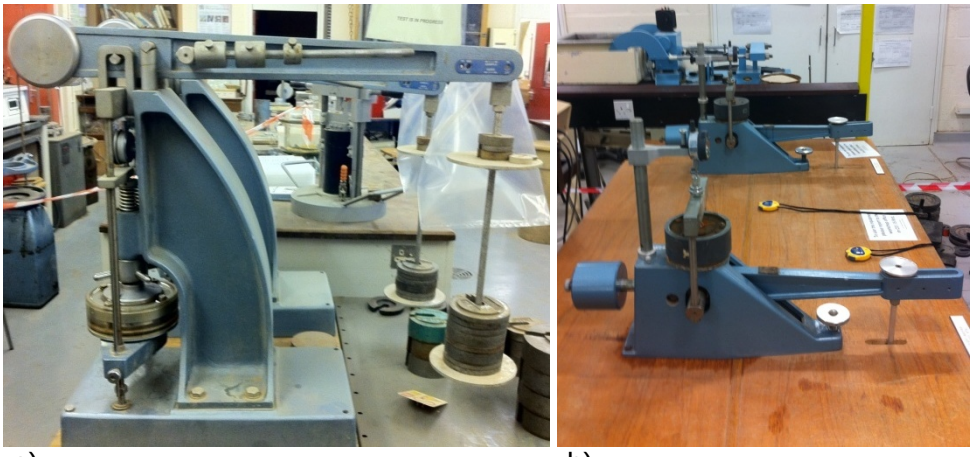

a) b)

Figure 5.1 Oedometer test apparatus a) Rear loaded b) Front loaded

5.4 Discussion on the results of UCS tests

5.4.1 Stress-Strain behaviour

Figure 5.2 to Figure 5.9 show the stress-strain behaviour of non-reinforced and fibre reinforced clay soil specimens. Non-reinforced C1 and C1-10B soil specimens prepared at dry unit weight of 17.8 kN/m^3 showed a very brittle behaviour with small strains at peak compression strength of 0.9% and 1.4% respectively. Failure strain (i.e. strain at peak compression strength) increased upon increasing fibre content, which denoted a gradual transformation from brittle behaviour to ductile one. Stress-strain curves of non-reinforced and fibre reinforced soil specimens with 1% ABF, 3% ABF and 1% GBF fibre content were indicative of strain-softening behaviour.

Although fibre reinforced soil specimens at lower fibre contents showed strain-softening behaviour, loss of their post peak strength was significantly less than that of non-reinforced soil specimens. At 5% ABF fibre content and more than 1% GBF fibre content, reinforced specimens showed strain-hardening behaviour. The observed behaviour was due to contribution of the tensile strength of fibres at higher strain values.

To quantify the influence of fibre addition on stress-strain behaviour of fibre reinforced clay soil specimens, energy absorption capacity was calculated using stress-strain curves. Energy absorption capacity is defined as the required energy to deform the specimen, which is equal to the area under the stress-strain curve (Maher and Ho, 1994).

Figure 5.10 shows the energy absorption capacity of non-reinforced and ABF/GBF fibre reinforced specimens (specimens tested in series one to three) up to failure strain, which is dependent upon dry unit weight, moisture content and fibre content. Maximum failure strain in the current testing programme was considered as 15% for specimens with strain hardening behaviour posing increased strength beyond 15% axial strain. With all specimens compacted at the same dry unit weight, increase in fibre content resulted in significant increase in absorbed energy. This was consistent with the results published by Maher and Ho (1994).

Increase in absorbed energy is a measure of increase in either failure strain or peak strength or both. In fibre reinforced specimens, a uniform distribution of fibres throughout the structure of soil specimen resulted in continuous energy absorption under compression. This can be interpreted as developing resisting forces by fibres when shear forces in weak zones overcome soil natural shear strength. Therefore, the rate of absorbed energy increased with increased fibre content due to more probability of intersecting weak zones by fibres. Moreover, this can also be attributed to absorbed energy by fibres which were in tension.

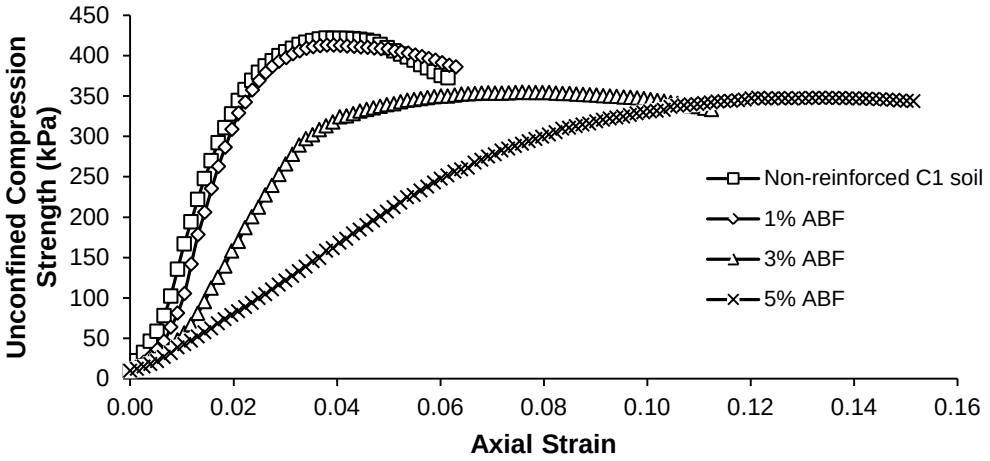

Figure 5.2 Stress-strain behaviour of ABFfibre reinforced C1 soil specimens compacted at their respective maximum dry unit weights

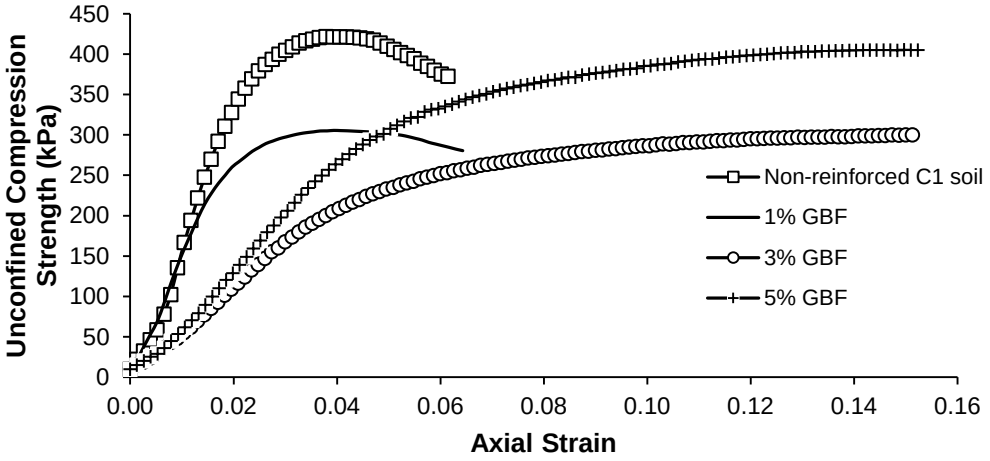

Figure 5.3 Stress-strain behaviour of GBF fibre reinforced C1 soil specimens compacted at their respective maximum dry unit weights

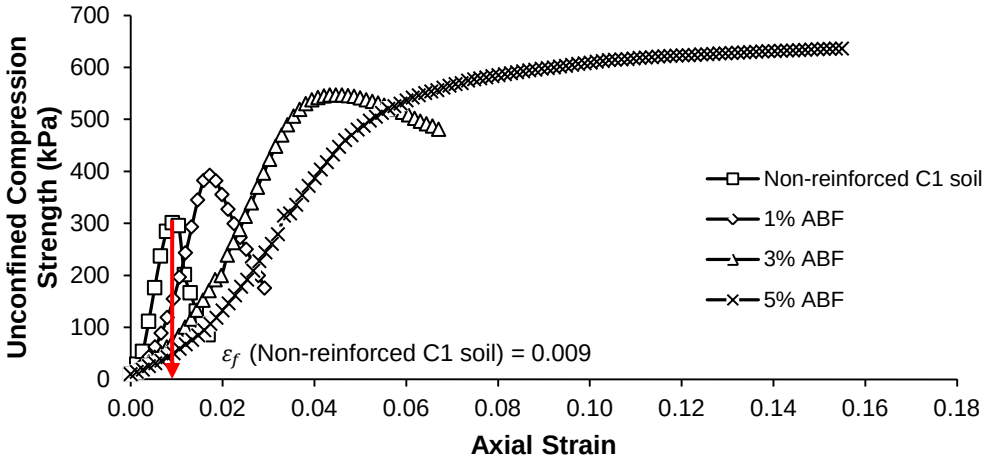

Figure 5.4 Stress-strain behaviour of ABF fibre reinforced C1 soil specimens compacted at dry unit weight of 17.8 kN/m^3

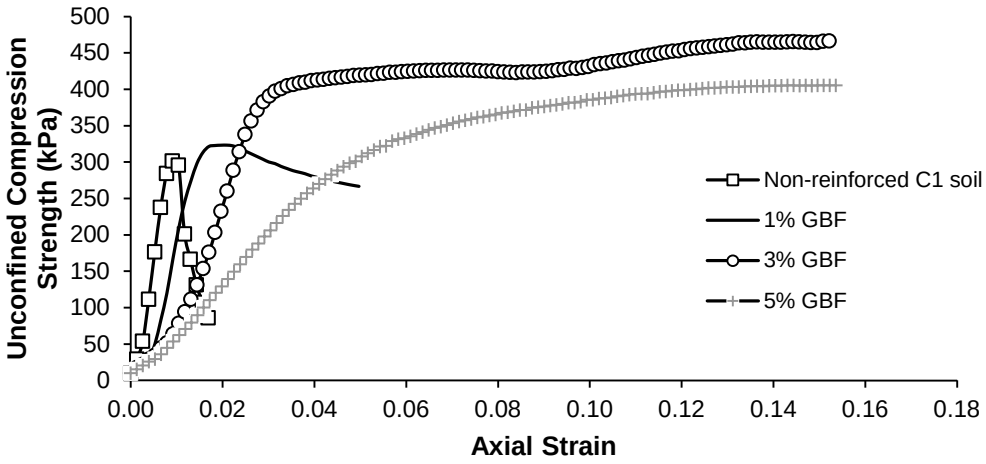

Figure 5.5 Stress-strain behaviour of GBF fibre reinforced C1 soil specimens compacted at dry unit weight of 17.8 kN/m^3

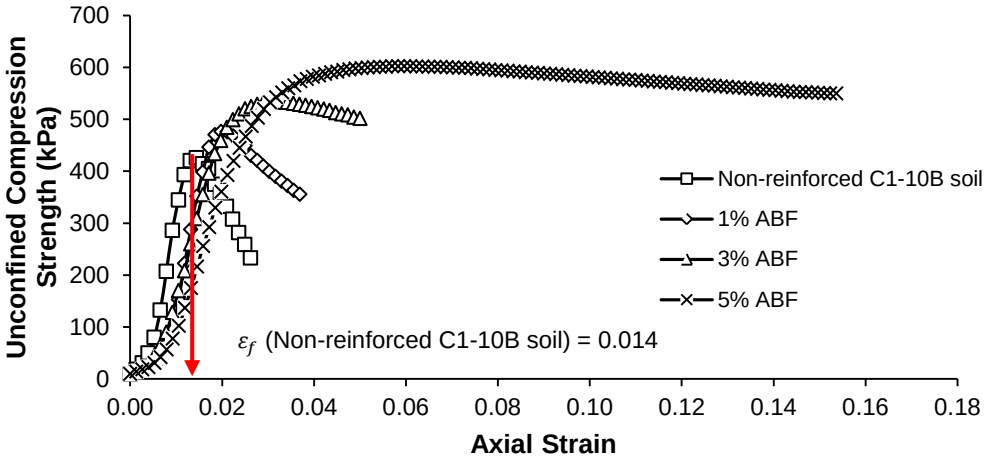

Figure 5.6 Stress-strain behaviour of ABF fibre reinforced C1-10B soil specimens compacted at dry unit weight of 17.8 kN/m^3

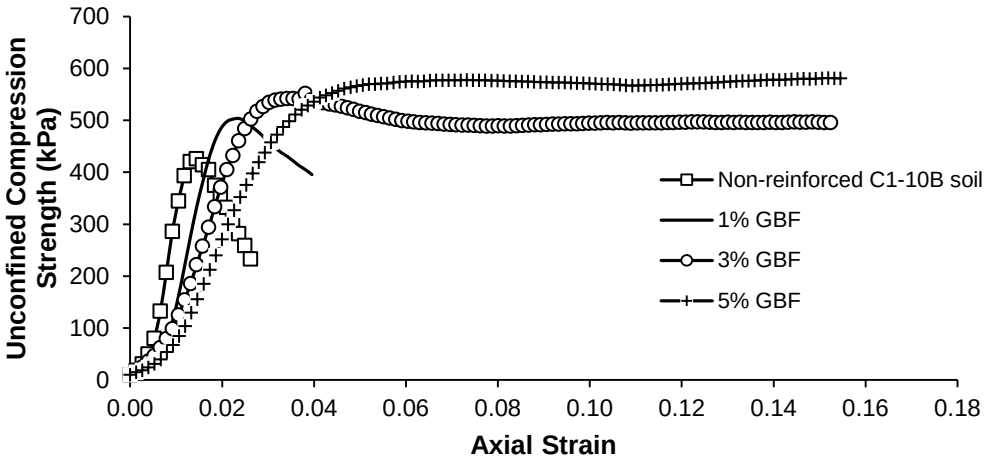

Figure 5.7 Stress-strain behaviour of GBF fibre reinforced C1-10B soil specimens compacted at dry unit weight of 17.8 kN/m^3

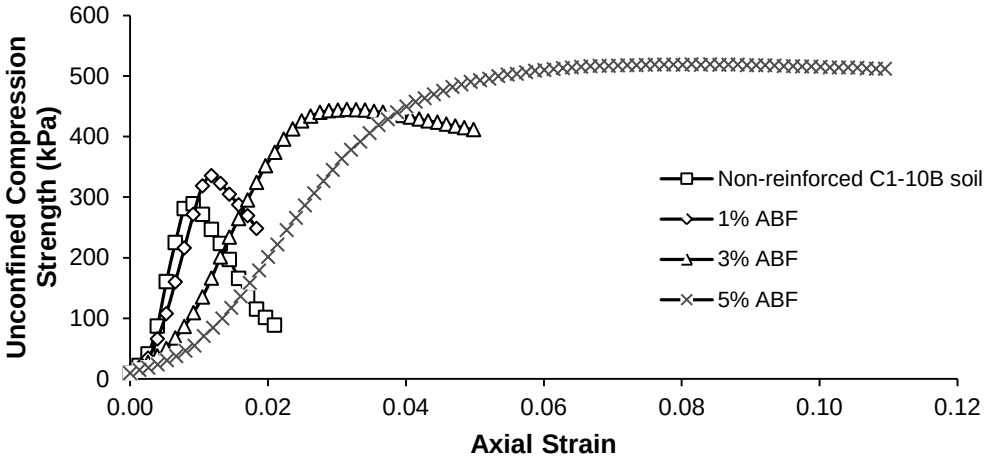

Figure 5.8 Stress-strain behaviour of ABF fibre reinforced C1-10B soil specimens compacted at dry unit weight of 17.2 kN/m^3

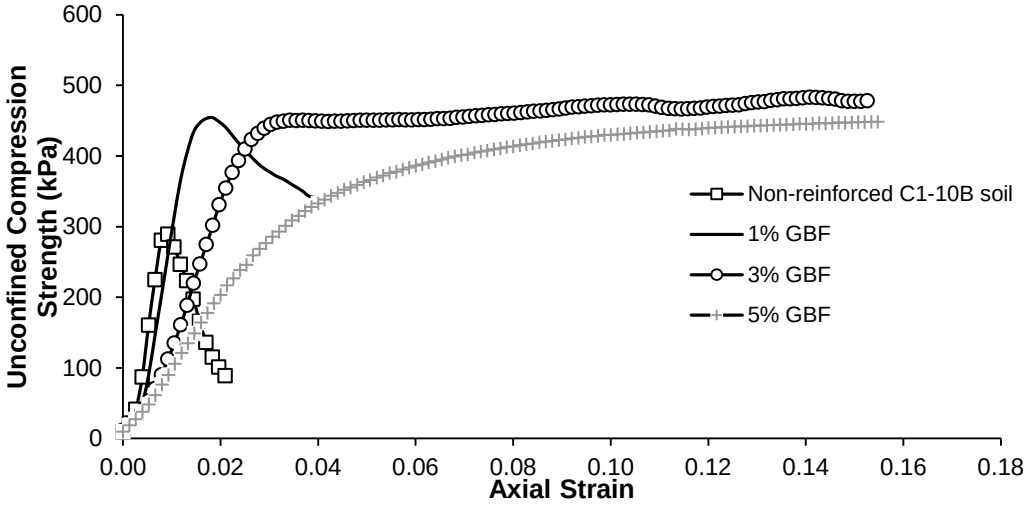

Figure 5.9 Stress-strain behaviour of GBF fibre reinforced C1-10B soil specimens compacted at dry unit weight of 17.2 kN/m^3

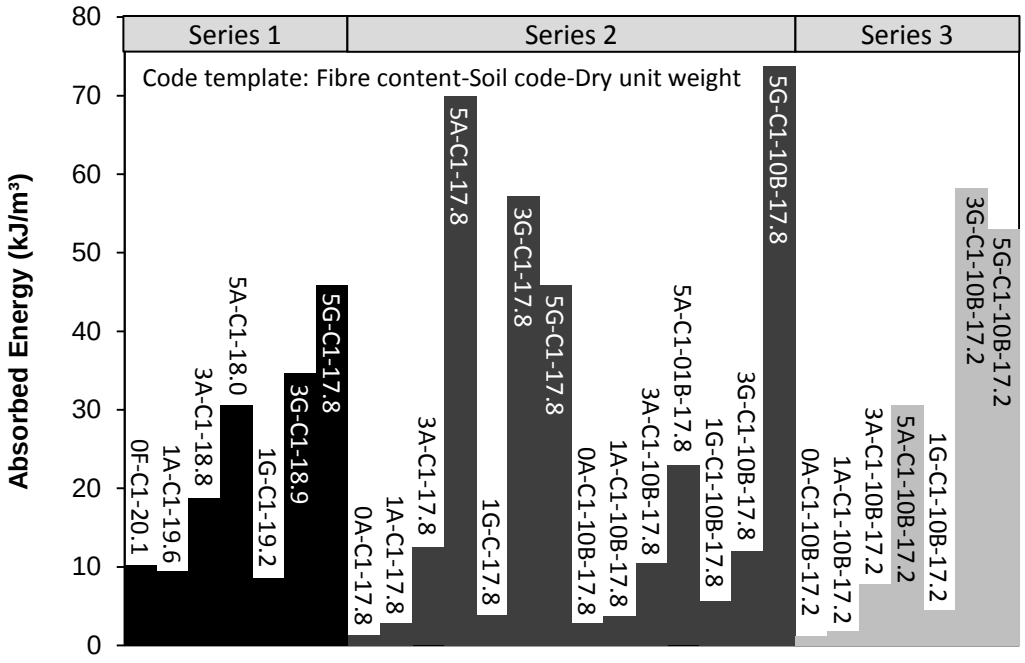

Figure 5.10 Energy absorption capacities of C1 and C1-10B soil specimens

As shown in Figure 5.10, C1-10B soil specimens induced more absorbed energy compared to C1 soil specimens. This might be attributed to higher plastic behaviour of C1-10B soil which resulted in more intertwining with fibres during compression.

According to Figure 5.10, in the first series, there was slight reduction in absorbed energy of specimens composed of 1% ABF fibre and 1% GBF fibre compared to that of non-reinforced C1 soil specimen. All these three specimens were prepared at the same moisture content and therefore, reduction in dry unit weight due to fibre addition resulted in lower absorbed energy.

5.4.2 Peak strength

Figure 5.11 shows peak unconfined compression strength of non-reinforced and fibre reinforced C1 soil specimens compacted at their respective maximum dry unit weights and optimum moisture contents (series 1). As shown in Figure 5.11, adding 1% ABF fibre to C1 soil would result in insignificant change in its UCS (i.e. almost 2% reduction).

There was a small difference between maximum dry unit weights of the non-reinforced C1 soil specimen (i.e. 20.1 kN/m^3) and 1% ABF fibre reinforced soil specimen (i.e. 19.6 kN/m^3) whilst their optimum moisture contents were the same (i.e. 11%). Therefore, the observed minor reduction of in UCS of 1% ABF fibre reinforced C1 soil specimen could be related to slight reduction in its dry unit weight compared to that of non-reinforced C1 soil specimen. This also confirmed that at the same moisture content, reduction in the specimen's dry unit weight would lead to decrease in unconfined compression strength. With further increase in ABF fibre content, the UCS value decreased significantly due to significant drop in the maximum dry unit weight as well as due to the increase in optimum moisture content.

Increase in GBF fibre content also led to decrease in UCS value due to decreased dry unit weight. At fibre content of 5%, a rise in UCS value was observed. Although the observed increase in UCS was still below that of non-reinforced C1 soil specimen, there was 35% incremental increase compared to that of 3% GBF fibre reinforced C1 soil. The incurred enhancement could be explained due to enhanced probability of intersecting developing shearing planes by fibres due to increase in their quantity.

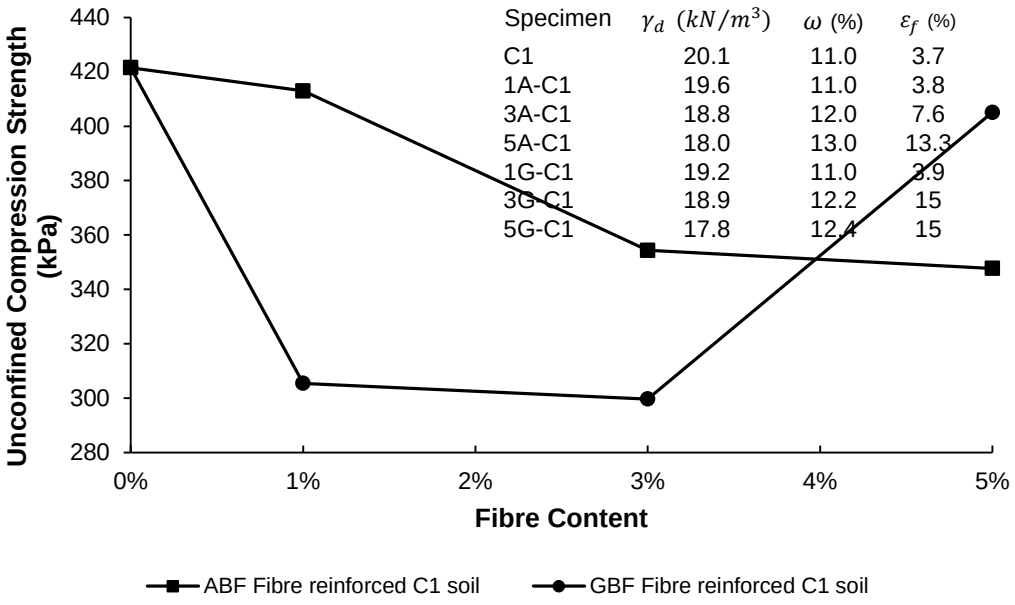

Figure 5.11 Peak compression strength of C1 soil specimens prepared at maximum dry unit weight and optimum moisture content

The variation in peak unconfined compression strength obtained from the second series of testing programme has been shown in Figure 5.12 and Figure 5.13. As can be seen in Figure 5.12, there was a continuous increase in UCS value of fibre reinforced C1 soil specimens with increase in ABF fibre content. UCS value of C1 soil reinforced with 5% ABF fibre content was just over twice that of non-reinforced C1 soil. A similar rate of enhancement was observed for C1-10B soil reinforced with increased ABF fibre content. The observed increase in UCS value of fibre reinforced soil due to increase in fibre content could be attributed to; (i) increased number of fibres intersecting failure zone, (ii) tensile strength of fibres, which adds benefit to the resulting strength and (iii) better interlocking and intertwining of fibres with clay soil particles.

The observed difference between behaviour of C1-10B soil and C1 soil reinforced with 3% and 5% ABF fibre content as well as 5% GBF fibre content could be because of:

a) Over compaction of C1-10B soil specimens at higher dry unit weight (i.e. 17.8 kN/m^3) than their corresponding maximum dry unit weight from compaction data for specimens containing 3% and 5% ABF fibre as well as 5% GBF fibre.

b) Inconsistency between dry unit weight value of 17.8 kN/m^3 and predicted moisture content of C1-10B soil specimens regardless of compaction curve for fibre reinforced C1-10B specimens

As shown in Figure 5.13, GBF fibre reinforced soil specimens showed different behaviour upon increasing fibre content. UCS value of GBF fibre reinforced C1 soil specimen with 3% fibre content increased by almost 54%, followed by 20% reduction at 5% fibre content compared to that of 3% fibre content.

Although UCS value of reinforced C1 soil with 5% GBF fibre content was less than that of 3% fibre content, its UCS value was still 34% more than UCS value of non-reinforced C1 soil. GBF fibre reinforced C1-10B soil specimens showed continuous increase in UCS value with increase in fibre content.

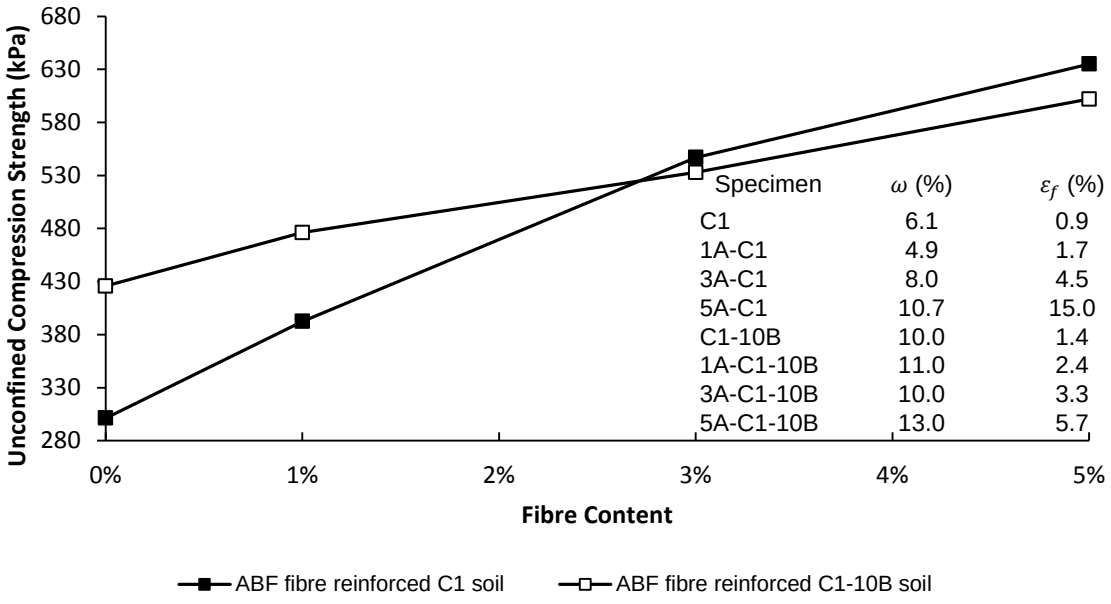

Figure 5.12 Peak compression strength of ABF fibre reinforced C1 and C1-10B soil specimens prepared at dry unit weight of 17.8 kN/m^3

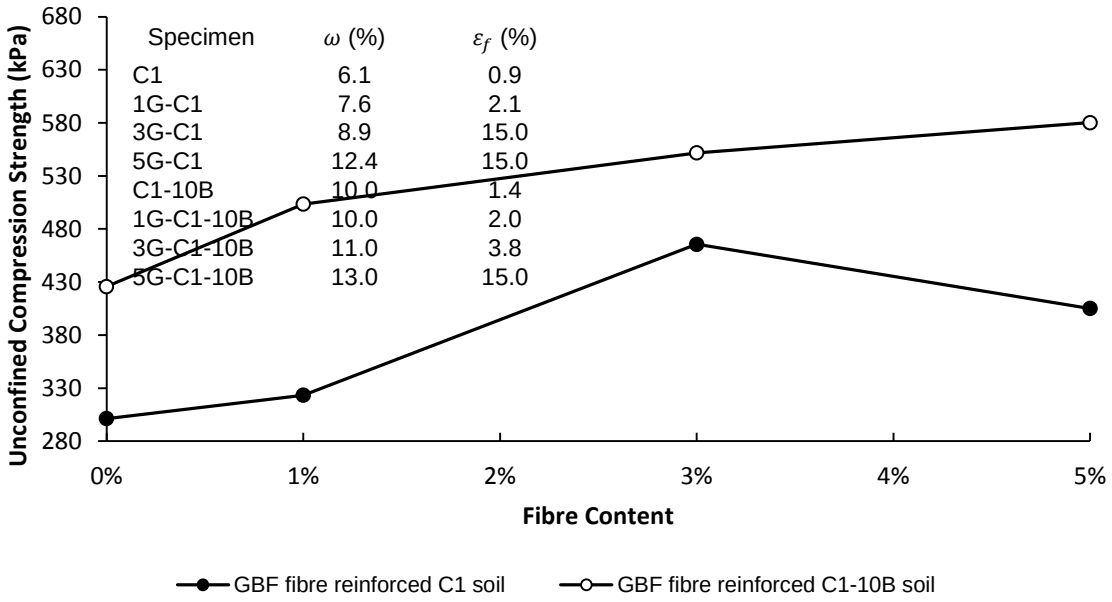

Figure 5.13 Compression strength of GBF fibre reinforced C1 and C1-10B soil specimens prepared at dry unit weight of 17.8 kN/m^3

In the second series of the testing programme, ABF fibre reinforced C1-10B soil specimens with 3% and 5% fibre content and GBF fibre reinforced C1-10B soil specimen with 5% fibre content were compacted at higher dry unit weight than their respective maximum dry unit weight. Moreover, moisture contents of these specimens were not chosen according to their compaction curves. In fact, addition of waste carpet fibres might have a detrimental effect on UCS if the dry unit weight is set to increase above the maximum achievable one from a compaction test.

Therefore, because of arisen dry unit weight-moisture content inconsistency, the revealed trend of UCS values of ABF fibre reinforced C1-10B soil specimens (with 3% and 5% fibre content) and 5% GBF fibre reinforced C1-10B soil specimen was not similar to that of fibre reinforced C1 soil specimens.

Thus, third series of testing experiment was set up to evaluate the UCS of ABF/GBF fibre reinforced C1-10B soil specimens compacted at dry unit weight and moisture content extracted from their respective compaction curves.

Figure 5.14 shows peak unconfined compression strength of C1-10B soil specimens prepared at a dry unit weight of 17.2 kN/m^3. ABF fibre reinforced C1-10B soil specimens showed continuous increase in UCS value upon increasing fibre content. This was the same behaviour as was seen for ABF fibre reinforced

C1 soil and C1-10B soil at dry unit weight of 17.8 kN/m^3. The maximum increase in UCS value was 79% belonging to reinforced C1-10B soil specimen with 5% ABF fibre. Fibre reinforced C1-10B soil specimen with 3% GBF fibre content showed an increase of 94% in UCS value followed by 20% reduction at 5% fibre content compared to that of 3% fibre content. However, it was still 55% higher than UCS value of the pure C1-10B soil specimen.

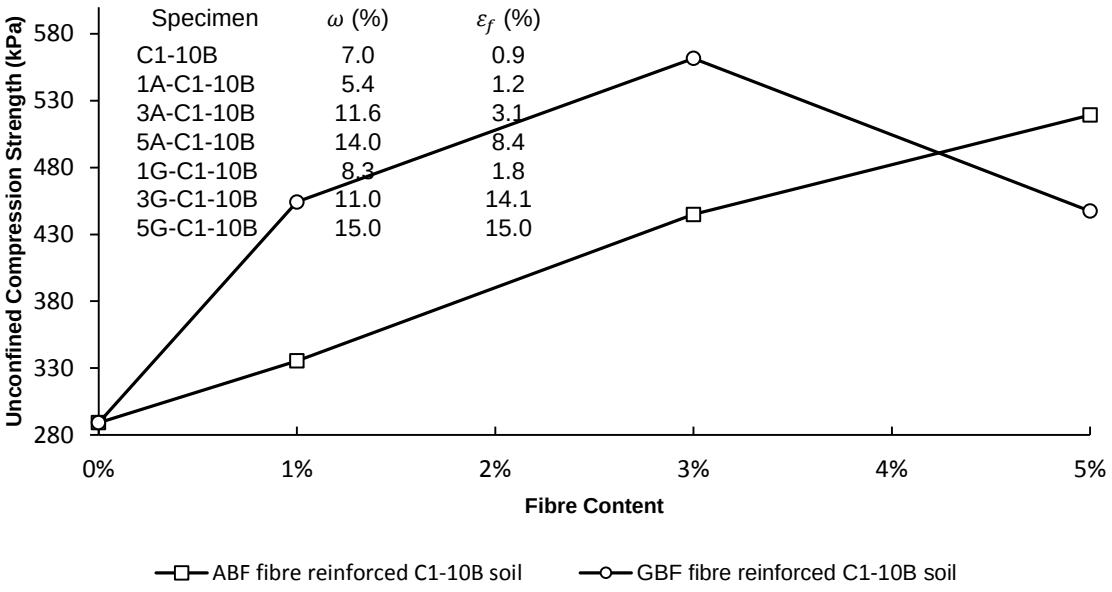

Figure 5.14 Peak compression strength of C1-10B soil specimens prepared at dry unit weight of 17.2 kN/m^3

Behaviour of the fibre reinforced soil is highly susceptible to the change in dry unit weight and/or moisture content conditions. Therefore, the fourth series of UCS experiments was carried out to elucidate the influence of change in dry unit weight on UCS of fibre reinforced soil specimens prepared at constant fibre content and moisture content. Furthermore, the results of these tests explained the influence of increased fibre content on UCS of specimens prepared at the same dry unit weight and moisture content. Figure 5.15 shows the results of the fourth series of UCS experiments on ABF fibre reinforced C1 soil specimens prepared at 12% moisture content and different dry unit weights of 15.8, 16.8, 17.8, and 18.8 kN/m^3**.**

Figure 5.15 shows that at the same moisture content and fibre content increase in dry unit weight of fibre reinforced soil resulted in significant increase in UCS. The data shown in this figure also confirmed that increase in fibre content in specimens

prepared at the same dry unit weight and water content resulted in increase in UCS. The improving effect of fibres on UCS enhanced with increase in dry unit weight.

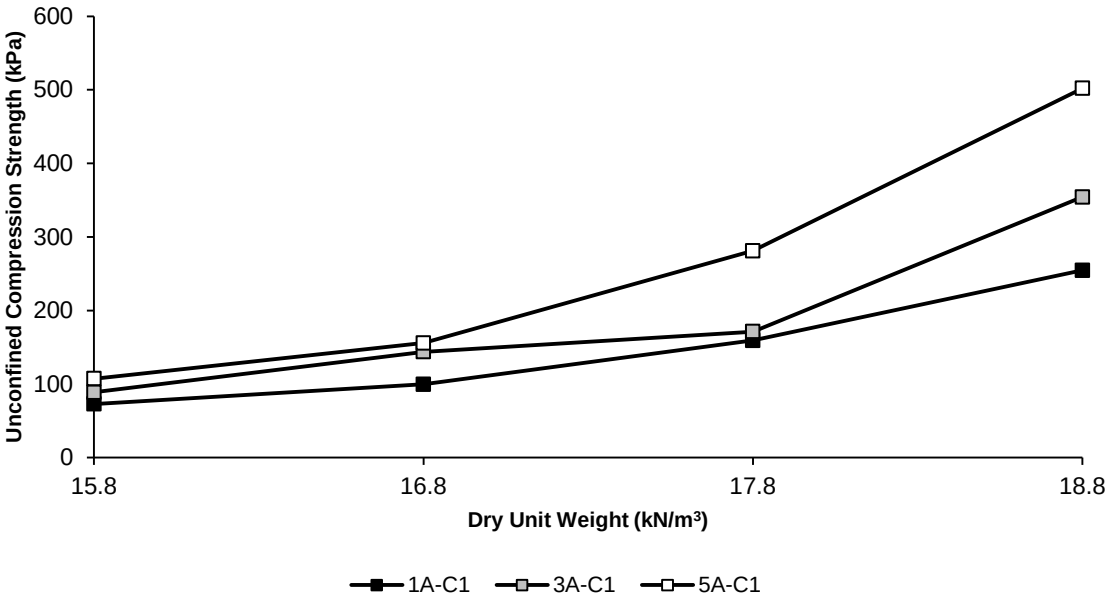

Figure 5.15 Influence of dry unit weight on UCS of fibre reinforced C1 soil specimens prepared at 12% moisture content

Figure 5.16 demonstrates the coupling effect of fibre content and dry unit weight on UCS of ABF fibre reinforced soil specimens (series 4) prepared at the same moisture content (i.e. 12%). It can be clearly seen in Figure 5.16 that, although individual increase in dry unit weight or fibre content resulted in increase in UCS of fibre reinforced soil, the coupling increase of these elements together led to a substantial increase in UCS of reinforced soil.

The improving effect of fibres on UCS of reinforced soils can be further supported by comparing data shown in Figure 5.11 to Figure 5.13. This revealed that UCS value of non-reinforced C1 soil specimen compacted at maximum dry unit weight (i.e. 20 kN/m^3) was 1.3 times that of compacted soil at dry unit weight of 17.8 kN/m^3**.** However, fibre reinforced C1 soil specimens compacted at dry unit weight of 17.8 kN/m^3 showed considerably more peak strength than the non-reinforced specimen prepared at maximum dry unit weight. This was also another indication of improving effect of fibres to enhance the UCS of clay soils.

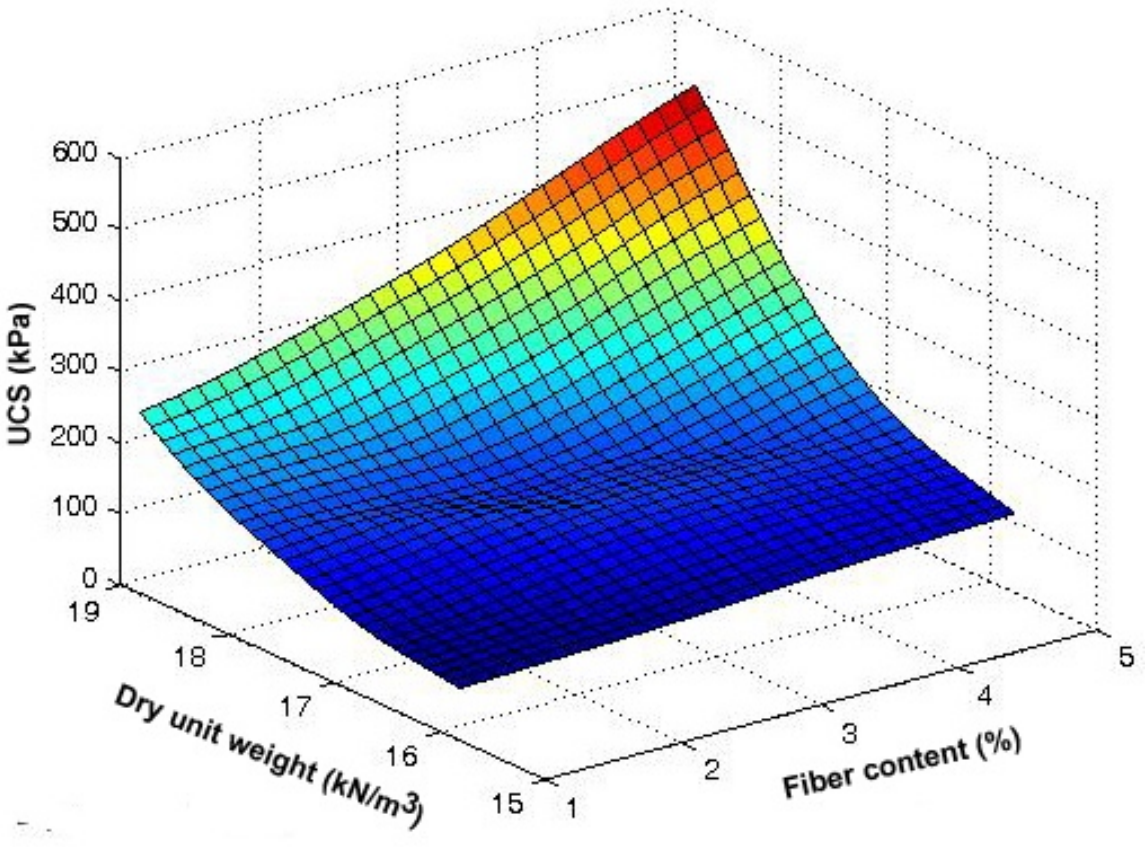

Figure 5.16 Coupling effects of fibre content and dry unit weight on UCS of ABF fibre reinforced specimens prepared at 12% moisture content

To evaluate the combined influence of changing dry unit weight and moisture content on UCS of specimens prepared at the same fibre content, the fifth series of UCS experiments were carried out on the reinforced specimens with 3% ABF fibre at dry unit weights of 15.8, 16.8, 17.8 and 18.8 kN/m^3 and moisture contents of 7%, 8%, 10% and 12% respectively. Figure 5.17 shows that the UCS value of fibre reinforced specimens increased with increase in both dry unit weight and moisture content.

To evaluate the effect of moisture content on UCS of reinforced specimens, further tests were carried out on specimens prepared at the same dry unit weight and fibre content with different moisture contents. Details of tested specimens and resulted UCS values have been shown in Table 5.4. Comparing results in Table 5.4 and previous data (Figure 5.12 and Figure 5.13) showed that at the same dry unit weight and fibre content, increase in moisture content resulted in significant reduction in UCS and increase in failure strain. However, according to the data

shown in Figure 5.17 it can be concluded that for the tested range of dry unit weights and moisture contents, the impact of dry unit weight on UCS of fibre reinforced specimens dominated the influence of moisture content.

To prove repeatability of the results mentioned in this study, few tests were repeated. Results of replicate test specimens showed maximum difference of ±12% from presented values. The occurred difference could be related to the fact that fibres were distributed in a random fashion in different specimens. However, based on the results of tests carried out on both C1 soil and C1-10B soil, they showed rather the same trend as fibre content was increased. This was indicative of reliability of the results considering that C1 and C1-10B soils had the same origin but different plasticity indices.

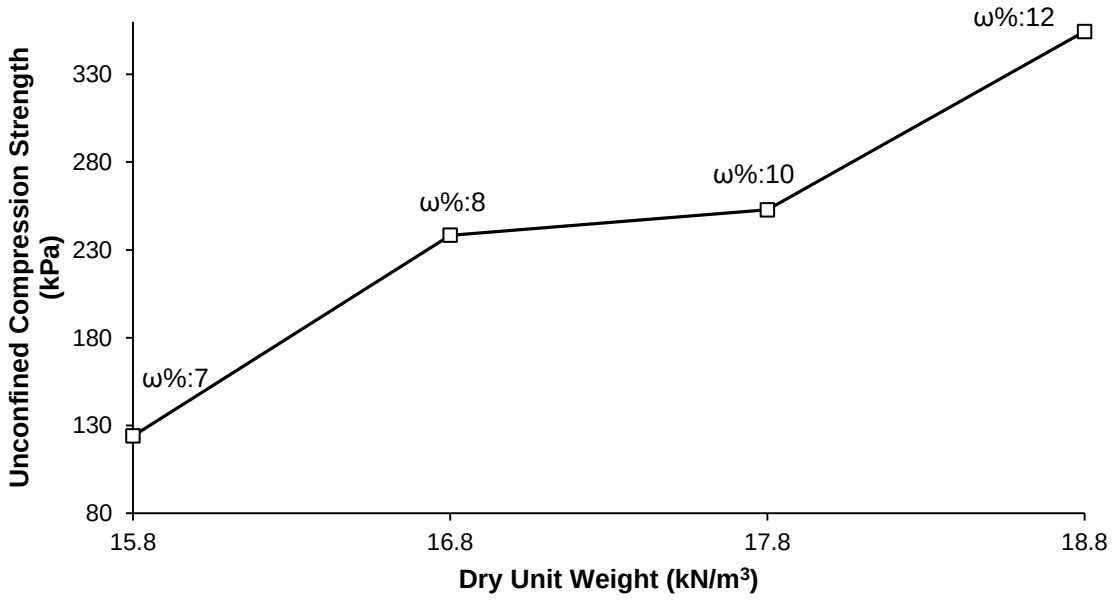

Figure 5.17 Combined effect of increase in both dry unit weight and moisture content on UCS of ABF fibre reinforced specimens with 3% fibre content

Table 5.4 Unconfined compression strengths of specimens at same dry unit weight of 17.8 kN/m^3 and different moisture contents

Specimen	Moisture content (%)	UCS (kPa)	Failure strain (%)
3A-C1	8.0	546.9	4.5
3A-C1	10.0	252.9	5.2
1G-C1	7.6	323.3	2.1
1G-C1	10.0	226.5	3.2
3G-C1	8.9	465.6	15.0
3G-C1	10.0	373.9	15.0
5A-C1-10B	13.0	601.9	5.7
5A-C1-10B	15.0	463.7	8.8
5G-C1-10B	13.0	580.3	15.0
5G-C1-10B	15.0	383.3	15.0

5.4.3 Failure Patterns

Figure 5.18 and Figure 5.19 show the failure patterns of C1 and C1-10B soil specimens compacted at dry unit weight of 17.8 kN/m^3. For some specimens, the depicted illustration is pertained to the shape of specimen at post peak failure (more than 15% of axial strain). Numbers below each picture indicates failure strain at which evidence was recorded. As it is shown in Figure 5.18(a) and Figure 5.18 (e), for non-reinforced C1 and C1-10B soil specimens, failure occurred at very small strain values and a major single vertical crack appeared throughout the entire specimens indicating a very brittle behaviour. Increasing ABF/GBF fibre content in both C1 and C1-10B soil specimens resulted in appearance of enormous amount of tiny cracks with no obvious single domination of shear failure plane as shown in Figure 5.18 (b) to Figure 5.18 (d) and Figure 5.19 (b) to Figure 5.19 (d).

With increase in fibre content, particularly to 5%, gradual increase in strain during compression, led to occurrence of a network of tiny cracks forming into progressive failure zones with barrel failure shape.

Therefore, the shape of failure of non-reinforced soil specimens was steep shear planes whereas with the addition of fibres, dominated shear failure planes were not evident. In higher fibre content specimens, due to abundant presence of fibres, they confined the soil particles and increased the global stability of the soil mass. Therefore, fibres could tolerate the influence of sudden displacement behaviour of soil particles (brittle behaviour) under axial load to that of a more gradual

deformation (ductile behaviour). Hence, soil specimen bulged laterally and reshaped to a barrel form.

Comparing Figure 5.18 and Figure 5.19 and considering failure strains depicted in Figure 5.12 to Figure 5.14 denoted that GBF fibre reinforced specimens failed at relatively higher strain values compared to corresponding ABF fibre reinforced specimens denoting more ductility.

The failure of all specimens happened at the lower part. This shows the non-uniformity of the dry unit weight at the height of the specimen by static compaction method in one layer (Murray et al., 2000). Therefore, specimens cracked from the lower part due to lower dry unit weight at bottom of the specimens. The uniformity of dry unit weight over height of the specimen can be improved significantly by increasing the number of layers in specimen preparation method (Saad et al., 2012).

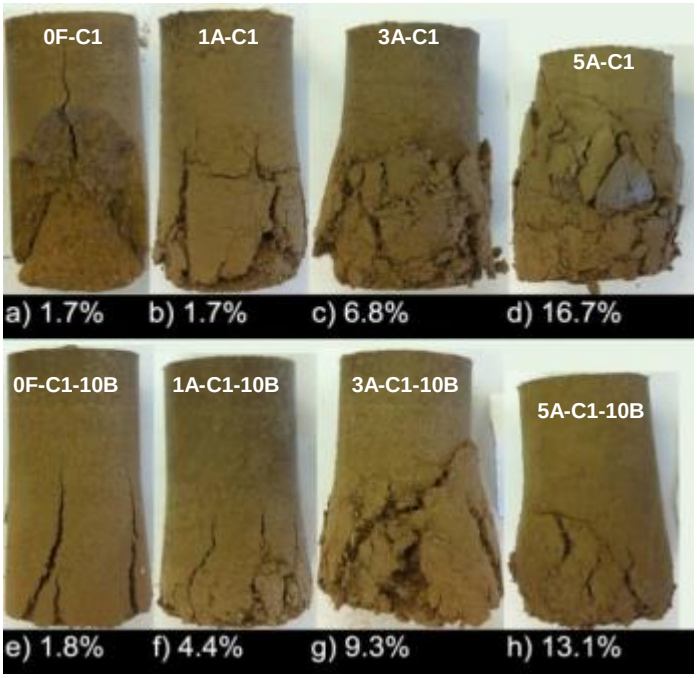

Figure 5.18 Failure pattern of ABF fibre reinforced C1 and C1-10B specimens compacted at dry unit weight of 17.8 kN/m^3

Note: Numbers shown in the picture, denote the strain value at which pictures have been taken

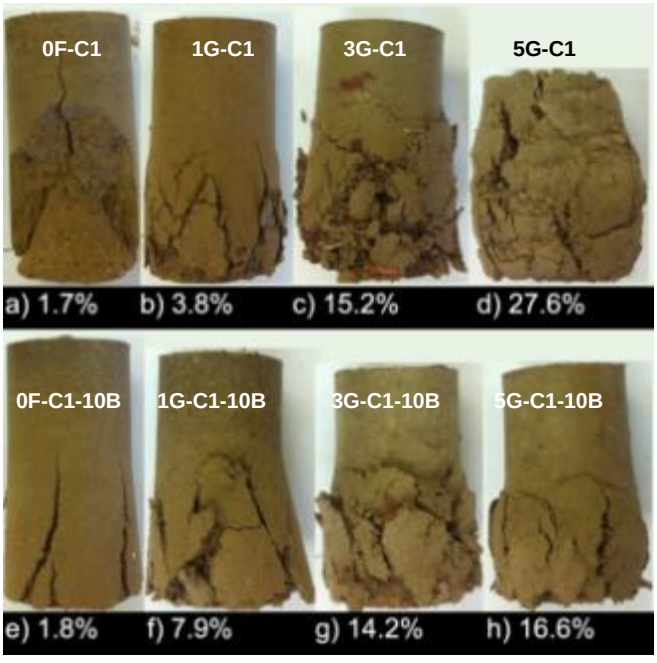

Figure 5.19 Failure pattern of GBF fibre reinforced C1 and C1-10B specimens compacted at dry unit weight of 17.8 kN/m^3

Note: Numbers shown in the picture, denote the strain value at which pictures have been taken

5.5 Discussion on the results of swelling pressure tests

Figure 5.20 shows the results of first series of swelling pressure tests in which all specimens were compacted at their maximum dry unit weights and optimum moisture contents.

Table 5.5 summarises the dry unit weights, moisture contents and attained swelling pressure from all tests in series one. The results indicated that swelling pressure reduced significantly with increased fibre content.

Continuous loss in the swelling pressure could be observed with the increase in ABF fibre content. However, adding 1% of GBF fibre was efficient in reducing a relatively large percentage of the swelling pressure. Any further addition of GBF fibres showed less mitigation.

Adding 5% ABF fibre resulted in 63% reduction in the swelling pressure of C1 soil which was not far from the 67% reduction when 5% of GBF fibre was added. These results are in good agreement with those obtained earlier by Al-Akhras et al. (2008) and Viswanadham et al. (2009) based on the use of different types of fibre. Their results were obtained from specimens prepared at 95% of maximum dry unit weight and 3% below the optimum moisture content of the non-reinforced soils. It should be noted that compacting the soil specimens to their respective maximum dry unit weights and optimum moisture contents means that with the increase in fibre content, specimens are prepared at a lower dry unit weight and higher water content. Simultaneous change of the dry unit weight and moisture content might have an interacting effect which prevents fair comparison.

In the second series of the testing programme, all specimens of C1 and C1-10B soil specimens were compacted to the same dry unit weights of 17.8 kN/m^3 and 17.2 kN/m^3 respectively. These values were obtained for C1 and C1-10B soil specimens with 5% GBF fibre content which were less than the maximum dry unit weight for most mixes. Figure 5.21, Figure 5.22 and Table 5.6 show the swelling pressure results of second series. It is clear from Figure 5.21 that adding 1% ABF fibre led to 21% and 19% reduction in swelling pressure of C1 and C1-10B soil specimens respectively. However, with further increase in ABF fibre content to 3%,

C1 soil and C1-10B soil specimens exhibited a significant increase in the swelling pressure. GBF fibre reinforced specimens experienced an increase in the value of the swelling pressure with increasing fibre content from 1% to 3% irrespective of the soil type. Based on the presented data, the peak swelling pressure of ABF and GBF fibre reinforced specimens was observed at 3% fibre content.

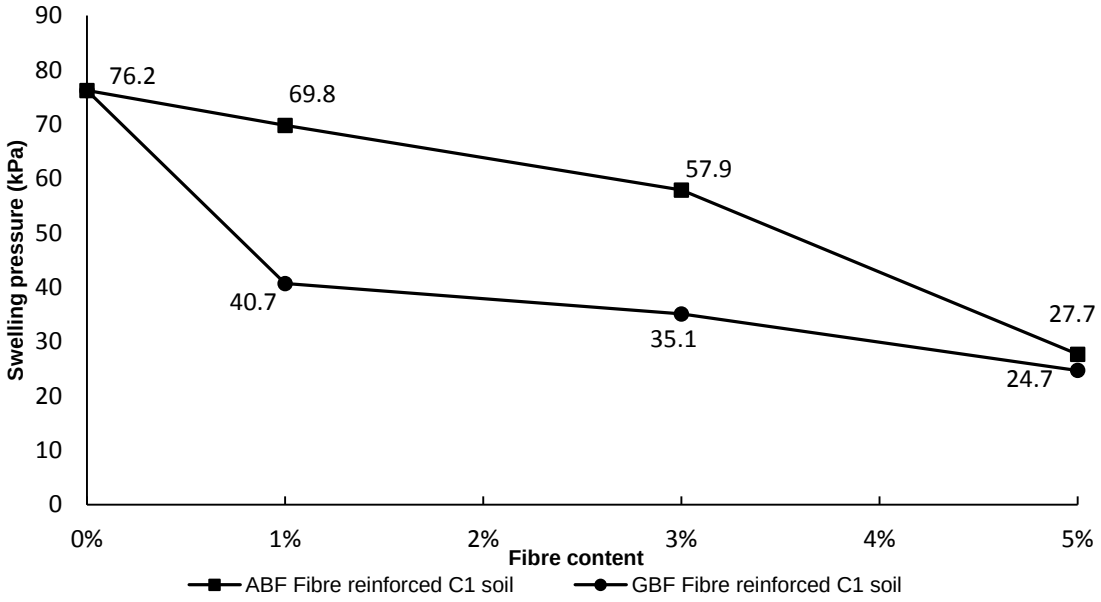

Figure 5.20 Swelling pressure of C1 soil specimens (series I)

Table 5.5 Swelling pressure of C1 soil specimens (series I)

Specimen	MDU (kN/m^3)	OMC (%)	Swelling pressure (kPa)
C1	20.1	11.0	76.2
1A-C1	19.6	11.0	69.8
3A-C1	18.8	12.0	57.9
5A-C1	18.0	13.0	27.7
1G-C1	19.2	11.0	40.7
3G-C1	18.9	12.2	35.1
5G-C1	17.8	12.4	24.7

MDU: Maximum dry unit weight
OMC: Optimum moisture content

Table 5.6 Swelling pressure of C1 soil and C1-10B soil specimens (series II)

Specimen	Dry unit weight (kN/m^3)	Moisture content (%)	Swelling pressure (kPa)
C1	17.8	6.1	26.7
1A-C1	17.8	4.9	21.1
3A-C1	17.8	8.0	47.4
5A-C1	17.8	10.7	36.6
1G-C1	17.8	7.6	34.5
3G-C1	17.8	8.9	44.9
5G-C1	17.8	12.4	24.7
C1-10B	17.2	7.0	47.8
1A-C1-10B	17.2	5.4	38.5
3A-C1-10B	17.2	11.6	89.1
5A-C1-10B	17.2	14.0	81.6
1G-C1-10B	17.2	8.3	64.9
3G-C1-10B	17.2	11.0	87.5
5G-C1-10B	17.2	15.0	72.5

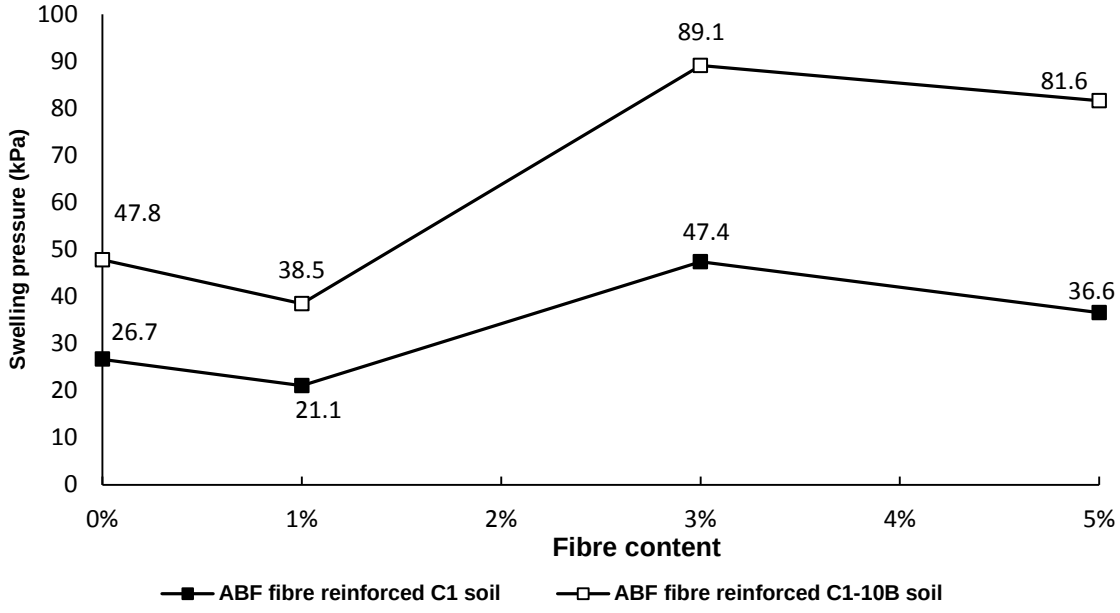

Figure 5.21 Swelling pressure of ABF fibre reinforced C1 and C1-10B soil specimens (series II)

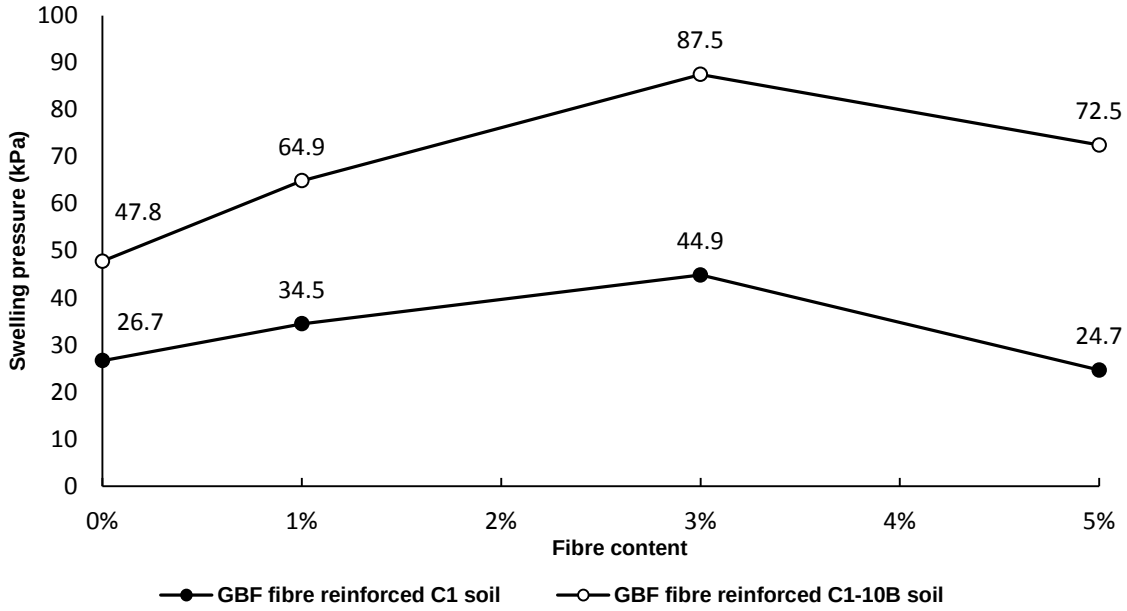

Figure 5.22 Swelling pressure of GBF fibre reinforced C1 and C1-10B soil specimens (series II)

Comparing the results of series I and series II clearly demonstrated that there was a large influence for the initial dry unit weight and moisture content on the subsequent swelling behaviour of fibre reinforced soils. Therefore, in series III, specimens with various combinations of dry unit weights and moisture contents were tested independently for better understanding of individual influences of dry unit weight and moisture content on obtained swelling pressure. The results of series III testing programme are shown in Figure 5.23. Data for the dry unit weight, moisture content and achieved swelling pressure are presented in Table 5.7.

In series III, the influence of changing dry unit weight at constant moisture content, change in moisture content at constant dry unit weight and changing both dry unit weight and moisture content on swelling pressure of fibre reinforced soil specimen with 3% ABF fibre content have been investigated.

Figure 5.23 (a) shows that increasing moisture content of C1 soil specimens that were reinforced with 3% of ABF fibre content and prepared at the same dry unit weight led to significant reduction in the attained swelling pressure. However, provided the dry unit weight increases, the value of the obtained swelling pressure becomes higher, as shown in Figure 5.23 (b). In general, Simultaneous increase in the dry unit weight and moisture content of fibre reinforced soil specimens (within the tested range) resulted in increase in the measured swelling pressure

(see Table 5.6). This may show that for the tested range of dry unit weights and moisture contents, the impact of initial dry unit weight on swelling pressure of fibre reinforced soils overrides the impact of change in the moisture content.

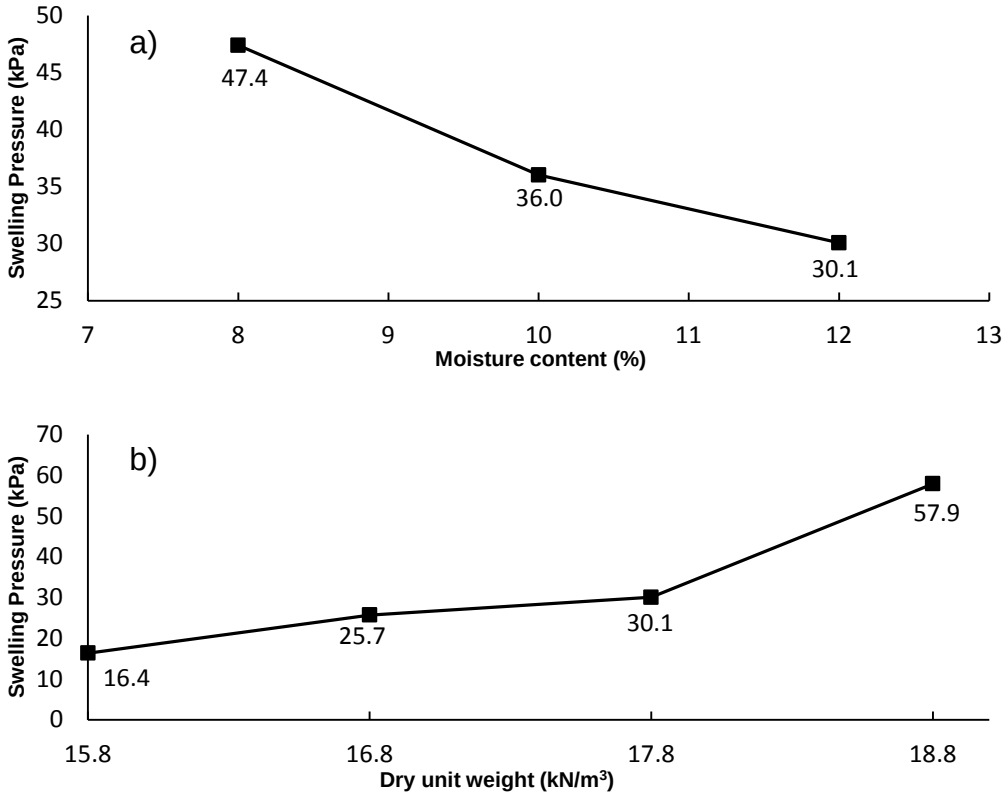

Figure 5.23 Swelling pressure of C1 soil with 3% ABF fibre content (series III) a) at constant dry unit weight of 17.8 kN/m^3 b) at constant moisture content of 12%

Table 5.7 Swelling pressure test results of series III

Specimen	Dry unit weight (kN/m^3)	Moisture content (%)	Swelling pressure (kPa)
3A-C1	15.8	12.0	16.4
3A-C1	16.8	12.0	25.7
3A-C1	17.8	12.0	30.1
3A-C1	18.8	12.0	57.9
3A-C1	17.8	8.0	47.4
3A-C1	17.8	10.0	36.0
3A-C1	17.8	12.0	30.1
3A-C1	15.8	7.0	12.6
3A-C1	16.8	8.0	16.2
3A-C1	17.8	10.0	36.0
3A-C1	18.8	12.0	57.9
3A-C1-10B	17.2	11.6	89.1
3A-C1-10B	17.2	15.0	77.5
3G-C1-10B	17.2	11.0	91.0
3G-C1-10B	17.2	14.5	87.9

5.5.1 Fibre content distribution

Careful observations made during specimen preparation might give an insight into the influence of the changing moisture content or dry unit weight on the swelling behaviour. Visual observations indicated that at low moisture contents, due to the lack of water in the soil/fibre mix, there may not be an effective and uniform entanglement between soil particles and fibres and this is worsened by increasing the fibre content. Therefore, in lack of enough moisture in the soil specimen fibres can tangle together and form fibre pockets that are surrounded by solid particles (Figure 5.24). In this case, the localised fibre pockets can behave like springs.

In addition, the reduced interaction between fibres and solid soil particles would mean an increase in the value of swelling pressure. With the increase in moisture content, better entanglement and interaction between fibres and soil particles are achieved since the possibility for forming fibre pockets is lessened.

It was observed that less fibre pockets are formed on specimens with GBF fibre which are described as long and thick fibres compared to short and thin ABF fibres.

To assess the distribution of fibres within the prepared specimens and to evaluate the efficiency of fibre/soil mixing method, a few specimens which were prepared for swelling pressure test were dried and cut in two equal sections. In order for the percentage of the fibres to be determined, each half of the specimen was dried, crushed and subsequently the fibre mass was measured by washing using a series of sieves.

Figure 5.25 shows a plot for the measured fibre content against expected amount. Reasonable fibre content distribution for GBF fibres was achieved. However, ABF fibre distribution was not consistent throughout the prepared specimens. This was a clear indication of concentration of the fibres in the other part of the specimen.

This might cause loss of accuracy. Therefore, it was decided to repeat several tests in order to increase the accuracy of the assessment procedure. The maximum difference between the measured swelling pressures was found to be 9%. Considering the nature and characteristics of the used fibres, this difference seemed acceptable.

Formation of fibre pockets at low moisture contents

Distribution of fibres at higher moisture content

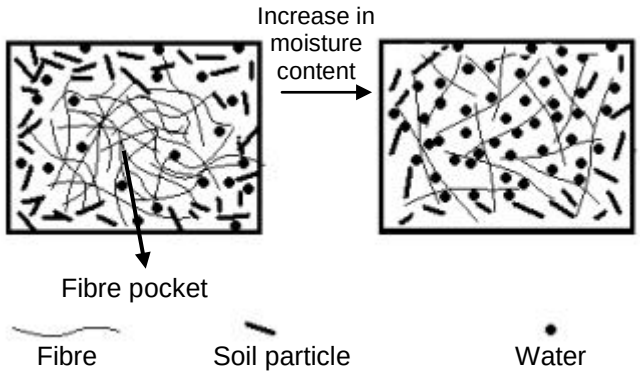

Figure 5.24 Observed formations of fibre pockets as a function of moisture content

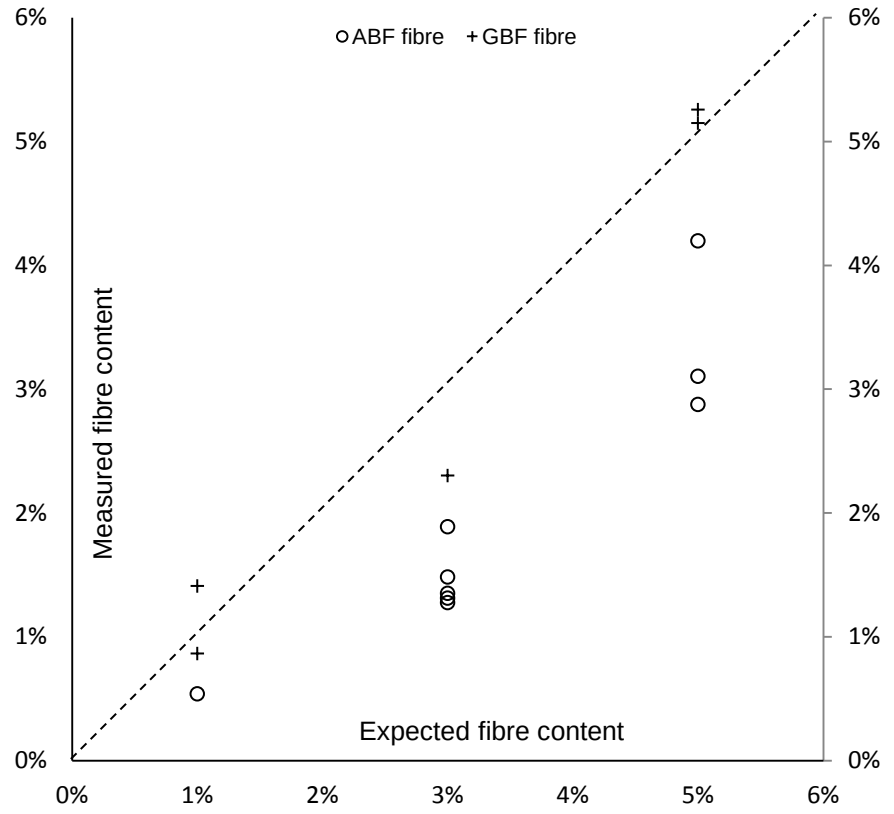

Figure 5.25 Fibre content in half section of swelling pressure test specimens

5.6 Discussion on the results of one-dimensional consolidation tests

A series of one-dimensional consolidation tests were carried out on non-reinforced and GBF fibre reinforced C2, C2-10B and C2-20B soil specimens. All these specimens were prepared at their respective maximum dry unit weights and optimum moisture contents. Results of one-dimensional consolidation tests were analysed by comparing changes in void ratio against applied stresses. Figure 5.26 shows the change in void ratio of C2, C2-10B and C2-20B under applied loading/unloading stresses.

For all one-dimensional consolidation tests, applied stress was doubled at periods of 24 hours unless swelling was observed. For C2, C2-10B and C2-20B soils, some swelling was observed at low stress levels. Once swelling was observed, stress was doubled to the next level. For these soils swelling was observed to cease at stress levels of 100 kPa, 200 kPa and 200 kPa respectively. For stress

levels below these values, void ratio was calculated based on the deformation of specimen before swelling.

For calculating void ratio values, it was assumed that the specimen was fully saturated at the last stage of the test. Therefore, final moisture content of specimen was used to calculate the final void ratio. Void ratio values at the end of other loading stages were calculated using backward method.

Compared to non-reinforced soil specimens, fibre reinforced soil specimens revealed more void ratio changes under applied stresses. This was due to the increased void ratio of the fibre reinforced soil specimens. Moreover, increased fibre content resulted in reduction in maximum dry unit weight at which the specimens were prepared. Therefore, specimens with lower dry unit weight with increased fibre content when subjected to axial load, showed higher compression and hence higher change in void ratio. This was intensified with increase in bentonite content for C2-10B and C2-20B soil specimens. Fibre reinforced C2, C2-10B and C2-20B soil specimens with 5% fibre content, showed the highest void ratio at all stress levels.

As it appears from Figure 5.26, with increase in bentonite content, void ratio of non-reinforced and fibre reinforced C2-10B and C2-20B soil specimens at 1600 kPa axial stress eventually converged.

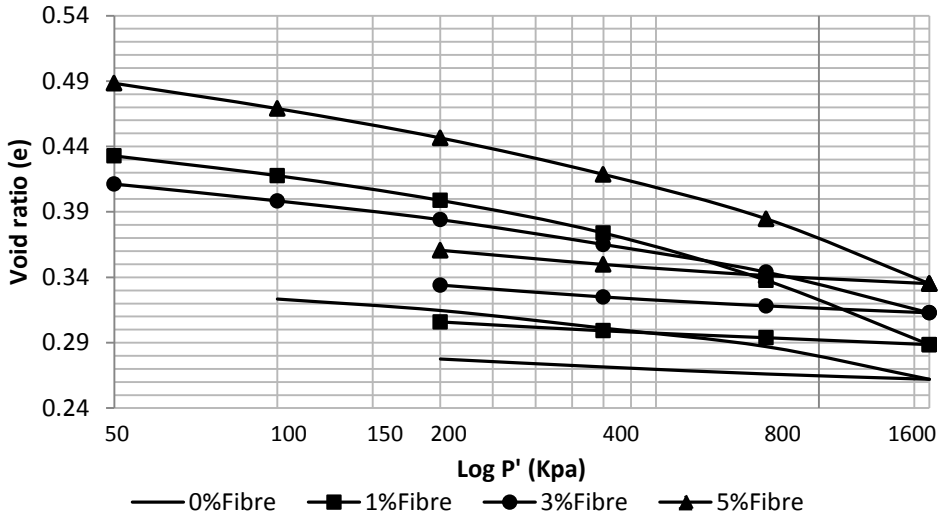

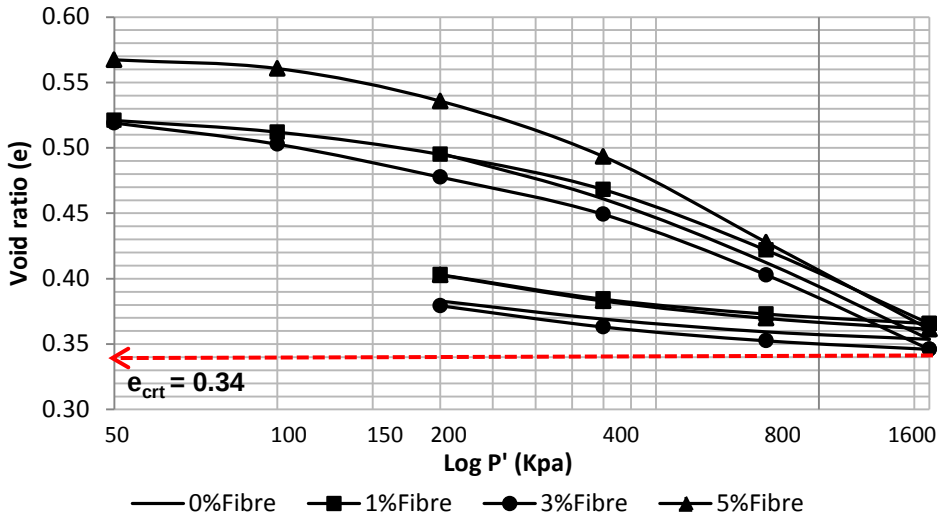

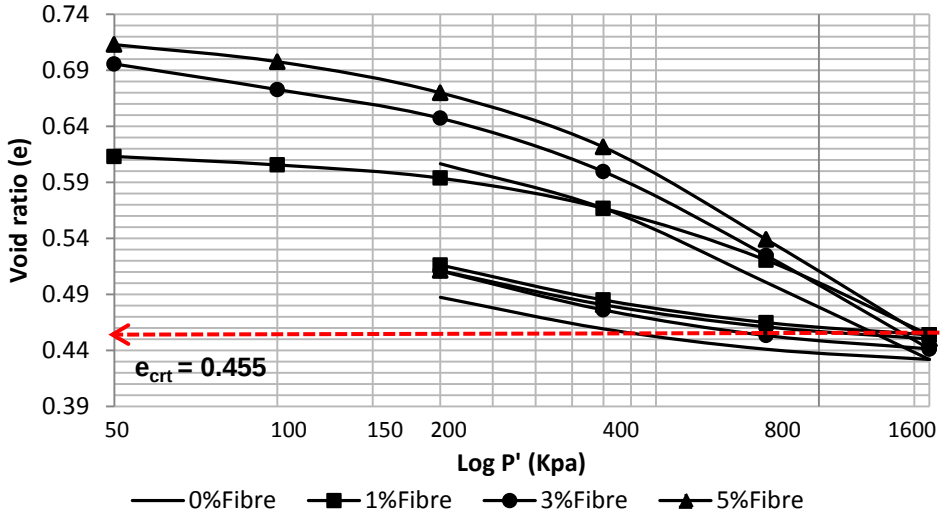

Figure 5.26 Curves of void ratio against axial stress for a) C2 soil b) C2-10B soil and c) C2-20B soil

Given the maximum dry unit weights of 20 kN/m^3 and 18.4 kN/m^3 for C2-10B and C2-20B soil specimens, the relationship between dry unit weight and void ratio (equation (5.1)) implies that the void ratio at maximum dry unit weight and optimum moisture content for these soils were 0.34 and 0.456 respectively.

$$\gamma_d = \frac{G_s \gamma_w}{1 + e} \tag{5.1}$$

Where:

γ_d Soil *d*ry unit weight

G_s Specific gravity

γ_w Dry unit weight of water (i.e. 10 kN/m^3)

Based on the presentations in Figure 5.26, at 1600 kPa of axial stress the void ratios of fibre reinforced C2-10B and C2-20B soil specimens converged to void ratios of non-reinforced C2-10B and C2-20B soil specimens at maximum dry unit weight and optimum moisture content (i.e. 0.34 and 0.45 respectively). However, the void ratio of fibre reinforced C2 soil specimens at 1600 kPa axial stress was not converged. This confirmed that with increase in bentonite content of fibre reinforced specimens under high stress levels, the void ratio was independent of fibre content and initial dry unit weight. Therefore, the final void ratio converged to void ratio of non-reinforced soil specimen at maximum dry unit weight and optimum moisture content.

As it is presented in Figure 5.26, void ratios of fibre reinforced C2 soil specimens were not converged at a certain void ratio at 1600 kPa axial stress. This was probably related to higher dry unit weight of C2 soil specimen compared to C2-10B and C2-20B soil specimens which made it relatively less compressible compared to C2-10B and C2-20B soil specimens.

For better exploration of influence of fibres on consolidation settlement of studied soils, change in void ratio versus fibre content for different soil specimens at stress levels of 400, 800 and 1600 kPa have been shown in Figure 5.27 to Figure 5.29.

These figures implied that increase in fibre content of fibre reinforced C2 soil resulted in increase in void ratio at all stress levels. However, insignificant change was observed for fibre reinforced C2-10B and C2-20B specimens.

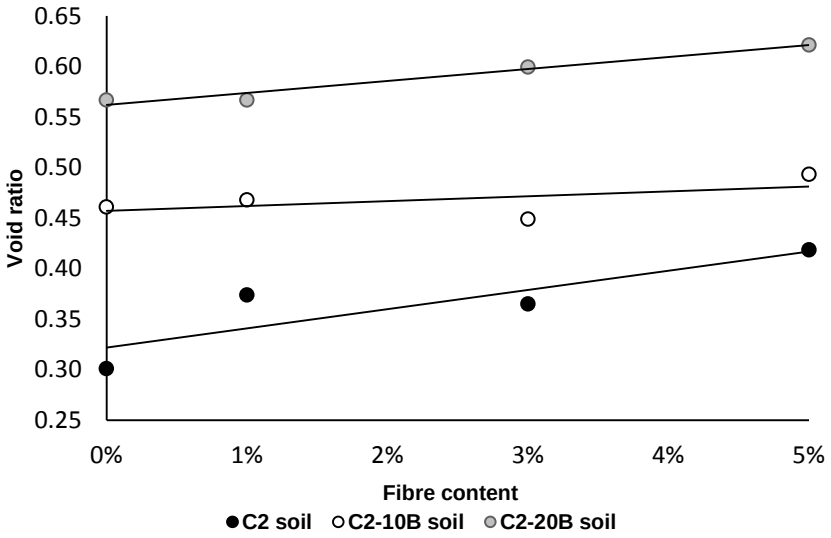

Figure 5.27 Influence of fibre on void ratio at 400 kPa loading stress

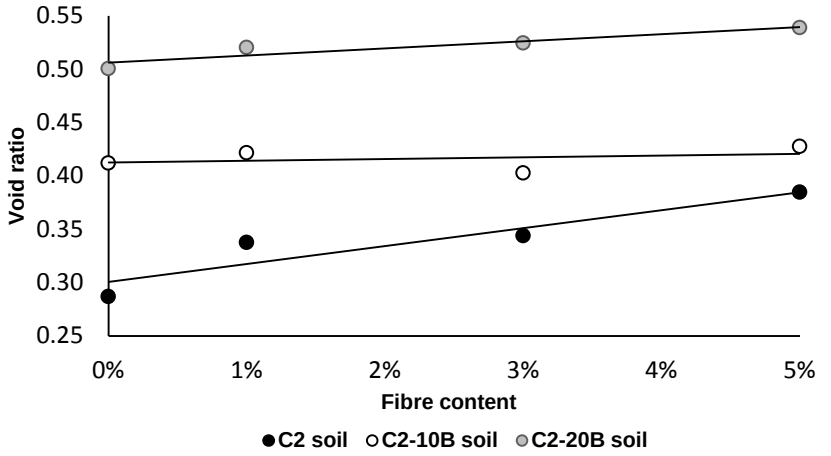

Figure 5.28 Influence of fibre on void ratio at 800 kPa loading stress

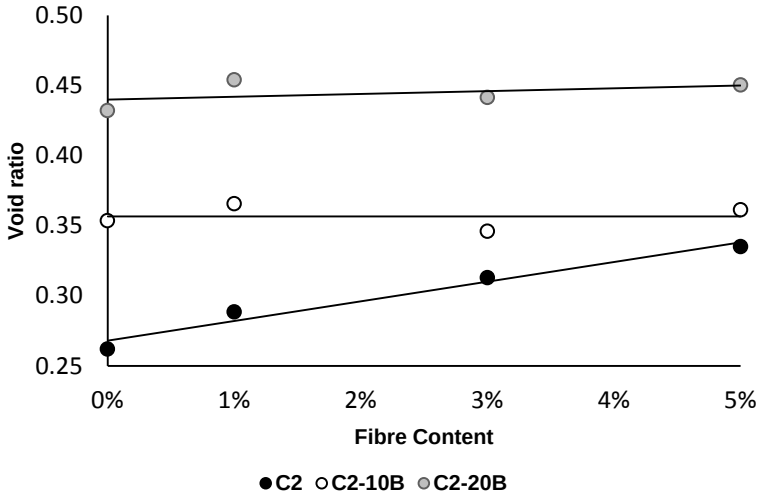

Figure 5.29 Influence of fibre on void ratio at 1600 kPa loading stress

5.7 Summary of the findings

In this chapter, results of a series of unconfined compression tests, swelling pressure tests and one-dimensional consolidation tests were presented. Based on the discussion made on the results of the experimental works the following conclusions can be drawn.

1) Unconfined compression strength of fibre reinforced clay soil specimens was highly dependent upon dry unit weight, moisture content and fibre content. At constant dry unit weight, increasing fibre content of both fibre types resulted in significant increase in UCS value. However, non-reinforced and fibre reinforced clay soil specimens prepared at their respective maximum dry unit weight and optimum moisture content, showed reduction in UCS value with increased fibre content.

2) Increase in dry unit weight of fibre reinforced clay soil specimens prepared at constant fibre content and moisture content resulted in significant increase in UCS.

3) Increase in moisture content of the fibre reinforced soil specimens at the same fibre content and dry unit weight resulted in reduction in UCS.

4) Increase in both dry unit weight and moisture content at constant fibre content (within the tested range) could result in an increase in UCS.

5) Stress-strain behaviour of non-reinforced soil specimens showed strain-softening behaviour with a large drop in post peak strength. With increase in fibre content to 5%, the stress-strain behaviour was transformed to strain-hardening behaviour.

6) Failure patterns of non-reinforced C1 and C1-10B soil specimens were evident as nearly vertical shear planes. With increase in fibre content, particularly at 5% fibre content, the failure pattern was gradually transformed to plastic bulging with appearance of networks of tiny cracks without apparent shear plane at failure.

7) Non-reinforced soil specimens showed brittle behaviour and failed at very small axial strain (i.e. less than 1%) while reinforced specimens at 5% fibre content failed at relatively large axial strain (i.e. 15% or more) in a ductile manner.

8) Increasing the fibre content of specimens prepared at maximum dry unit weight and optimum moisture content caused reduction in the attained swelling pressure. The observed reduction was continuous over the range of ABF fibre contents. However, significant drop occurred with the addition of 1% GBF fibres.

9) Minimum swelling pressure, irrespective of the soil type, was obtained on specimens mixed with 1% ABF fibres at a specific dry unit weight and the corresponding moisture content on the dry side of the compaction curve.

10) Maximum swelling pressure was observed on specimens compacted at a specific dry unit weight and the corresponding moisture content on the dry side of the compaction curve with 3% fibres irrespective of the soil type and fibre type.

11) Increasing the initial moisture content of the fibre reinforced soil was found to be effective in suppressing its swelling pressure.

12) Increasing dry unit weight of fibre reinforced soil while keeping constant moisture content caused an increase in the measured swelling pressure.

13) For the range of dry unit weights and moisture contents studied in this study, when both dry unit weight and moisture content of the fibre reinforced soil were changed, the influence of dry unit weight was dominant to increase the swelling pressure of the fibre reinforced clay soil.

14) Fibre distribution uniformity and formation of fibre pockets was dependent on the initial water content and type of fibre.

15) Fibre reinforced C2, C2-10B and C2-20B clay soil specimens revealed higher void ratio changes under applied stresses. This was intensified with increase in bentonite content

16) With increase in bentonite content, void ratio of the non-reinforced and fibre reinforced C2-10B and C2-20B soil specimens at 1600 kPa of axial stress eventually converged. Therefore, at high stresses the void ratio was independent of fibre content and initial dry unit weight. And void ratio of these specimens converged to void ratio of non-reinforced clay soil specimen at maximum dry unit weight and optimum moisture content.

Chapter 6 Results and Discussion (part two)

Summary

In this chapter, results of consolidated undrained (CU) triaxial compression tests are presented and discussed. Discussion is made on the stress-strain behaviour, excess pore-water pressure generation and stress path of the non-reinforced and fibre reinforced C1 soil specimens prepared at different dry unit weights.

6.1 Results of Consolidated undrained triaxial tests

6.1.1 Load-elapsed time relationship during specimen preparation

In this study a series of consolidated undrained triaxial compression tests was undertaken to determine the shear strength parameters of non-reinforced and fibre reinforced C1 soil specimens.

All soil specimens for triaxial tests were prepared in 38mm diameter mould. Static compaction method was employed for preparing triaxial soil specimens following the method described in Chapter 3 (section 3.9).

Figure 6.1 shows the required axial force for compressing the mixture of soil and fibre to form a cylindrical specimen of 76mm long. Figure 6.1, reports results of several repeated tests (empty markers) and average value (solid black markers).

As it can be seen in Figure 6.1 (a) for fibre reinforced specimens compacted at constant dry unit weight of 17.8 kN/m^3, increased fibre content resulted in increase in the maximum axial force required for compressing the soil/fibre mixture to a cylindrical 76mm heigh specimen.

The following explanations might help better understand the observed behaviour:

a) When a fibre reinforced clay soil is compacted, cohesion between clay soil particles alone is much stronger than that between clay soil particles and fibres. Therefore, for compressing a soil/fibre mixture more axial stress might be required.

b) Fibres may be accumulated to form relatively dry fibre pockets in local points during mixing procedure due to inefficient mixing procedure. This may prevent the uniform distribution of moisture content within the soil specimen. Local dry fibre pockets in compacted soil/fibre mixture behave like miniature springs. Therefore, possible presence of dry fibre pockets in soil/fibre mixture creates a spongy structure and leads to generate rebounding forces under compression. Hence, compared to non-reinforced

soil, compressing fibre reinforced specimens to the target height requires more axial force to overcome rebounding forces.

As it was mentioned earlier, ABF fibres are composed of very short single fibres however; GBF fibres include longer and thicker fibres in variety of single individual fibres to strands of tied fibres. Therefore, at constant fibre content, there are fewer number of GBF fibres. Hence, rebounding forces of GBF fibres reinforced specimens are less than that of specimens containing ABF fibres. Figure 6.1 (a) and Figure 6.1 (b) confirm the mentioned differences between behaviour of ABF and GBF fibre reinforced specimens.

As depicted in Figure 6.1 (b) there is a drop in the axial load required for compressing 3% ABF/GBF fibre reinforced soil specimens to their respective maximum dry unit weights compared to 1% and 5% fibre reinforced soil specimens. Axial load required for compressing ABF/GBF fibre reinforced soil specimen decreased with increase in fibre content from 1% to 3% due to reduction in dry unit weight. However, more axial stress is required for compressing fibre reinforced soil specimen with increase in fibre content from 3% to 5% due to higher fibre content and hence higher generated rebounding forces by fibres. Therefore, it seems that 3% fibre content is the optimum fibre content for compressing the fibre reinforced clay soil specimens to their maximum dry unit weights with minimal axial load.

Fibre reinforced specimens compacted at their respective maximum dry unit weights and optimum moisture contents showed distorted behaviours. Axial stress required for compressing soil/fibre mixture into 76mm long cylindrical specimen was found to be minimal for 3% fibre reinforced specimens.

Figure 6.2 and Figure 6.3 show the axial load against elapsed time at suitable intervals after reaching corrected target height (described in section 3.9) for different specimens.

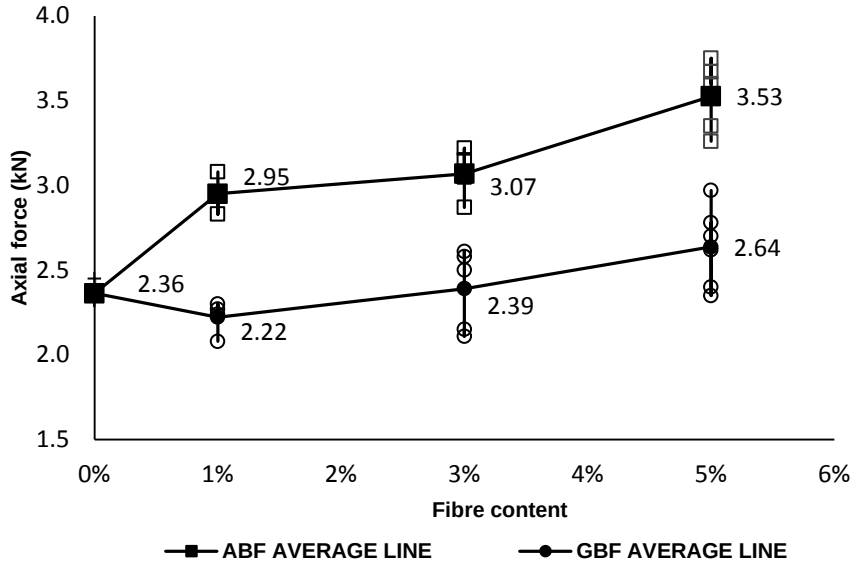

a) Compacted at dry unit weight of 17.8 kN/m^3

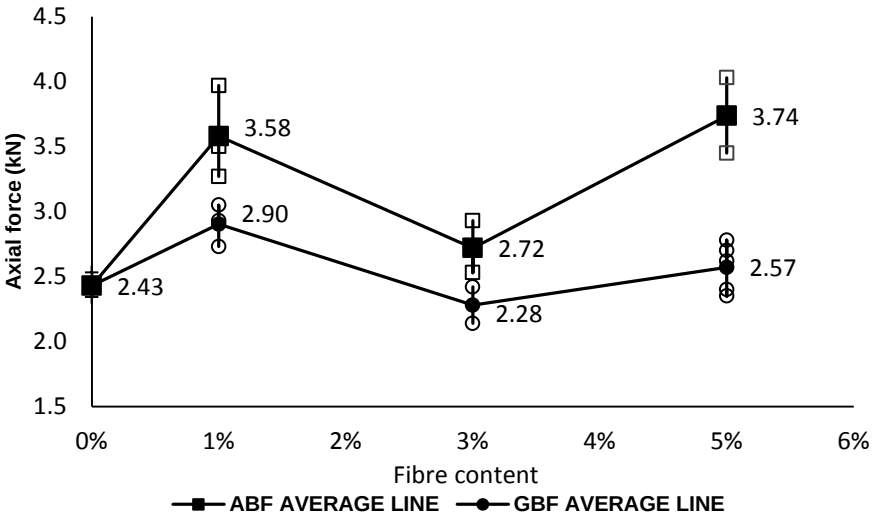

b) Compacted at maximum dry unit weight

Figure 6.1 Average axial load required for compressing the soil/fibre mixture into a cylindrical specimen

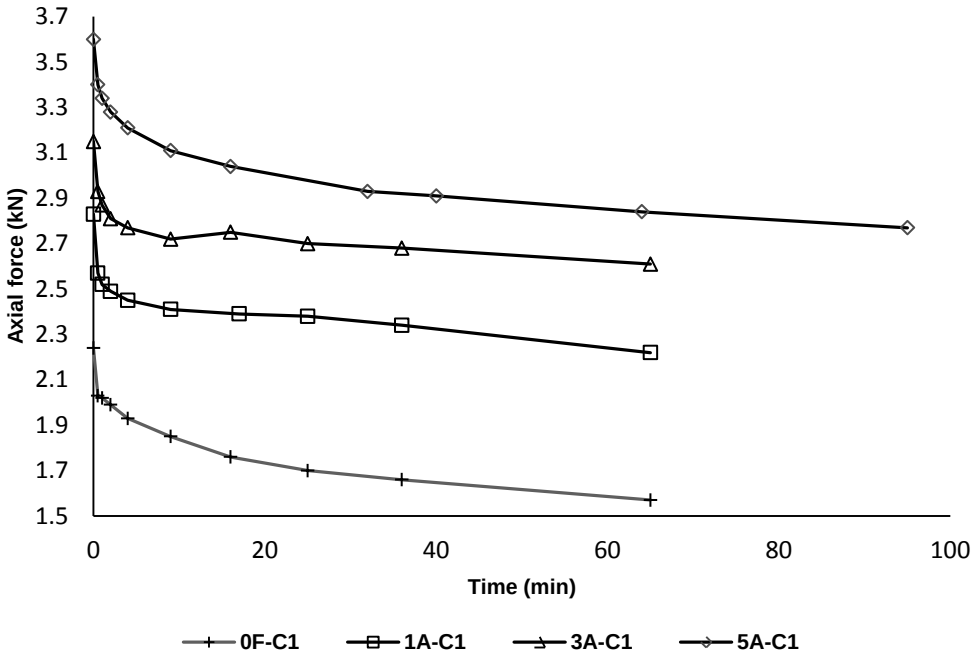

a) ABF fibre reinforced specimens

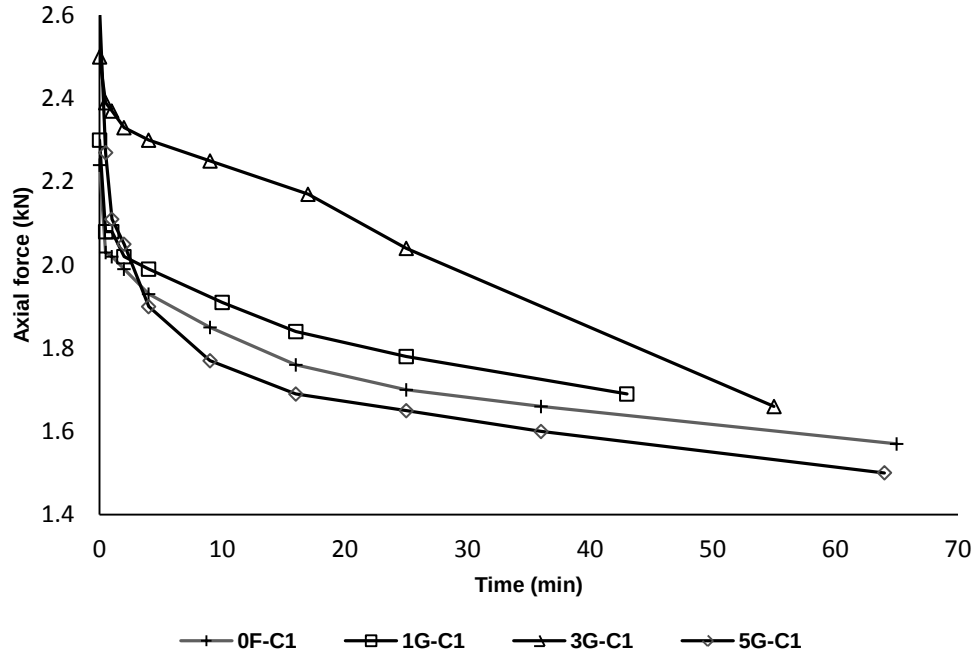

b) GBF fibre reinforced specimens

Figure 6.2 Load-Time relationships after reaching target height for specimens prepared at dry unit weight of 17.8 kN/m^3

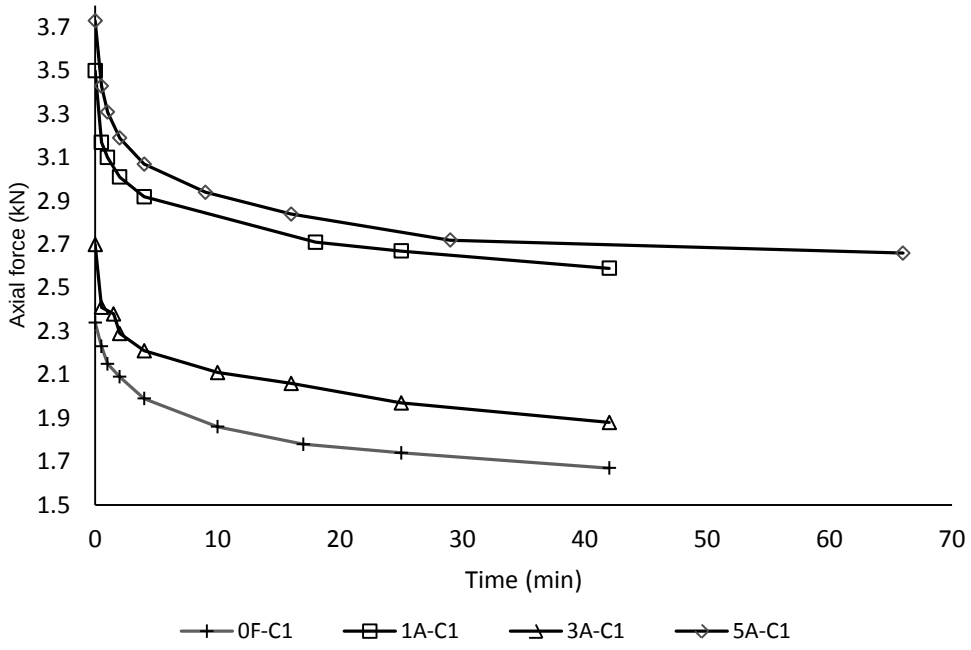

a) ABF fibre reinforced specimens

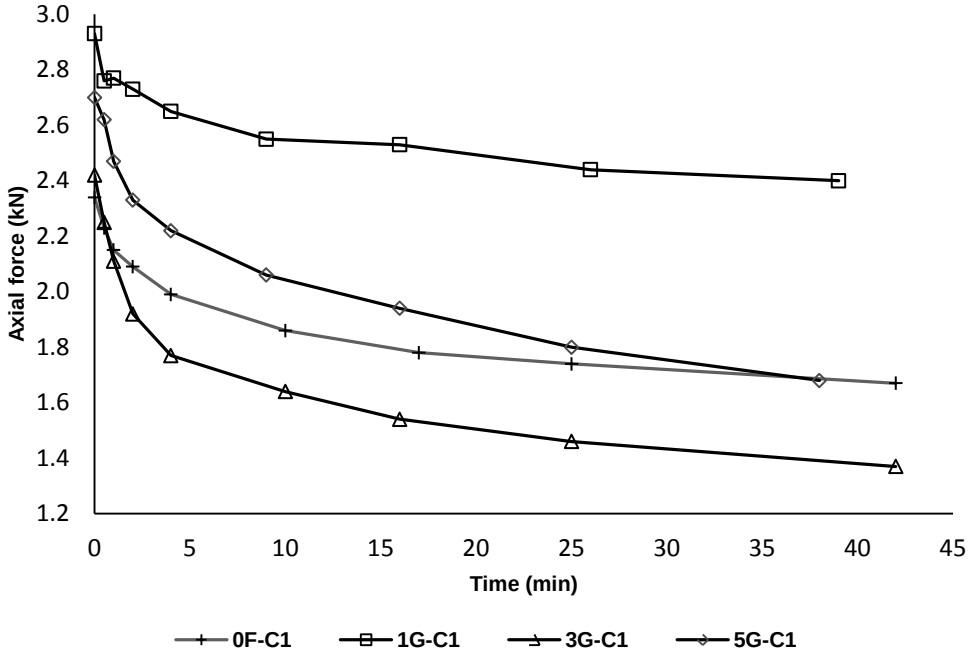

b) GBF fibre reinforced specimens

Figure 6.3 Load-Time relationships after reaching target height for specimens prepared at their respective maximum dry unit weight

6.1.2 Procedure of triaxial tests

At the beginning of the current study, three basic setups of triaxial test apparatus were available in the soil laboratory of the University of Bolton. The test setups relied on mercury column system to apply pressure (cell pressure and back pressure) to the specimen and mercury null-indicator to measure induced volume change of specimen. The maximum applicable back pressure and cell pressure to the specimen using the basic setups were 250 kPa and 400 kPa respectively due to the low height of the ceiling.

The whole system was transformed to a modern computerised system using sensors, data logger and appropriate software to collect data from sensors. Moreover, water/bladder cylinders were used to supply required back and cell pressures (i.e. up to 1000 kPa). Therefore, the following modification and/or additions were designed, made and implemented by the author:

1) Designing and making a six-way pressure panel for applying cell/back pressure, measuring pore-water pressure and deaerating water, (see Appendix A) in conjunction with air/water bladder cylinders for supplying required water pressure up to 1000 kPa

2) Programming a professional data logging software from scratch for collecting and analysing data from sensors through the data logger (see Appendix B).

3) Adopting and calibrating sensors for each set of triaxial apparatus including 3 pressure sensors for measuring cell/back pressure and pore-water pressure, load cell for measuring axial force and LVDT for measuring axial displacements.

4) Adopting new twin burette volume change devices (made by Controls S.R.I[12]) to the available triaxial apparatuses.

[12] www.Controls.it

5) Designing new arrangements of hose networks for all three sets of triaxial test apparatus to add new features such as new paths for applying carbon dioxide for saturating sand specimens, separate ball valves to manage different flow paths from top to bottom of specimen or reverse direction and extra valves for ease of de-airing of connection blocks and pipes.

Therefore, the improved sets of triaxial test apparatus together with data logging software made the procedure of the test more convenient, precise and easy to control.

To determine the influence of waste carpet fibres on shear strength of clay soil specimens, two series of consolidated undrained triaxial compression tests were carried out on C1 soil specimens. In the first series of triaxial testing programme, all specimens including non-reinforced and fibre reinforced C1 soil specimens were prepared at their respective maximum dry unit weight.

The second series of triaxial compression tests was carried out on specimens prepared at the constant dry unit weight of 17.8 kN/m^3. Table 6.1 shows the detailed specifications of all specimens prepared for triaxial compression test.

Table 6.1 Detailed specifications of specimens for soil triaxial compression test

	First series		Second series	
Specimen	Dry unit weight (kN/m^3)	Moisture content (%)	Dry unit weight (kN/m^3)	Moisture content (%)
C1	20.1	11.0	17.8	6.1
1A-C1	19.6	11.0	17.8	4.9
3A-C1	18.8	12.0	17.8	8.0
5A-C1	18.0	13.0	17.8	10.7
1G-C1	19.2	11.0	1.78	7.6
3G-C1	18.9	12.2	17.8	8.9
5G-C1	17.8	12.4	17.8	12.4

All soil triaxial compression tests were carried out according to BS1377-8 (1990). Two rubber membranes were used to isolate the specimen from cell fluid due to application of high confining stresses for saturating the specimen. And High vacuum grease was used as a lubricant between two rubber membranes.

Correction factors for considering the restraining effect of membranes were applied following the outlines mentioned in BS1377-8 (1990).

The saturation stage for all specimens was followed by the procedure described in Chapter 3 (Section 3.4.4) to reach a Skempton B-value of 97% or more. Once satisfactory B-value was achieved, specimens were consolidated at the predefined effective confining stresses. Shear test was undertaken at suitable strain rates calculated according to the results of consolidation stage. The procedure to calculate a suitable strain rate for shear test was earlier described in Chapter 3 (Section 3.4.5).

In this study, all the specimens were consolidated at three effective confining stresses of 50 kPa, 100 kPa and 200 kPa. A maximum shear strain rate of 0.002%/sec was used for shear test.

For the majority of specimens, the saturation stage was undertaken in a week and the consolidation stage was fulfilled in 1 hour to 3 days depending on the permeability of the specimens which in turn was related to the fibre content. The higher the fibre content, the higher the permeability of the specimen and the shorter consolidation time.

6.1.3 Results of triaxial tests

Results of triaxial compression tests are presented using graphs of deviator stress and excess pore-water pressure against axial strain. Moreover, to understand the behaviour of fibre reinforced specimens, stress paths for all specimens are analysed.

6.1.4 Deviator stress

Figure 6.4 and Figure 6.5 show the evolution of deviator stresses against axial strain at consolidation stresses of 100 kPa and 200 kPa for fibre reinforced specimens compacted at their respective maximum dry unit weights. Due to the large number of curves, stress-strain curves obtained at 50 kPa consolidation stress have not been shown here.

Both non-reinforced and fibre reinforced C1 soil specimens showed strain hardening behaviour at consolidation stresses of 50 kPa, 100 kPa and 200 kPa. Therefore, because there was no well-defined peak strength, the shearing resistance at 20% axial strain was used as the ultimate strength for all specimens. Of note, all tests were continued up to 30% axial strain to evaluate the behaviour of the fibre reinforced specimens at relatively large strains.

ABF fibre reinforced specimens showed continuous increase in deviator stress with increase in fibre content. According to Figure 6.4 slope of the deviator stress-axial strain curve increased with increase in the fibre content.

Shear strength of the soil specimen is highly dependent on environmental conditions, such as its initial moisture content and density (Lamb and Whitman, 1979). In general, shear strength of the soil decreases with increase in the moisture content. Density also plays a key role in defining strength of the soil. For a given level of compactive effort, density increases with increase in moisture content to optimum moisture content. However, beyond optimum moisture content, applied load is transferred increasingly to pore-water which acts as a lubricant between soil grains. Therefore, the strength of the soil specimen decreases (Newcomb and Birgisson, 1999).

Although the increase in fibre content accompanies an increase in the optimum moisture content and reduction in maximum dry unit weight of the fibre reinforced soil, ultimate deviator stress of ABF fibre reinforced soil specimens prepared at their respective maximum dry unit weights increased with increase in fibre content.

Thus, it may be concluded that ABF fibres contributed to the strength of fibre reinforced soil specimens. However, at all consolidation stress levels, specimens with 1% ABF fibre content, showed almost the same ultimate deviator stress as non-reinforced C1 soil specimen. The ultimate deviator stress of specimens with 3% and 5% ABF fibre content were also almost the same at all tested consolidation stresses. This implied that increase in ABF fibre content compensated strength losses due to combined effect of increase in moisture content and reduction in maximum dry unit weight.

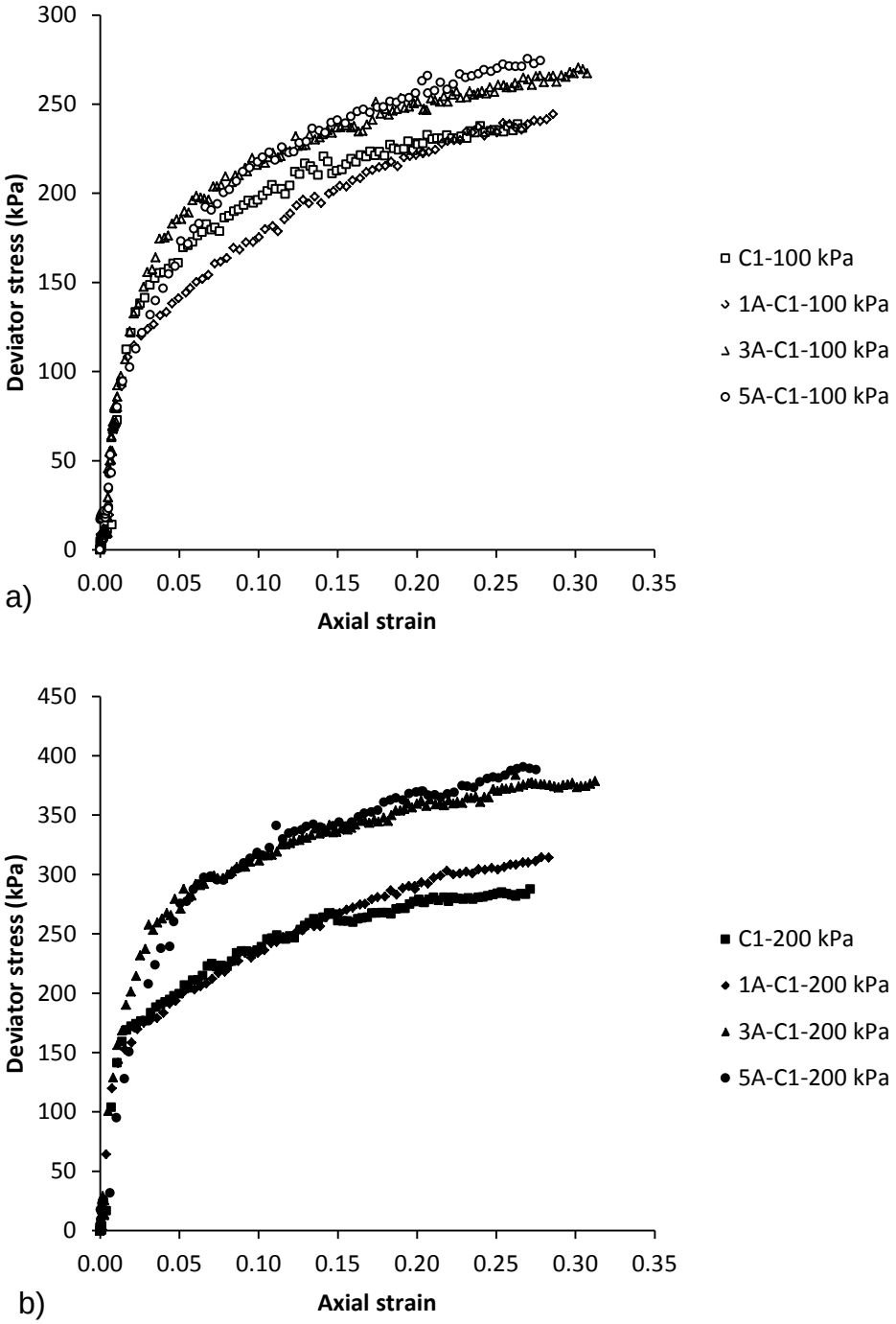

Figure 6.4 Deviator stress against axial strain curves for ABF fibre reinforced specimens compacted at their respective maximum dry unit a) at consolidation stress of 100 kPa b) at consolidation stress of 200 kPa

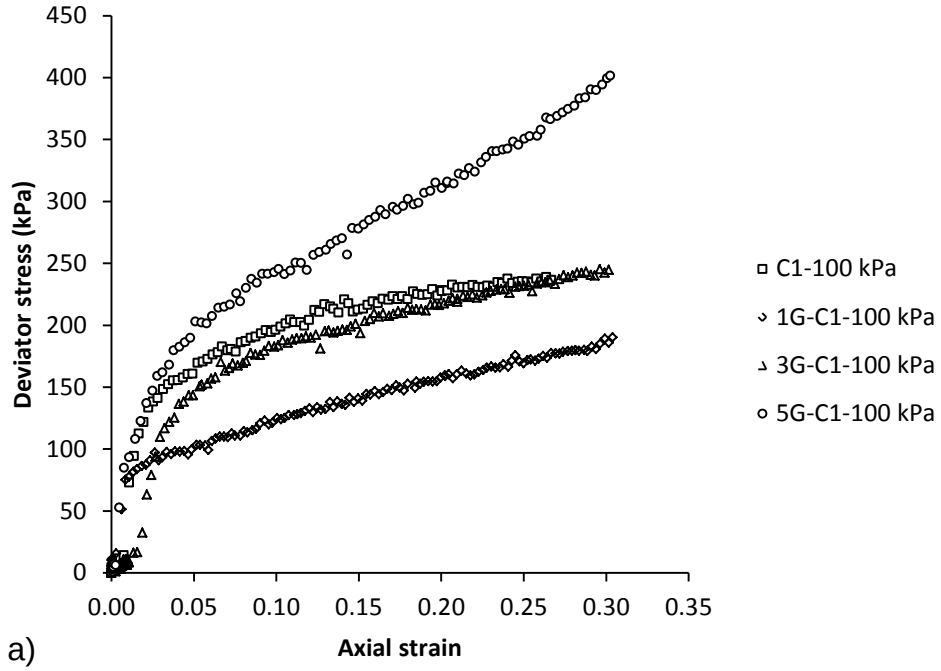

a)

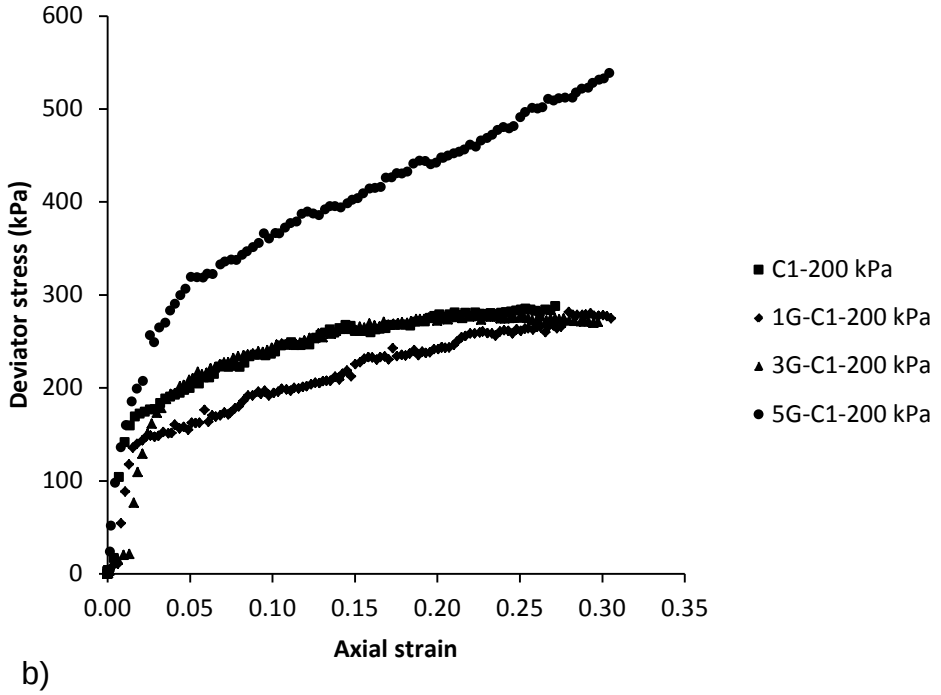

b)

Figure 6.5 Deviator stress against axial strain curves for GBF fibre reinforced specimens compacted at their respective maximum dry unit a) at consolidation stress of 100 kPa b) at consolidation stress of 200 kPa

Ultimate deviator stress of GBF fibre reinforced soil specimens also increased with fibre content. However, at all consolidation stress levels, the ultimate deviator stress of 1% and 3% fibre reinforced specimens was less than or equal to that of non-reinforced C1 soil specimen. 5% GBF fibre reinforced C1 soil specimens showed significant increase in deviator stress compared to that of non-reinforced C1 soil specimens at all consolidation stresses.

Figure 6.6 and Figure 6.7 show the influences of ABF and GBF fibres on deviator stresses of C1 soil specimens compacted at dry unit weight of 17.8 kN/m^3 respectively.

Non-reinforced C1 soil specimen compacted at dry unit weight of 17.8 kN/m^3 showed plastic behaviour however, increase in fibre content (both for ABF and GBF fibre types) followed by gradual transformation to strain hardening behaviour.

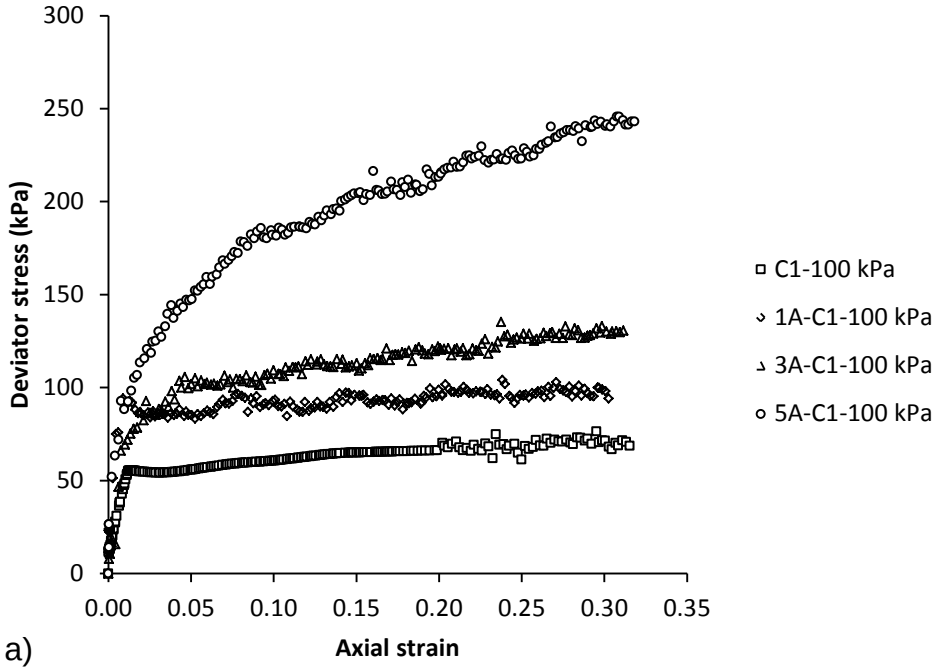

a)

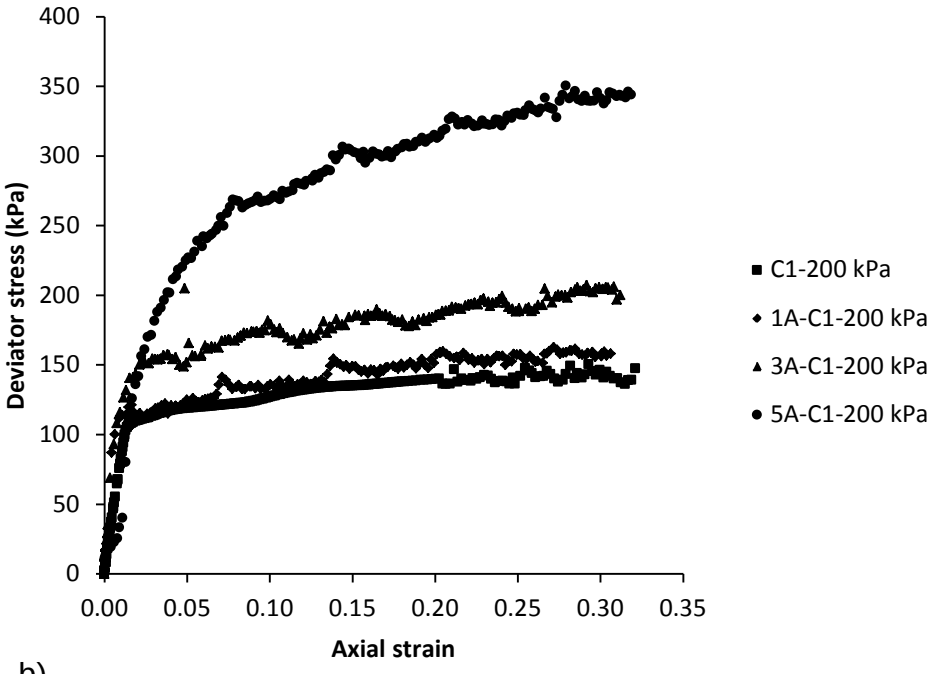

b)

Figure 6.6 Deviator stress against axial strain curves for ABF fibre reinforced specimens compacted at 17.8 kN/m^3 a) at consolidation stress of 100 kPa b) at consolidation stress of 200 kPa

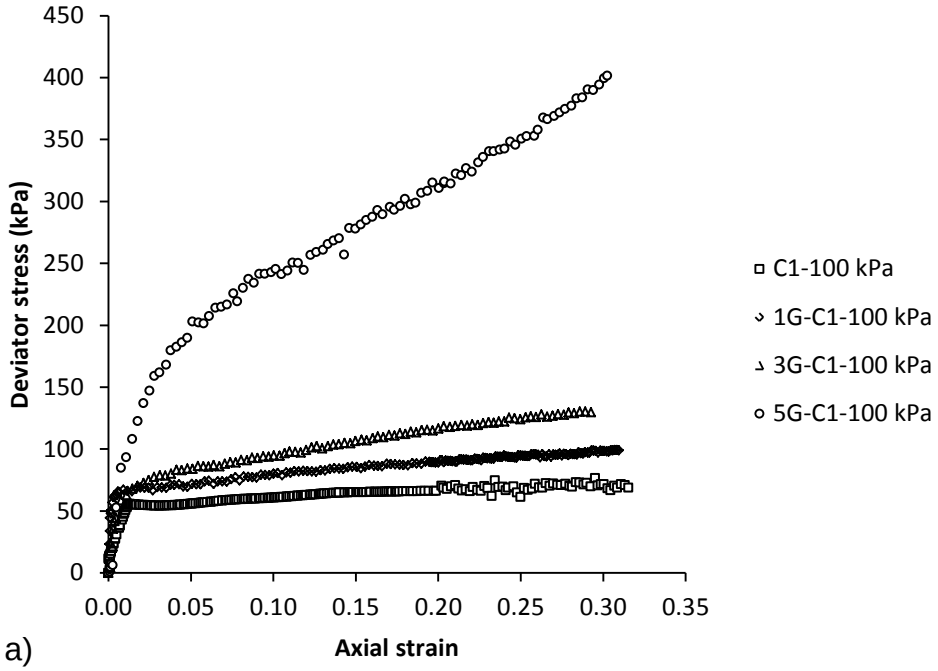

a)

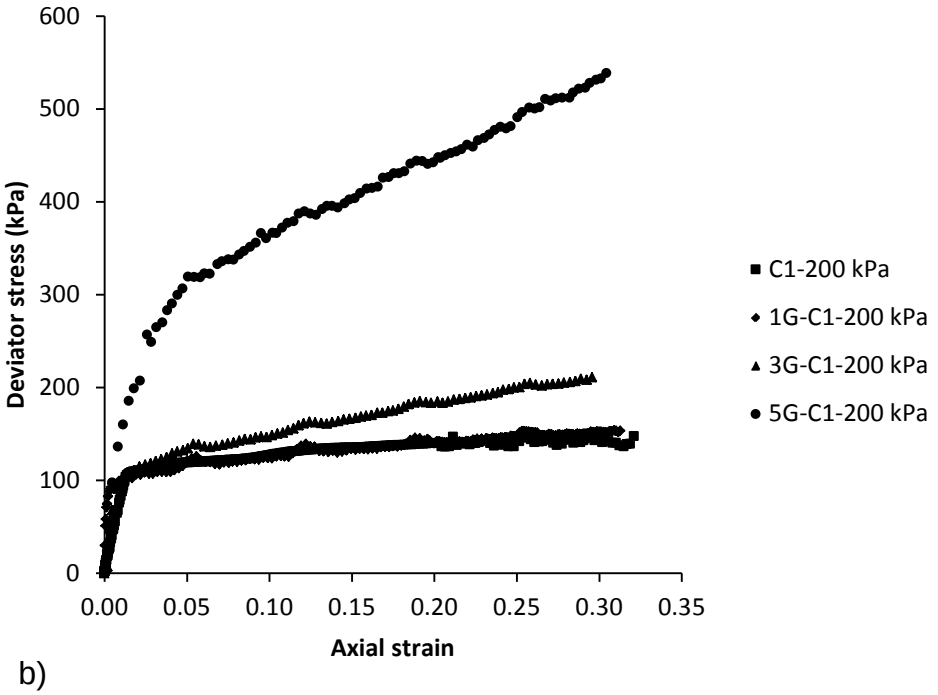

b)

Figure 6.7 Deviator stress against axial strain curves for GBF fibre reinforced specimens compacted at 17.8 kN/m^3 a) at consolidation stress of 100 kPa b) at consolidation stress of 200 kPa

Figure 6.8 and Figure 6.9 compare the ultimate deviator stress of ABF/GBF fibre reinforced C1 soil specimens compacted at maximum dry unit weight and at the same dry unit weight respectively. Comparing the graphs shown in Figure 6.8 and Figure 6.9 revealed that:

1) For both fibre types, including 1% and 3% fibre content did not increase the ultimate deviator stress significantly. However, adding 5% fibre followed a significant improvement in ultimate deviator stress.

2) It can be seen that GBF fibres contributed better than ABF fibres to enhancement of the ultimate deviator stress. This was due to differences in the physical properties of GBF and ABF fibres. GBF fibres included longer and thicker fibres compared to thinner and shorter ABF fibres. Therefore, GBF fibres exhibited better contribution to improved stress-strain behaviour by better interlocking with clay soils particles

3) Increase in fibre content resulted in significant increase in deviator stress at higher consolidation stress. This was also reported by Freilich et al. (2010). At higher consolidation stresses in shear stage, fibres stretched increasingly and therefore, they contributed better to distribution of the applied axial load in to a wider area. Moreover, at higher consolidation stresses, soil grains came closer to fibre filaments and the developed frictional forces between fibres and soil grains increased. This phenomenon limited the sliding and reorientation of soil grains under applied stresses. Therefore, fibres contributed better to strength at higher consolidation stresses.

According to Figure 6.9, the degrees of improvement in peak deviator stresses of fibre reinforced specimens (consolidated to 200 kPa) prepared at the same dry unit weight of 17.8 kN/m^3 were 1%, 32% and 220% (corresponding to increase in GBF fibre content to 1%, 3% and 5% respectively). Murray et al. (2000) reported increase in peak deviator stresses of reinforced sandy silt specimens with recycled carpet fibres (consolidated to 34.5 kPa) to 28.7%, 103.9% and 203.7% respectively with increase in fibre content to 1%, 2% and 3%. Regardless of the type of fibre in both studies and consolidation stress, this shows that the degree of

improvement in peak deviator stress of cohesionless soils (sandy silt) with increase in fibre content is more than that in cohesive soils.

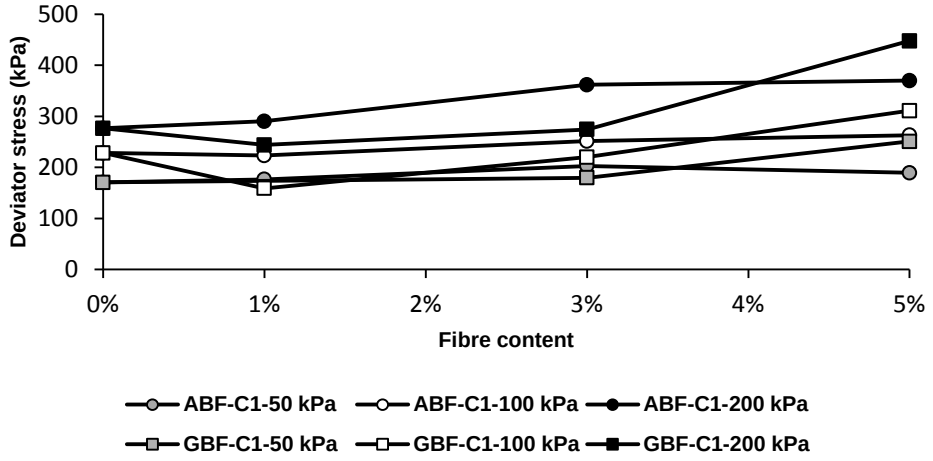

Figure 6.8 Ultimate deviator stress (at 20% axial strain) of ABF/GBF fibre reinforced specimens compacted at their respective maximum dry unit weight

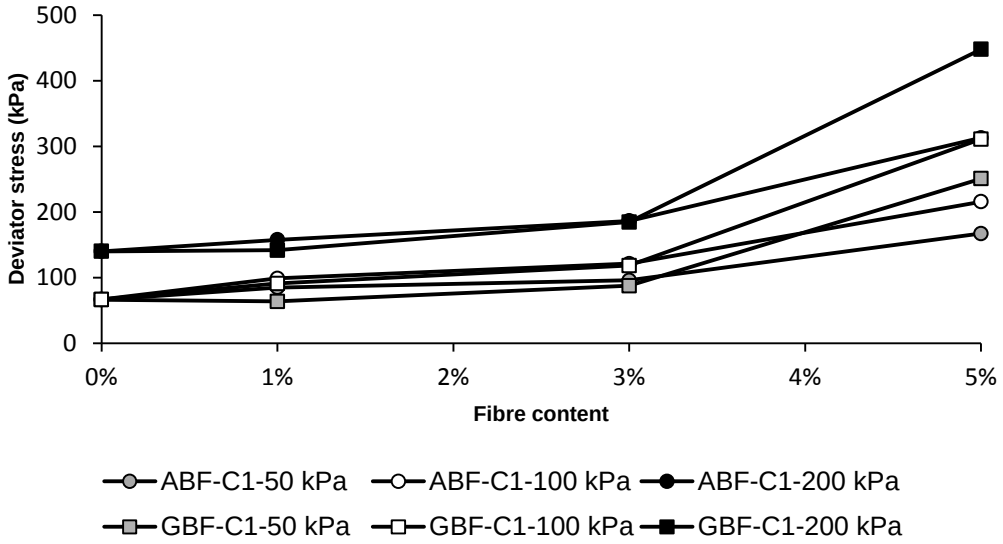

Figure 6.9 Ultimate deviator stress (at 20% axial strain) of ABF/GBF fibre reinforced specimens compacted at 17.8 kN/m^3

6.1.5 Pore-water pressure generation in fibre reinforced specimens

Excess pore-water pressure during shearing stage of consolidated undrained (CU) triaxial tests was measured from the bottom of specimens using an appropriate pressure sensor. Shearing stage was carried out at a very slow axial displacement rate of 0.10 mm/min to ensure equilibrium of the pore-water pressure distribution along vertical profile of the specimen.

For interpreting the results due to slow axial displacement rate at shearing stage, it was considered that measured pore-water pressure from bottom of the specimen would be representative of pore-water pressure across the whole specimen. However, because of random distribution of fibres in the specimen, there might be some locally generated pore-water pressures along interface of soil grains and fibres.

Figure 6.10 and Figure 6.11 show the excess pore-water pressure in ABF/GBF fibre reinforced C1 soil specimens compacted at their respective maximum dry unit weights. It can be observed that non-reinforced C1 and 1% ABF fibre reinforced C1 soil specimens reached a peak excess pore-water pressure at small strains followed by continuous reduction in excess pore-water pressure. For the case of non-reinforced C1 soil specimen, excess pore-water pressure even reached negative values beyond 15% axial strain. Reduction in excess pore-water pressure reflects the tendency of specimen for dilation (US Army Corps of Engineers, 2003). Therefore, under applied consolidation stresses, non-reinforced and 1% ABF fibre reinforced C1 soil specimens compacted at their respective maximum dry unit weights showed dilative behaviour which is the marked behaviour of over consolidated clay soils. However, increase in fibre content led to reduction in the post peak drop of excess pore-water pressure. Therefore, an increase in the fibre content under applied consolidation stresses gradually reduced the over consolidation ratio of the soil.

Li (2005) and Estabragh et al. (2011) also reported similar findings of excess pore-water pressures developed in fibre reinforced clay soil specimens tested in consolidated undrained condition. With increase in fibre content in fibre reinforced soil specimen, fibres distributed the stresses within the structure of the soil specimen and restrained the dilative deformation of the soil specimen. Therefore, excess pore-water pressure increased with increase in fibre content.

Another explanation to observed increase in excess pore-water pressure with increase in fibre content would be through the change in the void ratio of the fibre reinforced soil specimens. The results shown in Figure 6.10 and Figure 6.11 are pertained to specimens prepared at their respective maximum dry unit weights and optimum moisture contents. Reduction in maximum dry unit weight with increase

in fibre content led to increase in void ratio of the specimen. Therefore, at full saturation, specimens with more fibre content contained more voids filled with water. Hence, increase in deviator stress was accompanied with more increase in pore-water pressure.

As it is depicted in Figure 6.4 and Figure 6.5, Figure 6.9 and Figure 6.10, with increase in fibre content, the rate of increase in deviator stress exceeded the rate of increase in pore-water pressure. Therefore, although pore-water pressure increased with increase in fibre content, the effective major stress increased as well.

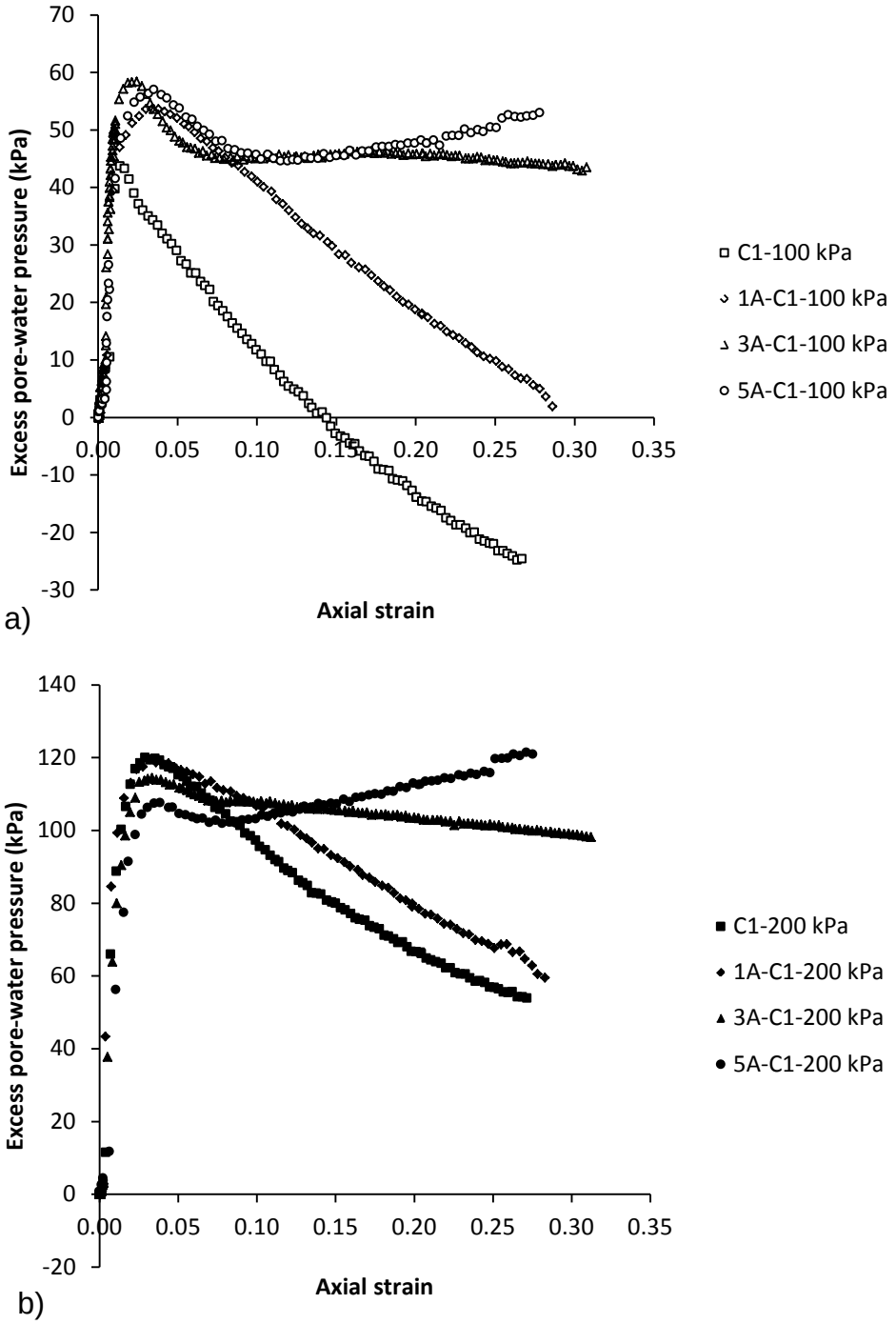

Figure 6.10 Excess pore-water pressure development in ABF fibre reinforced specimens compacted at their respective maximum dry unit weights a) at consolidation stress of 100 kPa b) at consolidation stress of 200 kPa

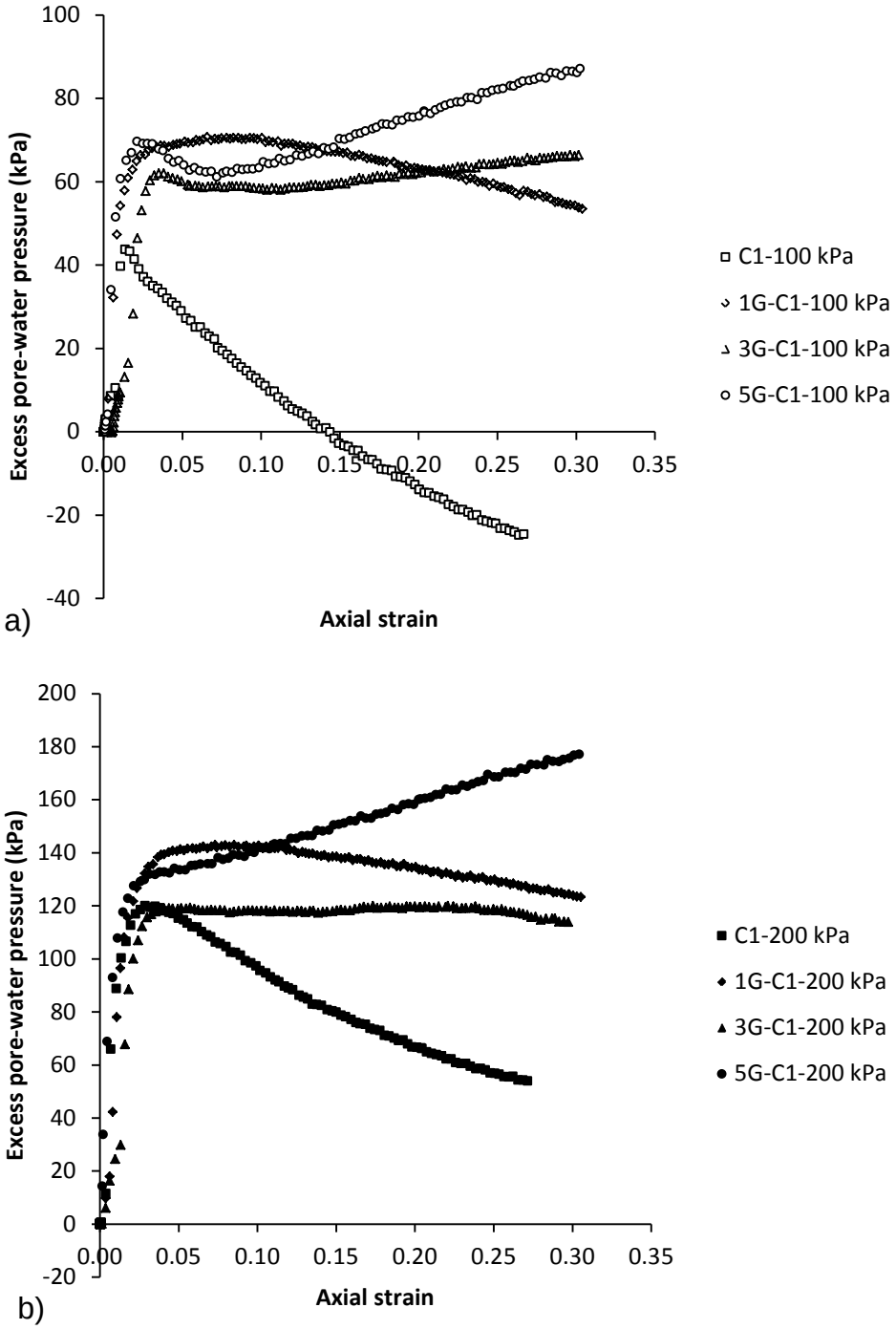

Figure 6.11 Excess pore-water pressure development in GBF fibre reinforced specimens compacted at their respective maximum dry unit weights a) at consolidation stress of 100 kPa b) at consolidation stress of 200 kPa

Comparing Figure 6.10 to Figure 6.11 shows that the pore-water pressures generated in GBF fibre reinforced soil specimens were relatively more than those generated in ABF fibre reinforced soil specimens. This was attributed to the differences in composition of the fibres. GBF fibres due to their higher lengths contributed better to confine the soil particles together and hence they led to more increase in the pore-water pressure of the fibre reinforced soil specimens.

Figure 6.12 and Figure 6.13 show the excess pore-water pressures developed in ABF/GBF fibre reinforced C1 soil specimens compacted at the same dry unit weight of 17.8 kN/m^3. There was a slight increase in pore-water pressure with increase in fibre content. This can pertain to the same initial void ratio of all specimens as long as their dry unit weights are the same.

Comparing results of excess pore-water pressures generated in specimens prepared at their respective maximum dry unit weights and those compacted at the same dry unit weight confirmed that for the range of fibre contents used in this study, increase in excess pore-water pressure of fibre reinforced specimens was more dependent on the dry unit weight rather than fibre content. However, Li (2005) and Estabragh et al. (2011) reported increase in excess pore-water pressure with increase in fibre content and explained this observation by relating it to tendency of fibres for restraining volume change (in the form of dilation) of fibre reinforced specimens.

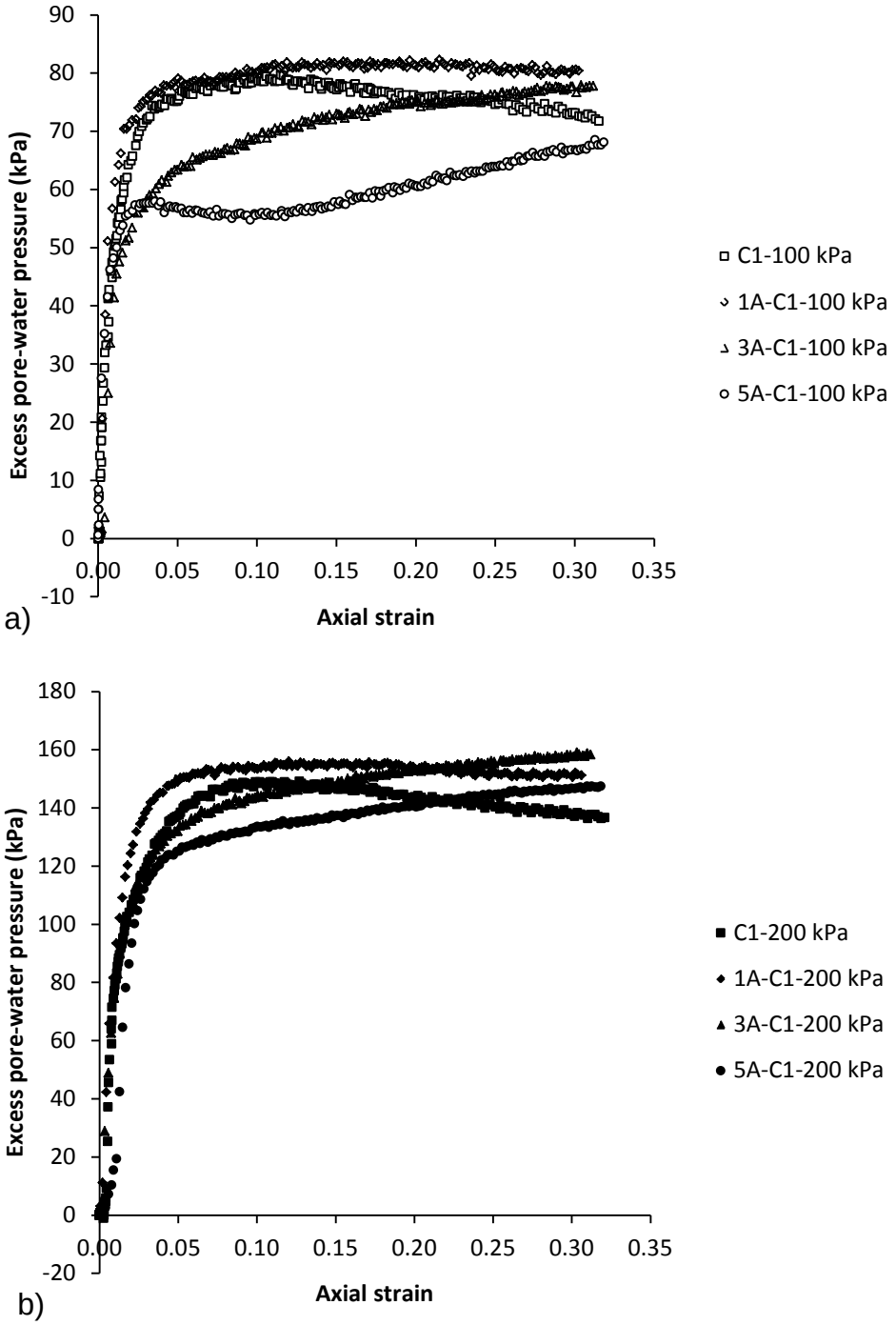

Figure 6.12 Excess pore-water pressure developments in ABF fibre reinforced specimens compacted at the same dry unit weight of 17.8 kN/m^3 a) at consolidation stress of 100 kPa b) at consolidation stress of 200 kPa

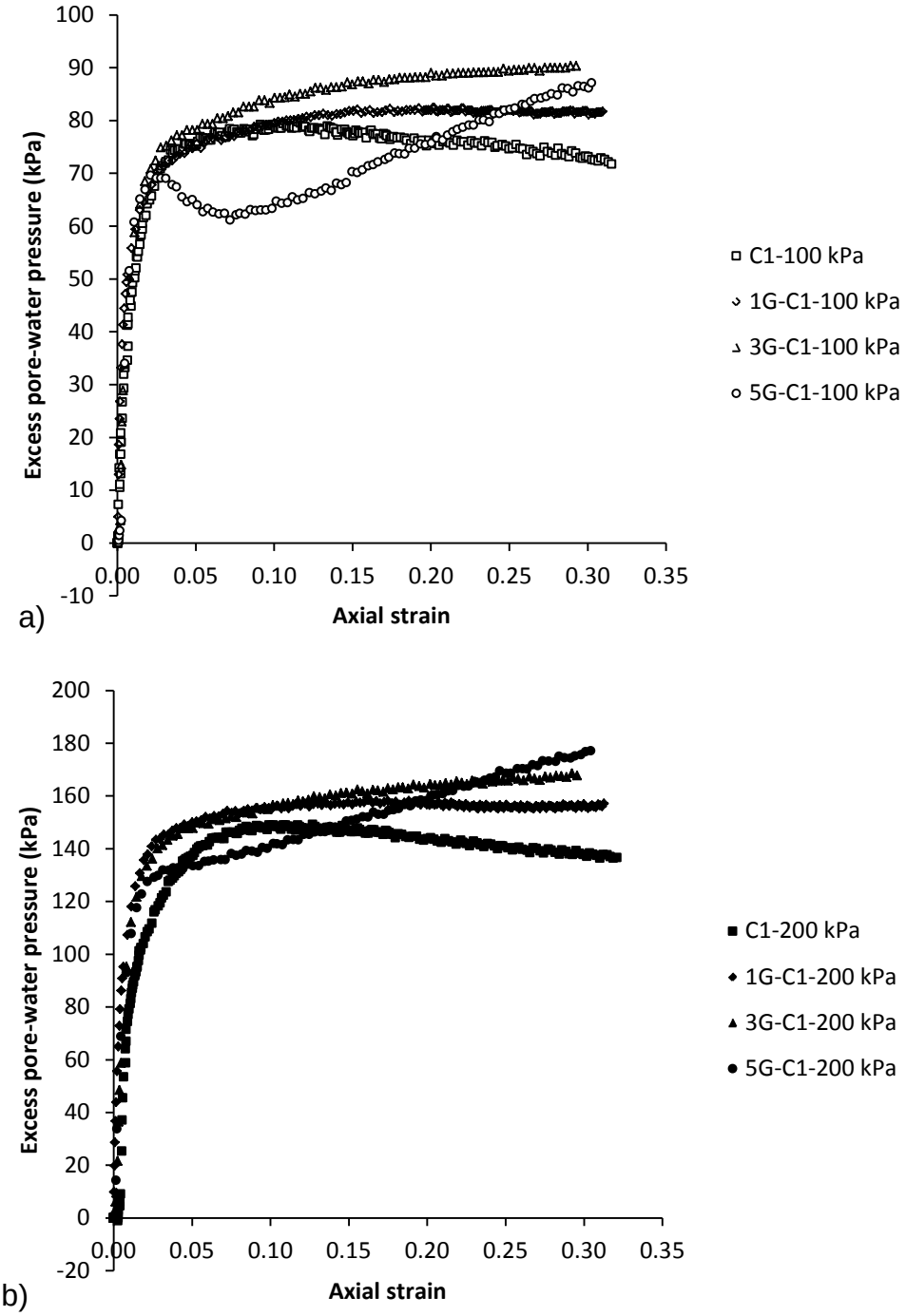

Figure 6.13 Excess pore-water pressure developments in GBF fibre reinforced specimens compacted at the same dry unit weight of 17.8 kN/m^3 a) at consolidation stress of 100 kPa b) at consolidation stress of 200 kPa

6.1.6 Stress path analysis of fibre reinforced specimens

The stress path field concept in soil mechanics was first introduced in 1958 by Roscoe, Schofield and Wroth (Head, 1998). Stress path shows the changes which

happened in state of the soil specimen under loading/unloading stresses by means of graphical explanation. Stress path parameters are defined as:

$$p' = \frac{\sigma_1' + \sigma_2' + \sigma_3'}{3}$$ Mean effective stress (6.1)

$$q' = \sqrt[2]{\frac{(\sigma_1' - \sigma_2')^2 + (\sigma_2' - \sigma_3')^2 + (\sigma_1' - \sigma_3')^2}{2}}$$ Deviator stress (6.2)

Where:

σ_1'	Major effective principal stress
σ_2'	Intermediate effective principal stress
σ_3'	Minor effective principal stress

In isotropic triaxial tests, minor principal stress and intermediate stresses are the same and equal to the confining stress. Therefore equation (6.1) and equation (6.2) can be simplified as:

$$p' = \frac{\sigma_1' + 2\sigma_3'}{3}$$ Mean effective stress in isotropic triaxial test (6.3)

$$q' = (\sigma_1' - \sigma_3')$$ Deviator stress in isotropic triaxial test (6.4)

At any stage, the relationship between p' and q' can be written as:

$$p' = \sigma_3' + q/3$$ Relationship between p' and q (6.5)

Figure 6.14 explains the stress path and corresponding changes in the volume change against natural logarithm of effective confining stress of clay soils in drained and undrained shear tests. In this figure isotropic consolidation line (NCL) has been defined as upper limit of volume change of clay soils under isotropic compression. At critical state, soil continues plastic shearing without change in deviator stress or mean effective stress (Wood, 1990).

In the undrained test, specific volume (i.e. equals void ratio plus one) during shear test is remained unchanged. Therefore, the only possible stress paths for clay soils in undrained test are HIJ (for heavily over consolidated clay soils), EFG

(for lightly over consolidated clay soils) or AD (for normally consolidated clay soils). Description of the critical state concept is beyond the scope of this thesis and readers can find related materials elsewhere (Wood, 1990).

Stress path analysis was conducted using equation (6.3) and equation (6.4) for all the undertaken consolidated undrained triaxial tests in this study. Figure 6.15 and Figure 6.16 show the stress path diagrams of non-reinforced and fibre reinforced C1 soil specimens compacted at their respective maximum dry unit weights.

It can be observed that at the same consolidation stress, increase in fibre content resulted in increase in the slope of stress path. Increase in the slope of stress path of the fibre reinforced soil specimen with increase in fibre content indicated combined effect of increase in deviator stress and pore-water pressure (see Figure 6.4, Figure 6.5, Figure 6.10 and Figure 6.11). Moreover, excess pore-water pressure of non-reinforced and 1% fibre reinforced soil specimens compacted at their respective maximum dry unit weights reduced after emerging a peak excess pore-water pressure at small axial strains. Therefore, the mean effective stress of these specimens increased and hence their stress path slopes distinctively decreased compared to those of 3% and 5% fibre reinforced soil specimens.

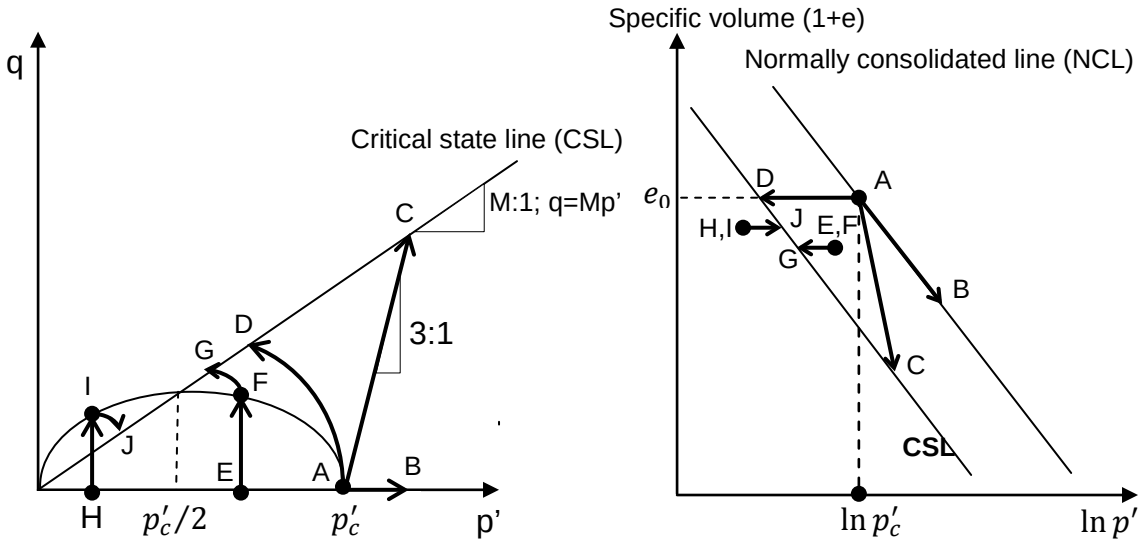

AB: Isotropic compression
AC: Normally consolidated clay-drained test
HIJ: Heavily over consolidated clay-undrained test

AD: Normally consolidated clay-undrained test
EFG: Lightly over consolidated clay-undrained test

Figure 6.14 Illustrative stress paths of different types of clay soils to reach critical state behaviour

Comparing the stress-strain curves of the non-reinforced and fibre reinforced soil specimens compacted at their respective maximum dry unit weights revealed that at the beginning of shear test at axial strains of less than 3%, stress paths of all the specimens were similar. This might be pertained to minimum strain required for enabling fibres as tensile elements in the soil specimen. With increase in axial strain, stress path state of soil specimens began to be more distinctive such that stress path of 5% ABF fibre reinforced C1 soil specimen at large strains tended to be almost perpendicular to mean effective stress (p') axis.

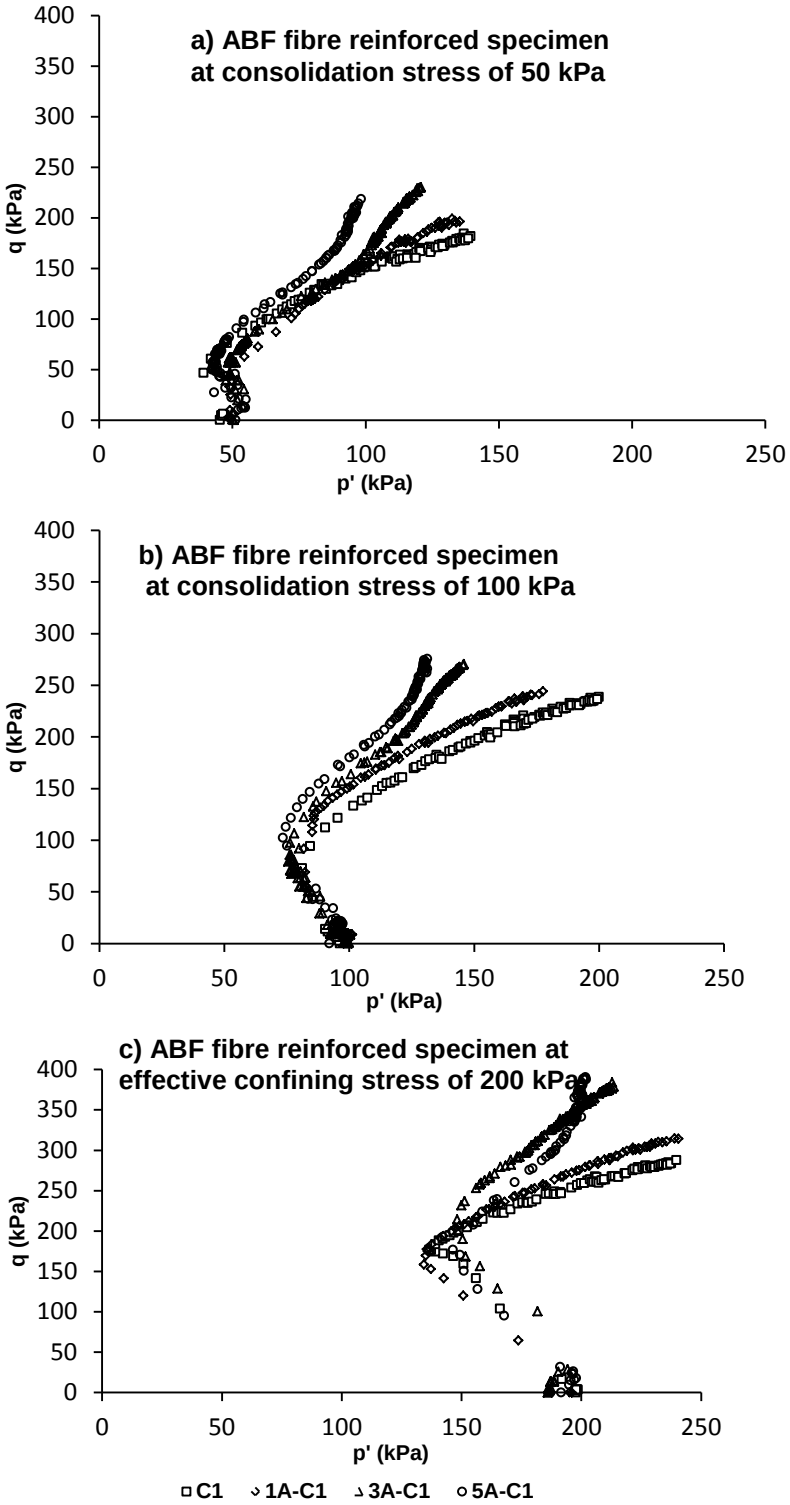

Figure 6.15 Stress paths of ABF fibre reinforced specimens at their respective maximum dry unit weights

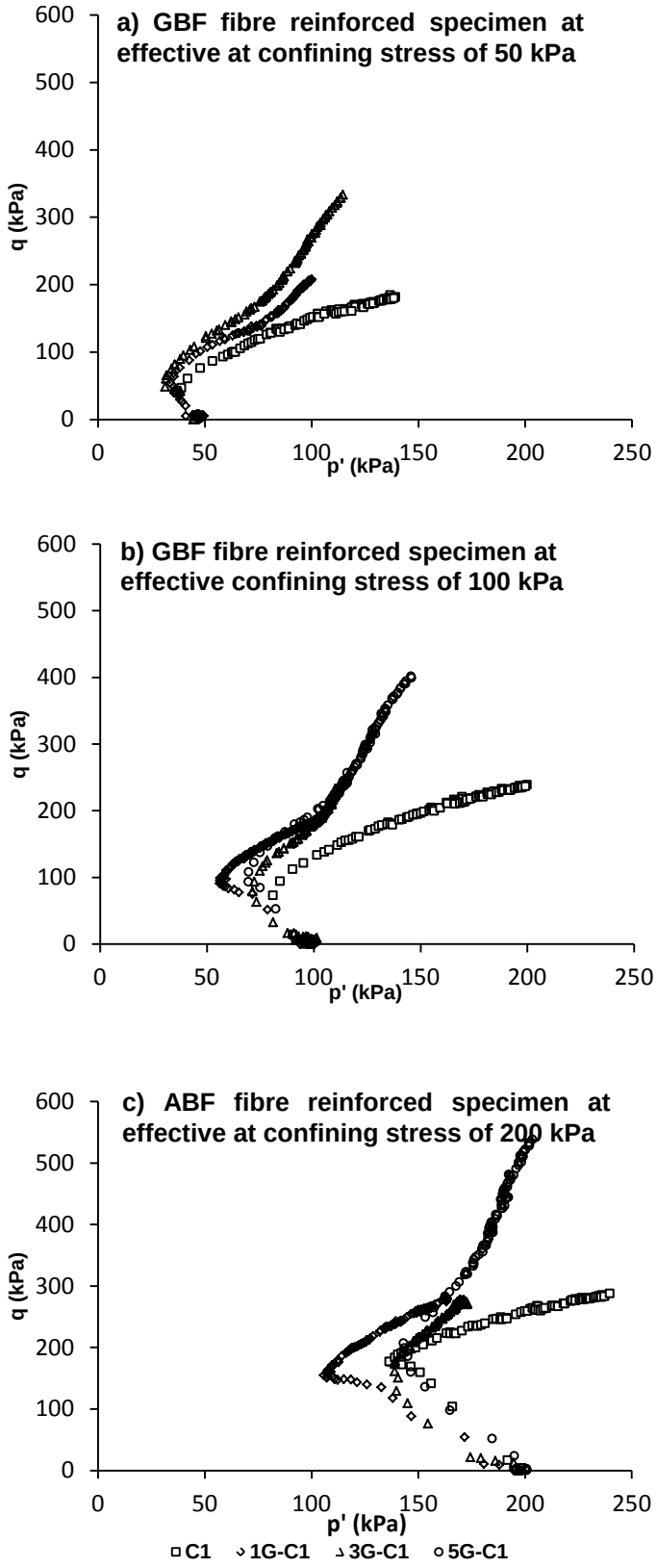

Figure 6.16 Stress paths of GBF fibre reinforced specimens compacted at their respective maximum dry unit weights

Figure 6.17, Figure 6.18 and Figure 6.19 show the stress path for non-reinforced and ABF/GBF fibre reinforced C1 soil specimens compacted at the same dry unit weight of 17.8 kN/m^3 respectively. According to Figure 6.6 and Figure 6.12, deviator stress and excess pore-water pressure of non-reinforced soil at all studied consolidation stresses reached steady state (zero-change) condition with increase in axial strain. Moreover, Figure 6.17 shows that, stress paths of this soil reached a unique straight line. Hence, it can be concluded that non-reinforced C1 soil specimen has reached the critical state line in q:p' space with slope (i.e. M) of 1.43.

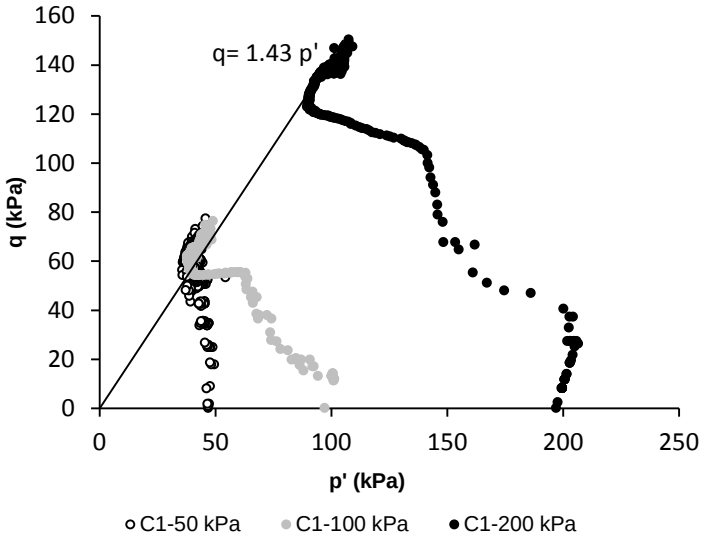

Figure 6.17 Stress paths of non-reinforced C1 soil specimens compacted at the dry unit weight of 17.8 kN/m^3

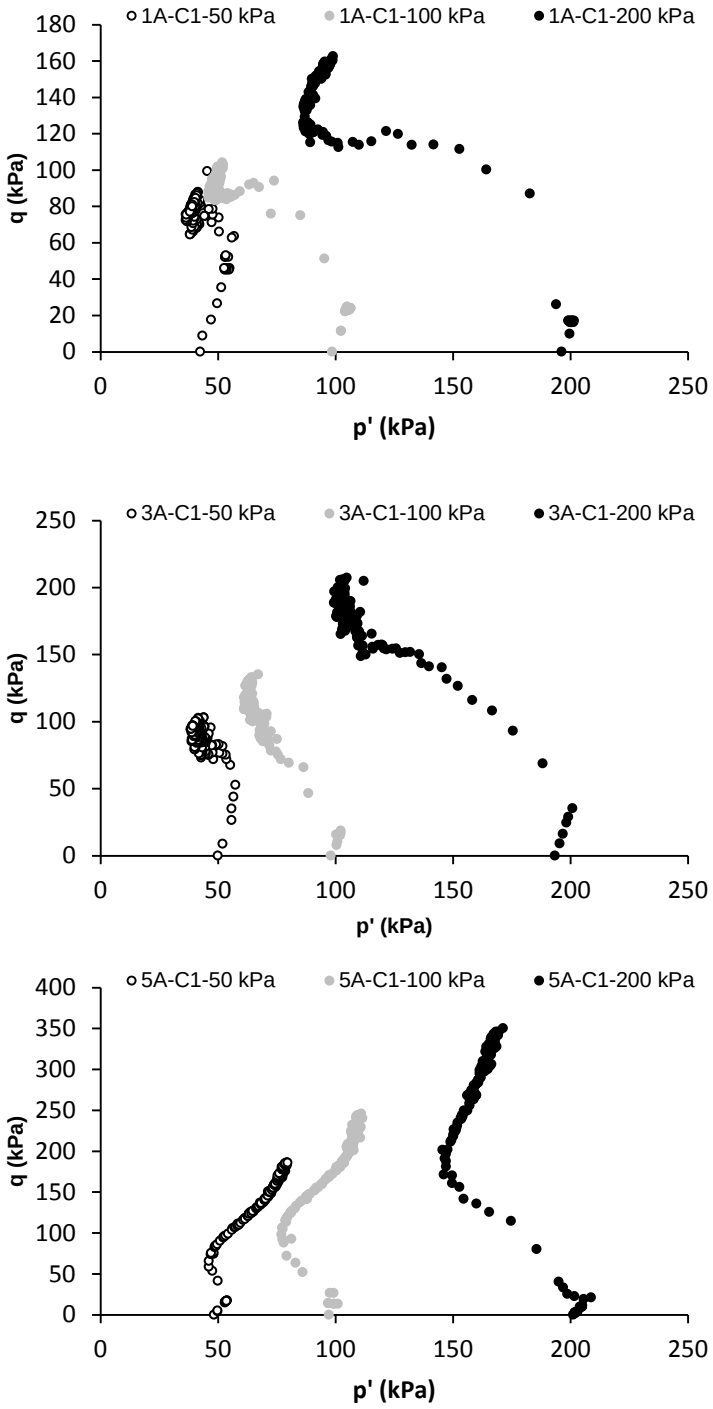

Figure 6.18 Stress paths of ABF fibre reinforced C1 soil specimens compacted at the dry unit weight of 17.8 kN/m^3

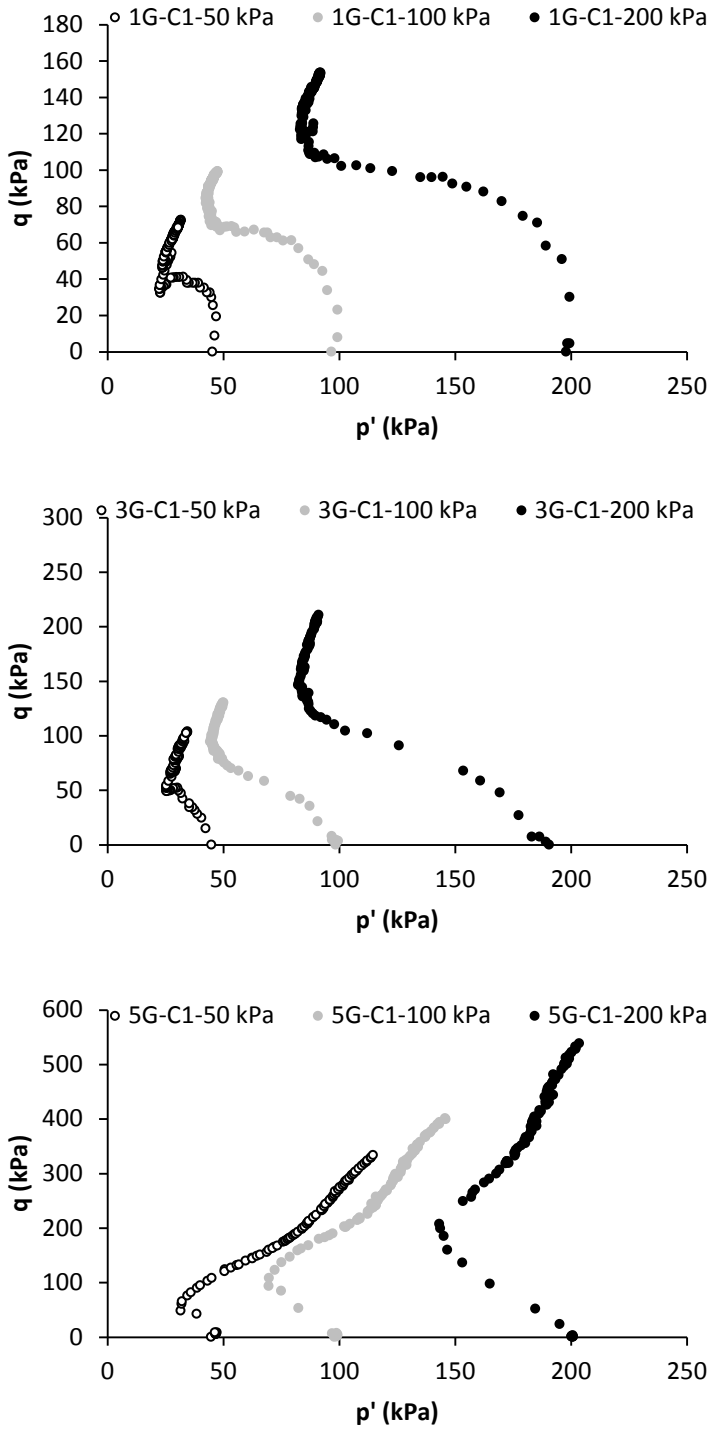

Figure 6.19 Stress paths of GBF fibre reinforced C1 soil specimens compacted at the dry unit weight of 17.8 kN/m^3

Equation (6.5) showed the relationship between mean effective stress (p') and deviator stress (q). Differentiating both sides of this equation gives:

$$\frac{\partial p'}{\partial \varepsilon_a} = \frac{\partial \sigma_3}{\partial \varepsilon_a} + \frac{\partial q}{3\partial \varepsilon_a} - \frac{\partial u}{\partial \varepsilon_a} \tag{6.6}$$

Where:

ε_a Axial strain

u Pore-water pressure

During conventional undrained shear test minor total stress remains constant and therefore:

$$\frac{\partial p'}{\partial \varepsilon_a} = \frac{\partial q}{3\partial \varepsilon_a} - \frac{\partial u}{\partial \varepsilon_a} \quad or\ \Delta p' = \frac{\Delta q}{3} - \Delta u \tag{6.7}$$

Figure 6.20 and Figure 6.21 show the changes of excess pore-water pressure versus deviator stress of ABF and GBF fibre reinforced specimens prepared at their respective maximum dry unit weights respectively. All specimens showed peak excess pore-water pressure at deviator stress equal to 0.95 to 1.30 times of consolidation stress. Following the peak value, the excess pore-water pressure of non-reinforced and 1% fibre reinforced C1 soil specimens decreased. However, increasing the fibre content to 3% and 5% resulted in gradual increase in excess pore-water pressure whereas, specimens with 5% fibre content showed continuous increase in excess pore-water pressure.

The slopes of plots shown in Figure 6.20 and Figure 6.21 show the tendency of specimens for either contractive or dilatancy behaviour. Increase in the slope of excess pore-water pressure indicates contractive behaviour. However, reduction in the slope shows the tendency of specimen to dilation.

According to Figure 6.20 and Figure 6.21, the slopes of post peak excess pore-water pressure of non-reinforced and 1% ABF/GBF fibre reinforced soil specimens were negative. However, the magnitude of their slopes decreased slightly with increase in consolidation stress. Therefore, these specimens showed dilative behaviour after reaching peak excess pore-water pressure. And their dilation behaviours were limited with increase in consolidation stress.

At 3% ABF/GBF fibre content the slope of post peak pore-water pressure versus deviator stress did change significantly. However, the slope of post peak excess pore-water pressure versus deviator stress of 5% ABF fibre reinforced C1 soil specimen increased from 0.19 at consolidation stress of 50 kPa to 0.34 at consolidation stress of 200 kPa. For 5% GBF fibre reinforced soil the slope of the post peak excess pore-water pressure versus deviator stress also increased from 0.1 at consolidation stress of 50 kPa to 0.2 at consolidation stress of 200 kPa.

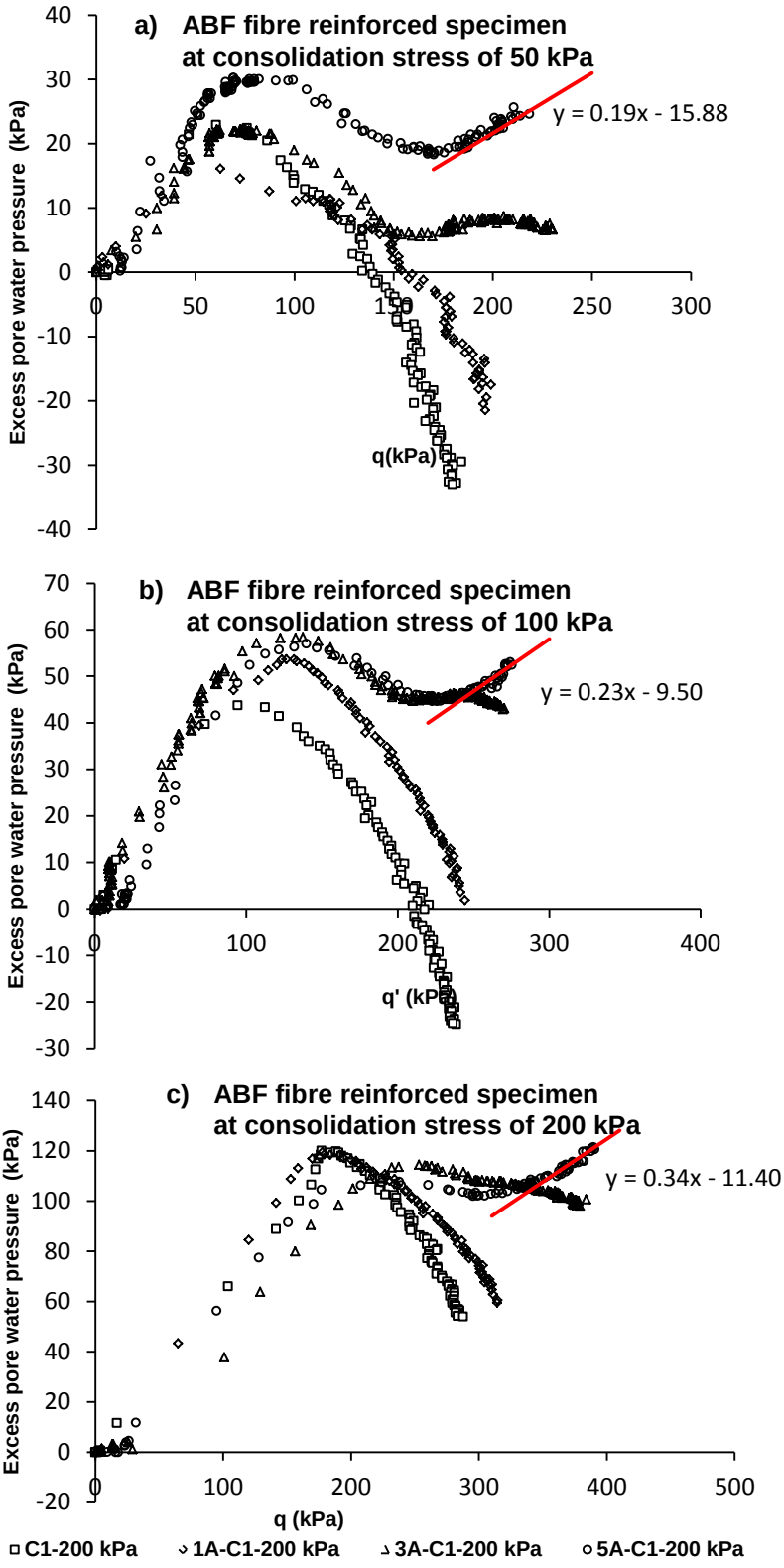

Figure 6.20 Excess pore-water pressure versus deviator stress of ABF fibre reinforced specimens compacted at their respective maximum dry unit weight

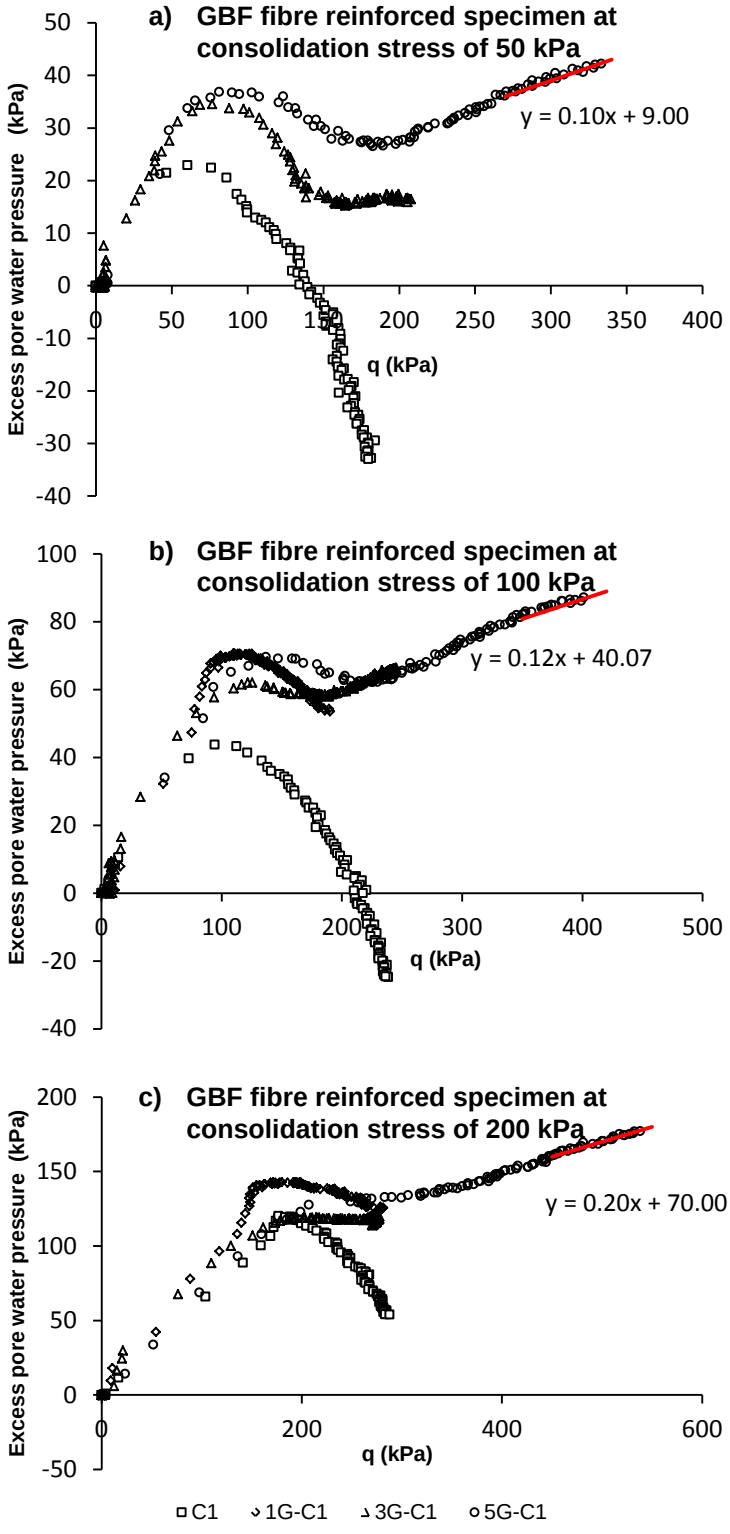

Figure 6.21 Excess pore-water pressure versus deviator stress of GBF fibre reinforced specimens compacted at their respective maximum dry unit weight

Equation (6.7) recalls that mean effective stress would be constant in condition that excess pore-water pressure becomes equal to one third of change in deviator stress. Shear test for most of the tests carried out in this study were stopped when axial strain reached 30%. Therefore, unfortunately the behaviour of the soil specimens beyond 30% axial strain is not available. However, the arisen condition may be predicted by stress path concept. For example for 5% ABF fibre reinforced C1 soil specimen compacted at its maximum dry unit weight and consolidated to 200 kPa, one the following scenarios might take place beyond 30% axial strain:

1. The first scenario would be following the condition that $\Delta u = \Delta q\ /3$ and excess pore-water pressure increases with the current slope versus deviator stress (i.e. ≈ 0.34). Therefore, mean effective stress would be constant. During undrained test there is no volume change in the specimen. Therefore, the stress state of specimen on $e - \ln p'$ diagram would not change at all. This means that the soil specimen would never reach critical state which is contradictory. Hence, this is not the case.

2. The second scenario would be in condition that $\Delta u < \Delta q\ /3$. Therefore, mean effective stress would increase. According to Figure 6.14, this does happen if and only if the soil specimen is highly over consolidated and its stress state is located on the left side of critical state line (CSL).

3. The third scenario would be in condition that $\Delta u > \Delta q\ /3$. Therefore, mean effective stress would decrease. According to Figure 6.14, this does happen if and only if the soil specimen is lightly over consolidated and its stress state is located on the right side of critical state line (CSL).

Due to the method of specimen preparation used in this study (i.e. remoulding), the stress history of the specimens during preparation was not available. However, comparing the stress paths of 5% ABF fibre reinforced C1 soil specimen with illustrations in Figure 6.14, shows that the revealed stress path is similar to the behaviour of lightly over consolidated clays. Therefore, the third scenario would be more probable for change of excess pore-water pressure versus deviator stress

beyond 30% axial strain. Hence, mean effective stress beyond 30% axial strain would decrease and stress path may lean backward to reach the critical state.

6.1.7 Effective shear strength parameters of fibre reinforced soil specimens

Effective shear strength parameters including c' and φ' were calculated for non-reinforced and fibre reinforced C1 soil specimens using Mohr circle diagrams of shear stress versus principal effective stresses. Figure 6.22 to Figure 6.25 compare the effective apparent cohesion (c') and effective internal friction angle (φ') of non-reinforced and 5% fibre reinforced soil specimens. All Mohr circles were drawn based on the effective principal stresses at 20% axial strain. Table 6.2 shows the summary of the results.

Effective internal friction angle of ABF Fibre reinforced soil specimens compacted at the maximum dry unit weight increased significantly with increase in fibre content. The value of effective internal friction angle of ABF fibre reinforced soil specimens increased by 48% with adding 5% fibre. Effective apparent cohesion of ABF fibre reinforced soil specimens did not change significantly with increase in fibre content.

GBF Fibre reinforced soil specimens compacted at the maximum dry unit weight, showed significant increase in effective internal friction angle with increase in fibre content. However, at 3% GBF fibre content slight reduction in internal friction angle was observed. The reduction in internal friction angle at 3% GBF fibre content was followed by significant increase in apparent cohesion.

Although increase in fibre content of C1 soil specimens prepared at their respective maximum dry unit weights was accompanied with reduction in dry unit weight, the resultant effective shear strength parameters increased significantly. The effective apparent cohesion of fibre reinforced soil specimens did not change significantly however, the effective internal friction angle improved significantly.

The most striking improvement was achieved with adding 5% GBF fibre. Whereas the effective internal friction angle of 5% ABF fibre reinforced soil specimen increased by 82% compared to that of non-reinforced C1 soil specimen.

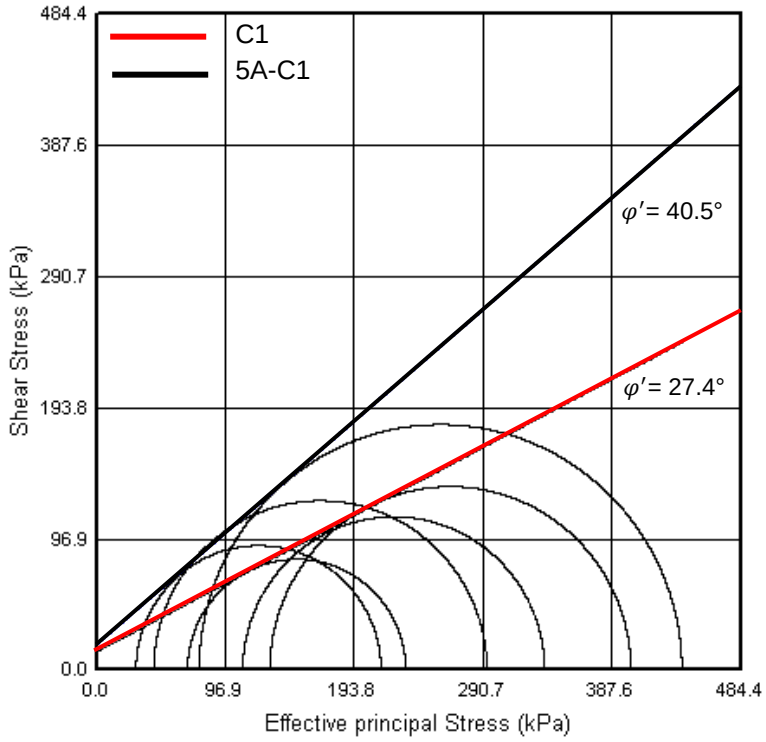

Figure 6.22 Mohr circle diagrams of non-reinforced and 5% ABF fibre reinforced C1 soil specimen prepared at their respective maximum dry unit weight

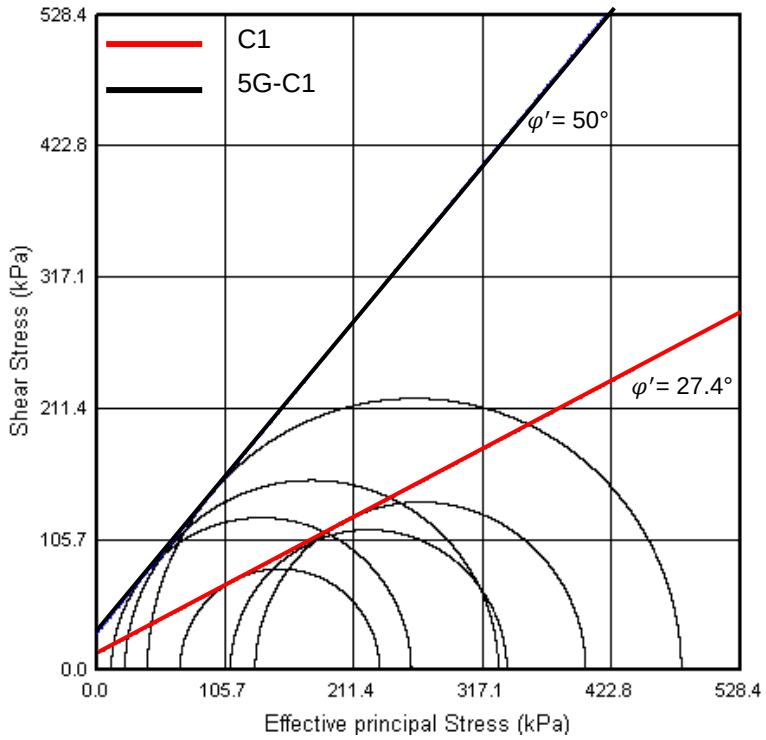

Figure 6.23 Mohr circle diagrams of non-reinforced and 5% GBF fibre reinforced C1 soil specimen prepared at their respective maximum dry unit weight

Shear strength parameters of non-reinforced and fibre reinforced C1 soil specimens prepared at dry unit weight of 17.8 kN/m^3 were also increased significantly with increase in fibre content. It may be concluded that GBF fibres improved both frictional angle and cohesion intercept of the studied clay soil. However, ABF fibres were more effective in improving frictional angle. GBF fibres, because of their rough surface increased the bonding forces between the soil/fibre matrices.

Fibres increased the bonding forces in the soil/fibre matrix physically by linking the soil particles together and making a more uniform continuum. To explain the behaviour of fibres it may be useful to suppose that the soil specimen is made up of micro elements. Therefore, when a soil element is moved under applied shear stresses, it transports the displacement to the very next micro element. This mechanism may cause a movement in the whole group of soil elements unless the applied force is dissipated against arisen friction between them. When fibres are engaged in the soil specimen, they tangle up soil elements together and therefore, form larger macro elements, made up of small elements. In this case, the strength of the whole specimen is increased against applied shear stresses.

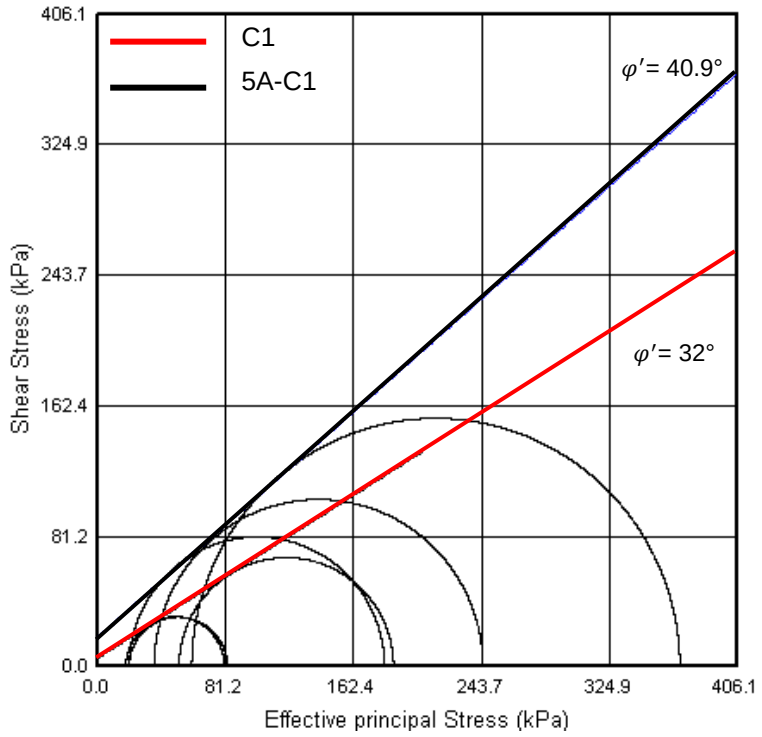

Figure 6.24 Mohr circle diagrams of non-reinforced and 5% ABF fibre reinforced C1 soil specimen prepared at dry unit weight of 17.8 kN/m^3

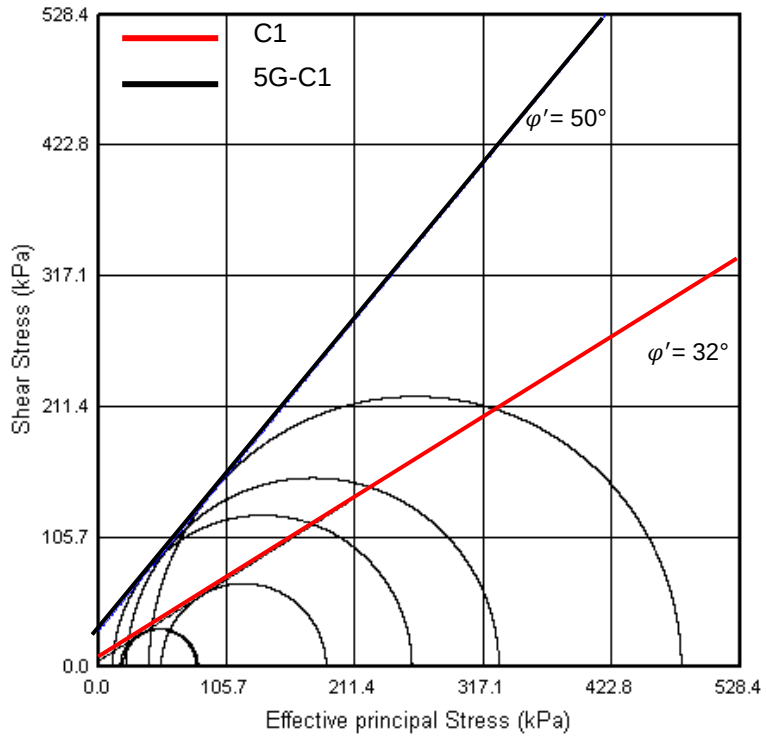

Figure 6.25 Mohr circle diagrams of non-reinforced and 5% GBF fibre reinforced C1 soil specimen prepared at dry unit weight of 17.8 kN/m^3

Table 6.2 Shear strength parameters of C1 soil specimens

Specimen	Dry unit weight (kN/m^3)	c' (kPa)	φ' (Degree)
C1	20.1	13.4	27.4
1A-C1	19.6	16.7	29.7
3A-C1	18.8	9.8	40.8
5A-C1	18.0	18.8	40.5
1G-C1	19.2	16.7	36.0
3G-C1	18.9	36.0	30.1
5G-C1	17.8	29.3	50.0
C1	17.8	5.3	32.0
1A-C1	17.8	15.3	32.0
3A-C1	17.8	14.8	36.9
5A-C1	17.8	18.2	40.9
1G-C1	17.8	13.1	32.5
3G-C1	17.8	16.6	42.3
5G-C1	17.8	29.3	50.0

6.1.8 Evaluating the fibre distribution in specimens

Mixing waste carpet fibres which consist of different materials, shapes and dimensions with cohesive clay soils is not an easy task while fibres tend to become twisted together and create pockets of fibres during mixing. Therefore, mixing efficiency is greatly affected by mixing duration and effort. To evaluate the mixing efficiency of soil and fibres, several GBF fibre reinforced C1 soil specimens were decomposed to evaluate the distribution of fibres. Soil specimens were prepared and cut into three sections and fibre content of each section was determined. Therefore, each section was oven dried to measure the moisture content and subsequently it was crushed using mortar and pestle. To separate the fibres from soil, the whole mixture was washed through 2mm, 1.18mm and 0.150mm sieves accordingly. Clay part of the specimen was washed completely however, fibres specially very short and thin fibres were required to be separated from solid particles. Large clean fibres were retained on 2mm sieve and could be separated easily by hand. The retained materials on 1.18mm and 0.150mm sieves were transferred to a beaker and filled with water. After few seconds of shaking the beaker, solid particles were settled down while fibres were floated on top of the water. By transferring the water including short fibres on 0.150mm sieve, clean short fibres could be collected easily. Table 6 shows the distribution of GBF fibre

content in different parts of the specimens. As inferred from Table 6.3 it is quite obvious that distribution of fibres along the specimen height was relatively uniform however, with increase in fibre content, uniformity of fibre distribution in soil specimens was decreased.

Table 6.3 Variation of fibre distribution in compacted C1 soil specimens (GBF Fibre)

		No	#1	#2	#3	#4	#5
		Fibre content					
Expected Fibre Content	1% Fibre	Top	0.83	0.48	0.65	0.82	0.60
		Middle	1.29	1.39	0.98	1.15	1.19
		Bottom	0.64	0.97	1.02	0.79	0.93
	3% Fibre	Top	1.66	1.91	1.96	1.73	2.68
		Middle	3.00	2.67	3.42	2.68	2.54
		Bottom	3.88	3.23	3.17	2.80	1.98
	5% Fibre	Top	3.60	4.37	3.21	3.38	3.34
		Middle	4.08	5.04	3.85	4.19	3.72
		Bottom	5.28	4.98	4.83	5.01	5.27

6.2 Repeatability of results

The strength parameters and stress-strain behaviour of fibre reinforced soil specimens with random fibre distribution may depend strictly on the alignment of fibres. Therefore, repeatability of the results may also be affected. In order to examine the repeatability of the results, six triaxial tests including three tests on C1 soil specimens prepared at maximum dry unit weight of 20.1 kN/m^3 and three tests on C1 soil specimens with 5% ABF fibre at dry unit weight of 17.8 kN/m^3 were carried out. Figure 6.26 and Figure 6.27 compare the results of the main and repeating tests.

Figure 6.26 shows the deviator stress and excess pore-water pressure of C1 soil specimens prepared at maximum dry unit weight. Results of triaxial consolidated undrained at consolidation stresses of 50 kPa, 100 kPa and 300 kPa showed great degree of repeatability of the results. Shear strength parameters of repeating tests were calculated as c'=8.8 kPa and φ'=28.9°. Comparing the repeated test results to the data shown in Table 6.2 shows that although the apparent effective

cohesion was decreased slightly, the effective frictional angle was almost the same.

Figure 6.27 also shows the deviator stress and excess pore-water pressure of 5% ABF fibre reinforced C1 soil specimens prepared at dry unit weight of 17.8 kN/m^3. Repeating consolidated undrained triaxial tests were carried out at consolidation stresses of 50 kPa, 100 kPa and 200 kPa. Although the fibre distribution plays a key role in repeatability of the results, the successful method of fibre reinforced soil specimen preparation proved high degree of repeatability. Shear strength parameters of repeating 5A-C1 soil specimens were calculated as c'=10.6 kPa and φ'=43.3°. Comparing these results with the data shown in Table 6.2, shows great repeatability of the results.

Effective friction angle values of the repeated tests for non-reinforced and 5% ABF fibre reinforced soil specimens were almost the same. However, the effective apparent cohesion values were reduced by 30% to 40%. Given the fact that the effective apparent cohesion values of the main tests were very small, the arisen reduction in repeating tests is not significant. Moreover, according to the data shown in Table 6.2, fibres used in this study contributed better in enhancing the frictional angle of C1 soil specimens and their influence on apparent cohesion was insignificant.

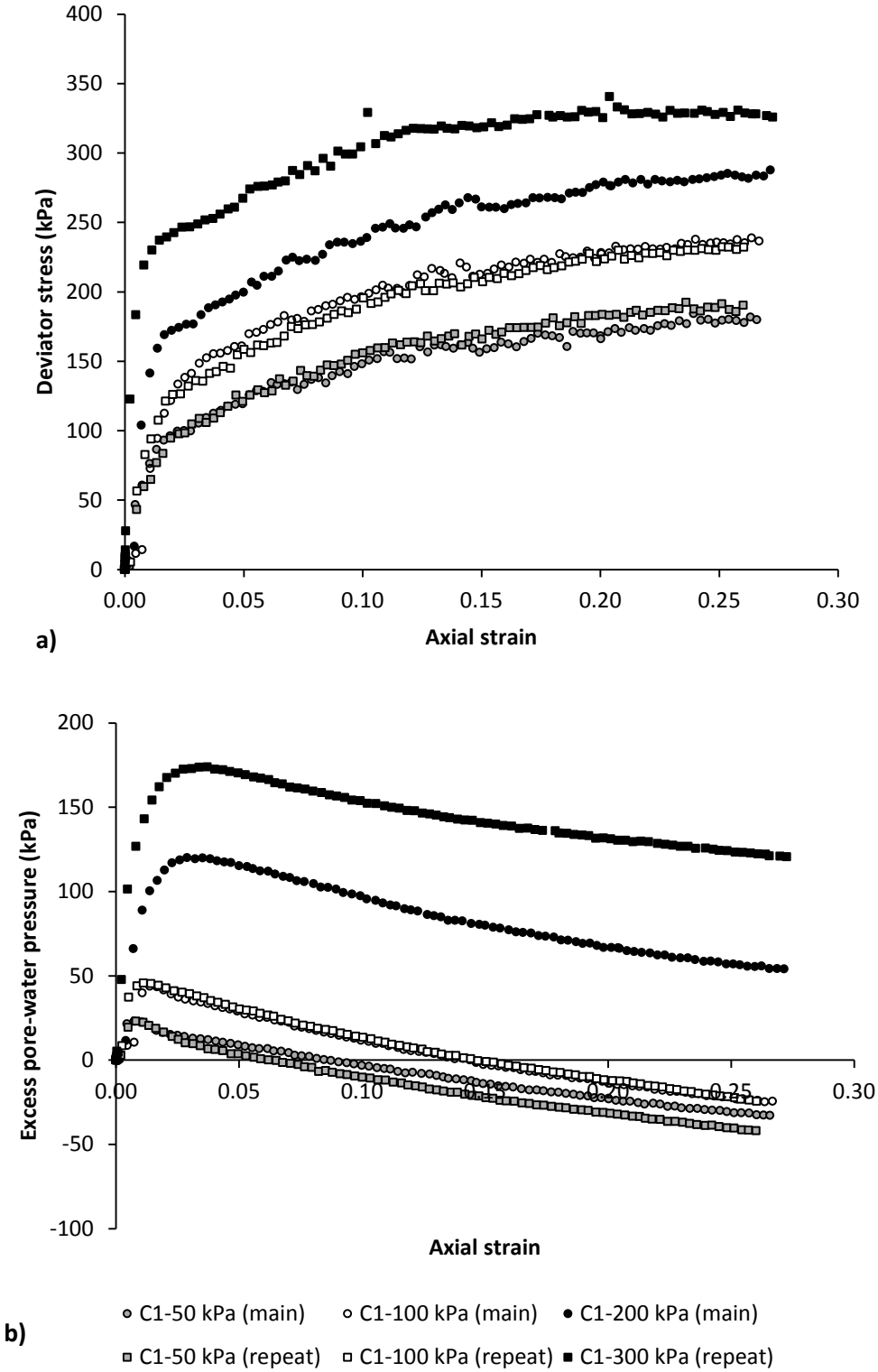

Figure 6.26 Results of repeating tests of C1 soil specimen prepared at maximum dry unit weight of 20.1 kN/m^3
a) Deviator stress b) Excess pore-water pressure

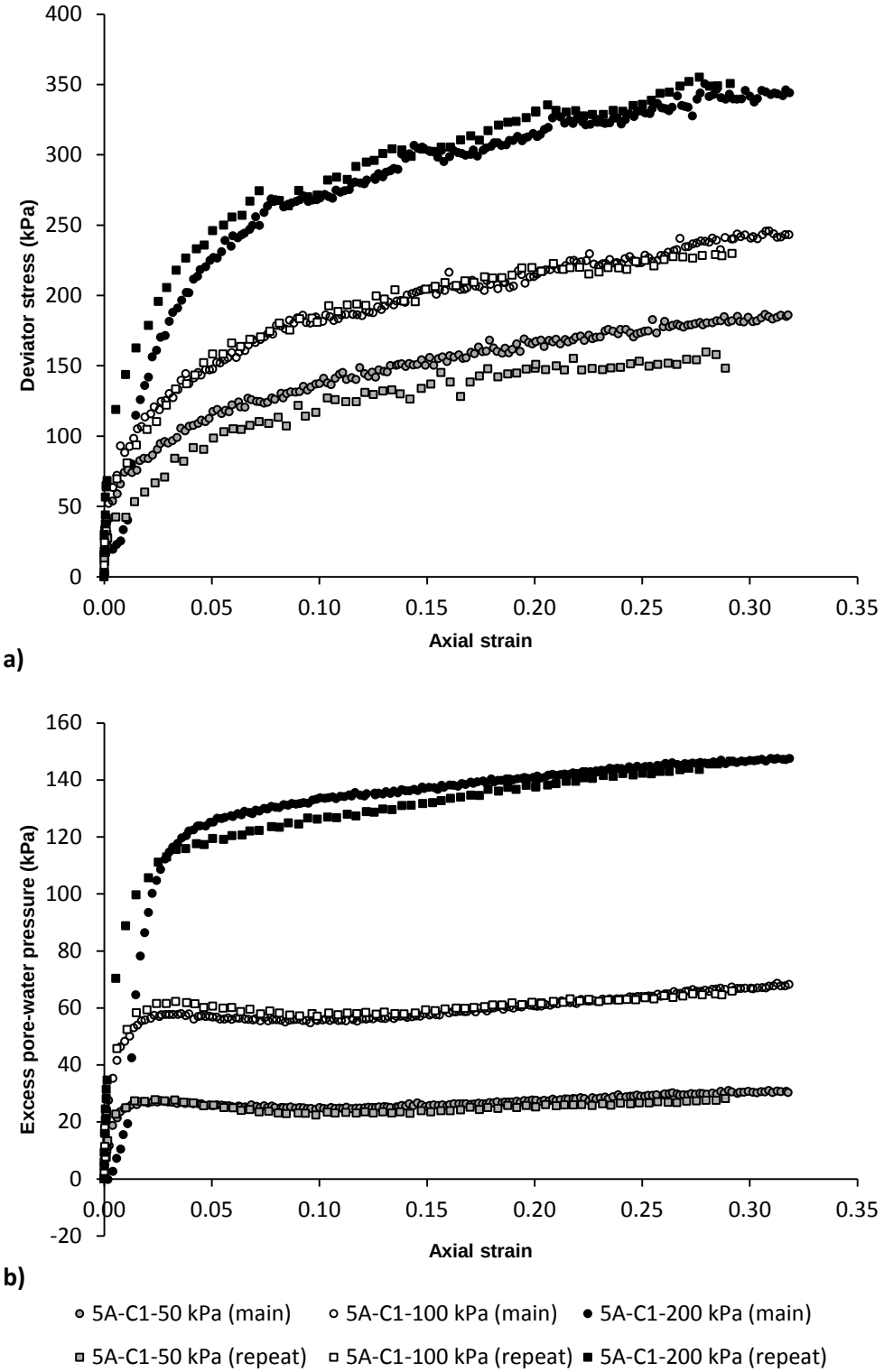

Figure 6.27 Results of repeating tests of C1 soil specimen with 5% ABF fibre prepared at dry unit weight of 17.8 kN/m^3 a) Deviator stress b) Excess pore-water pressure

6.3 Summary of the findings

Based on the results of the consolidated undrained triaxial tests carried out on non-reinforced and fibre reinforced soil specimens prepared at different initial density and moisture content conditions the following conclusions are made:

1) Although increase in fibre content resulted in reduction in maximum dry unit weight of the fibre reinforced soil, the shear strength of the reinforced soils increased significantly with increase in fibre content.

2) Cohesion intercept and internal friction angle of the fibre reinforced soil specimens prepared at their respective maximum dry unit weight increased significantly with increased fibre content. For example the cohesion intercept and internal friction angle increased from 13.4 kPa and 27.4 degree respectively for non-reinforced soil to 29.3 kPa and 50 degree for 5% GBF fibre reinforced. This implied 82% increase in internal friction angle of the reinforced soil with including 5% GBF fibre content.

3) For specimens prepared at the same dry unit weight of 17.8 kN/m^3, the shear strength parameters also increased significantly with increase in fibre content. For example the cohesion intercept and internal friction angle of non-reinforced soil (i.e. 5.3 kPa and 32 degree respectively) increased to 29.3 kPa and 50 degree with increase in GBF fibre content to 5%.

4) Non-reinforced soil specimens compacted at their maximum dry unit weight showed dilative behaviour. And pore-water pressure reduced significantly with evolution of axial strain after reaching a peak at small strains.

5) Increase in fibre content of specimens prepared at their maximum dry unit weights resulted in increased pore-water pressure. However, for specimens prepared at the same dry unit weight, the pore-water pressure did not change significantly. This showed that the pore-water pressure in undrained condition was more dependent on initial void ratio of the specimen rather than its fibre content. Increased initial void ratio resulted in increased pore-water pressure during shear stage.

Chapter 7 Neural network analysis

Summary

Artificial Neural Networks (ANNs) are information-processing systems which resemble human's consecutive cells known as neurons. Artificial neural networks are widely used in science to solve complex problems involving multitudes of variables.

In this chapter, an introduction to artificial neural networks is given. A neural network analysis is carried out on the results of the consolidated undrained triaxial shear tests of fibre reinforced C1 soil. Hence, a neural network model is developed for predicting the deviator stress of fibre reinforced C1 soil specimens. A coupling effect analysis is also carried out on the predictions of the proposed model.

7.1 What are Artificial Neural Networks

An artificial neural network is an information-processing system that has been intrigued by its common characteristics with biological neural networks. A neural network includes multitudes of simple processing elements (i.e. known as neurons, units, cells, or nodes) which work in parallel.

Architecture of a neural network consists of weighted interconnections between neurons by means of directed communication links. The weights are used by the network to solve a problem. Each neuron has an activity level, which is a function of the values of input parameters (Fausett, 1993). In the current study the term 'Artificial Neural Network' may interchangeably be used by short form of 'Neural Network'.

In fact, neural networks can be defined as powerful pattern recognisers and classifiers. A neural network can be considered as a black box, model-free, and adaptive tool to perceive and learn behaviour of a complex system using systematic inter-relations between input data.

Neural networks have extensively been used in variety of problem solving strategies in science and engineering. Successful applications of neural networks in civil engineering including structural analysis and design (Adeli and Yeh , 1989, Vanluchene and Sun, 1990), design automation and optimisation (Adeli and Park, 1995) and finite element mesh generation (Manevitz et al. 1997) have been reported repeatedly.

Geotechnical engineering complex problems have also not been excepted from the ongoing application of neural networks in engineering. Neural networks have been used in wide variety of problems in geotechnical engineering such as evaluating the CPT calibration chamber test data (Goh, 1995), modelling stress-strain and volume change of soil in triaxial compression test (Penumadu and Zhao, 1999, Banimahd et al., 2005), prediction of the Oedometer test results on the basis of the basic soil properties (Turk et al., 2001), prediction of shear strength parameters of fibre reinforced sand (Ghiassian et al., 2006), prediction of shear strength parameters of clay soils (Goktpe et al., 2008).

7.2 Architecture and processing technology of Neural Networks

A very close analogy resembles the structure of the processing element (artificial neuron) in neural networks to a biological neuron. Figure 7.1 shows general structure of a biological neuron cell. A biological neuron has three types of components including dendrites, soma, and axon. Dendrites receive signals from other neurons. Signals in fact consist of electric impulses that are passed through a synaptic gap by means of a chemical process. The chemical process alters the input signals (by scaling the frequency of the input signals). The soma, or cell body, sums the incoming signals. Once, sum of incoming signals reaches sufficient level, a signal transmits over axon to other cells (Fausett, 1993).

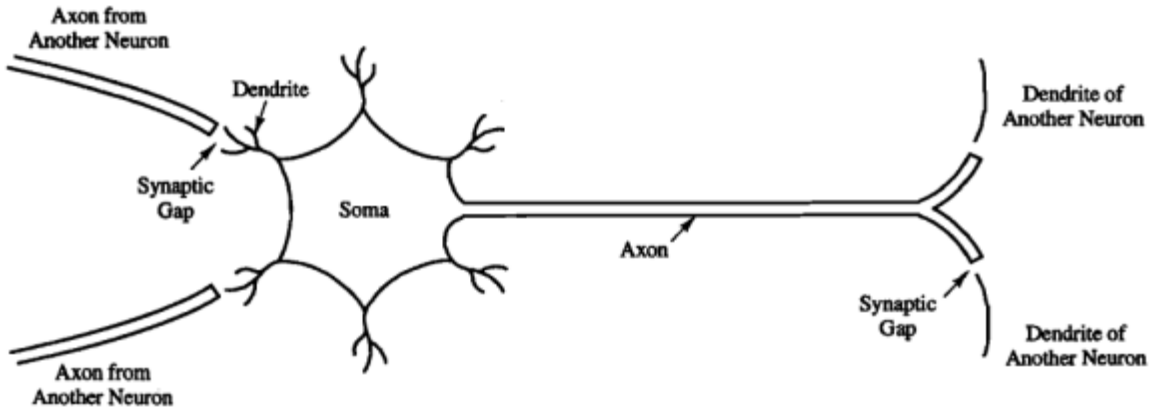

Figure 7.1 Structure of the human brain's neuron cells (Fausett, 1993)

Figure 7.2 shows architecture of a neural network. A generic structure of neural network incorporates a number of processing elements (i.e. nodes) which are arranged in three types of layer:

a) an input layer
b) one or more hidden layers
c) an output layer

The relation between input layer and hidden layer(s) is adjusted by a series of inter-connection weights which define the intensity of inputs to hidden layer(s). A hidden layer also is connected to the successive hidden layer or output layer by means of weighted inter-connections. All weights in the neural network must be optimised somehow to correlate the input layer to the output layer. The process of weight optimisation of a neural network is called 'Learning' or 'Training' algorithm.

Training of the neural network model can be performed in several ways. Back propagation is the most widely used and understood supervised learning method for training neural networks. Its simple architecture and easy to understand learning process have made it the default choice for most of neural network models.

The back propagation scheme comprises two major steps including forward activation and backward error flows. Therefore, input values of each neuron (processing element) is multiplied by corresponding connection weight (w_{ji}). All weighted input values of each neuron are summed and a threshold value (θ_j) is also added. Output value (Y_j) is then produced by applying a nonlinear transfer function ($f(.)$) on the combined input (I_j). Equations (7.1) and (7.2) show the neural network internal calculations (Shahin et al., 2002).

$$I_j = \sum w_{ji} X_i + \theta_j \tag{7.1}$$

$$Y_j = f(I_j) \tag{7.2}$$

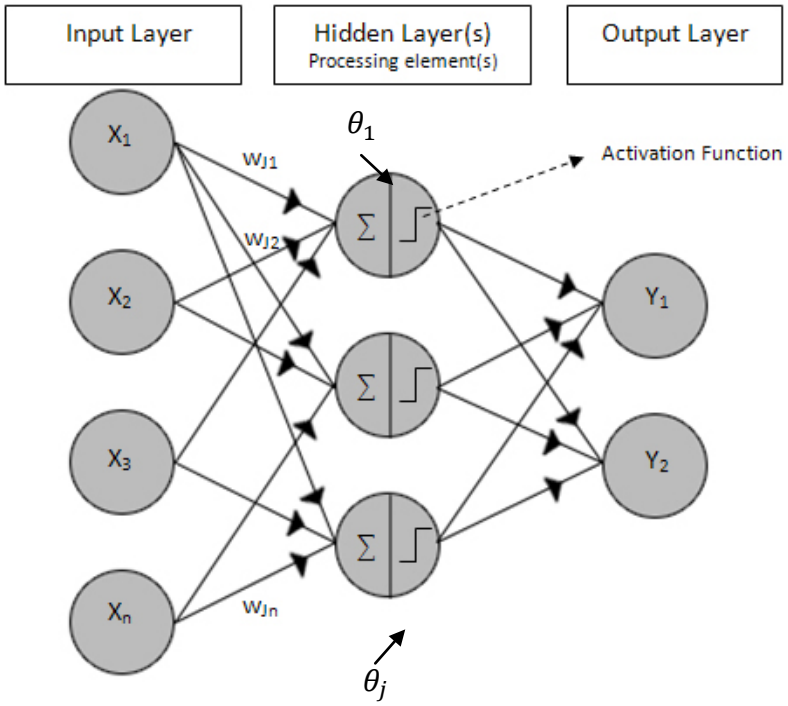

Figure 7.2 Structure of an artificial neural network

The propagation of information in neural network initiates at the input layer with introducing a set of input data and the corresponding (desired) outputs. Initially, a set of arbitrary weights are attributed to the nodes' inter-connections. After first round of calculations, the actual output(s) of the network is then compared with the desired output(s) and error is calculated. This error is used along a learning rule; to re-adjust the weights (Back propagation method). This process repeats until a set of weights is resulted in such manner that produces the input/output mapping with the smallest possible error. Once the learning process is carried out successfully, the performance of the trained model has to be validated using an independent set of data used for validation.

Detailed procedure and techniques about neural network modelling is beyond the scope of the current chapter. A comprehensive explanations and details of the neural network modelling such as type of network (i.e. feed back, feed forward) and type of training algorithm (i.e. supervised, unsupervised) can be found elsewhere (e.g. Fausett, 1993, Maier and Dandy, 2000 and Galushkin, 2007).

Therefore, the resulted neural network model learns from set of data examples which are presented to the model by adjusting the inter-connection weights to perceive the relationship between the input variables and the corresponding output(s).

Neural network model does not need any previous knowledge about the nature of the relationships between the input/output variables. This can be considered as one of the benefits of neural networks compared with the other empirical and statistical methods (shahin et al., 2002).

7.3 Review of application of neural networks for fibre reinforced soils

Neural network modelling for constitutive modelling of materials behaviour was first introduced by Ghaboussi et al. (1990) for bi-axial behaviour of concrete. Neural network modelling has also been used extensively in diverse range of applications in geotechnical engineering. A multilayer neural network with enough nodes in hidden layer(s) has been proved to approximate a nonlinear function to high degree of accuracy on a compact set of input-output knowledge

(He and Li, 2009). There are also examples of using neural networks for modelling mechanical behaviour of reinforced soils.

Ghiassian et al. (2006) examined a neural network on the results of 125 triaxial drained tests on silty sand reinforced with carpet waste in form of strips. Their neural network model consisted of an input layer including fibre content, fibre aspect ratio, confining stress and an output layer including peak deviator stress, residual stress, axial and volumetric strain at peak strength and the maximum modulus. They used back propagation method on a neural network comprising of two hidden layers and reported very high correlation coefficient for testing data which showed the efficiency of the trained network.

He and Li (2009) carried out a neural network analysis on the results of consolidated undrained triaxial tests of sand reinforced with short fibres and lime. Input parameters of 34 triaxial tests including effective confining stress, fibre and lime content, specimen curing period and axial shear strain were used to train a neural network with four nodes (as a hidden layer) to predict the axial shear stress of the soil specimen using back propagation method. Parameter's sensitivity and coupling effect of input parameters were also analysed using the constructed neural network model. The results showed satisfactory predictions by constructed neural network model and it was concluded that mechanical properties of the studied soil are more sensitive to lime content rather than fibre content.

Edincliler et al. (2010) developed a neural network with 5 inputs, 3 hidden layers and a single output for predicting deviator stress of mixture of sand and tyre waste using quick undrained and consolidated drained triaxial tests. Input parameters were chosen as waste tyre content, type of waste tyre, effective confining stress, test type and strain value and the only output was deviator stress. The proposed neural network was found to perform fairly satisfactory and the results were accurate enough.

7.4 Modelling results of CU triaxial tests with neural network

The results of consolidated undrained triaxial compression tests which were demonstrated in previous chapter were used to model the deviator stress of the

fibre reinforced C1 soil specimens. In this study MATLAB package was used for simulating and modelling. The following parameters were used as input of the neural network:

a) Type of fibre (1: No fibre, 2: ABF fibre, 3: GBF fibre)
b) Fibre content (0: 0%, 1: 1%, 3: 3%, 5: 5%)
c) Dry unit weight (kN/m^3)
d) Effective confining stress at start of shear stage (consolidation stress(kPa))

Deviator stress at 20% axial strain was correlated as a single output parameter to input parameters.

Performance of neural networks is highly dependent on its architecture and parameter settings. It has been shown that a three-layer neural network (including input layer) with differential transfer functions and sufficient number of neurons in hidden layer can approximate any nonlinear relationship (Banimahd et al., 2005). Moustafa (2011) carried out a research on optimisation of architecture of neural networks via several examples. He concluded that using a single hidden layer with number of neuron equal to the square of the number of inputs leads to an optimal neural network by means of minimising the number of iterations (training stages) which in essence diminishes the processing time required to train the network.

In the current study results of 45 consolidated undrained triaxial compression tests where used to train a neural network with 4 inputs, 16 nodes in the only hidden layer and one output. For maintaining continuity in predicted data by neural network model, some repeating data were also included in the input data set. These data were consisting of fibre reinforced soil specimens by setting fibre content to zero (representing specimen without fibre: i.e. specimen with 0% ABF/GBF fibre content which is the same data set with specimen with no fibre). Therefore, the number of input data sets was virtually increased to 57.

The Levenberg-Marquardt back propagation algorithm was used to train the neural network model with 80% of the results (45 tests) by random. The rest of data (i.e. 20%) were used to validate and test the neural network model. Training set was used to adjust the weights and biases of the network model by back

propagation method. However, a validation set of data was also used to measure network generalisation to stop the training once it stopped improving. Testing set was an independent set of data which had not yet been introduced to the model and therefore it was used to measure the performance and accuracy of the model. The hyperbolic tangent sigmoid function (equation (7.3)) was applied for the hidden layers:

$$f(x) = \frac{e^{x} - e^{-x}}{e^{x} + e^{-x}} \qquad \text{Sigmoid function} \qquad (7.3)$$

The Purelin activation function which is a linear function was used to transfer output of hidden layer to output layer. The initial weights and biases of the inter-connections between neurons in a network model are chosen by random and therefore, there must be enough training iterations to achieve lowest level of error (difference between actual targets and predicted outputs by model).

Mean squared error was used as a mean of measuring error in the proposed model. Hence, the training process was repeated several times and the final weights that led to lowest mean squared error were used in the model. Figure 7.3 shows the architecture of the neural network model used in the current study. Table 7.1 lists all weights and biases used in the current model. Table 7.1 also shows the mean squared error of the network for training, validating and testing data sets. Regression correlation factor (R^2) for training, validating and testing data sets were highly close to unity and therefore, the relationships between target data and predicted values were close enough to rely on the results of neural network model.

Figure 7.4 and Figure 7.5 compare the deviator stress values from results of the triaxial tests and predicted values by neural network for soil specimens with dry unit weight of 17.8 kN/m^3. These figures show that the predicted results using neural network model data were fairly satisfactory and precise and the proposed neural network model was highly efficient. It seems that the developed neural network model can predict deviator stress of GBF fibre reinforced specimens more precisely compared to that of ABF fibre reinforced soil specimens. However, the accuracy of the model can be enhanced by introducing more input data set to cover a wider range of input parameters.

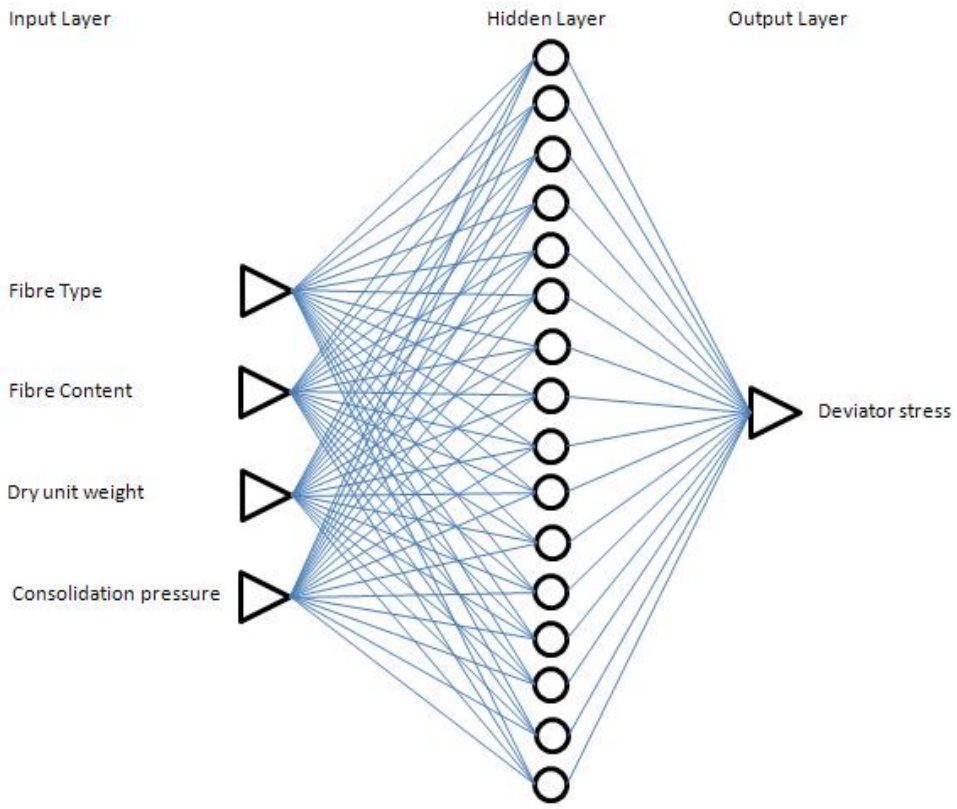

Figure 7.3 Architecture of the neural network model used in the current study

Table 7.1 Values of weights and biases of the trained neural network

W^1 (Weights to hidden layer) (16x4)	-1.0289	-1.8666	0.78048	1.0092
	-1.3669	-1.1606	-2.1216	0.36142
	-1.0629	1.3718	-2.2199	-0.11053
	0.14073	1.5552	0.68602	□.4224
	1.2041	-0.04182	-2.2773	0.024521
	-0.15174	-0.89845	2.2463	-2.1777
	-0.56486	-1.3811	-0.9938	-2.1873
	1.1815	-0.82188	-1.7372	-1.4814
	1.9695	-0.28808	-2.3306	0.16904
	-2.0877	-0.92105	-1.035	-0.16407
	-2.4809	-1.3149	-0.77147	0.62937
	0.058776	-1.6584	-1.9575	-1.5817
	-1.9332	1.454	-0.95024	0.26604
	0.29785	1.0236	0.40491	-2.292
	-0.6994	-1.3318	-1.918	-1.9316
	-0.21861	2.4395	-0.70823	-0.76574

W^2 (Weights to output layer (1x16) (from left to right)

-0.062156 0.049177 0.024545 1.0365 -0.4033 -0.3799 0.26889 -0.10728 0.16121 0.086636 -0.1654 -0.53987 -0.68142 0.0069184 0.11527 0.3964

Biases to hidden layer (16x1) (from left to right)

2.9364 2.5382 1.9365 -1.7824 -1.5364 1.2742 0.39668 0.0567 0.56262 -0.44155 -1.2481 -0.93496 -1.8614 2.1593 -2.2145 -2.8463

Bias to output (1x1)	0.42369	
	Mean Squared Error (MSE)	R^2 (Regression correlation factor)
Training set	109.7484	0.9935
Validation set	275.7583	0.9918
Testing set	93.7088	0.9949

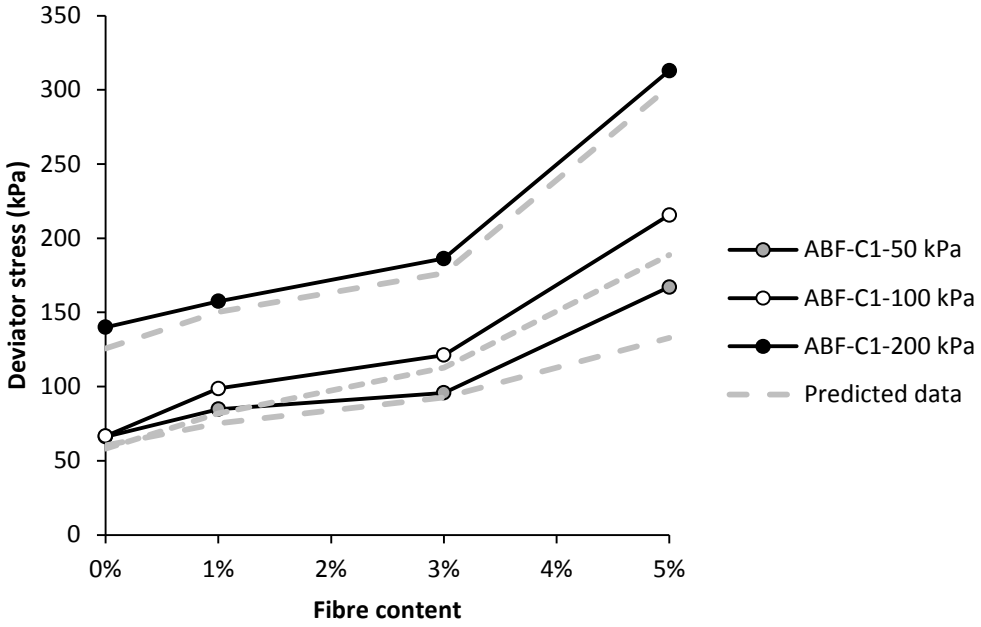

Figure 7.4 Comparison between test results and model predictions for ABF fibre reinforced soil specimens prepared at 17.8 kN/m^3

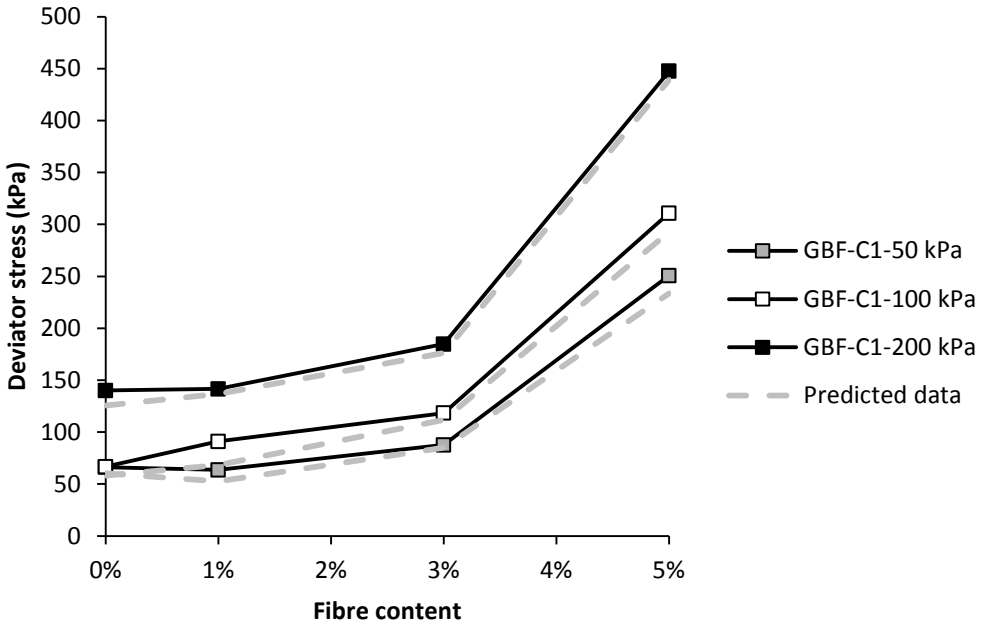

Figure 7.5 Comparison between test results and model predictions for GBF fibre reinforced soil specimens prepared at 17.8 kN/m^3

7.5 Coupling effect of the model's input parameters

In order to investigate the coupling effect of input parameters, a simple code was written in MATLAB to simulate wide range of input parameters using the developed neural network model and draw the changes in fibre content, consolidation stress and deviator stress in a 3D graph. Figure 7.6 and Figure 7.7 show the influence of fibre content and consolidation stress on deviator stress of specimens compacted at dry unit weight of 17.8 kN/m^3.

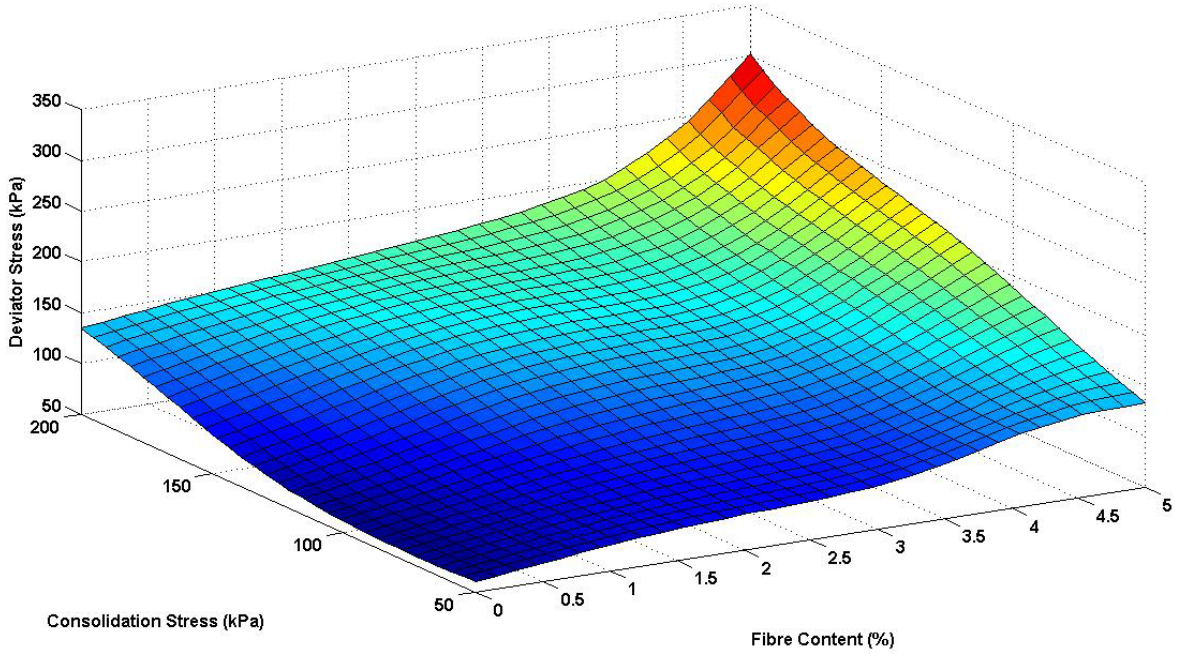

Figure 7.6 Coupling effect of fibre content and consolidation stress on deviator stress of ABF fibre reinforced specimens compacted at 17.8 kN/m^3

It can be seen in Figure 7.6 that at zero fibre content increase in consolidation stress from 50 kPa to 200 kPa resulted in increase in deviator stress with relatively low exponential growth rate. However, the rate of growth was reduced in vicinity of 200 kPa of consolidation stress.

At 5% ABF fibre content increase in consolidation stress to 200 kPa was followed by high exponential growth in deviator stress. However, it seems that beyond consolidation stress of 200 kPa, the deviator stress may increase dramatically with fibre content. Of course, the current neural network model can not effectively

support the relationship between deviator stress, fibre content and consolidation stress beyond the limit of the input parameters. And further input data sets are required to conclude such relationships.

On the other side, at low consolidation stress (i.e. 50 kPa) the deviator stress increased almost linearly with increase in fibre content. However, increase in consolidation stress turned this relationship into an exponential growth. Therefore, it can be concluded that addition of ABF fibres as well as increase in consolidation stress, significantly influenced the deviator stress of ABF fibre reinforced C1 soil specimens.

Figure 7.7 shows that increase in GBF fibre content at all consolidation stresses (from 50 kPa to 200 kPa) resulted in high exponential growth in deviator stress. This shows that the stress-strain relationship of GBF fibre reinforced C1 soil specimens is more sensitive to fibre content rather than consolidation stress. Comparing Figure 7.6 and Figure 7.7 denotes that contribution of GBF fibres in enhancing the deviator stress of the C1 soil was more significant compared to that of ABF fibres.

Increase in both consolidation stress (from 50 kPa to 200 kPa) and fibre content (from 0% to 5%) simultaneously resulted in continuous increase in deviator stress. The proposed neural network model may only be valid for input data within the tested range. Therefore, further tests are required for increasing the size of the database of input data to increase the extent of prediction by proposed neural network model.

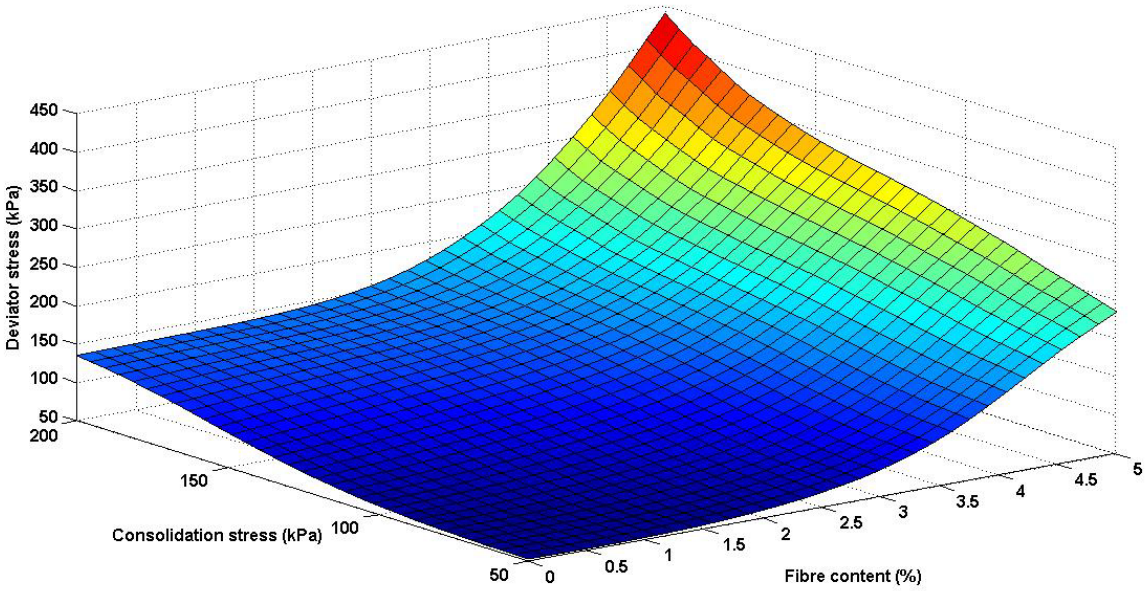

Figure 7.7 Coupling effect of fibre content and consolidation stress on deviator stress of GBF fibre reinforced specimens compacted at 17.8 kN/m^3

7.6 Summary of the findings

A neural network model was developed based on the results of 45 consolidated undrained triaxial shear tests to predict the maximum deviator stress at failure. The architecture of the developed neural network model comprised 4 input parameters of type of fibre, fibre content, dry unit weight and consolidation stress, 16 nodes in a single hidden layer and an output of maximum deviator stress.

The results showed that predicted results using the neural network model were fairly satisfactory and the proposed neural network model was highly efficient.

The introduced model was used to investigate the coupling effect of fibre content and consolidation stress on deviator stress at failure of soil specimens prepared at the same dry unit weight. The results showed that at the same consolidation stress, the rate of increase in deviator stress increased exponentially with increase in fibre content.

At constant consolidation stress, increase in deviator stress due to increase in fibre content changed from a linear relationship to an exponential one.

Coupling increase in fibre content and consolidation stress significantly enhanced the deviator stress and hence mechanical behaviour of fibre reinforced soil.

The number of triaxial tests for developing a comprehensive neural network was limited and therefore, the precision of the proposed model can be further improved by including more input data set into the data base.

The current model was adjusted based on the results of triaxial test on C1 soil specimens and cannot be used for other soils unless the proposed neural network model is trained along with intrinsic characteristics of different soils such as clay content, plasticity index, and specific gravity.

Chapter 8 Determination of bearing pressure of fibre reinforced embankments with the aid of Particle image velocimetry analysis

Summary

In this chapter, to evaluate the bearing pressure of fibre reinforced embankments, laboratory scaled model slopes are studied. Strip footing load is applied at top of the model slope at different distances from crest of the slope. Applied load on the strip footing, settlement of footing, induced total pressure at the bottom of model and pore-water pressure within the soil are measured using appropriate instruments.

Particle image velocimetry method is used to study the displacements occurred under footing. The results of stress-strain behaviour and generated pore-water pressure in the soil are discussed accordingly.

.

8.1 Model slope tests

8.1.1 Introduction

A laboratory model slope was designed and built at the University of Bradford in order to evaluate the bearing pressure and settlement behaviour of strip footing resting on the fibre reinforced clay soil. Therefore, a wooden tank was made with dimensions of 800mm (L) x 300mm (W) x 500mm (H). The tank was made rigidly to avoid any volume change during preparation of the slope and also during the test. The front door was especially designed so as to open after compaction of soil to sprinkle dyed sand to facial view of the slope. Dyed sand was sprinkled to the front view of the slope to produce suitable texture for recognising displacement of particles between consecutive images using particle image velocimetry[13] (PIV) method. After sprinkling the dyed sand, the front door was firmly fastened using two pairs of large bolts on both sides of the frame.

The front side of the tank was made of a thick transparent Perspex glass (i.e. thickness of 15mm) to make it possible to observe the deformation of the compacted soil during the test and to minimise its deformation. Figure 8.1 shows the tank used for this experiment. A mesh of 6x4 circular holes was created on the rear side of the box for installing suction probes. In the case of not intending to use the holes, they could be sealed separately using special plugs.

8.1.2 Instrumentation

A loading frame with capacity of 5kN was used to apply axial load on the strip footing. The moving beam of the loading frame was equipped with a load cell to measure the axially applied load. A long steel extension rod was connected to the bottom end of the load cell to transfer the applied load to the strip footing.

A solid steel plate with dimensions of 280mm (L) x 50mm (W) x 5mm (T) was used as footing on the soil slope. Therefore, the L/B ratio of 5.6 (i.e. greater than 3)

[13] Particle Image Velocity method: method to calculate the particle's displacement by comparing successive acquired images

confirmed the behaviour of the footing as strip footing. Two LVDT sensors were installed on both sides of the strip footing for measuring settlement of the footing.

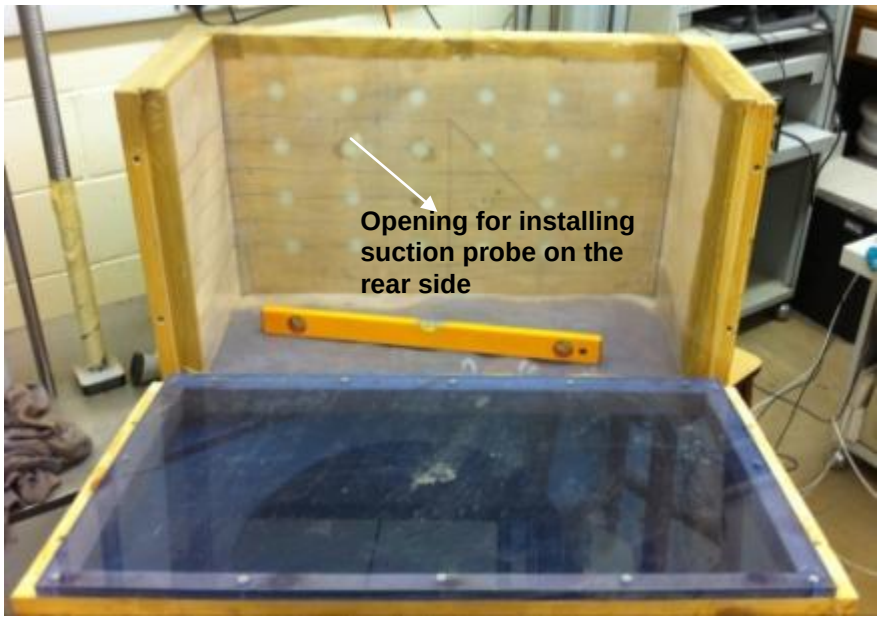

a) opening side of the tank

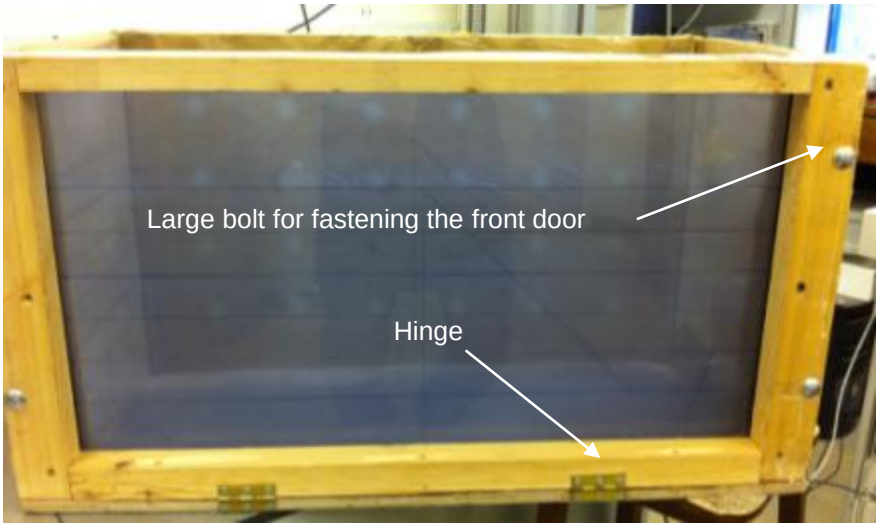

b) front transparent side of the tank hinged to the base

Figure 8.1 Rigid tank made for bearing pressure tests

For evaluating the influence of fibres on distribution of the applied stress to the lower layers, three pressure cells were installed on the base of the tank to measure the distributed total stress on the base of the tank.

Two mini suction probes were also installed on the rear side of the tank to measure the possible negative pore-water pressures in tension zones. Details of the structure and method of calibration of the developed suction probes have been previously discussed in Chapter 4.

8.1.3 Strip footing loading tests

According to the results of triaxial consolidated undrained tests, it was concluded that GBF fibres contributed better to increase the shear strength of the C1 soil specimens. Hence, in this testing programme, influence of GBF fibres on stress-deformation relationships and ultimate bearing pressure of the fibre reinforced model slopes was investigated. Figure 8.2 shows the schematic features and dimensions of the model slope. The model slope was made of C2 soil on a layer of compacted fine sand with thickness of 100mm. C2 soil had the same origin with C1 soil and their particle distribution curves were almost the same with difference in their fine content. Therefore, the plasticity index of C2 soil was less than that of C1 soil.

A total of 11 model slopes were constructed and tested under different conditions of varying fibre content and varying distances of footing from crest of slope. Table 8.1 shows the details of the experiments and location of the sensors in each experiment. Distance of footing from crest of slope was defined as non-dimensional parameter of ratio of distance of footing from crest and width of footing.

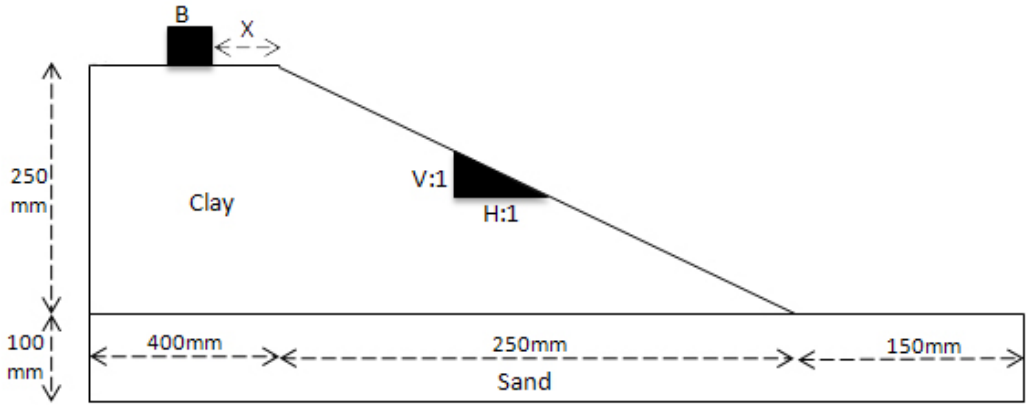

Figure 8.2 Dimensions of the model slope

Table 8.1 Details of the strip footing loading experiments

Test No.	B (mm)	X/B	Fibre content (%)	Horizontal position of pressure cells (relative to the centre of footing)(mm)	[14]Horizontal position of suction probes (relative to the centre of footing)(mm)
1	50	0	0	-75, 0, +75	-50, +70
2	50	0	1	-75, 0, +75	-50, +70
3	50	0	3	-75, 0, +75	-50, +70
4	50	0	5	-75, 0, +75	-50, +70
5	50	1	0	-75, 0, +75	-120, 0
6	50	1	1	-75, 0, +75	-120, 0
7	50	1	3	-75, 0, +75	-120, 0
8	50	3	0	-75, 0, +75	-20, +100
9	50	3	1	-75, 0, +75	-20, +100
10	50	3	3	-75, 0, +75	-20, +100
11	50	3	5	-75, 0, +75	-20, +100

8.1.4 Mixing fibres and soil in large scale quantities

The method of preparation of fibre reinforced soil specimens was earlier described in section 03.9. However, the mass of the soil required for preparation of model slope was not comparable with that required for preparation of small 38mm diameter soil specimen for triaxial test. For each soil model slope experiment

[14] All suction probes were installed at the same depth underneath the footing (i.e. 152mm)

approximately 71 kg of C2 soil was used. However, for preparing a triaxial soil specimen approximately 150 to 180 grams of soil was used.

Therefore, to adapt the previous procedure to mass soil mixing, the same procedure as that described in Chapter 3 was used to mix GBF fibres with C2 soil using a rotary drum mixer. For each layer, the whole amount of C2 soil, fibre and water were divided in to three equal portions and mixed accordingly. Mixing was continued for 5 to 8 minutes for each trial. The achieved mixture was uniform enough to be used for compaction in layers. Figure 8.3 shows the mixing procedure using a rotary drum mixer.

8.2 Procedure for preparation of the model slope

To evaluate the influence of GBF fibres on load carrying capacity and load-deformation relationship of the C2 soil, a common value for dry unit weight and moisture content for all experiments was chosen. Therefore, C2 soil was compacted at dry unit weight of 17.8 kN/m^3 and 16.5% moisture content in 5 equal layers. The model slope was underlain by a sand layer with a thickness of 100 mm compacted at dry unit weight of 18.0 kN/m^3 and 7% moisture content as a base layer for the slope to provide a relative hard natural boundary.

An impervious plastic was used to cover all internal sides of the tank to reduce the effect of interface friction between the soil and the tank. The procedure of the experiment started with positioning the pressure cells at predefined locations (See Table 8.1). Afterwards, the sand layer was compacted followed by compaction of the clay soil in five equal layers. A small stainless steel plate was used to compact the soil layers inside the tank manually. To control the compaction, the boundary of each layer was previously marked on the plastic cover. All layers were compacted in 50mm layers. However, the weight of material for each layer was calculated in such way that the dry unit weight remained constant (i.e. 17.8 kN/m^3). Care was taken to maintain the angle of the front side of the slope at 45 degrees. In order to do this, a steel plate slope regulator with two handles was used to regulate the front slope to a given angle. After preparation of the slope, its surface was further checked using a spirit level to be levelled.

For each test, suction probes were saturated under 1800 kPa overnight and they were calibrated and installed on the rear side of the tank just before starting the experiment. Surface of the suction probes were smeared with a thin layer of wet kaolinite to create better interface between soil and ceramic disc of the suction probe. Figure 8.4 shows procedure of the preparation of the model slope. Once the model slope was made, sensors including LVDT and load cell were brought in contact with the strip footing and their initial values were set to zero.

Figure 8.3 Mixing fibres and soil in large quantities using rotary drum mixer

Figure 8.4 Procedure of preparation of model slope

8.2.1 Preparation of slope for particle image velocimetry

In order to operate the PIV image processing method for analysing the displacement induced in the model slope, a recognisable texture was required to be added to its exposed plane using coloured 'flock' material or fine sand (White et al., 2001). In this study, a mixture of light and black (dyed) sand was used as artificial texture of the clay soil. Therefore, tracking the displacements of the clay soil particles under loading by means of post image processing was made easier.

After compaction of the soil layers, the front door of the tank was opened carefully in such a way to reduce disturbance of the compacted soil. Mixture of light and

black dyed sand was sprinkled randomly on to the front plane of the model slope in a thin uniform layer.

One of the most critical issues in acquiring suitable images for analysing by PIV method is to adjust light sources. Any type of light source which can create constant light intensity on the spot can be used. In this project two bulb light projectors were used at relatively wide angle to normal plane to the Perspex glass. The angle of the light projectors to normal plane to the Perspex glass was chosen based on trial and error to reduce the light reflection from the surface of the Perspex glass and also to create a uniform intensity of light on the surface of the glass.

After adjusting the location of the camera and light projectors, a calibrating board (product of Dantec Dynamics[15]) was placed at centre line of footing for calibration of the camera and few pictures were taken. Experiment was carried out in a completely dark room with just the light projectors as the only source of light.

All experiments were carried out at footing axial displacement rate of 1 mm/min and data captured by the load cell, LVDT, pressure cells and suction probes were recorded using a data logger. Consecutive pictures were taken at intervals of 20 seconds. To correlate the pictures with the data recorded by the data logger, the sampling rate of the data logger was also set to 3 samples per minute (1 sample at interval of 20 seconds). Figure 8.5 shows the setup of the experiment.

[15] http://www.dantecdynamics.com

Figure 8.5 Setup of the model slope and positioning of the camera and projectors

8.3 Image-based deformation analysis

Precise measurement of deformation is one of the key requisites in most geotechnical testing and modelling practices. Traditional methods of measuring deformation of geotechnical materials under loading sequences have been mostly involved with using locally attached mechanical dial gauges and sensors such as LVDT. These methods are usually accompanied with continuous measurement of deformation at exterior point(s) on boundary of the soil mass and do not give a vector field of deformations inside the soil mass. However, the application of these methods to determine the deformation of spot point(s) does not require any post-experiment calculation and an online measure of deformation can be read out during the experiment.

The other available methods for measurement of deformation in planar exposed view of the soil mainly rely on intrusive target markers on the soil and video image capturing. Therefore, artificially intrusive markers are tracked on the spot area through consecutive photographs taken at suitable intervals. These methods (known as image-based techniques) involve a series of post-experimental analysis to determine gradual movement of the spot markers during the experiment.

Various image-based techniques have been developed to determine the deformation in model experiments including X-ray (Roscoe et al., 1963, Phillips, 1991) and stereo-photogrammetric methods (Butterfield et al., 1970; Andrawes & Butterfield, 1973). Roots of these methods can be found in the research carried out by Garber (1929) who used X-ray to measure displacements within a soil mass using embedded lead shots in the soil model. His methodology included tracking of the markers' displacement by successive radiograph shots (White et al., 2001).

Stereo-photogrammetric methods involve determination of three-dimensional coordinates of spot points on the model using photographs taken from different views. Comparing the coordinates of the displaced points from successive images provides an estimation of occurring deformation. The drawbacks of these methods mainly include inconsistencies between presence of artificial markers and spot soil mass. A dense network of markers may influence the behaviour of the soil mass or

sparse network of markers may reduce the number of reference points. Moreover, soil particles may partly cover the artificial markers during the experiment and thus prevent successful tracking procedure by post-analysing of the photographs (White et al., 2001).

8.3.1 Fundamentals of particle image velocimetry method

PIV theory was first introduced by Adrian (1991) in the field of fluid mechanics. The technique included photography of seeded flow with small marker particles. The velocity of the flow could be determined by tracking the particles and movement of the small patches of an image within consecutive images.

PIV method has been modified partly to fit in with geotechnical engineering experiments by introducing soil texture instead of seeded flow. The add-in texture creates a suitable contrast to be recognisable when illuminated. Application of PIV method in naturally textured soils such as sand with different-coloured grains does not require any extra process to create pseudo-texture. However, in clay soils which may not have inherent texture, extra texture can be added by addition of coloured ‘flock’ material or dyed sand (White et al., 2003).

Recently PIV method has been used frequently in geotechnical engineering testing and modelling practices. Unlike former image-based techniques, application of PIV method is independent of intrusive markers on the spot area of the soil.

White and Take (2002) developed a MATLAB module (GeoPIV) to implement a suitable PIV analysing method for geotechnical engineering practice.

White et al. (2003) validated the precision and accuracy of the GeoPIV through a series of bench-scale experiments. In their setup, known horizontal incremental displacements were applied to clay/sand soil using a micrometer. Photographs taken during incremental movement was then analysed using GeoPIV. The results confirmed excellent precision and reliable displacement for both sand and clay soils. They used an inexpensive Kodak DC280 digital camera with image size of 1760 x 1160 pixels and they could achieve high precision of $1/15^{th}$ pixel (within a field of view of 300mm x 200mm) which was equivalent to 17μm.

Figure 8.6 shows the basic presentation of PIV method. The PIV analysing algorithm compares the consecutive images by spatial variation in brightness (i.e. texture). In order to fulfil this, the initial image is divided into a mesh of small patches. Consider a given patch that is located at coordinate of (u_1, v_1) in image 1, moves to the new location of (u_2, v_2). In order to find (u_2, v_2) in image 2, a comparison is made by degree of match (correlation) of the patch in image 1 within a larger interrogation area from the same part of image 2. The location with the greatest correlation factor indicates the position of (u_2, v_2).

This procedure is repeated for whole patches in image 1 and therefore, trajectories of all test patches are produced. This algorithm is so called cross correlation algorithm.

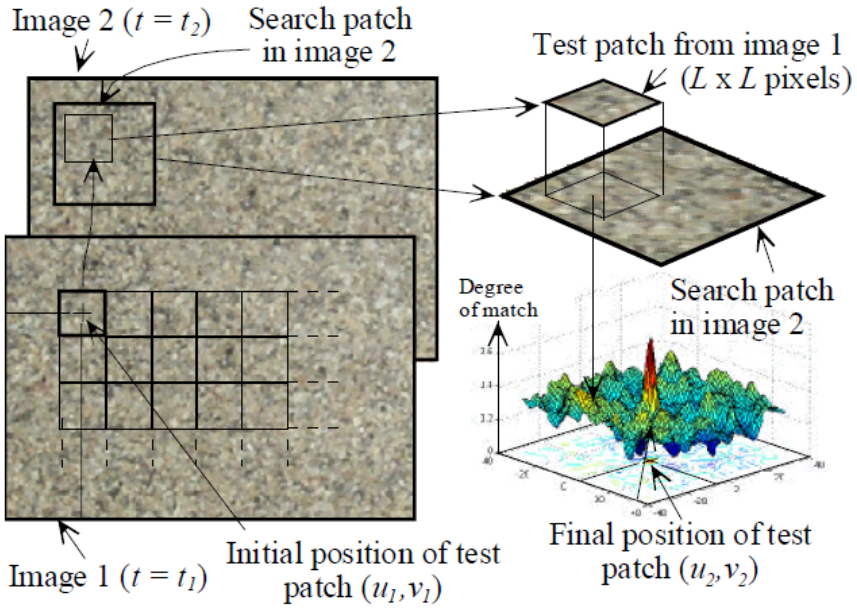

Figure 8.6 Procedure of PIV method (White et al., 2001)

8.3.2 Application of PIV method in the current study

In this study DynamicStudio package[16] was used to perform PIV analysis on the acquired images. DynamicStudio has been mainly designed for acquiring, storing and analysing image-based data. It has a flexible database structure and advanced data analysis modules such as image processing modules,

[16] www.DantecDynamics.com

vector/image interpolating and image calibrating modules. This package is mainly used for analysing the velocity of the flow in hydraulics. Therefore, time interval between acquired images is required to calculate the velocity of the flow. However, in this study since the displacement of the soil particles is investigated, the time interval between acquired images was set to one second. Therefore, the calculated velocity of the soil particles was equal to their displacements.

8.3.3 Adaptive correlation versus cross correlation PIV method

In order to divide the whole field of view into smaller sub-regions, a suitable size image patch must be selected. For increasing the accuracy of the analysis, each patch must contain sufficient textures to be identifiable within the successive images. The standard dimensions of image patches available in DynamicStudio are 16, 32, 64, 128 and 256 pixels. In order to find the degree of similarity of an image patch within pool of patches in the successive images, a correlation algorithm must be used to find the displacement vector of the initial image patch within successive image.

Cross correlation algorithm is the most conventional procedure which has been utilised in PIV analysis to measure the similarity of an image patch within the interrogation windows of successive images (Keane, 1992).

The reliability of the cross correlation method is dependent on some factors such as particle size and shape, number of particles per interrogation area, relative displacement of recognisable particles between successive images. If the number of particles per interrogation area is not enough, the PIV analysis will not produce meaningful statistics. If the relative displacement of particles between two images is large, the number of related pairs (i.e. comprising the location of original particle in the first image and location of displaced one in the second image) will reduce and therefore, the spatial correlation will diminish (Keane, 1992). The efficient number of particle pairs in each interrogation window must be at least 7 and the two dimensional displacement between successive images should not exceed 25%~30% of the interrogation window size (Yaodong, 2004).

In conventional cross correlation algorithm, the position of the image patches is fixed within successive images and as a result if the relative displacement of the particles in the interrogated windows increases, the correlated area reduces (Liu and Iskander, 2004). Therefore, the accuracy of this algorithm reduces with increase in relative displacement of the particles.

An adaptive correlation algorithm is an improved cross correlation algorithm to track the movement of the particles within successively acquired images with higher degree of accuracy. In this method a number of refinement steps (i.e. N) is used to reduce the size of the interrogation area from an initially large size (i.e. N times the size of the final interrogation area) to the final size to obtain a general direction of movement. Therefore, in this method size and position of the interrogation area are changed in several iterations to determine the optimal displacement vectors.

For both cross correlation and adaptive correlation methods, the overlap between interrogation areas can be defined to compensate for the loss of vector field resolution during the processing. In this study overlap of 25% was used for all analyses to reduce the volume of calculations and hence to reduce the calculation time. This value was also recommended by DynamicStudio.

A comparison was made between accuracy of cross correlation and adaptive correlation methods. In order to perform this comparison, an image was translated virtually by known pixels along X and Y directions using an image editing software. PIV analysis was performed on the images using cross correlation and adaptive correlation methods with different interrogation area sizes from 16x16 pixels to 128x128 pixels. Table 8.2 compares the results. In this table average of displacement measured by PIV analysis and root mean squared error (RMSE) as a measure of precision of the methods have been calculated. Data in Table 8.2 show that adaptive correlation far outweighs cross correlation in precision. The selection of patch size is dependent mainly on the maximum displacement of the patches. Patch sizes smaller than the applied displacement incur erratic measurement. Therefore, the size of the patches should be larger than the estimated displacement of the particles between successive images. Although

larger patch sizes may reduce the RMSE, they produce lower number of patches within a fixed size of field of view. Therefore, lower number of displacement vectors is produced.

The field of view of images used for evaluating the accuracy of cross correlation and adaptive correlation methods was 391.7mm by 262.4mm corresponding to 4293 pixels by 2877 pixels. The RMSE errors of adaptive correlation method in moderate image translation (i.e. $\Delta u = 10px, \Delta v = -5px$) for 32x32 patches were 0.0273 pixel and 0.0170 pixel in X and Y directions respectively. Comparing to the size of the field of view, these errors are equivalent to 0.00249mm and 0.00155mm in X and Y directions respectively which are quite satisfactory comparing to the rate of displacement of footing (i.e. 1mm/min).

Therefore, adaptive correlation method and 32x32 pixels patches with overlap of 25% were used in this study to analyse the images of fibre reinforced model slope. Furthermore, 2 steps of refinement were used in adaptive correlation method to reduce the size of the interrogation area from 128x128 pixels to final size of 32x32 pixels.

Table 8.2 Average and RMSE error for different patch analysed by cross correlation and adaptive correlation methods

Patch size	Applied translation	Average of displacement (pixels) ($\Delta \boldsymbol{u}, \Delta \boldsymbol{v}$)		RMSE[1] (pixels) $(\boldsymbol{\sigma_u}, \boldsymbol{\sigma_v})$[2]	
		CC[3]	AC[4]	CC	AC
16x16 pixels	$\Delta u = 2px, \Delta v = -2px$	1.2673,-1.2880	1.9996, -2.0003	0.9929, 0.9604	0.0435, 0.0195
	$\Delta u = 5px, \Delta v = -5px$	2.4889, -2.7260	4.9951, -4.9988	3.7815, 3.5292	0.1987, 0.1057
	$\Delta u = 10px, \Delta v = -5px$	-0.4262, -1.1811	9.9158, -4.9583	11.2498, 5.0873	1.3860, 0.9551
	$\Delta u = 30px, \Delta v = -15px$	0.3111, 0.3647	6.7601, -1.8680	30.5278, 15.0839	30.1406, 21.40
	$\Delta u = 60px, \Delta v = -30px$	-0.3518, -0.3130	-0.9903, -0.7460	60.4608, 29.9059	63.267, 33.450
32x32 pixels	$\Delta u = 2px, \Delta v = -2px$	1.6542, -1.6630	1.9985, -1.9988	0.4698, 0.4509	0.0214, 0.0143
	$\Delta u = 5px, \Delta v = -5px$	4.4445, -4.4774	4.993, -4.9971	1.3841, 1.3286	0.0682, 0.0674
	$\Delta u = 10px, \Delta v = 5px$	8.4639, -3.9747	9.9986, -4.9986	3.9944, 3.1481	0.0273, 0.0170
	$\Delta u = 30px, \Delta v = -15px$	-0.3684, -0.6052	29.8316, -14.937	31.4173, 16.5724	2.3874, 1.6506
	$\Delta u = 60px, \Delta v = -30px$	-0.0503, -0.0203	10.0591, -4.2417	60.5907, 31.0274	64.030, 43.122
64x64 pixels	$\Delta u = 2px, \Delta v = -2px$	1.8427, -1.8497	1.9982, -1.9984	0.1920, 0.1766	0.0168, 0.0152
	$\Delta u = 5px, \Delta v = -5px$	4.8260, -4.8375	4.9952, -4.9954	0.3622, 0.2785	0.0882, 0.0871
	$\Delta u = 10px, \Delta v = -5px$	9.7123, -4.7496	9.9912, -4.9953	2.0075, 1.5588	0.1709, 0.0860
	$\Delta u = 30px, \Delta v = -15px$	5.5016, -3.0315	29.8988, -14.986	30.2689, 19.2208	2.2478, 0.6714
	$\Delta u = 60px, \Delta v = -30px$	-0.2629, -1.5531	55.8837, -29.819	62.5623, 33.1398	9.8049, 2.2568
`128x128 pixels	$\Delta u = 2px, \Delta v = -2px$	1.9148, -1.8596	-1.9951, -0.9585	0.1236, 0.3569	0.0350, 0.2035
	$\Delta u = 5px, \Delta v = -5px$	4.9006, -4.7483	4.9847, -4.9171	0.2427, 0.9276	0.1469, 0.4046
	$\Delta u = 10px, \Delta v = -5px$	9.9400, -4.7514	9.9829, -4.9164	0.6907, 0.9291	0.2365, 0.4117
	$\Delta u = 30px, \Delta v = -15px$	28.8718, -14.224	6.7601, -1.8680	7.1613, 3.8576	30.140, 21.403
	$\Delta u = 60px, \Delta v = -30px$	13.1075, -8.2984	55.6555, -29.591	59.8404, 36.9054	26.5010, 9.602

[1] Root Mean Squared Error as a measure of precision
[2] u: Displacement along X axis, v: Displacement along Y axis
[3] Cross correlation method
[4] Adaptive correlation method

Figure 8.7 shows different patch sizes on the image used for evaluating the accuracy of the correlation processes. This figure shows that 32x32 and 64x64 pixels patches include reasonable number of textures. Figure 8.8 compares the displacement vector fields obtained by cross correlation and adaptive correlation methods using 32X32 pixels patch size on virtually translated image by 10 pixels and 5 pixels alongside X and Y directions respectively. This figure shows that the vector field obtained from adaptive correlation is more uniform and consistent compared to the one obtained from cross correlation method.

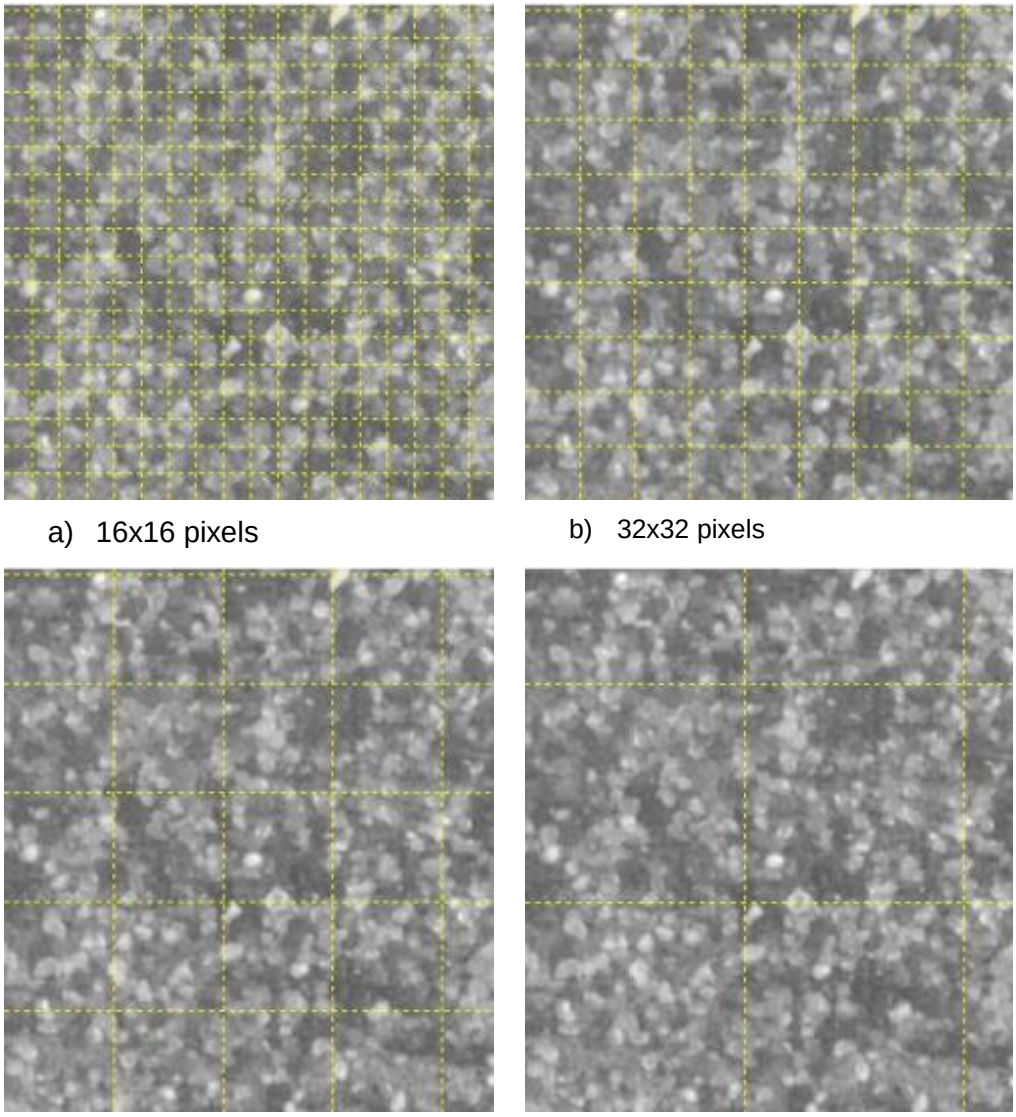

a) 16x16 pixels

b) 32x32 pixels

c) 64x64 pixels

d) 128x128 pixels

Figure 8.7 Different patch sizes

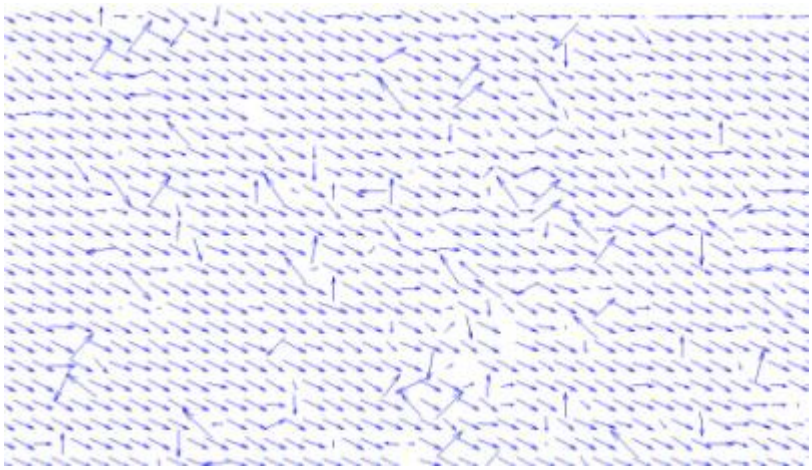

a) Displacement vector obtained by cross correlation method

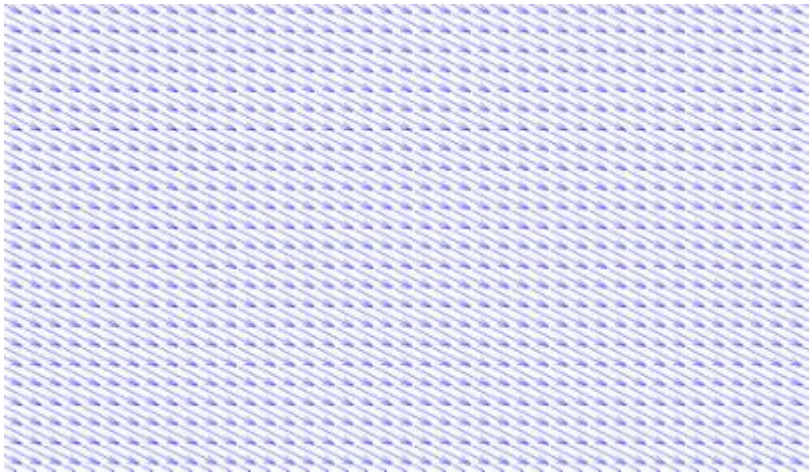

b) Displacement vector obtained by adaptive correlation method

Figure 8.8 Comparison between displacement vector fields of cross correlation and adaptive correlation methods

8.3.4 Camera calibration

A Nikon D90 (12M Pixel) camera was used in this study. The camera was positioned 100cm away with its optical axis at right angle to the surface of the Perspex glass. The resolution of the acquired image was 4288x2848 pixels. The size of the field of view was 387.4x257.3 mm. Therefore, the scale of field of view to the image was 0.090345 mm/pixel.

For each test few images were acquired by placing the calibrating board in front of the Perspex glass of the tank to calibrate the camera. The calibrating board (dot matrix calibration target) included a large dot (zero marker) surrounded by

four smaller dots (axis markers) and equally spaced dots (main markers) on a white background. These markers were used to identify the origin of the coordinate system. And based on known dot spacing (X,Y)-coordinates of the markers, the scale factor of the image could be determined. Figure 8.9 shows the calibrating board used in this study.

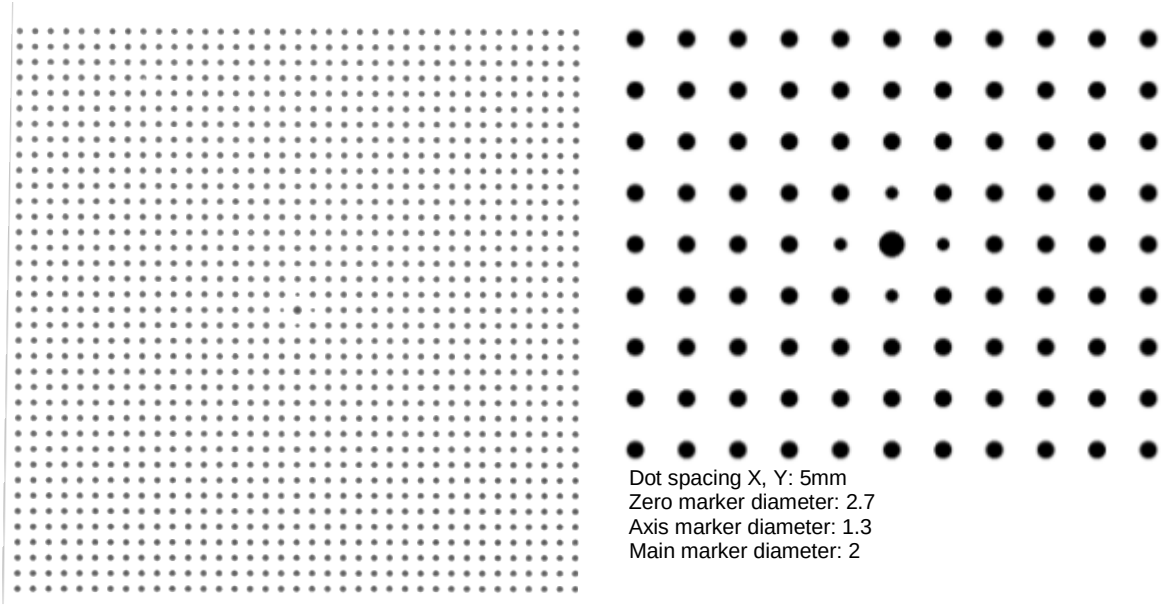

Figure 8.9 Calibrating board

The camera calibration model (Imaging model fit) is a mathematical model that correlates the "Object Space" (typically using mm-coordinates) to the "Image Plane" (where positions are measured in pixel coordinates). Acquired Images of the calibrating board were used to calibrate the camera using imaging model fit implemented in the DynamicStudio.

DynamicStudio can calibrate the camera using three built-in calibrating models including direct linear transform (DLT), third order XYZ polynomial and pinhole camera model. The latter includes compensation for lens distortion which is more suitable for the commercial cameras. Therefore, in the current study, pinhole camera model was used to calibrate the camera.

8.3.5 Corrections due to camera movement and vector distortion

Although the optical axis of camera was positioned at right angle to the surface of the Perspex glass, there were some discrepancies during image acquiring because of minor movement of the camera whilst triggering the camera. Therefore, the camera might be off-axis, looking at the Perspex glass at an angle instead of normal to it. Moreover, because of the large size of the field of view, far points from its centre were distorted through the lens of the camera.

Images acquired with an off-axis camera suffer from perspective distortion, due to non-constant scale factor across the field of view. For solving this issue, two corrections were applied to the images and resulted deformation vector field.

The first correction was applied using a MATLAB code to compensate the movement of the camera during image acquirement. In this code it was assumed that soil particles in a small patch, at the lower left corner of the field of view, were not displaced. Therefore, any offset of this small patch in consecutive images was considered as movement of the camera. And the calculated offset was compensated by translating the whole image.

The second correction was applied to the distorted vectors. DynamicStudio contains numerical models describing the perspective distortion to compensate and correct the images or the vectors derived from the distorted images.

By applying distortion correction (known as dewarping procedure) on the distorted images, pixels of the distorted images with trapezoidal section would be corrected to pixels with square section. The same considerations were applied for correcting distorted vectors of the displacement vector field. In this study all vectors of displacement vector field were dewarpped using the pinhole camera calibration data.

After dewarping the vectors, the location of the initial patches are changed due to applied dewarping correction. Therefore, the final vector field must be interpolated to attain a uniform map of patches. All the neighbouring vectors were interpolated

to attain a map of 40 patches in X direction and 40 patches in Y direction. Therefore, after interpolation process, each vector filed contained 1600 patches.
The consecutive deformations of the acquired images were exported as Microsoft Excel CSV files. A code was written in MATLAB to superimpose the consecutive deformations at each patch through all successive images to derive the cumulative deformation of each patch and to generate deformation contours and vector map of each experiment.

8.4 Results and discussion

8.4.1 Model slope with footing distance ratio of 3B

Figure 8.10 to Figure 8.13 show the footing pressure versus footing settlement ratio of non-reinforced and fibre reinforced C2 soil with footing distance ratio of 3B (i.e. 150mm).

The footing settlement was expressed as non-dimensional ratio of settlement over widths of the footing (S/B). Results showed that for all model slope tests carried out in this study there was no apparent peak bearing capacity. Increase in settlement ratio (S/B) was accompanied with continuous increase in footing pressure. Therefore, the value of the footing pressure at an arbitrary displacement ratio of 20% was used to compare the bearing pressure of the model slopes.

The settlement ratio was calculated by the average readings of LVDT sensors installed on both sides of the footing and the corresponding pressure-settlement curves were shown by solid lines in Figure 8.10 to Figure 8.13. However, the displacement of the footing was also measured using the PIV analysis. The corresponding pressure-settlement curves were shown by dashed-type lines in the same figures. It should be noted that in these figures the same value of footing pressure has been used for both methods. However, the displacement ratio measured by PIV analysis was less than that measured by LVDT sensors. Therefore, the dashed-type curve shifted to the left.

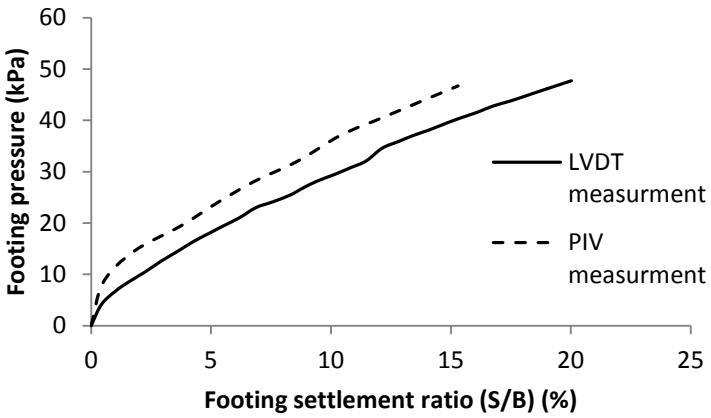

Figure 8.10 Pressure-settlement ratio curves for model slope (non-reinforced C2 soil, X:3B)

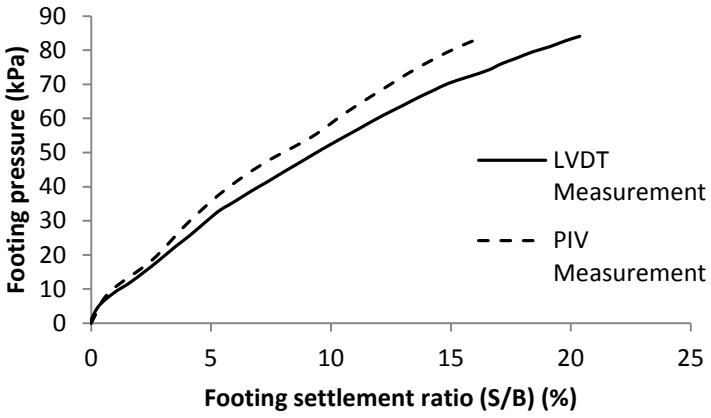

Figure 8.11 Pressure-settlement ratio curves for model slope (1% fibre reinforced C2 soil, X:3B)

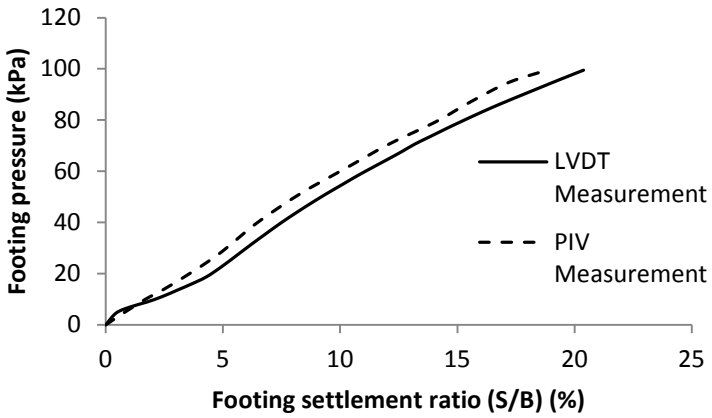

Figure 8.12 Pressure-settlement ratio curves for model slope (3% fibre reinforced C2 soil, X:3B)

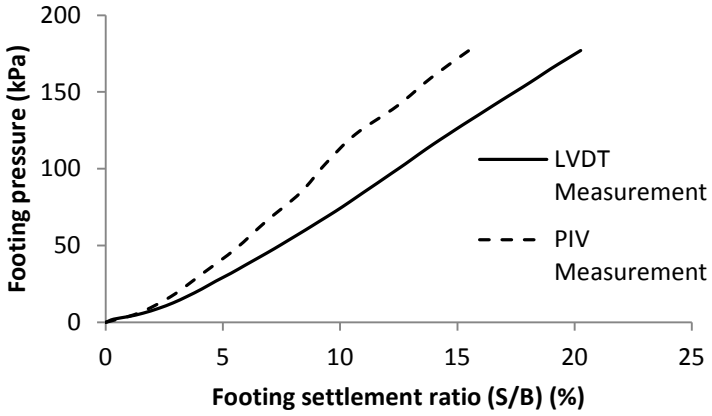

Figure 8.13 Pressure-settlement ratio curves for model slope (5% fibre reinforced C2 soil, X:3B)

The measured displacements of footing using PIV analysis was deviated from the measured displacements using mounted LVDT sensors installed on the footing. The incurred difference could be related to:

a) Minor movement of the camera during image capturing
b) Relative displacement of texturing particles to the clay particles
c) Failing of texturing process to maintain a uniform and regularly recognisable texture on the front view of the clay model slope.

Although all the images as mentioned in section 8.3.5 were corrected for minor camera movements using developed MATLAB code, there was still some inevitable non-corrected image shifting which caused error in measured displacement of the footing using PIV image analysis. The incurred discrepancy can be avoided by using a remote control trigger to capture the images without touching the camera capturing button. However, in the current study such device was not available.

Randomly sprinkling artificial recognisable texture to the frontal surface of the clay using coloured sand may not always ensure a regular and homogeneous density of contrasting colours in every single small patch of the soil surface. Therefore, this can reduce the number of recognisable pairs of particles in successive images.

On the other hand, the sprinkled coloured sand particles were not part of the body of the clay and they might reveal some relative displacements apart from displacements occurred in the clay particles. The relative displacement could be pertained to either the friction between sand particles and Perspex glass or small gap between footing and Perspex glass (i.e. 2mm). Figure 8.14 shows the effect of friction between sand particles and surface of Perspex glass and also the effect of relative displacement of the sand particles due to the gap between the footing and Perspex glass. The gap between the footing and Perspex glass should be reduced as much as possible to prevent the sand particles from off-plane movement. Moreover, the gap must be set in such way that, there is no risk of scratching the Perspex glass. These considerations help reducing the inconsistencies between measured value of footing displacement using LVDT and calculated value using PIV method.

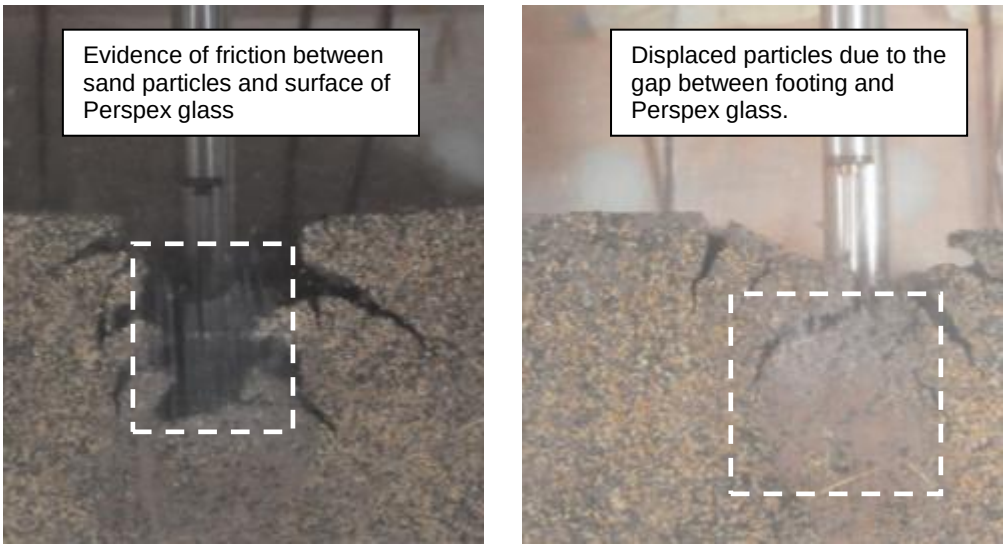

Figure 8.14 Relative displacements of sprinkled sand particles due to friction effect and increased pore-water pressure effect

Therefore, the measured displacement in clay soils using PIV analysis is not always satisfactory. However, in sand soils because of the natural texture of the sand particles (by reflection of light), the mentioned discrepancies between real displacement of particles and measured values by PIV analysis diminishes significantly. Liu and Iskander (2004) showed that the displacements of the footing on a compacted sand layer measured by PIV analysis agree well with those measured by LVDT sensor.

Figure 8.10 to Figure 8.13 show that increase in fibre content; enhanced the bearing pressure of the fibre reinforced model slope significantly. The bearing pressure increased by almost 271% with increasing the fibre content from 0% to 5% (i.e. change from 47.7 kPa to 177 kPa). This can be attributed to contribution of fibres to increase the shear strength of the soil against applied footing load.

Fibres limited the induced shear strains due to applied footing pressure. This can be further described using graphs of two-dimensional displacement (i.e. total displacement comprising displacements along X axis (u) and Y axis (v),$\sqrt{u^2+v^2}$) of model slopes at depth of 0.5B underneath the footing (Figure 8.15). Displacements shown in Figure 8.15 are cumulative displacements up to 20% settlement ratio. This figure shows that the displacement underneath footing decreased with increase in fibre content. The two-dimensional

displacement was highest under the centre of footing and it diminished away from centre of footing.

As it can be seen in Figure 8.15, total displacement at right side of the footing was higher than that at left side of the footing. This was attributed to the boundary condition of the model slope which implied confinement of the soil at left side of the footing by sides of the tank. However, soil at right side of the footing was exposed and therefore, displacement of soil particles at right side of the footing was more than that at left side of the footing.

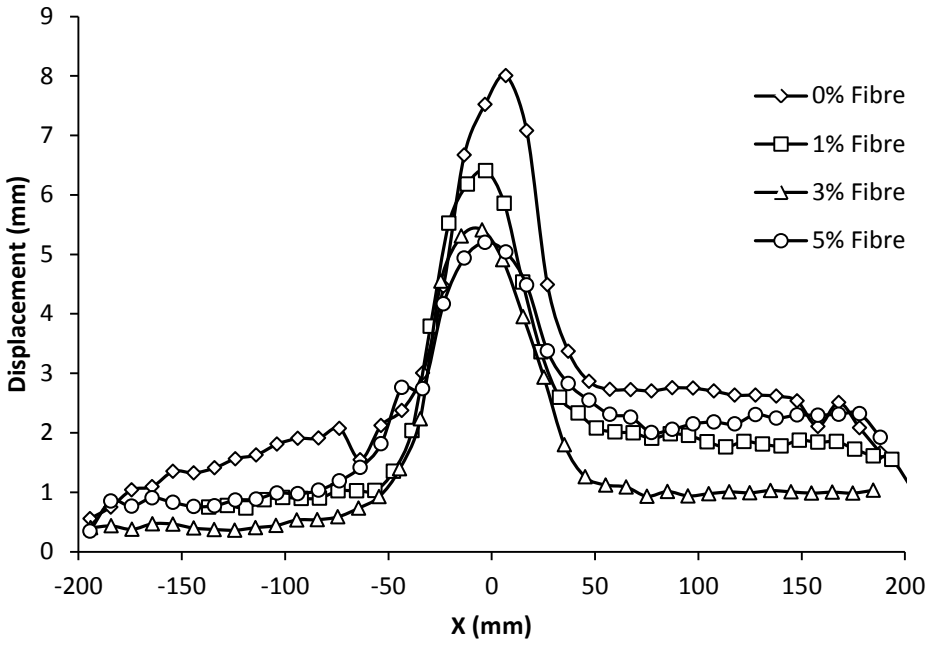

Figure 8.15 Two dimensional displacement at depth of 0.5B under the footing (X:3B)

Figure 8.16 shows the evolution of excess pore-water pressure before (i.e. at (-)0.4B, i.e. 40mm) and after (i.e. at 2B, i.e. 100mm) the footing.

Increased pore-water pressure at left side of the footing showed compression behaviour of the soil. At location of 0.4B before footing as it can be seen in Figure 8.15, non-reinforced and fibre reinforced soil have undergone relatively extreme compression. Figure 8.17 and Figure 8.18 show the displacement contours of non-reinforced and 5% fibre reinforced soil respectively. All displacement contours shown in this chapter are based on cumulative displacements up to 20% footing settlement ratio which was considered as failure of the model slope.

As can be seen in Figure 8.17(a) and Figure 8.18(a), the direction of displacement of the soil at location of (-)0.4B for both non-reinforced and 5% fibre reinforced soil was downward which confirmed the compression behaviour of the soil in this region.

The excess pore-water pressure of 5% fibre reinforced soil at location of (-)0.4B was significantly less than that of non-reinforced soil. This was truly representative of higher permeability of reinforced soil compared to non-reinforced soil which helped better dissipation of generated pore-water pressure in fibre reinforced soil under compression.

At right side of the footing (i.e. X:2B), the resultant displacement was towards right, which implied tension behaviour in the soil mass in this region. Therefore, as it is shown in Figure 8.16 negative pore-water pressure was expected.

The observed pore-water pressure was just slightly negative due to unconfined boundary condition of portion of slope at right side of the footing.

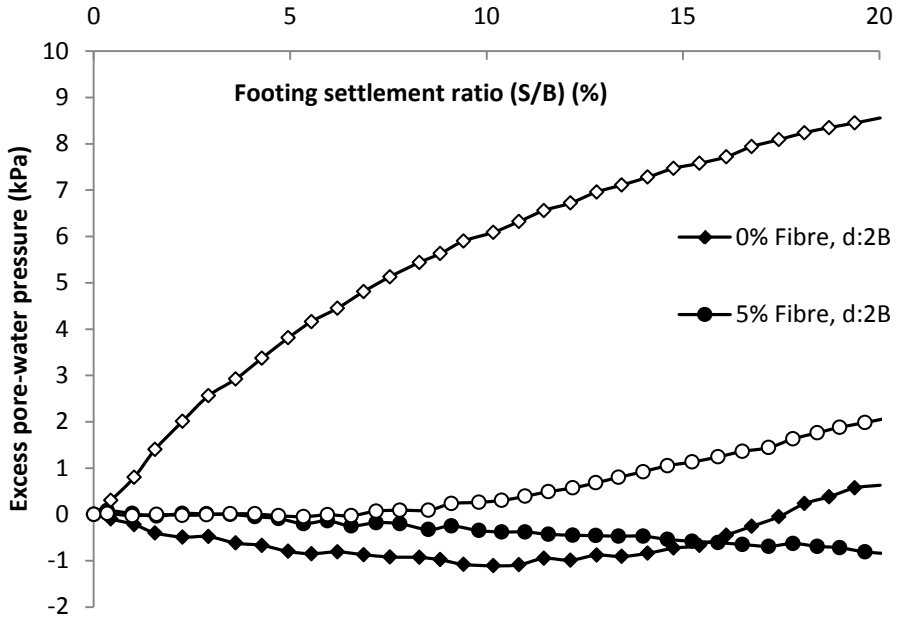

Figure 8.16 Excess pore-water pressure before and after footing (X:3B)

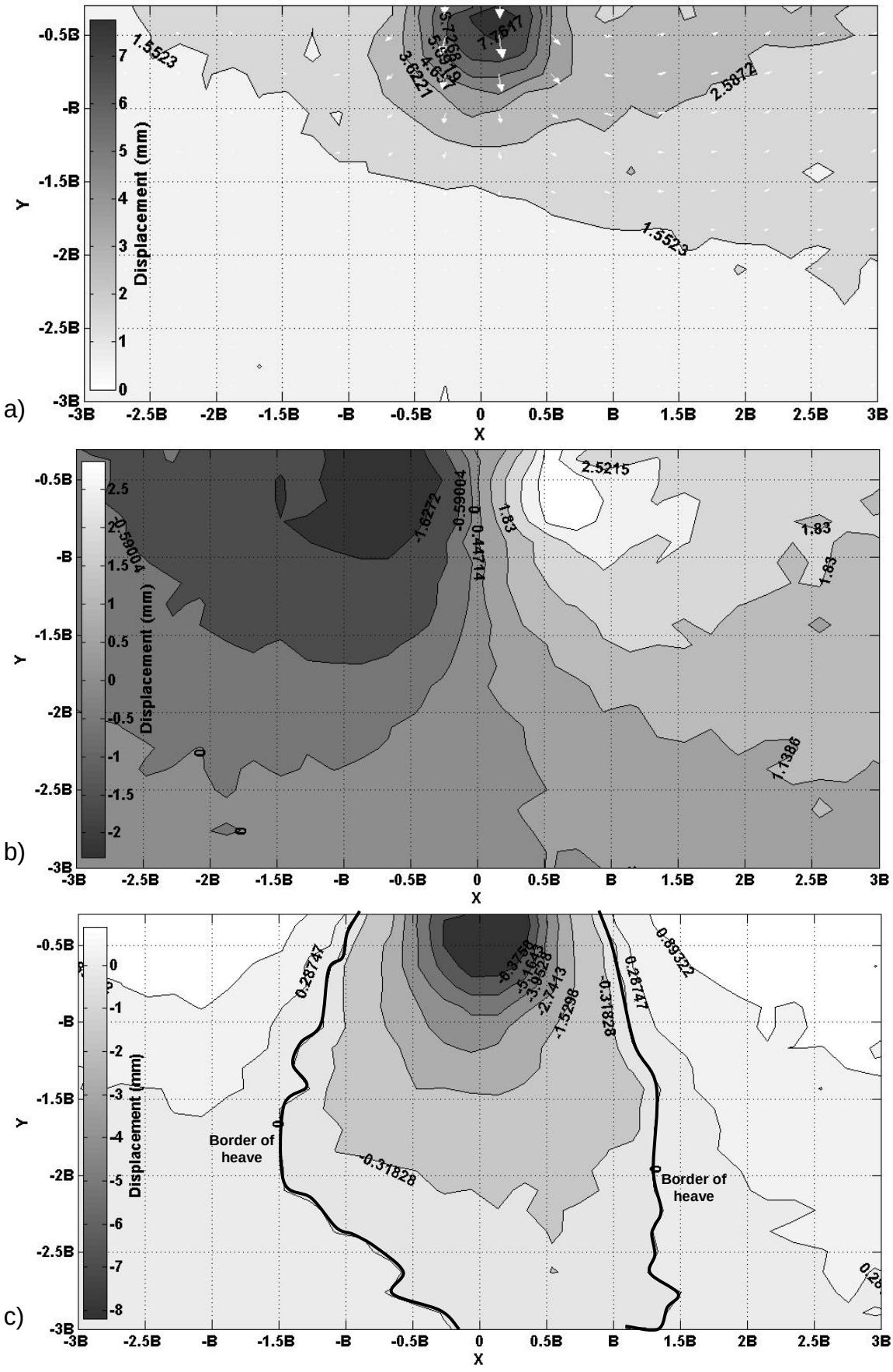

Figure 8.17 Contours of displacement under footing at failure (0% Fibre, X:3B) a) Total b) Horizontal c) vertical displacement

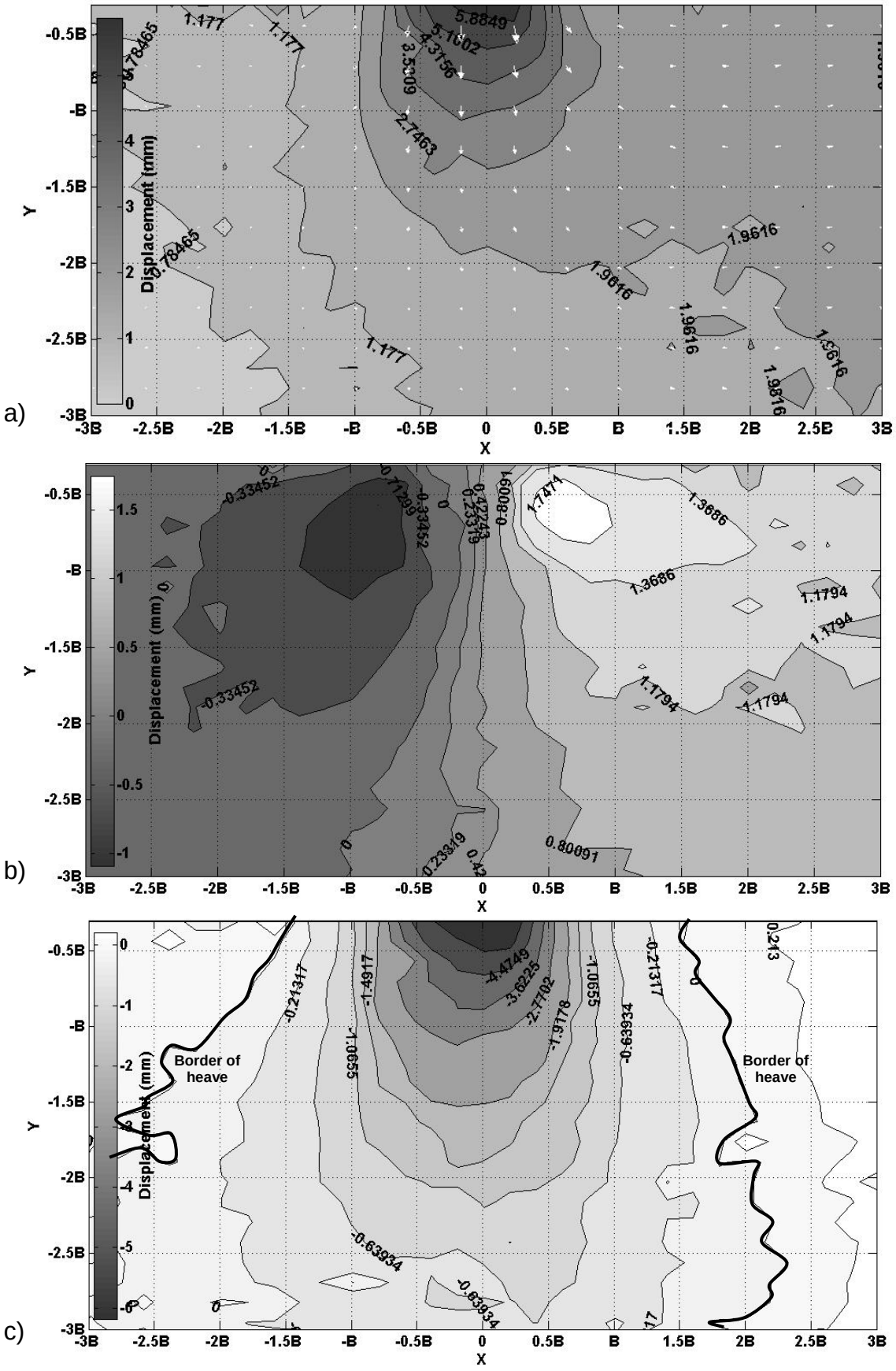

Figure 8.18 Contours of displacement under footing at failure (5% Fibre, X:3B) a) Total b) Horizontal c) vertical displacement

Displacement contours (Figure 8.17 and Figure 8.18) of non-reinforced and fibre reinforced soil showed different characteristics of the soil during loading. The horizontal contours of total displacement for both non-reinforced and fibre reinforced soil showed two distinctive blocks of soil displacement around the footing. At failure, the block of soil at right side of the footing moved to the right and the left block moved to the left. This showed almost symmetrical direction of displacement at sides of the footing. However, because of unconfined boundary condition at right side of the slope, the magnitude of horizontal displacements was accordingly higher than those at left side of the footing.

The location of maximum horizontal displacement for both non-reinforced and fibre reinforced soil was from 0.5B to B at both sides of the footing. Maximum horizontal displacement for fibre reinforced soil was located at 0.5B to 0.75B deep of footing. However, for non-reinforced soil location of highest horizontal displacement was at depth of 0 to 0.75B.

In non-reinforced soil, the extent of the soil mass between heave borders (settled region) lied between (-)1.5B and 1.5B (Figure 8.17 (c)). However, for 5% fibre reinforced soil this limit extended to a region between (-)3B and 2.25B (Figure 8.17(c)). Beyond these regions, soil heaved. Therefore, in fibre reinforced soil the size of the displacement bulb confined between zero vertical displacement contour lines was significantly larger than that of non-reinforced soil.

This was indicative of the capability of the fibre reinforced soil to distribute the stresses underneath footing over successively wider area. The observed behaviour was pertained to stress distribution role of fibres within the body of the fibre reinforced soil which maintained lower stress concentration in deeper layers of soil under footing.

The reduced excess stress (i.e. because of footing pressure) under footing was measured using pressure cells installed on the rigid base of the tank at centreline and 1.5B away of centreline of footing. Table 8.3 shows the results. In this table the rate of excess stress reduction defined as the difference between stress applied on the footing and measured stress at the centre line of footing on the base of model slope divided by height of the slope. The rate of excess stress

reduction can be used to compare the stress distribution measure under the footing for different model slopes.

The data shown in Table 8.3 shows that rate of excess stress reduction was changed from 0.133 kPa/mm to 0.478 kPa/mm with increase in fibre content from 0% to 5%. The measured change showed that in fibre reinforced soil, applied stress on the footing distributed over wider area and hence the rate of reduction of normal excess stress along the depth under footing increased. This was consistent with the displacement contours shown in Figure 8.18 which showed increased size of vertical displacement bulbs of fibre reinforced soil compared to that of non-reinforced soil.

Table 8.3 Measured excess stresses at failure at the base of model slope (X:3B)

	pressure measured (kPa) at:				
Fibre content	Surface of slope at centre of footing	Tank base at -1.5B away from centre of footing	Tank base at centre of footing	Tank base at +1.5B away from centre of footing	Rate of reduction of stress at centre of footing along height of slope (kPa/mm)
0%	47.7	0.18	1.25	0.49	0.133
1%	84.1	0.46	3.38	0.39	0.231
3%	99.5	N/A*	N/A	N/A	N/A
5%	177.0	2.13	9.83	6.45	0.478

* data of pressure cells for model slope with 3% fibre content was not available

The state of the displacement contours showed that in fibre reinforced soil, the failure surface was deeper and fibres contributed to increase the mobilised shear resistance along the failure surface. That was why, fibre reinforced soil could sustain higher bearing pressure.

To investigate the shape of the failure surface, the displacement vector fields obtained from PIV analysis of two images before and after reaching 20% settlement ratio were used to sketch the failure surface of the model slopes. Figure 8.19 to Figure 8.22 shows the results.

Two apparent slip surfaces were recognised in these figures including a shallow slip surface with maximum depth equals to width of the footing at left side of the footing and a deep slip surface at right side of the footing. The slip surface at left

side of the footing was mainly controlled by boundary conditions of the tank and its extents decreased slightly with increase in fibre content.

For non-reinforced slope, the slip surface at right side of the footing was extended to almost 2B deep away from surface of slope. The depth of the slip surface at right side of the footing increased to 2.4B, 3.6B and more than 4B for model slopes constructed with 1%, 3% and 5% fibre content respectively. Increase in depth of slip surface with increase in fibre content showed that fibres confined soil particles together and hence tended to involve larger block of soil during failure. And hence, the mobilised strength along the slip surface increased. This resulted in requirement of higher footing pressure to bring the model slope into failure state. This was consistent with the pressure-settlement ratio graphs which showed increased bearing pressure with increase in fibre content.

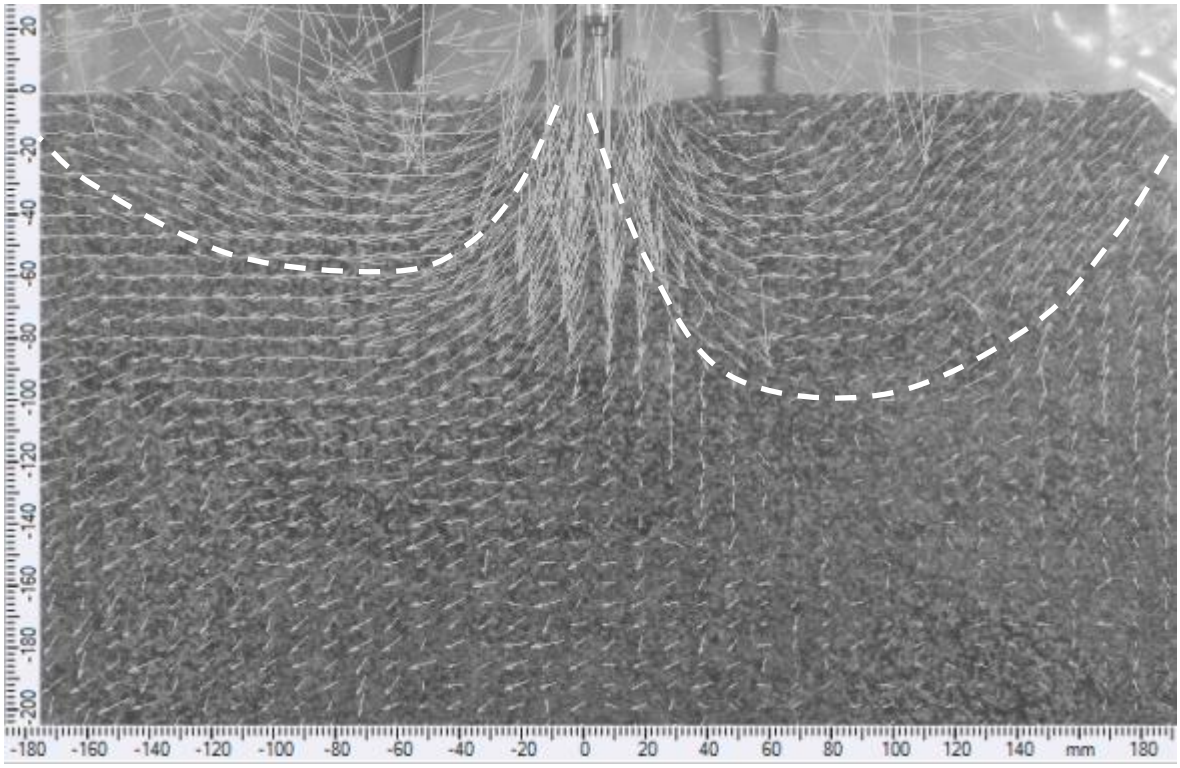

Figure 8.19 Slip surface of non-reinforced model slope (X:3B)

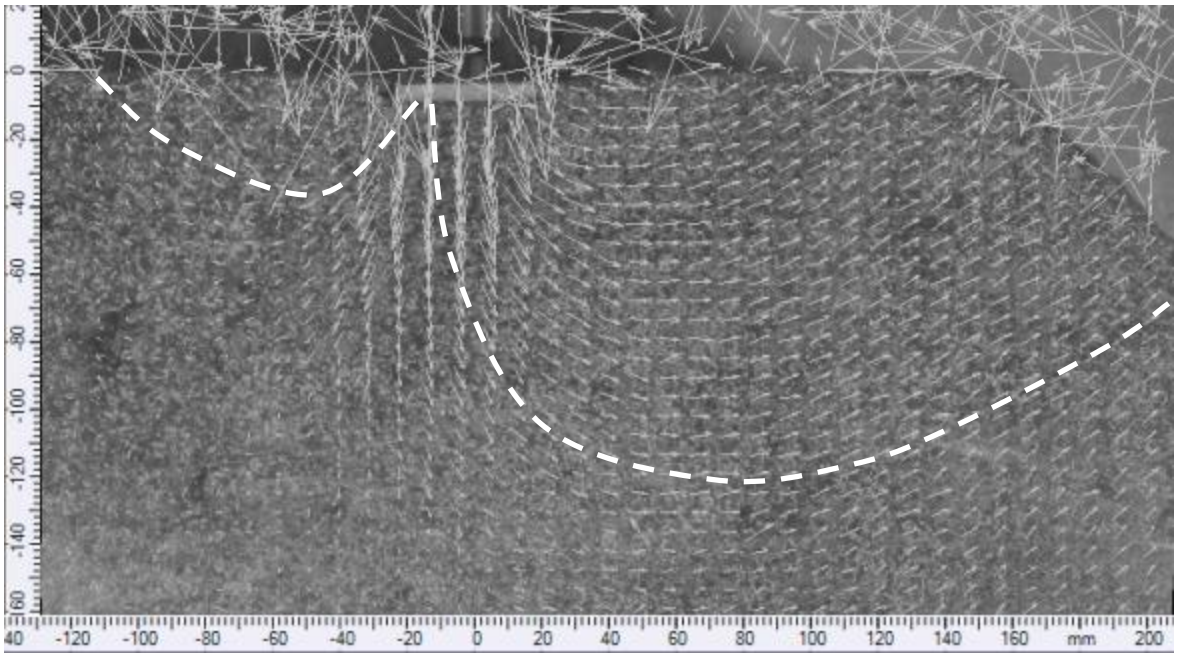

Figure 8.20 Slip surface of 1% fibre reinforced model slope (X:3B)

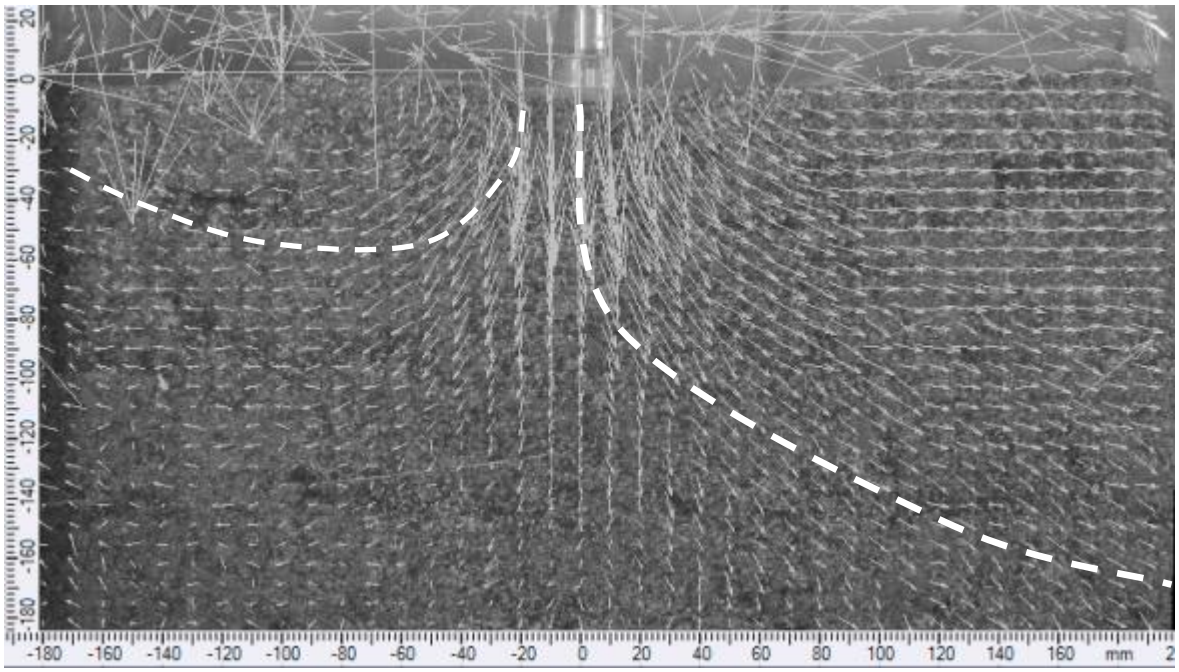

Figure 8.21 Slip surface of 3% fibre reinforced model slope (X:3B)

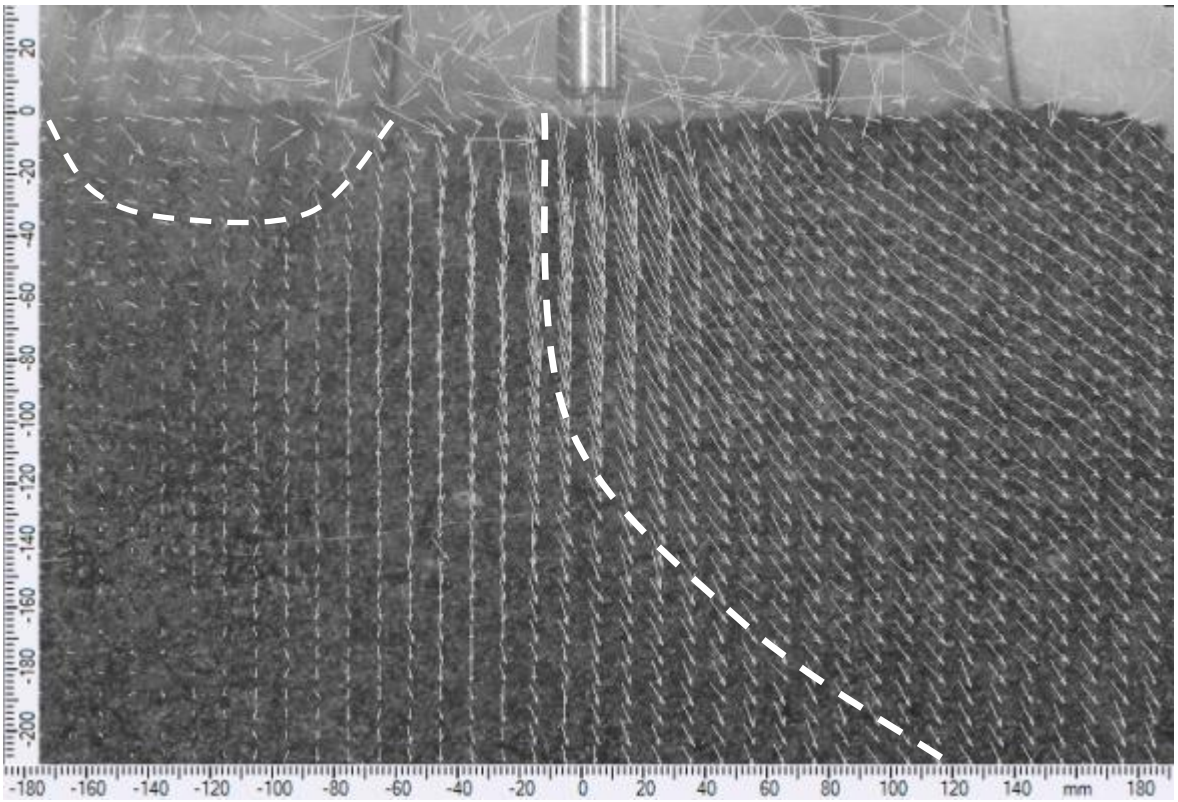

Figure 8.22 Slip surface of 5% fibre reinforced model slope (X:3B)

8.4.2 Model slope with footing distance ratio of 1B

Non-reinforced and fibre reinforced (i.e. with 1% and 3% fibre content) model slopes were loaded from top using a strip footing located at distance equal to width of footing (i.e. 50mm) from crest of slope. Figure 8.23 to Figure 8.25 show the change of footing pressure against settlement ratio of non-reinforced and fibre reinforced model slopes.

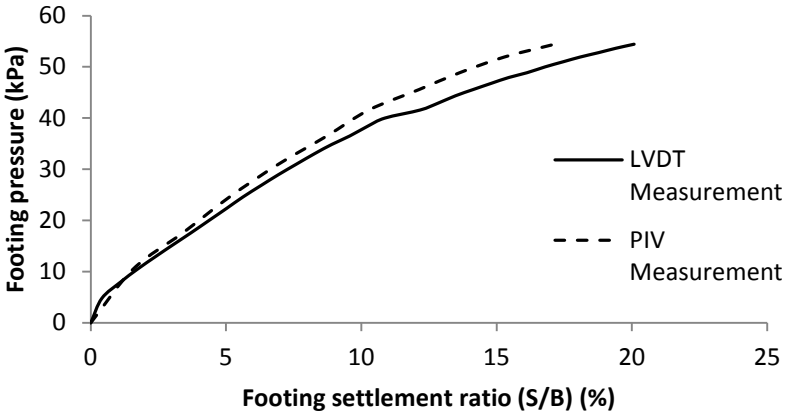

Figure 8.23 Pressure-settlement ratio curves for model slope (non-reinforced C2 soil, X:1B)

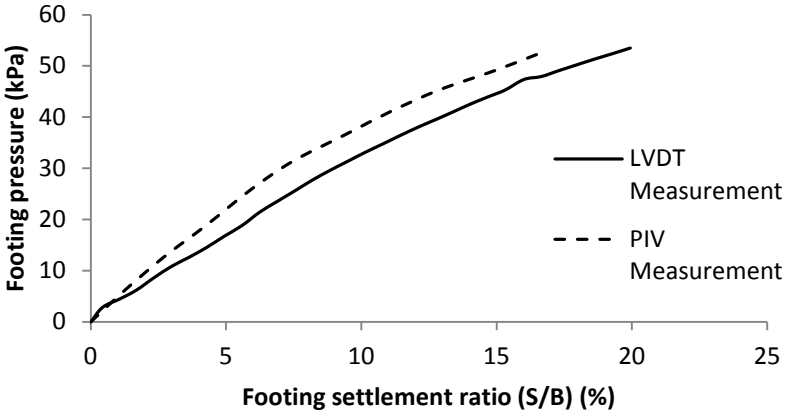

Figure 8.24 Pressure-settlement ratio curves for model slope (1% fibre reinforced C2 soil, X:1B)

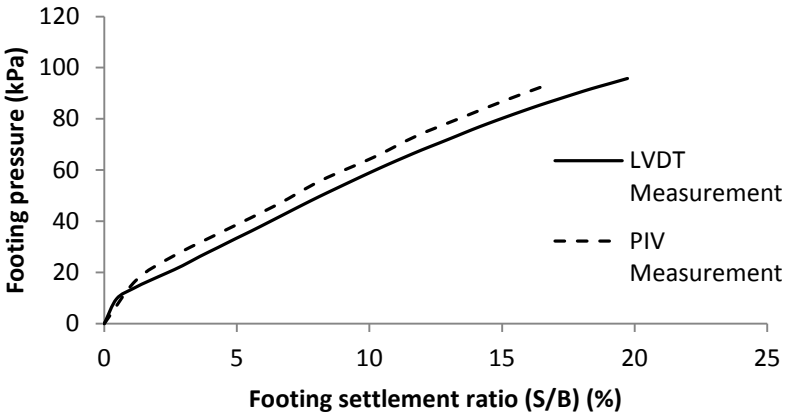

Figure 8.25 Pressure-settlement ratio curves for model slope (3% fibre reinforced C2 soil, X:1B)

Figure 8.23 and Figure 8.24 show that model slope with non-reinforced and 1% fibre reinforced soil reached almost the same bearing pressure (i.e. 54.5 kPa). However, bearing pressure of the 3% fibre reinforced model slope increased by 79% to 97.6 kPa.

Total displacement of the non-reinforced and fibre reinforced model slopes at 0.5B deep of footing has been shown in Figure 8.26. Similar to the results presented in the last section (8.4.1), the total displacement at 0.5B under footing reduced with increase in fibre content. This denoted confinement effect of fibres to limit the displacement of the soil particles by integrating the smaller soil blocks to form larger blocks. Therefore, larger blocks of soil were mobilised against applied stress by footing, and hence, the arisen displacement reduced due to the increased shear strength of the integrated blocks. The described hypothesis can be clearly proved by comparing Figure 8.27 (a), Figure 8.28 (a) and Figure 8.29 (a) which indicated growths of extent of two dimensional displacement contours and shrinkage of displacement vectors with increase in fibre content.

Peak total displacements at right side of the footing in Figure 8.26, shows the sudden displacements of some particles. This might happen due to the unconfined boundary condition of slope at right side of the footing. Therefore, some particles might be displaced horizontally especially in non-reinforced slope.

Figure 8.27 (b), Figure 8.27 (b) and Figure 8.29 (b) show the contour lines of horizontal displacement of non-reinforced and fibre reinforced model slopes. For non-reinforced model, the maximum horizontal displacement happened at horizontal extent of 0.5B to 1.25B away footing and vertical extent of 0.3B to 0.8B away footing. Increase in fibre content to 3% shifted the location of maximum horizontal displacement downward to the right (i.e. 0.5B to 1.75B and 0.4B to 1.25B in X and Y directions respectively).

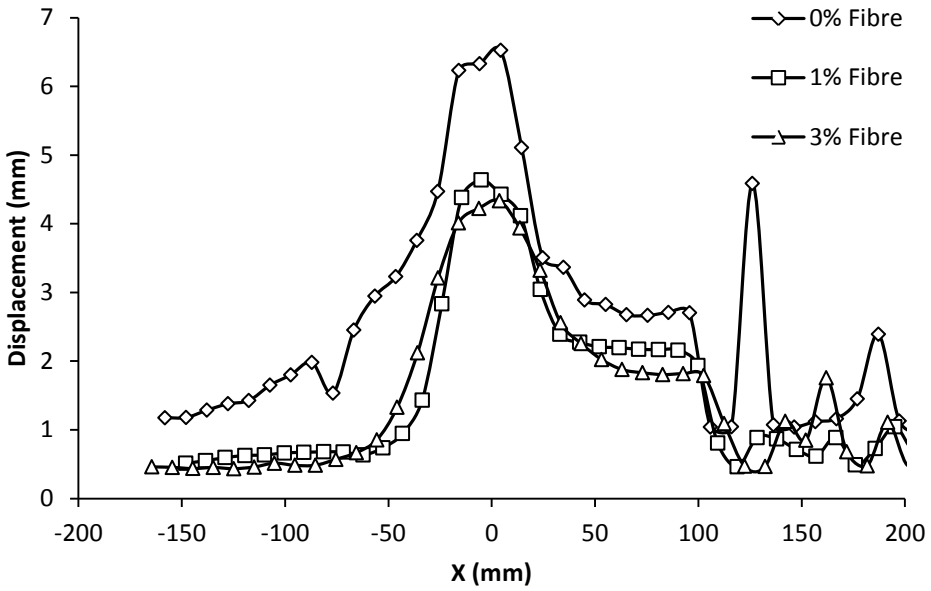

Figure 8.26 Two dimensional displacement at depth of 0.5B under the footing (X:1B)

Vertical displacement contours in Figure 8.27 to Figure 8.29 show that the soil under footing behaved in compression. With increase in fibre content, the border of heave shifted more to the left (Figure 8.27 (c), Figure 8.28 (c) and Figure 8.29 (c)).

Figure 8.30 shows the excess pore-water pressure of non-reinforced and 3% fibre reinforced soil before (i.e. (-)2.4B) and under footing. The excess pore-water pressure of 3% fibre reinforced soil at left side of the footing was lower than that of non-reinforced soil. This showed that the soil in this region was in tension resulting from almost pure horizontal displacement to the left (see Figure 8.29 (c)).

Measurement of excess pore-water pressure under footing showed higher values for non-reinforced soil which was indicative of higher compression behaviour of non-reinforced soil compared to 3% fibre reinforced soil. This was consistent with the results shown in Figure 8.26 which showed reduction in displacement under footing with increased fibre content.

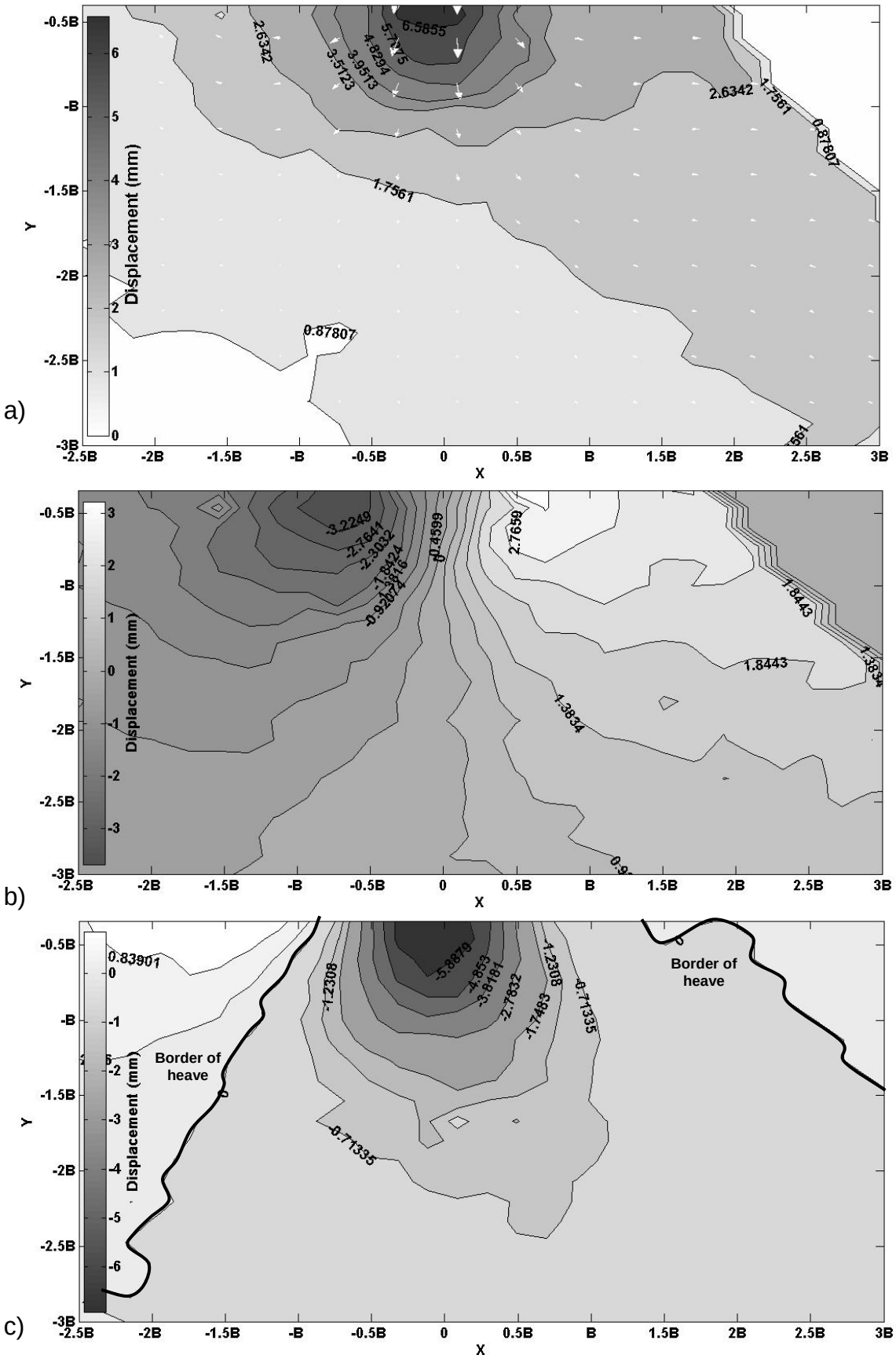

Figure 8.27 Contours of displacement under footing at failure (0% Fibre, X:1B) a) Total b) Horizontal c) vertical displacement

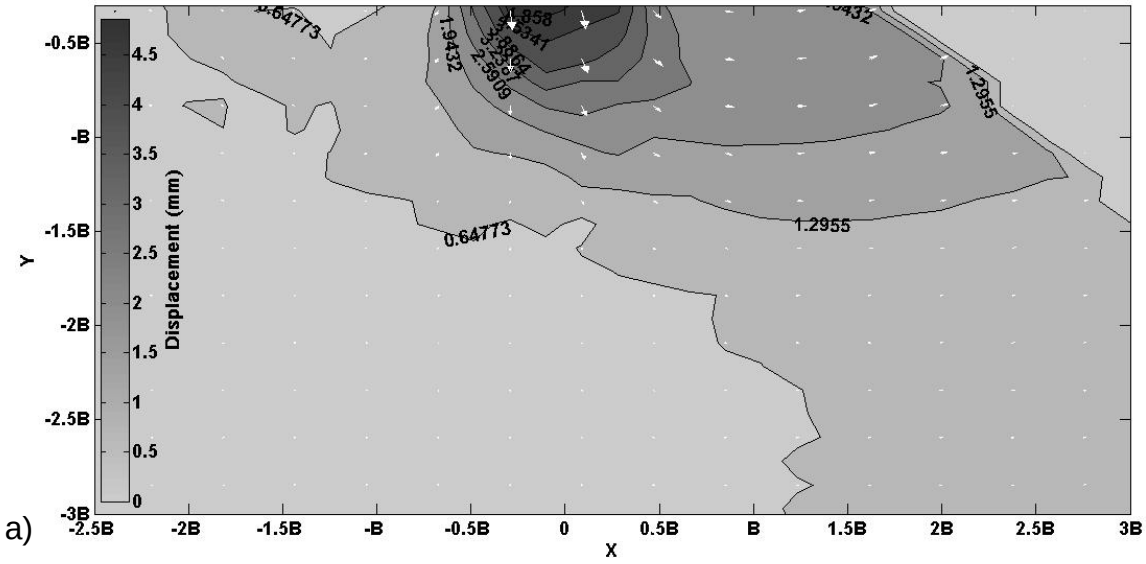

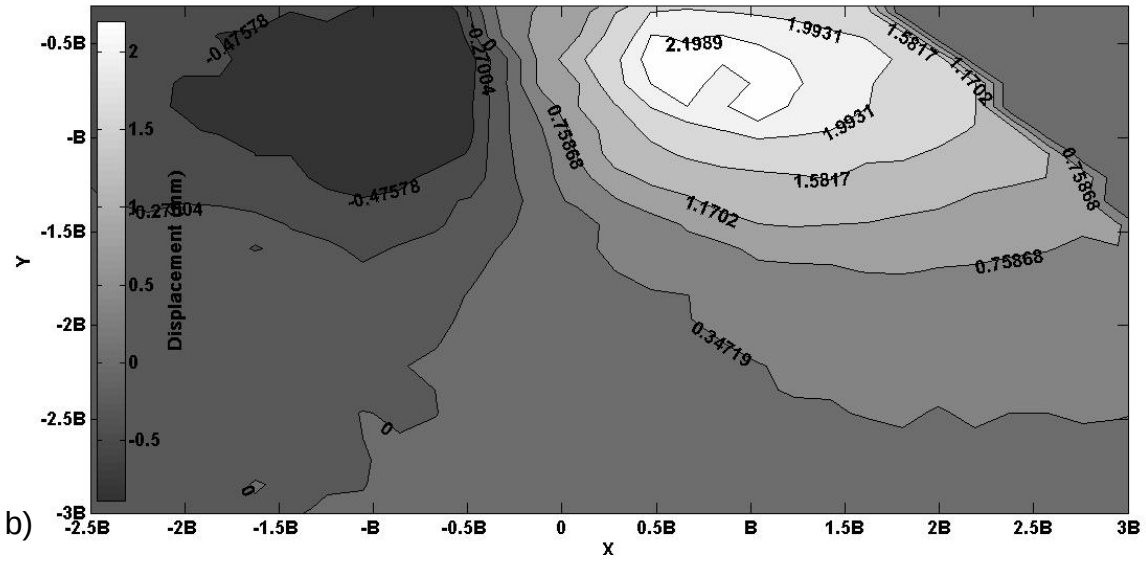

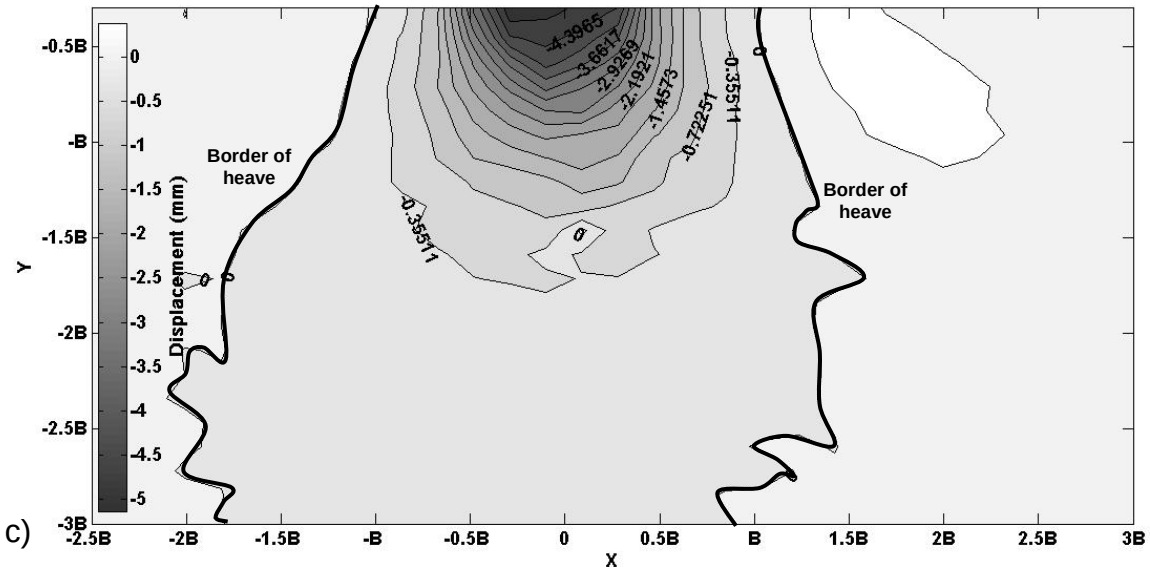

Figure 8.28 Contours of displacement under footing at failure (1% Fibre, X:1B)
a) Total b) Horizontal c) vertical displacement

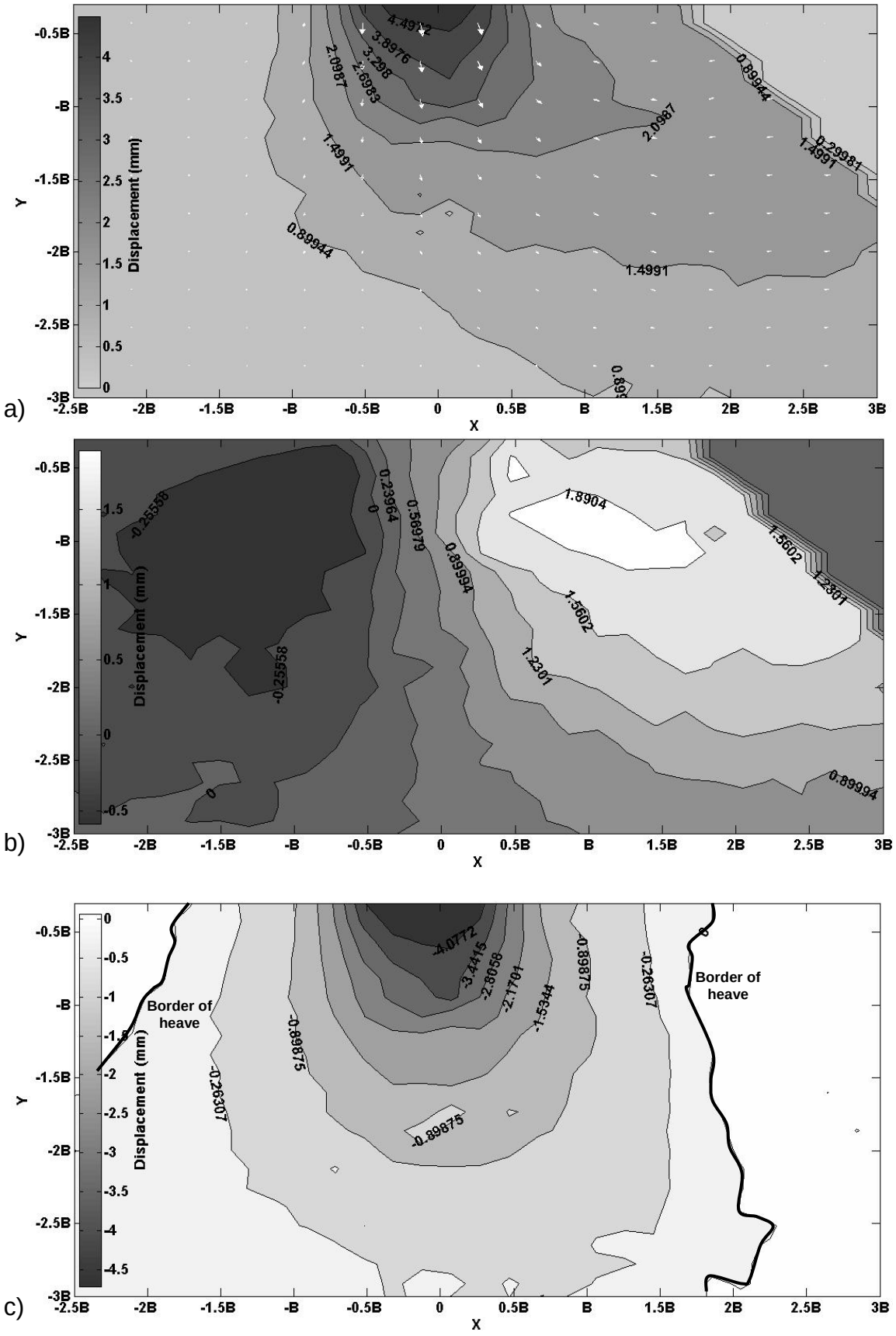

Figure 8.29 Contours of displacement under footing at failure (3% Fibre, X:1B)
a) Total b) Horizontal c) vertical displacement

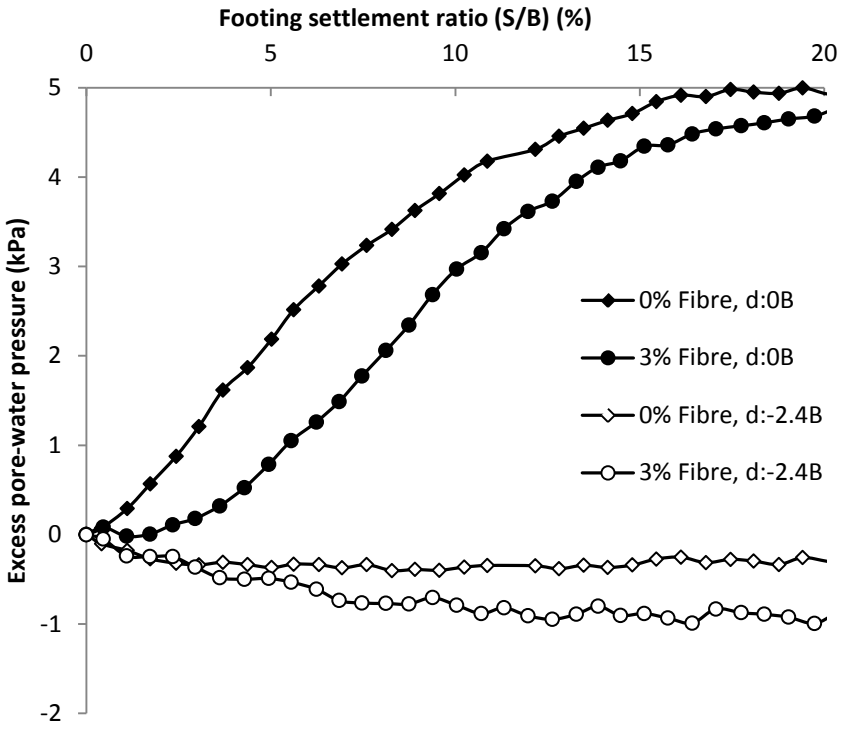

Figure 8.30 Excess pore-water pressure before and after footing (X:1B)

Table 8.4 shows the measured excess stresses at the bottom of the model slope. The rate of reduction of applied footing pressure along depth of soil increased with increase in fibre content. This was the direct outcome of the growing size of vertical displacement contours and integrating effect of fibres which resulted in distributing the applied stresses in wider area under footing.

Table 8.4 Measured excess stresses at failure at the base of model slope (X:1B)

Fibre content	pressure measured (kPa) at: Surface of slope at centre of footing	Tank base at -1.5B away from centre of footing	Tank base at centre of footing	Tank base at +1.5B away from centre of footing	Rate of reduction of stress at centre of footing along height of slope (kPa/mm)
0%	54.4	0.52	1.06	0.50	0.152
1%	54.5	0.29	0.98	1.38	0.153
3%	97.6	1.48	3.85	1.59	0.268

Figure 8.31 shows the sketched slip surface of non-reinforced model slope obtained from displacement vector field at 20% displacement ratio. This figure shows that the vertical extent of slip surface at right side of the footing was up to 1B deep away from surface of the model slope. As it is obvious in this figure, there

are other probable slip surfaces extending to higher depth. However, due to the large horizontal soil displacements at right side of the footing at 0.5B deep of surface of slope, the drawn slip surface is most probable. Figure 8.32 and Figure 8.33 show that, the extent of slip surface at right side of the footing increased with increase in fibre content. This was consistent with the results presented in the previous section (8.4.1). With increase in fibre content the slip surface at left side of the footing was shrunk. Whereas, at 3% fibre content there was no slip surface at left side of the footing

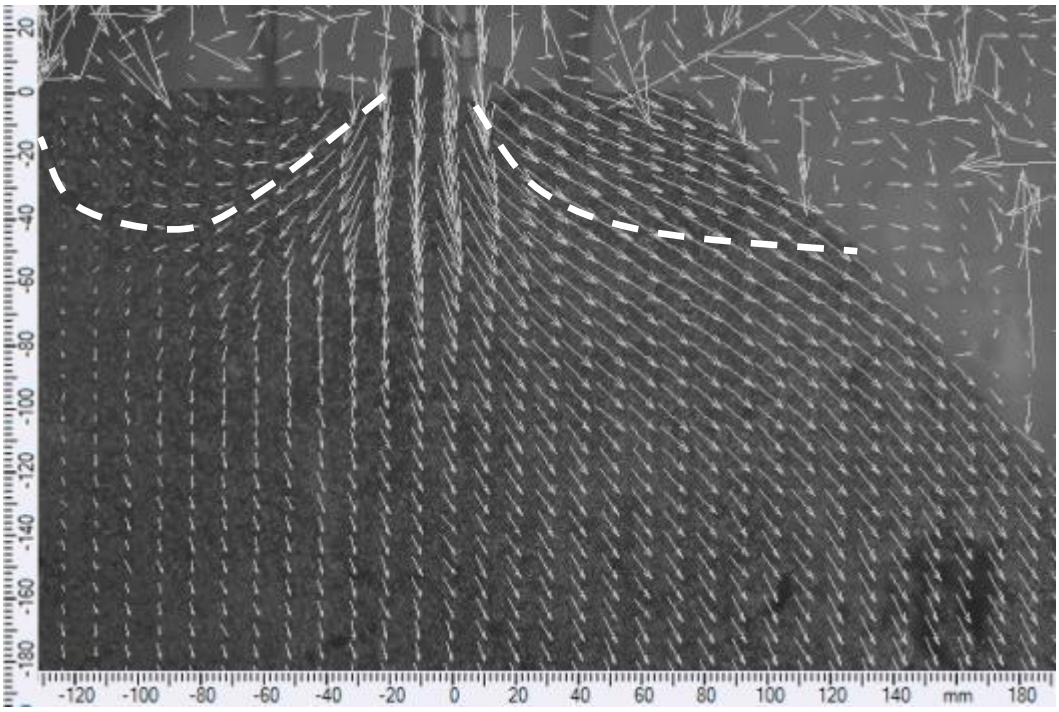

Figure 8.31 Slip surface of non-reinforced model slope (X:1B)

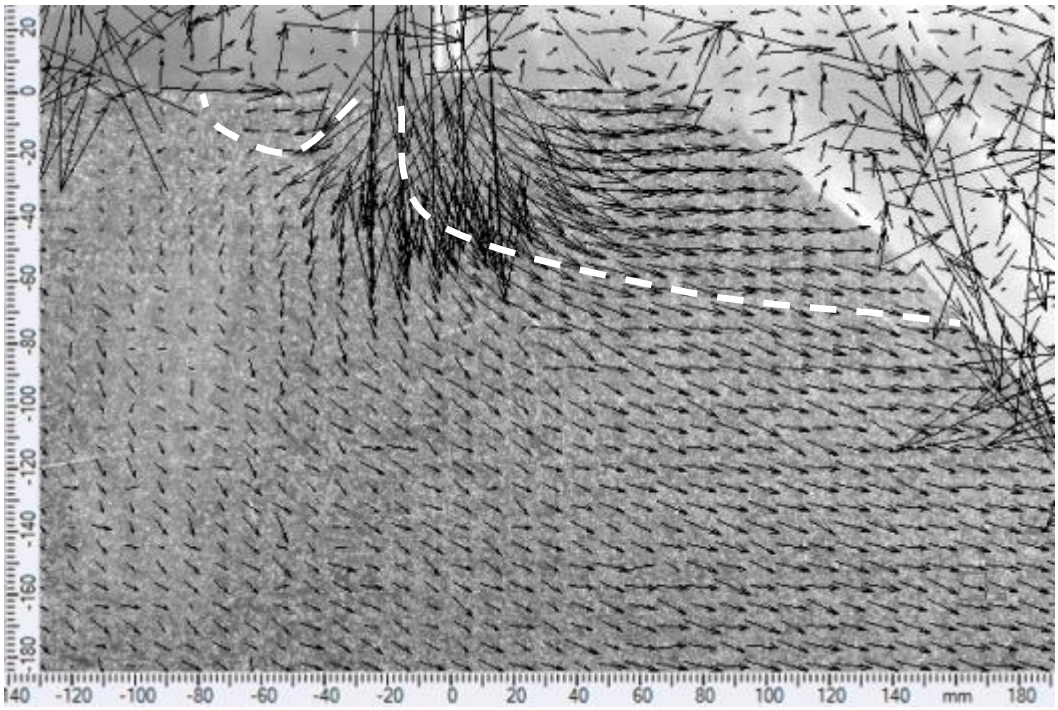

Figure 8.32 Slip surface of 1% fibre reinforced model slope (X:1B)

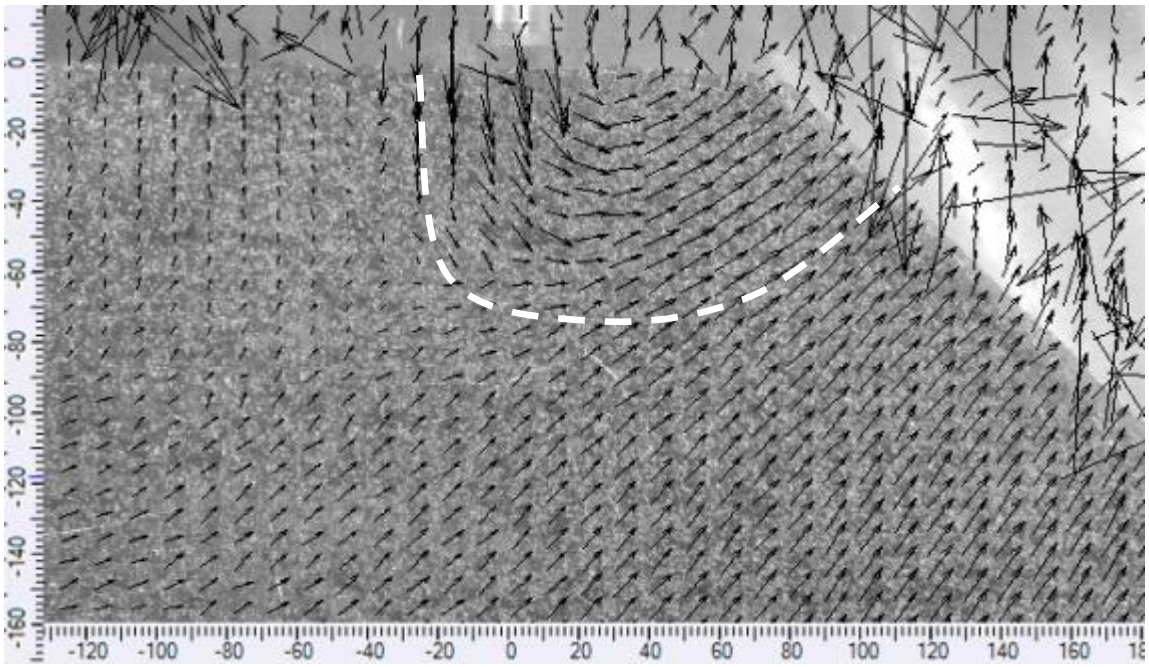

Figure 8.33 Slip surface of 3% fibre reinforced model slope (X:1B)

8.4.3 Model slope with zero footing distance ratio

Model slope tests were also carried out with placing the footing on the crest of slope. Different fibre contents were used to construct the model slope (i.e. 0%, 1%, 3% and 5%). The relationships between footing pressure and settlement ratio of model tests are shown in Figure 8.34 to Figure 8.37.

It was seen that the bearing capacities of the model slopes increased with increase in fibre content from 52.5 kPa (for non-reinforced soil) to 151.2 (for 5% fibre reinforced soil) which was equivalent to 188% increase in bearing pressure.

In the recent arrangement of the test, shear strength along a smaller block of soil was mobilised against shear stress applied by footing. Although, this increased the instability of the slope, its bearing pressure was improved with adding fibre inclusions.

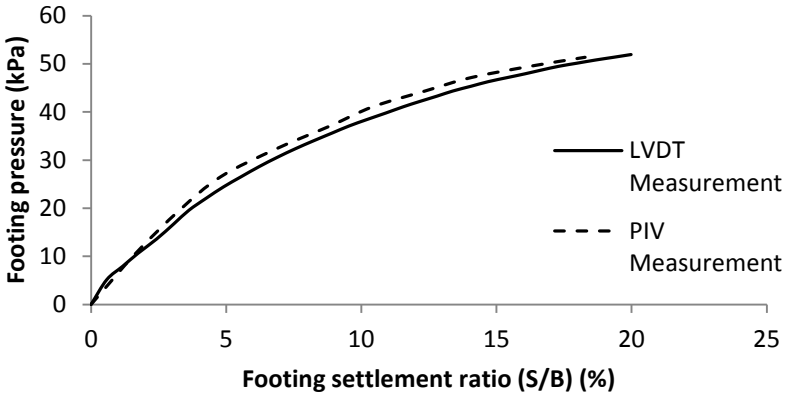

Figure 8.34 Pressure-settlement ratio curves for model slope (0% fibre reinforced C2 soil, X:0)

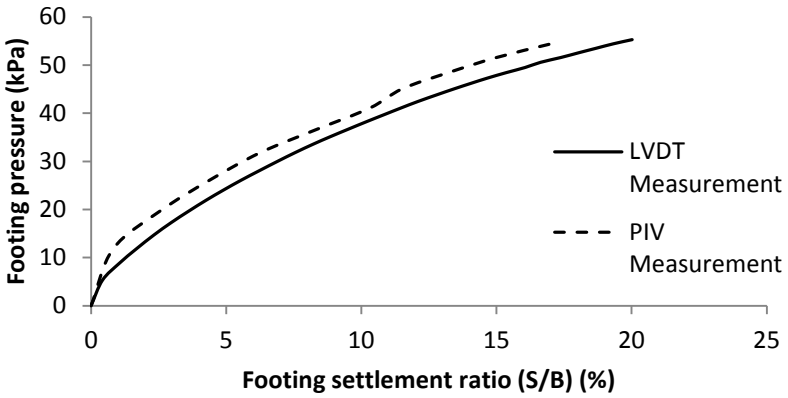

Figure 8.35 Pressure-settlement ratio curves for model slope (1% fibre reinforced C2 soil, X:0)

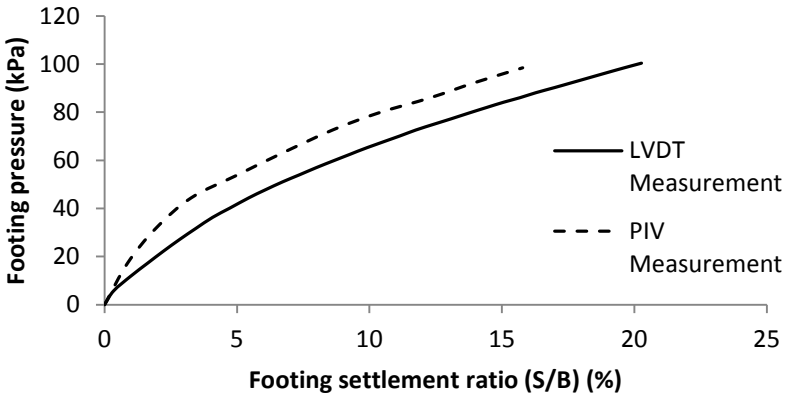

Figure 8.36 Pressure-settlement ratio curves for model slope (3% fibre reinforced C2 soil, X:0)

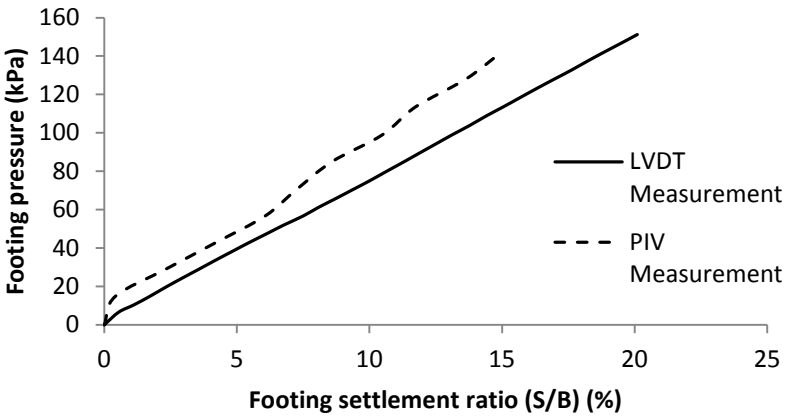

Figure 8.37 Pressure-settlement ratio curves for model slope (5% fibre reinforced C2 soil, X:0B)

Figure 8.38 shows the two dimensional displacement of soil at depth of 0.5B underneath footing. The highest displacement happened under footing and it diminished away from centre of the footing. Highest displacement under footing belonged to non-reinforced soil and it decreased with increase in fibre content. Displacements obtained from PIV analysis for right side of the slope were turbulent due to the large displacements occurred in frontal side of the slope.

All model slopes in this study were kept under loading to experience large settlement ratios to observe the shape of the complete failure. However, just in recent tests that footing was placed at crest of the slope, a well distinguished failure was observed. Figure 8.39 shows that non-reinforced soil failed with obvious sliding in frontal face of the slope. However, adding fibres to the soil reduced the extent of failed block.

The test carried out on model slope reinforced with 5% fibre content, was terminated at a relatively smaller settlement ratio (compared to other tests in recent series) because of reaching upper limit of load cell. For the other model slopes, the test terminated due to exceeding the upper displacement limit of the LVDT sensors.

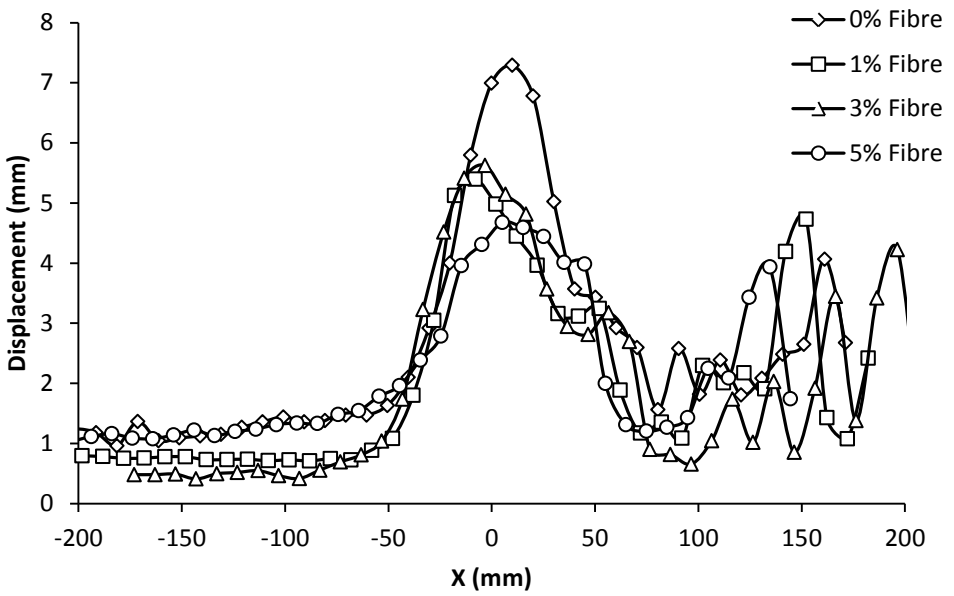

Figure 8.38 Two dimensional displacement at depth of 0.5B under the footing (X:0B)

Non-reinforced soil (S/B:105%)

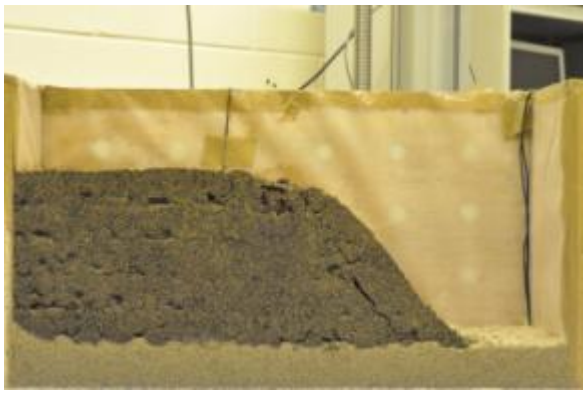

1% fibre reinforced soil (S/B: 154%)

3% fibre reinforced soil (S/B:154%)

5% fibre reinforced soil (S/B: 66%)

Figure 8.39 Failed model slopes at large settlement ratios (X:0B)

Two dimensional displacement vectors and displacement contours of non-reinforced and 5% fibre reinforced model slopes have been shown in Figure 8.40 and Figure 8.41.

For non-reinforced soil maximum horizontal displacement occurred at a depth from zero to 0.5B deep of footing. However, for 5% fibre reinforced soil this happened at depth of zero to B under footing. Vertical displacement contours showed that, the extent of compression zone (positive vertical displacement) increased with increase in fibre content which can be related to integrating effect of fibres to combine the soil masses together to form larger blocks.

Figure 8.42 shows the evolution of excess pore-water pressure at locations of (-)B at left side of the footing and 1.4B at right side of the footing. For non-reinforced soil, negative excess pore-water pressure was measured at right side of the footing which was related to the formation of tension cracks in the model slope (Figure 8.39). However, with increase in fibre content the pore-water pressure measured for 5% fibre reinforced soil after footing tended to zero. This was due to reduction in tension cracks with increase in fibre content. Moreover, increase in permeability of the reinforced soil with increased fibre content resulted in higher rate of pore-water pressure dissipation.

At left side of the footing, excess pore-water pressure exhibited positive pressure which was indicative of compression behaviour under footing (Figure 8.40, Figure 8.41).

Increase in extent of the vertical displacement contours with increase in fibre content supported the increase in rate of excess stress distribution under footing (Table 8.5).

Figure 8.43 to Figure 8.46 show the slip surfaces of non-reinforced and fibre reinforced model slopes with footing placed at crest of the slope. Two slip surfaces can be seen in each model slope, with the left one wider and shallower than the right one.

The depth of both slip surfaces at left side of the footing increased with increase in fibre content which was indicative of confining effect of fibres. However, at the right

side of the footing the slip surfaces were not consistent due to the unconfined boundary condition of slope at right side.

Compared to previous model slope tests, it was observed that, the efficiency of the fibre reinforcement for improving the bearing pressure of the model slopes was reduced with reducing footing distance ratio. This was mainly due to the unconfined boundary condition of the slope at crest of slope which increased the instability of the involved soil block under footing.

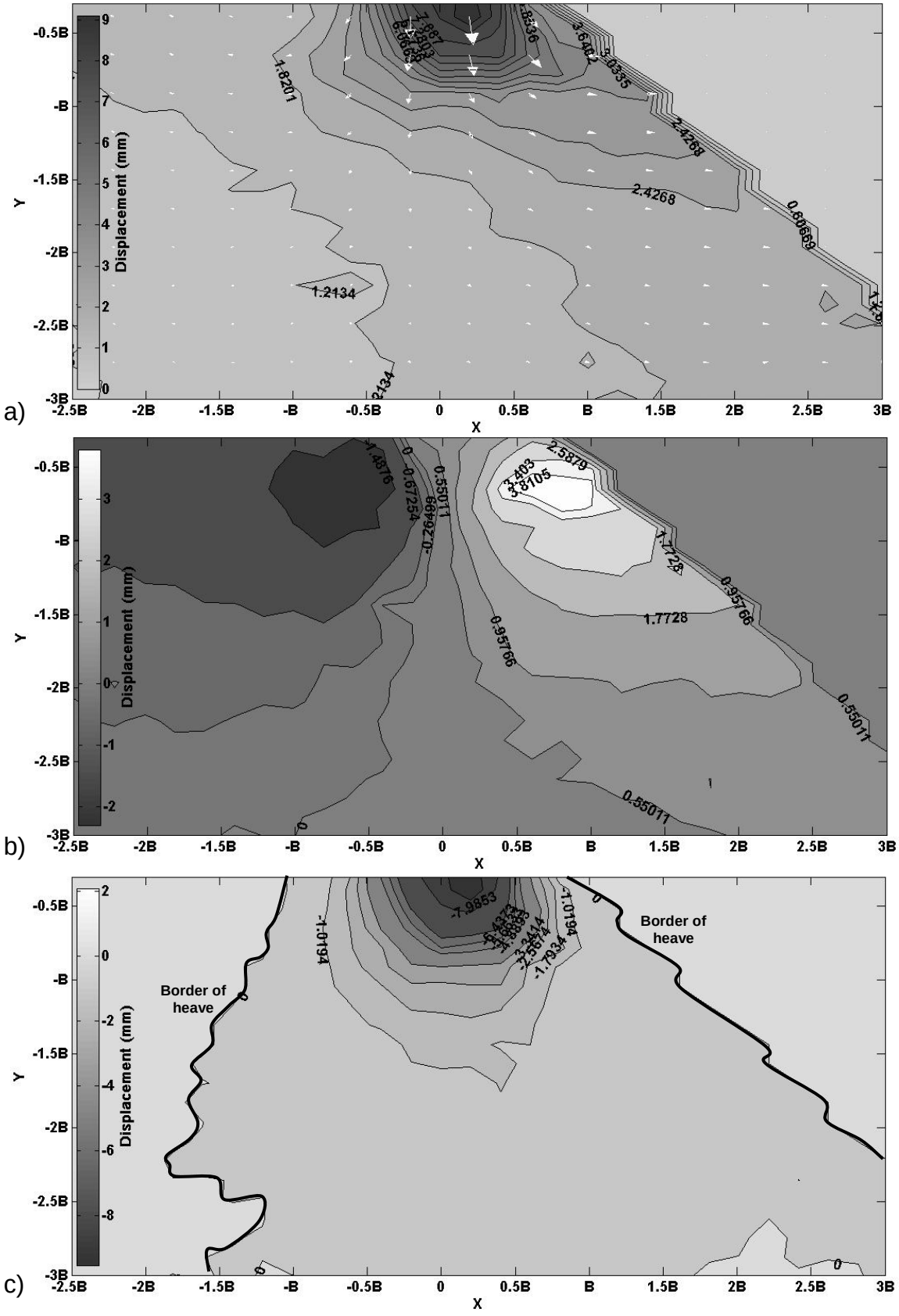

Figure 8.40 Contours of displacement under footing at failure (0% Fibre, X:0B) a) Total b) Horizontal c) vertical displacement

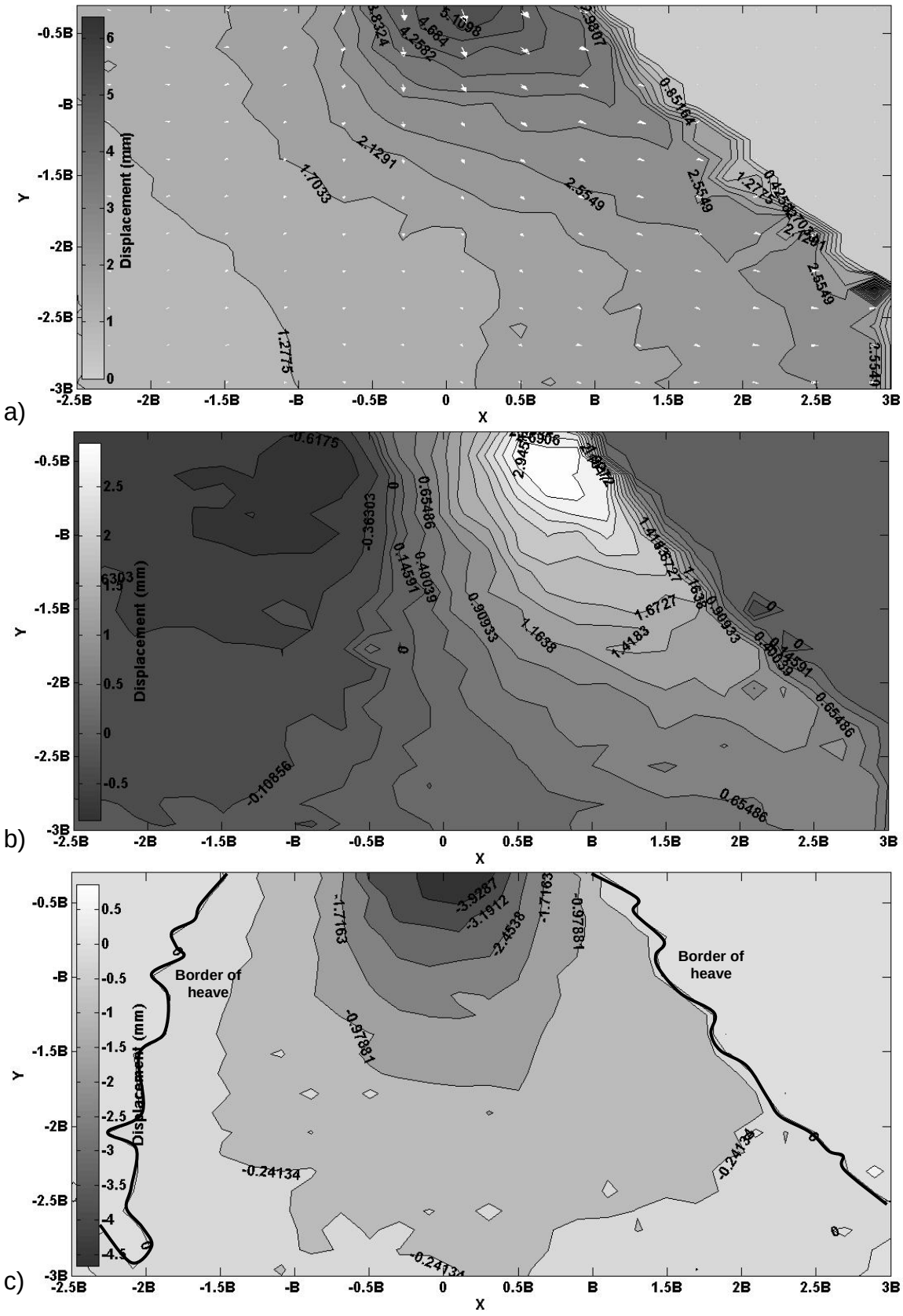

Figure 8.41 Contours of displacement under footing at failure (5% Fibre, X:0B) a) Total b) Horizontal c) vertical displacement

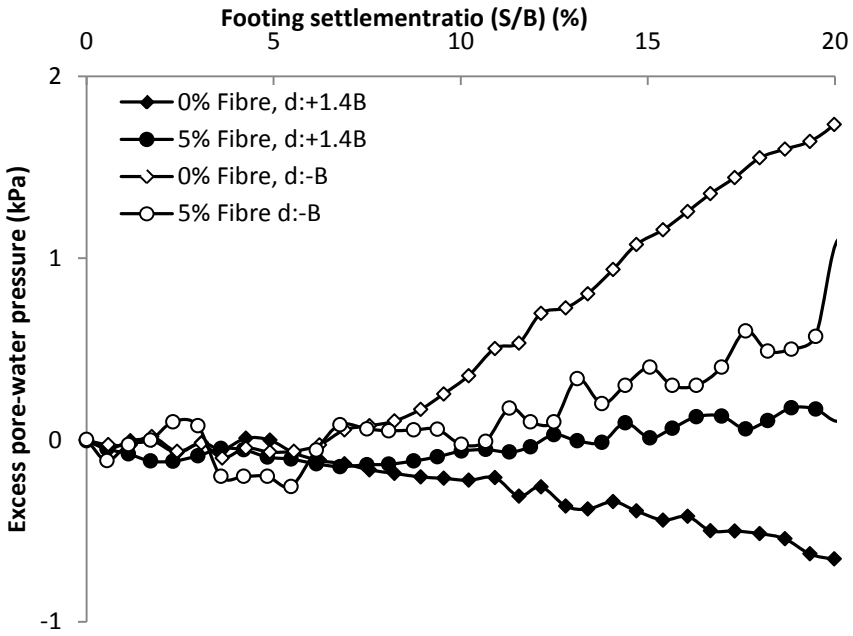

Figure 8.42 Excess pore-water pressure before and after footing (X:0B)

Table 8.5 Measured excess stresses at failure at the base of model slope (X:0B)

Fibre content	pressure measured (kPa) at: Surface of slope at centre of footing	Tank base at -1.5B away from centre of footing	Tank base at centre of footing	Tank base at +1.5B away from centre of footing	Rate of reduction of stress at centre of footing along height of slope (kPa/mm)
0%	52.5	0.16	1.43	0.99	0.146
1%	55.3	0.31	1.59	0.21	0.153
3%	100.4	0.81	2.40	1.85	0.280
5%	151.2	2.22	6.70	5.09	0.413

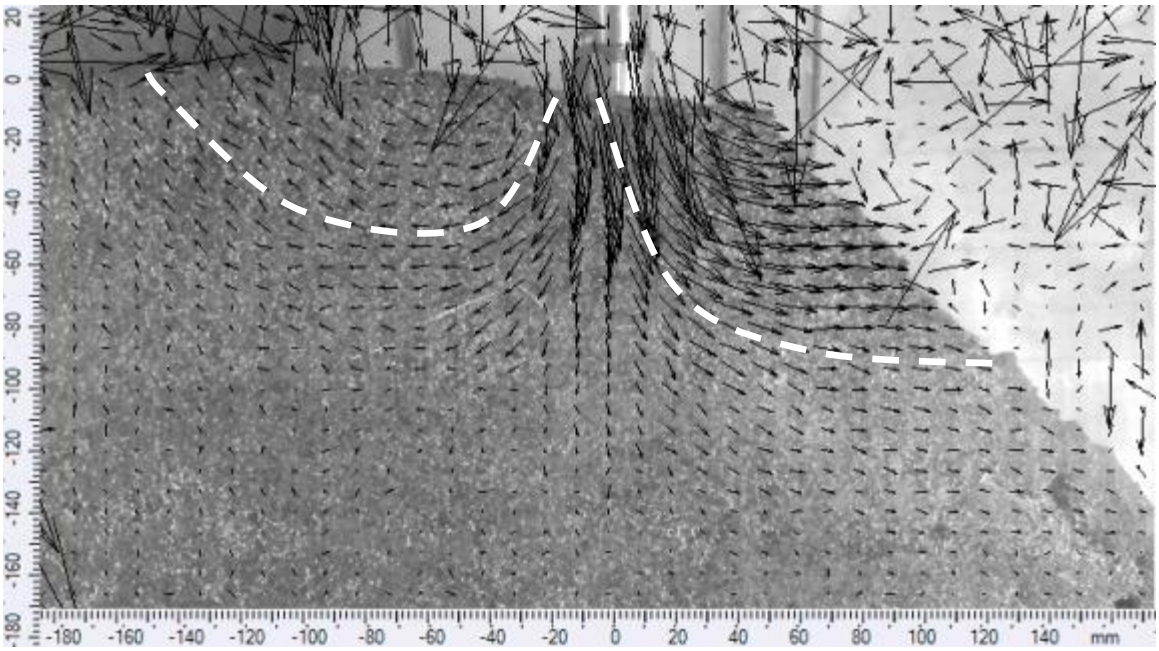

Figure 8.43 Slip surface of non-reinforced model slope (X:0B)

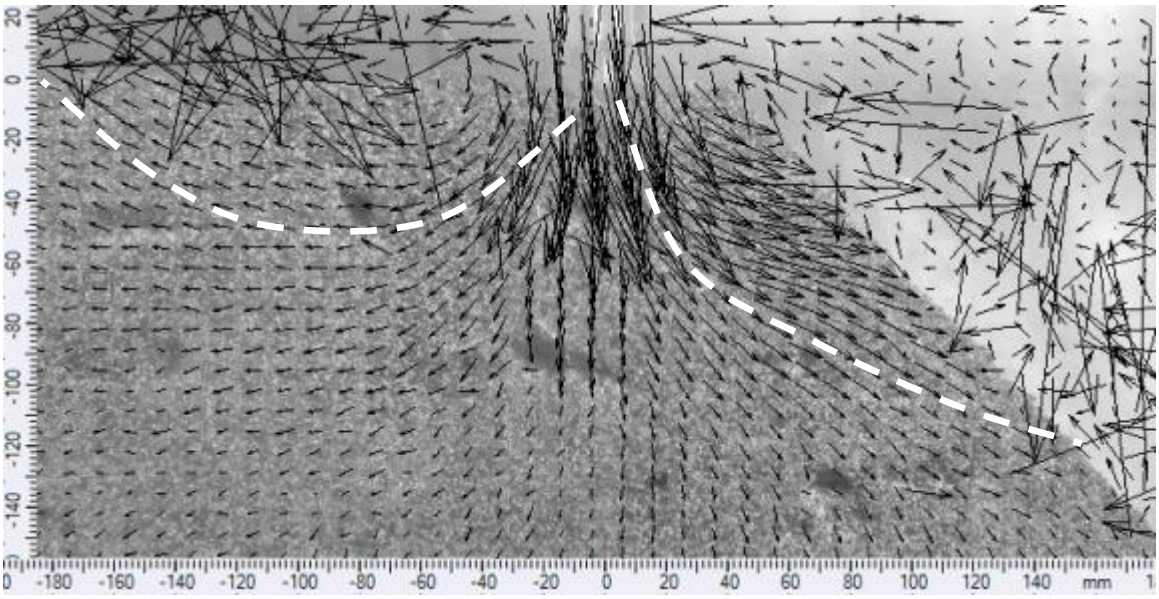

Figure 8.44 Slip surface of 1% fibre reinforced model slope (X:0B)

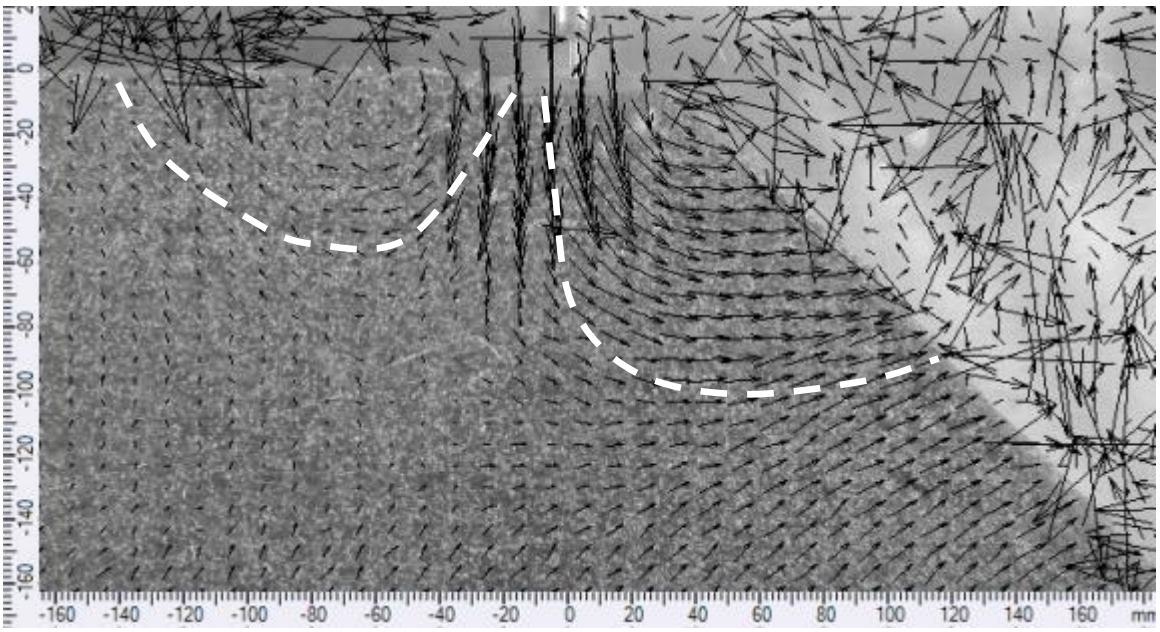

Figure 8.45 Slip surface of 3% fibre reinforced model slope (X:0B)

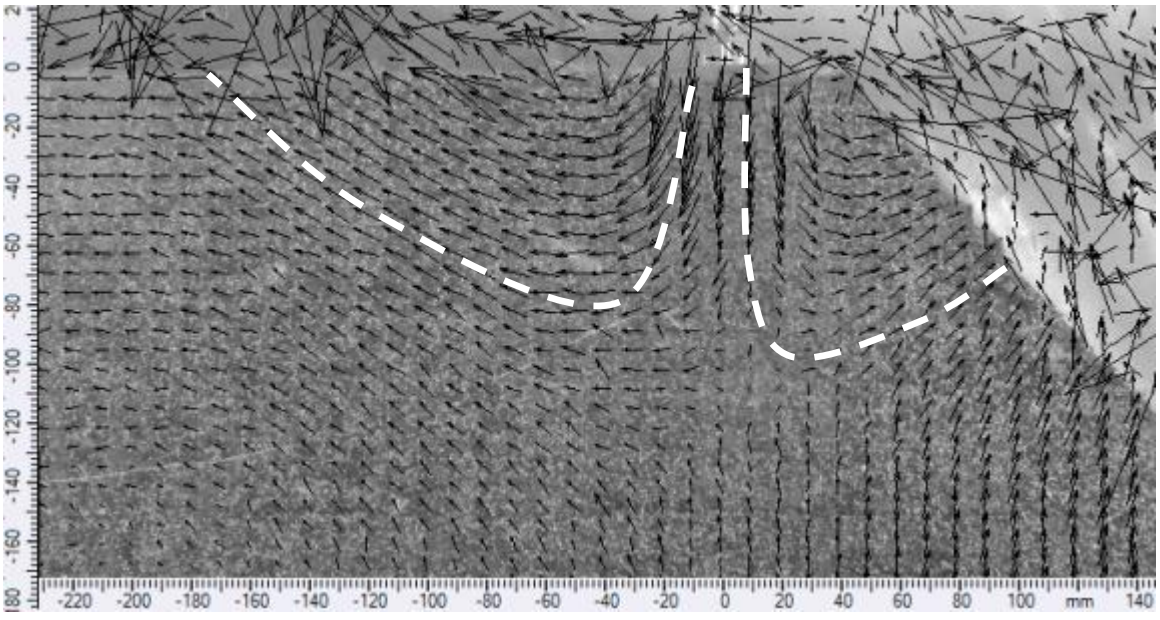

Figure 8.46 Slip surface of 5% fibre reinforced model slope (X:0B)

8.4.4 Summary of the findings

1) Model slope tests that carried out in this study showed that increase in the distance of the footing from crest of slope would result in increasing the bearing pressure. However, there was no apparent change observed by increasing the footing distance ratio from zero to 1. The highest gain in bearing pressure by increasing the footing distance ratio was achieved by increasing the distance ratio from zero to 3 for model slope prepared with 1% fibre content (i.e. 52% increase, change from 55.3 kPa for X:0 to 84.1 kPa for X:3B).

2) Fibre reinforcement increased the bearing pressure of the model slopes significantly. And the rate of improvement was increased with increase in fibre content of the reinforced soil. Including 5% fibre in model slope with footing distance ratio of 3, increased its bearing pressure by 271% compared to non-reinforced model slope at the same footing distance ratio. For model slope with footing distance ratio of zero, the rate of improvement with 5% fibre was reduced to 188%.

3) The location of maximum horizontal displacement under footing for all non-reinforced and fibre reinforced model slopes was happened at depth of almost equal to the width of footing. For a given footing distance ratio, dimensions of the slip surface increased with fibre reinforcement.

4) Results of footing model tests reported in this study were based on a prototype laboratory model. Small scale models are widely used in geotechnical engineering to investigate the behaviour of a full scale problem. However, due to the scale effects and nature of soils especially cohesive soils, the laboratory models may not behave in the same way as real structure does. This is primarily due to the differences in stress levels between the model tests and real structures.

5) The magnitude of the stresses under the scaled model footing is much lower than that experienced under a full scale footing. Because of great degree of dependency between cohesion and fiction angle of clay soils and

applied normal and confining stresses, the average shear strength mobilised along a slip line in laboratory scaled model is quite different with that occurred under a real size foundation. However, the main purpose of this investigation was to investigate the efficiency of waste carpet fibres for increasing the bearing pressure of clay slopes and also to use the particle image velocimetry to track the displacement of soil particles under footing. And therefore, the results of these experiments can be utilised to adopt reinforcement of real size slopes with waste carpet fibres.

Chapter 9 Conclusion and recommendation

Fibre reinforcement of the soil is a viable replacement of traditional soil improvement methods which can be applied to variety of problematic soils including low shear strength clays, expansive clays as well as loose sands.

In this study different types of clay soils covering plasticity index ranges of low to high, and 2 types of waste carpet fibre which were mainly synthetic fibres were used.

An experimental research was conducted to investigate the mechanical behaviour of low shear strength clay soils reinforced with waste carpet fibres. The experimental programme comprised a series of Proctor compaction tests, unconfined compression tests, swelling pressure tests, one-dimensional consolidation tests and consolidated undrained triaxial tests. A neural network model was also developed based on the results of the triaxial shear tests to predict the deviator stress of fibre reinforced soils at failure.

To validate the findings, a relatively large scale laboratory tank was employed to perform a series of laboratory model slope tests on fibre reinforced clay soils. The displacement behaviour of the model slope was analysed by PIV (Particle Image Velocimetry) method to study the displacements of the fibre reinforced model slope under strip footing load.

As part of the research during the study, several equipment and facilities were designed and developed. These consisted of a pressure distribution panel for triaxial test apparatus, full automatic data logging system including hardware and software, appropriate soil moulds for specimen preparation, suction probe, suction probe saturator/calibrator and pressure cell calibrator.

9.1 Conclusions

The following conclusions can be drawn from the analysis of the experimental data and modelling obtained in this study:

1) Majority of the previous research on fibre reinforcement of soils was focused on quantitative examination of effect of small percentage of fibres (i.e. less than 1%) on mechanical properties of soils. In this study, since carpet fibre is classified as waste material, it was decided to investigate the addition of high percentage of waste carpet fibres (i.e. up to 5%). Therefore, fibre contents of 1%, 3% and 5% of dry mass of soil were selected. Because of reduced workability and practical difficulties to mix higher fibre contents evenly with the soil, the maximum fibre content used in this study was limited to 5%.

2) Unconfined compression strength of the clay soils can be effectively improved by including fibres whilst controlling the dry unit weight and moisture content of the fibre reinforced soil. The relative gain in compression strength increased with increase in dry unit weight and reduction in moisture content of the soil. However, fibre reinforced soil specimens compacted at their respective maximum dry unit weight and optimum moisture content showed reduction in compression strength with increased fibre content.

3) Under constant dry unit weight condition and moisture content, with increase in the fibre content, compression strength of the fibre reinforced soil increased linearly at lower dry unit weights and it grew exponentially at higher dry unit weights.

4) Although at the same dry unit weight, increasing moisture content affected the obtained compression strength to a lower value, increase in both dry unit weight and moisture content improved the strength of the soil.

5) Fibre reinforced soils showed increased ductility and higher energy absorption capacity compared to those of non-reinforced soil with brittle failure. The projected ductile behaviour of fibre reinforced soils was manifested in reduced size of main cracks with apparent increase in number of small cracks. Furthermore, the strain softening stress-strain behaviour of

non-reinforced soil was gradually transformed to strain hardening one with increasing fibre content.

6) Swelling pressures of fibre reinforced soils prepared at their respective maximum dry unit weight and optimum moisture content reduced significantly with increase in fibre content.

7) ABF fibres were found to be particularly more effective in increasing the unconfined compression strength of the studied clay soils. However, GBF fibres diminished the swelling pressure of the clay soils significantly.

8) Increase in dry unit weight of the fibre reinforced soil at constant moisture content and fibre content showed increased swelling pressure. However, swelling pressure of fibre reinforced soils was found to be reduced with increase in moisture content at constant fibre content and dry unit weight.

9) The void ratio of the fibre reinforced soil with increase in bentonite content at high stresses was independent of the fibre content and initial dry unit weight of the soil. Therefore, its void ratio converged to void ratio of non-reinforced soil specimen compacted at its maximum dry unit weight.

10) Shear strength parameters of fibre reinforced soil increased with increase in fibre content. For example cohesion intercept and internal friction angle of 5% GBF fibre reinforced soil compacted at dry unit weight of 17.8 kN/m^3 increased by 118% and 82% respectively compared to those of non-reinforced soil compacted at dry unit weight of 20.1 kN/m^3.

11) Neural network model developed in this study was found to be well predictive of the deviator stress of the fibre reinforced soils at failure. The developed model showed that, at the same consolidation stress, the rate of increase in deviator stress increased exponentially with increase in fibre content. Moreover, it showed that at constant consolidation stress, increase in deviator stress due to increase in fibre content grew from a linear relationship to an exponential one.

12) The bearing pressure of the model slopes tested in this study improved significantly with increased fibre content. The rate of improvement increased with increase in footing distance ratio from crest of the slope. For example, including 5% fibre in model slope with footing distance ratio of 3, increased its bearing pressure by 271% compared to the non-reinforced model slope at the same footing distance ratio. For model slope with footing distance ratio of zero, the rate of improvement was reduced to 188% corresponding to inclusion of 5% fibre.

13) Mixing fibres and clay soils requires careful attention as fibres due to their random distributions tend to become twisted together and create pockets of fibre. This may defect the strength of the compacted fibre reinforced soil due to increased local void ratios. Through comparing several methods for mixing clay soils and fibres in this study, it was found that the most suitable results in terms of uniform distribution of fibres in the soil are achieved by mixing dry soil and fibres initially and spraying water on the mixture of soil/fibre. The quantitative evaluation of fibre distribution in several soil specimens showed that GBF fibres are distributed more uniformly in the soil compared to ABF fibres. However, the uniformity of fibre distribution reduced slightly with increase in fibre content

14) In order to extend the results of laboratory experiments on fibre reinforced soil to field application and maintain the consistency between outcomes of both practices, several factors regarding depot of fibres must be considered. These include continuous supply of fibres, consistency in the fibre's quality. Moreover, fibres must be environmentally free of contamination. As far as fibres used in this study are of waste by product of carpet manufacturing companies, such waste is always available and can be used for soil fibre reinforcement application. The quality of the waste fibres depends mainly on the dimensions and type of the fibres. Dimension of the fibres can be controlled through shredding process. However, type of the fibres may vary due to the variable compositions of the manufactured carpet. Therefore, it must be ensured that fibres with the same type or at least fibres with major identical type are used.

15) Based on the results of the conducted study, it is difficult to recommend a general fibre reinforcement solution for improving all the mechanical aspects of the clay soils. For example, it was found that there is no asymptote in improving the deviator stress and shear strength parameters of the clay soils with increase in fibre content (within the studied range). Unconfined compression strengths of the fibre reinforced specimens increased significantly with increase in fibre content (with no asymptote observation for specimens prepared at the same dry unit weight). However, for specimens prepared at their own maximum dry unit weight and optimum moisture content increase in fibre content resulted in reduction in unconfined compression strength.

Reduction in swelling pressure of the fibre reinforced clay soils is highly dependent on the initial moisture content and dry unit weight of the soil. According to the results, for specimens prepared at the same dry unit weight, 1% ABF fibre was found optimal for reducing the swelling pressure. However, provided the condition that fibre reinforced specimens are prepared at their own dry unit weights and optimum moisture contents, there is no asymptote for reduction in swelling pressure with increase in fibre content (within the studied range).

9.2 Recommendation for future work

The findings in this research help to understand the behaviour of reinforced clay soils with waste carpet fibres. The following research is recommended to extend the results of the this study into a broader level

1) In this study the shear strength behaviour of fibre reinforced clay soil was investigated at consolidated undrained condition on fully saturated specimens which was representative of shear strength behaviour at the short term. However, in order to investigate the effect of fibre reinforcement on long term shear strength behaviour of clay soils, it is required to carry out consolidated drained triaxial tests on fully saturated clay soil specimens. Moreover, as most of the soils at service condition are not fully saturated especially in areas with intense seasonal changes, it is recommended to study the effect of fibre reinforcement on shear strength of unsaturated clay soil specimens using double cell triaxial apparatus.

2) The mixing procedure of waste carpet fibres including fibres with a variety of dimensions with cohesive clay soils was examined by preparing small triaxial/swelling pressure specimens. Moreover, the procedure was adapted to prepare the model slope as a large scale laboratory model. The results found to be satisfactory in terms of uniformity of the fibre content in the fibre reinforced soil. However, the results of this study can be adapted to field trials to investigate the findings of this study in field application. Further study is also required to improve the mixing efficiency of waste carpet fibres with cohesive clay soils in field trials.

   There are a few successful instances of using fibre reinforcement concept for reinforcing road base or repairing highway embankments. Mouchel consulting company[17,18] (2011) reported successful application of geofibres (polypropylene fibres) for reinforcing defected embankment located on A1(M)

[17] www.mouchel.com

[18] http://www.ice.org.uk/ICE_Web_Portal/media/northwest/2012flyers/NWGG-Flyer-9-November-2011--Fibre-Reinforced-Soil.pdf

junction to the north of the M25 motorway in United Kingdom by carrying out full scale field trial tests. The earthwork defect comprised full height soil failure with extensive slope desiccation cracking. To reduce difficulties during mixing geofibres to the full depth of the soil, loose fill material were placed in 100mm lifts and fibres were spread over the soil. Mixing procedure was successfully carried out using Bob Cat T250 skid steer with a tiller attachment. The results confirmed reduction in desiccation cracking comprising reduction in depth and length of cracks.

For reducing the difficulties of mixing fibres with cohesive soils, it may be useful to increase the workability of the soil by mixing the soil with proportionate amount of additives such as lime or cement. Therefore, fibres can be mixed in the mixture of lime/soil easier. The extent of such recommendation must be examined through full scale field tests.

3) Beneficial application of waste carpet fibres for reinforcing cohesive soils was investigated in this study. However, to establish a generalised conclusion and to verify the observed behaviour in different soils, it is required to study the behaviour of reinforced sand soils with waste carpet fibres by conducting a series of triaxial shear tests. The results of such tests can be inputted to the developed neural network to extend the prediction range of such network for different types of soil.

4) A model test was developed in this study to investigate the behaviour of fibre reinforced slope under footing load. The sought parameters included footing distance ratio and fibre content. Further parameters such as angle of slope and height of slope can be incorporated into the study to investigate the effect of fibres on slopes with different geometry.

5) In the current study triaxial shear test was not carried out on non-reinforced and fibre reinforced C2 soil specimens and therefore, the shear strength parameters of these soil specimens were not available to study the factor of safety of the model slopes. Further study is required to determine the shear strength parameters of the fibre reinforced C2 soil to determine the factor of safety for each model slope. The model slope can be simulated in the

geotechnical finite element software such as PLAXIS to compare the observed behaviour of model slope with predicted behaviour by software.

6) The general benefit of including waste carpet fibres in model slopes was examined using several model slope tests. The indicated improvement in behaviour of footing resting at the top of a reinforced clay slope provided a useful basis for carrying out full scale tests or centrifuge model tests to enhance the understanding of the real behaviour and application of soil reinforcement with waste carpet fibres. Therefore, it is recommended to conduct centrifuge tests to study the behaviour of model slope at elevated rates of gravity to simulate the conditions in the field.

7) The environmental issues of mixing fibres in the soils require further investigation. Waste carpet fibres may include contaminations and colour pigments which can be released into the soil in long term. Moreover, durability of fibres in harsh conditions such as acidic, alkaline or saline soils should be investigated. Therefore, it is recommended to conduct a series of differential scanning calorimetry (DSC) tests on waste carpet fibres aged in different pH buffers to evaluate their thermodynamical properties such as melting point.

References

1. Abdi, M. R., Parsapajouh, A. and Arjomand, M. A. (2008). Effects of Random Fibre Inclusion on Consolidation, Hydraulic Conductivity, Swelling, Shrinkage Limit and Desiccation Cracking of Clays. *International Journal of Civil Engineering*. Vol.6 (4), pp.284-292

2. Abe, K., Ziemer, R.R., (1991a). Effect of tree roots on shallow-seated landslides. USDA Forest Service Gen. Tech. Rep. PSW-GTR-130, pp.11-20

3. Abe, K., and R. R. Ziemer (1991b). Effect of tree roots on a shear zone: Modelling reinforced shear stress, Can. J. For. Res., Vol.21,pp.1012-101

4. Adeli, H. and Park, H. S. (1995). A neural dynamics model for structural optimization: Theory. *Journal of Computers and Structures*. Vol.57 (3), pp.391–390

5. Adeli, H. and Yeh, C. (1989). Perceptron learning in engineering design. *Journal of Microcomputers in Civil Engineering*. Vol.4 (4), pp.47-56

6. Adrian, R. J. (1991). Particle imaging techniques for experimental fluid mechanics. Annual Review of fluid Mechanics, Vol.23, pp.261-304

7. Akbulut, S., Arasan, S. and Kalkan, E. (2007). Modification of clayey soils using scrap tyre rubber and synthetic fibres. *Journal of Applied Clay Science*. Vol.38, pp.23-32

8. Al-Akhras, N. M., et al. (2008). Influence of fibres on swelling properties of clayey soil. *Geosynthetics International Journa. Vol.*15 (4), pp.304-309

9. Al-Refeai, T.O. (1991). Behaviour of granular soil reinforced with discrete randomly oriented inclusions. *Geotextiles and Geomembranes journal*. Vol.10, pp.319-333

10. American Society of Civil Engineers (2010). Compaction Grouting Consensus Guide (ASCE Standard 53-10), USA: ASCE

11. Andersland, O. B. and Khattak, A. S. (1979). Shear strength of kaolinite/fiber soil mixture. *In: Proc. of 1st Int. Conf. on Soil Reinforcement*, Paris, pp.11-16

12. Banimahd, M., Yasrobi, S. and Woodward, P.K. (2005). Artificial neural network for stress–strain behaviour of sandy soils: Knowledge based verification, *Journal of Comput. Geotech*., Vol.32, pp 377-386

13. Bell, F. G. (1993). Engineering Treatment of Soils. Luton: Taylor & Francis

14. Bergado, D. T. (1996), Soft Ground Improvement in Lowlands and other Environments. USA: American Society of Civil Engineers

15. Bhardwaj, D. K. and Mandal J. N. (2008). Study on Polypropylene Fibre Reinforced Fly Ash Slopes. In*: The 12th International Conference of International Association for Computer Methods and Advances in Geomechanics*. Goa, India

16. Bjerrum, L. (1973). Problems of soil mechanics and construction on soft clays and structurally unstable soils. *In: Proc. 8th Int. Con. Soil Mechanics and Foundation Eng*. Vol.3, pp.109-159

17. Boutrup, Eva, Holtz, R. D. (1982). Fabric Reinforced Embankments Constructed on Weak Foundations: Final Report. West Lafayette, In: Purdue University

18. British Standards, BS1377-2:1990, Classification tests

19. British Standards, BS1377-4:1990, Compaction-related tests

20. British Standards, BS1377-5:1990, Determination of swelling and collapse characteristics

21. British Standards, BS1377-6:1990, Consolidation and permeability tests in hydraulic cells and with pore pressure measurement

22. British Standards, BS1377-7:1990, Determination of unconfined compression strength

23. British Standards, BS1377-8:1990, Shear strength tests effective stress

24. BS EN ISO 14688-1:2002, Geotechnical investigation and testing, Identification and classification of soil, Part 1: Identification and description

25. Burak, Sapaz (2004). Lateral versus vertical swell pressures in expansive soils. Dissertation (MSc), Middle East Technical University, Cyprus

26. Cai, Y.,et al. (2006). Effect of polypropylene fibre and lime admixture on engineering properties of clayey soil. *Journal of Geotechnical and Geoenvironmental Engineering*. Vol.87, pp.230-240

27. Casagrande, M. D. T. and Coop, M. R. (2006). Behaviour of a Fibre-Reinforced Bentonite at Large Shear. *Journal of Geotechnical and Geoenvironmental Engineering*. Vol.132, pp.1505-1508

28. CEN ISO/TS 17892-6:2004 Geotechnical investigation and testing - Laboratory testing of soil - Part 6: Fall cone test

29. Cetin, H., Fener, M. and Gunaydin, O. (2006). Geotechnical properties of tire-cohesive clayey soil mixtures as a fill material. *Journal of Engineering Geology*. Vol.88, pp.110-120

30. Chauhan, M.S.,Mittal, S., Mohanty, B. (2008). Performance evaluation of silty sand subgrade reinforced with fly ash and fibre, Journal of Geotextiles and Geomembranes, Vol.26. Issue 5, pp. 429-435

31. Chen, C. W. and Loehr, J. E. (2008). Undrained and drained triaxial tests of fibre-reinforced sand. In*: Proceedings of the 4th Asian Regional Conference on Geosynthetics*. Shanghai, China, pp.114-120

32. Consoli, N. C. et al. (2003). Plate load test on fibre-reinforced soil. *J. Geotech. Geoenviron. Eng*. Vol.129 (10), pp.951-955

33. Consoli, N. C., et al. (2007). Shear strength behaviour of fibre-reinforced sand considering triaxial tests under district stress paths. *Journal of Geotechnical and Geoenvironmental Engineering*. Vol.133, pp.1466-1469

34. Consoli, N.C. et al., (1998). Influence of fibre and cement addition on behaviour of sandy soil. *Journal of Geotechnical and Geoenvironmental Engineering*. Vol.124 (12), pp.1211-1214

35. Edincliler, A., Firat, C. A. and Cagatay, A. (2010). Triaxial compression behaviour of sand and tire wastes using neural networks. *Neural Computing & Applications* Journal., pp.1-12

36. Erol, A. O. and Ergun, U. (1994). lateral swell pressures in expansive soils. *In: 8th Int. Conf. on Soil Mech. and Found. Eng*. New Delhi, India, pp.1511-1514

37. Esna-ashari, M. and Asadi, M. (2008). A study on shear strength and deformation of sandy soil reinforced with tire cord waste. *In: Proceedings of 4th Asian Regional Conference on Geosynthetics*. Shanghai, China, pp. 355-359

38. Estabragh, A., Bordbar, A., Javadi, A. (2011). Mechanical Behaviour of a Clay Soil Reinforced with Nylon Fibres. *Geotechnical and Geological Engineering* Journal. Vol.29, pp.899-908

39. Eurocode 7, BS EN 1997-2:2007, Geotechnical design Part 2: Ground investigation and testing

40. Evans, Ianto (2002). The Hand-Sculpted House: A Philosophical and Practical Guide to Building a Cob Cottage. Vermont: Chelsea Green Publishing Company

41. Falorca, I. M.C.F.G., Pinto, M. I.M. and Ferreira, G. L. M. (2006). Residual shear strength of sandy clay reinforced with short polypropylene fibres randomly oriented. *In: Proceeding of 8th internation conference on geosynthetics (8ICG)*, Yokohama, Vol.4, pp.1663-1666

42. Fang, H. Y. (1990), Foundation Engineering Handbook. 2nd ed. Norwell: Kluwer Academic Publishers

43. Fausette, L. (1994). Fundamentals of Neural Networks Architectures, Algorithms, and Applications. 1st ed. NJ, USA: Prentice-Hall Inc

44. Freilich, B. J., Li, C. and Zornberg, J. G. (2010). Effective Shear Strength of Fibre-Reinforced Clays. *In: 9th International Conference on Geosynthetics*. Brazil, pp.1997-2000

45. Freitag, D. R. (1986). Soil randomly reinforced with fibres. *Journal of Geotechnical Engineering*. Vol.112 (8), pp.823-826

46. Galushkin, A. I. (2007). Neural Network Theory. 1st ed. New York, USA: Springer Berlin Heidelberg

47. Garber, E. (1929). Untersuchungen uber die Druckverteilungim Oertlick Belasteten Sand. Dissertation (MSc.), Technische Hochschule, Zurich

geotechnical testing. CUED/D-Soil/TR-322., Cambridge University, UK.

48. Ghaboussi, J., Garret, JH. Jr., Wu, X. (1990). Material modelling with neural networks. *In: Proceedings of the international conference on numerical methods in engineering: Theory and applications.* Swansea, UK, pp.701-717

49. Ghavami, K., Filho, R. D. T. and Barbosac, N. P. (1998). Behaviour of composite soil reinforced with natural fibres. *Journal of Cement and Concrete Composites*. Vol.21, pp.39-48.

50. Ghiassian, H., Poorebrahim, G. and Gray, D. (2004). Soil Reinforcement with Recycled Carpet Wastes. *Waste Management & Research Journal.* Vol.22, pp.108-114

51. Goh, A. T. C. (1995). Neural networks for evaluating CPT calibration chamber test data. *Journal of Microcomputers in Civil Engineering*. Vol.10 (2), pp.147–51

52. Gohl, B. (2005). Explosive Compaction. Available: http://www.explosivecompaction.com/Pages/explosive_compaction.htm. Last accessed 10 April 2012

53. Gray, D. H. (1970). Role of woody vegetation in reinforcing soils and stabilizing slopes. *In: Proc. Symp. on Soil Reinforcement and Stabilizing Techniques.* pp.253-306

54. Gray, D.H. and Ohashi, H. (1983). Mechanics of Fibre Reinforced in Sand. *Journal of\ Geotechnical and Geoenvironmental Engineering*. Vol.109 (3), pp.335-353

55. Gregory, Garry H. and Chill, David S. (1998). Stabilization of earth slopes with fibre reinforcement. *In: Sixth International Conference on Geosynthetics*, Atlanta

56. Guan, Y. and Fredlund, D. G (1997). Use of the tensile strength of water for the direct measurement of high soil suction. *Canadian Geotechnical Journal*. Vol.34, pp.604-614

57. Harianto, T., et al. (2008). Effects of Fibre Additives on the Desiccation Crack Behaviour of the Compacted Akaboku Soil as A Material for Landfill Cover Barrier. *Journal of Water, air, and soil pollution*. Vol.194, pp.141–148

58. Head, K. H. (1998). Manual of Soil Laboratory Testing: Effective Stress Tests v.3: Effective Stress Tests Vol.3, 2nd ed. England: John Wiley and Sons.

59. Heineck, K. S., Coop, M. R.; Consoli, N., (2005). Effect of microreinforcement of soils from very small to large shear strains. *Journal of Geotechnical and Geoenviromental Eng*. Vol.131 (8), pp.1024-1033

60. Huat, B.K., Ali, F. H. and Maail, S. (2005). The Effect of Natural Fibre on the Shear Strength of Soil. *American Journal of Applied Sciences*., pp.9-13

61. Ikizler, S. B., Aytekin, M. and Türker, E. (2009). Effect of fibres on swelling characteristics of bentonite. *In: Second International Conference on New Developments in Soil Mechanics and Geotechnical Engineering*. Nicosia, North Cyprus, pp.328-335

62. Keane, R.D. and Adrian, R.J. (1992). Theory of cross-correlation analysis of PIV images. *Journal of Applied Scientific Research*, Vol.49, pp.191-215

63. Kumar, A., Walia, B.S. and Bajaj, A. (2007). Influence of fly ash, lime, and polyester fibres on compaction and strength properties of expansive soil. *Journal of Materials in Civil Engineering*. Vol.19 (3), pp.242-248

64. Kumar, A., Walia, B.S. and Mohan, J. (2006). Compressive strength of fibre reinforced highly compressible clay. *Construction and Building Materials*. Vol.20, pp.1063-1068

65. Kumar, S. and Tabor, E. (2003). Strength Characteristics of Silty Clay Reinforced with Randomly Oriented Nylon Fibres. *Electronic Journal of Geotechnical Engineering*. Vol.10

66. Ladd, R.S. (1998). Preparing test specimens using under compaction. *Geotechnical Testing Journal*. Vol.1, pp.16-23

67. Lambe, T. W.; Whitman, R. V. (1979). Soil mechanics, SI version. USA: John Wiley & Sons.

68. Li, Chunling (2005). Mechanical response of fibre reinforced soil. Thesis (PhD), University of Texas at Austin

69. Liu, J., Iskander, M. (2004). Adaptive Cross Correlation for Imaging Displacements in Soils, *Journal of Computing in Civil Engineering*, Vol.18 (1), pp.46-57

70. Loehr, J. E.; Axtell, P. J. and Bowders, J. J., (2000). Reduction of soil swell potential with fibre reinforcement. *In: proc. of GeoEng 2000*. Melbourne, Australia

71. Lourenço, S. D. N., et al. (2006). Development of a Commercial Tensiometer for Triaxial Testing of Unsaturated Soils. *In: Proceedings of the Fourth International Conference on Unsaturated Soils*. Vol.2, Reston, USA, pp.1875-1886

72. Maher, M. H. and Ho, Y. C. (1994). Mechanical properties of kaolinite/fibre soil composite. *Journal of Geotechnical Engineering*. Vol.120 (8), pp.1381-1393

73. Maher, M.H. and Gray, D.H. (1990). Static Response of Sand Reinforced with Distributed Fibres. *Journal of Geotechnical Engineering*. Vol.116 (11), pp.1661-1677

74. Maheshwari, K. V. (2011). Performance of Fibre Reinforced Clayey Soil. Electronic *J. of Geotech. Eng.* Vol.16, pp.1067-1082

75. Makiuchi, K. and Minegishi, K. (2001). Strain-induced toughness and shearing characteristics of short-fibre reinforced soils. *In: Proceedings of International Symposium of Earth reinforcement*, Vol.1, pp. 83-88

76. Manevitz, L., Yousef, M. and Givoli, D. (1997). Finite element mesh generation using self-organizing neural networks. Journal *of Computer Aided Civil and Infrastructure Engineering*. Vol.12 (4), pp.233–50

77. Marandi, S. M., et al. (2008). Strength and Ductility of Randomly Distributed Palm Fibres Reinforced Silty-Sand Soils. *American Journal of Applied Science*. Vol.5 (3), pp.209-220

78. McGown, A., et al. (1981). Strain Behaviour of Soil-Fabric Model Embankments. *In: Proceedings of the Tenth International Conference on Soil Mechanics and Foundation Engineering*. Vol.3, Stockholm, pp.739-744

79. Meilani, I., et al. (2002). Mini suction probe for matric suction measurements. *Canadian Geotechnical Journal*. Vol.39, pp.1427-1432

80. Miller, C.J., Rifai, S. (2004). Fibre reinforcement for waste containment soil liners. *Journal of Environmental Engineering*. Vol.130 (8), pp.981–985

81. Mirzababaei, M., Yasrobi, S. and Al-Rawas, A. A. (2008). Effect of polymers on swelling potential of expansive soils. *Ground Improvement Journal*. Vol.162 (3), p. 111-119

82. Mitchell , J. M., Jardine, F. M. (2002). A Guide to Ground Treatment. London: CIRIA

83. Moir, J.; Letts, J. and Marie, J. (1999). Thatching in England 1790-1940. England: James & James (Science Publishers) Ltd

84. Moustafa, A. A. (2011). Performance evaluation of artificial neural networks for spatial data analysis, *Journal of Contemporary Engineering Sciences*, Vol.4 (4), pp. 149-163

85. Murray, J. J.; Frost, J. D. and Wang, Y. (2000). Behaviour of a sandy silt reinforced with discontinuous recycled fibre inclusions. *Transportation Research Record* Journal. Vol.1714, pp.9-17

86. NA to BS EN 1997-2:2007, UK National Annex to Eurocode 7: Geotechnical design – Part 2: Ground investigation and testing

87. Naeini, S.A. and Sadjadi, S.M. (2008). Effect of waste polymer materials on shear strength of unsaturated clays. *Electronic Journal of Geotechnical Engineering*. Vol.13

88. Newcomb, D. E., Birgisson, B. (1999). Measuring In Situ Mechanical Properties of Pavement Subgrade Soils. National Cooperative Highway Research Program, Project 20-5FYA 1996, Washington, USA

89. Özkul, Z. H., Baykal, G. (2006). Shear strength of clay with rubber fibre inclusions, *Journal of geosynthetics international*, Vol.13 (5), pp.173-180

90. Özkul, Z. H., Baykal, G. (2007). Shear Behavior of Compacted Rubber Fiber-Clay Composite in Drained and Undrained Loading. *Journal of Geotechnical and Geoenvironmental Engineering*, Vol.133 (7), pp.767-781

91. Park, S. (2009). Effect of fibre reinforcement and distribution on unconfined compressive strength of fibre-reinforced cemented sand. *Geotextiles and Geomembranes* Journal. Vol.27, pp.162-166

92. Park, S. (2011). Unconfined compressive strength and ductility of fibre-reinforced cemented sand. *Construction and Building Materials* Journal. Vol.25(2), pp.1134-1138

93. Penumadu, D. and Zhao, R. (1999). Triaxial compression behaviour of sand and gravel using artificial neural networks (ANN). *Journal of Computers and Geotechnics*. Vol.24, pp.207-230

94. Petros, P., Abramson, L. W. and Bruce, D. A. (1994). Ground Control and Improvement. New York: John Wiley & Sons

95. Plastics and the environment: A Handbook (2003). 'Recycling of Carpet and Textile Fibres' In: A. L. Andrady (ed), Wang, Y., et al. 1st ed. 2003: New York pp.697-725

96. Prabakar, J. and Sridhar, R. S. (2002). Effect of random inclusion of sisal fibre on strength behaviour of soil. *Journal of Construction and Building Materials*. Vol.16, pp.123-131

97. Punthutaecha, K., et al. (2006). Volume Change Behaviours of Expansive Soils Stabilized with Recycled Ashes and Fibres. Journal *of Materials in Civil Engineering*. Vol.18 (2), pp.295-306

98. Puppala, A.J. and Musenda, C. (2000). Effect of fibre reinforcement on strength and volume change behaviour of two expansive soils. *Journal of the Transportation Research Board*. Vol.1736, pp.134-140

99. Rahman, M. M., Siddique, A. (2010). Effects of Sampling Disturbance and its Minimization in Reconstituted over-consolidated Dhaka Clays. *DUET Journal*. Vol.1 (1)

100. Raj, P. (1999), Ground Improvement Techniques. New Delhi: Laxmi Publications

101. Ramires, M. C. P. (1993). Study of the behaviour of small diameter bored piles in a homogeneous residual soil layer. Dissertation (MSc), Federal Univ. of Rio Grande do Sul, Porto Alegre, Brazil

102. Ridley, A.M. and Burland, W.K. (1993). A new instrument for the measurement of soil moisture suction. *Geotechnique journal*. Vol.43 (2), pp.321-324

103. Rowe, R. K. (2000). Geotechnical and geoenvironmental engineering hand book. Norwell: Kluwer Academic Publishers

104. Saad, S., Mirzababaei, M., Mohamed, M., Miraftab, M. (2012). Uniformity of density of compacted fibre reinforced clay soil samples prepared by static compaction, Submitted to the 5th European Geosynthetics Congress, Valencia, Spain

105. Shahin, Mohamed A., Jaksa, Mark B. and Maier, H. R. (2002). Artificial Neural Network based Settlement Prediction Formula for Shallow Foundations on Granular Soils. *Journal and News of the Australian Geomechanics Society*. Vol.37(4), pp.45-52

106. Shouling, H., Jiang, Li. (2009). Modeling nonlinear elastic behaviour of reinforced soil using artificial neural networks, *Journal of applied soil computing*, Vol.9, 954-961

107. Sjoblom, K. (1996). The mechanisms involved during the desaturation process of a porous matrix. Thesis (PhD), Massachusetts Institute of Technology, USA

108. slopes in Japan, *In: Proc. Symp. on Effects of Forest Land Use on Erosion and Slope Stability*, Honolulu, Hawaii, pp. 63-72

109. Smoltczyk I, U. (2003). Geotechnical Engineering Handbook, Volume 1: Fundamentals. USA: John Wiley & Sons

110. Sudjianto, A. T., et al. (2009). Behaviour of Expansive Clay of Ngawi Region (East Java) Under Water Content Variation. *Journal of Civil Engineering Dimension*. Voil.11 (2), pp.100-105

111. Take, W.A. and Bolton, M.D (2003). Tensiometer saturation and the reliable measurement of soil suction. *Geotechnique Journal*. Vol.53 (2), pp.159-172

112. Tang, C., et al. (2007). Strength and mechanical behaviour of short polypropylene fibre reinforced and cement stabilized clayey soil. *Geotextiles and Geomembranes* Journal. Vol.25, pp.194-202

113. Tsukamoto, Y, and Kusabe, O. (1984). Vegetative influence on debris slide occurrence on steep

114. Turk, G., Logar, J., Majes, B. (2001). Modelling soil behaviour in uniaxial strain conditions by neural networks. *Journal of Advances in Engineering Software*, Vol.32, pp.805-812

115. Ud-din, S., Marri, A. and Wanatowski, D. (2011). Effect Of High Confining Pressure On The Behaviour Of Fibre Reinforced Sand. *Geotechnical Engineering Journal of the SEAGS & AGSSEA*. Vol.42 (4), pp.69-76

116. US Army Corps of Engineers. (2003) Engineering and Design – Slope Stability.Soil, USA

117. Van Impe, W. F. (1989). Soil Improvement Techniques and their Evolution, Rotterdam: A.A. Balkema

118. Vanluchene, R. D. and Sun, R. (1990). Neural networks in structural engineering. Journal of Microcomputers in Civil Engineering. Vol.5 (3), pp.207–15

119. Viswanadham, B.V.S., Phanikumar, B.R. and Mukherjee, R. V. (2009). Swelling behaviour of a geofibre-reinforced expansive soil. Geotextiles and Geomembranes. Vol.27, pp.73-76

120. Waldron, L. J. (1977). The shear resistance of root-permeated homogeneous and stratified soil. *Soil Science Society of American Journal*. Vol.41 (3), pp.843-849

121. Waldron, L.J., Dakessian, S. (1981). Soil reinforcement by roots: calculation of increased soil shear resistance from root properties. *Soil Science Journal*. Vol.132, pp.427-435

122. White D.J., Take W.A, Bolton M.D. (2001). Measuring soil deformation in geotechnical models using digital images and PIV analysis. *In: Proc. 10th Int. Conf. Computer Methods & Advances in Geomechanic*. Tucson, Arizona, pp.997-1002

123. White, D. J., et al. (2001). A deformation measuring system for geotechnical testing based on digital imaging, close-range photogrammetry, and PIV image analysis. *In: Proc. 15th Int. Conf. Soil Mech. & Geotech. Eng.* Istanbul, Turkey, pp.539-542

124. White, D. J., Take, W. A. and Bolton, M. D. (2003). Soil deformation measurement using particle image velocimetry (PIV) and photogrammetry. *Geotechnique Journal*, Vol.53 (7), pp.619-631

125. White, D.J., Take, W.A. (2002). GeoPIV: Particle image velocimetry (PIV) software for use in

126. Wood, D. M. (1990). Soil behaviour and critical state soil mechanics. 1st ed. England: Cambridge University Press

127. Wu, T. H., Beal, P. E., Lan, C. (1988). In situ shear test of soil-root system. *Journal of Geotechnical and Geoenvironmental Engineering*, ASCE, Vol.114 (12), pp.1376-1394

128. Wu, T.H. (1976). Investigation of landslides on Prince of Wales Island, Alaska. Department of Civil Engineering, Ohio State University, Columbus. Geotech. Eng. Rep. No.5

129. Yadong, Zhang (2004). An embedded improved soil berm in an excavation mechanisms and capacity. Thesis (PhD), National University of Singapore

130. Yetimoglu, T. and Salbas, O. (2003). A study on shear strength of sands reinforced with randomly distributed discrete fibres. *Geotextiles and Geomembranes Journal*. Vol.21, pp.103-110

131. Ziegler, S., Leshchinsky, D. and Ling, H. I. (1998). Effect of Short Polymeric Fibres on Crack Development in Clays. *Journal of Soils and Foundations*. Vol.38 (1), pp.247-253

132. Zornberg, J. G. and Li, C. (2003). Design of fibre-reinforced soil. *In: 12th Panamerican Conference on Soil Mechanics & Geotechnical Engineering*, Cambridge, Vol.2, pp.2193-2200

Appendix A Manual for use and maintenance of in-house built triaxial pressure distribution panel

A.1 Introduction

There are different approaches to supply water pressure for triaxial test apparatus. These include:

1. Mercury/water pressure control system
2. Oil/water pressure control system
3. Air/water bladder cylinder
4. Digital pressure/volume change controller

In the following sections a basic summary of each approach is given.

A.1.1 Mercury/water pressure control system

This system is based upon the design of Prof A.W. Bishop. The principle of Mercury/water setup to generate pressurised water is based on the weight of the elevated pot(s) of mercury on a pot of water which is directly connected to the triaxial chamber. The system comprises of one upper and one lower mercury/water pot, made from seamless acrylic tubes, a winch and a carriage assembly with calibrated suspension springs for upper pot; aluminium guide rails for the carriage; wooden stand for lower pot; a laminated panel suitable for wall mounting, fitted with a hand operated pressure pump, control valves, a water reservoir and a pressure gauge. This system requires high ceiling in laboratory to create sufficient pressure head. Moreover due to high price of mercury and its toxic nature, this system has been obsolete and replaced by new systems. Figure A.1 (a) shows the basic schematic of mercury/water pressure control system.

A.1.2 Oil/water pressure control system

This system is designed to give a constant pressure for wide range of applications. The design of this system incorporates an oil pump driven by an electric motor during the entire period of operation to maintain the regulated pressure. A hand

pump is also provided for quick initial build up of pressure. Therefore, required pressure can be adjusted using the provided regulator. A transparent acrylic chamber works as the oil/water reservoir. A pressure gauge is included in the circuit as a checking device for monitoring the working function of the unit. Figure A.1 (b) shows oil/water pressure system.

A.1.3 Air/water pressure cylinder

This system comprises of a Perspex chamber and a bladder inside the chamber and operates in conjunction with an air compressor to inflate the bladder. Therefore, the bladder acts as an interface between air and water. Air pressure is regulated using an air pressure regulator. By increasing the air pressure in the bladder, water around the bladder is pressurised and delivered to the triaxial test chamber. This system provides a simple and accurate mean of supplying required water pressure for triaxial test apparatus. Moreover, using bladder as an interface between air and water ensures introduction of deaerated water to the soil specimen during triaxial tests. Figure A.1 (c) shows an air/water pressure cylinder.

A.1.4 Digital pressure/volume change controller

This device is a microprocessor-controlled screw pump for the precise regulation and measurement of fluid pressure and volume change. As a standard research device in commercial and teaching soil mechanics laboratories, it offers the highest level of accuracy, resolution and control. Figure A.1 (d) shows a digital pressure/volume change controller.

A.2 Change over to air/water bladder cylinder

The initial means of applying cell pressure and back pressure for triaxial test apparatus available in the soil laboratory of university of Bolton was based on mercury control system. Due to the limited height of ceiling, the maximum pressure head that could be supplied to triaxial chamber was limited to 250 kPa for back pressure and 400 kPa for cell pressure. Figure A.2 shows the old mercury/water pressure controlling system at the University of Bolton. The system was capable of supplying cell pressure and back pressure for three sets of triaxial test apparatus at the same time.

To carry on the current research the mercury/water system was changed over to air/water bladder system along with using an air compressor.
In the new system that I designed and built, 6 air/water bladder cylinders were used for supplying pressure to three triaxial test apparatus. A pressure distribution panel was also designed and made in-house to deliver the pressurised water to the triaxial chambers. The new design of the pressure distribution panel made it easy to fulfil the following requirements:

a) Delivery of pressurised water to up to 6 triaxial cells at the same time
b) Deaerating water
c) Filling/emptying triaxial chambers using compressed air to force water into the chambers or evacuating water out of the chambers by applying vacuum pressure to the chambers.
d) Extra vacuum for stretching triaxial rubber membrane
e) Extra valves for deaerating water hoses connected to the test chambers
f) Digital display read out unit for displaying cell pressure, back pressure and pore-water pressure for three triaxial apparatus

In the new setup, pressure sensors were fitted to measure the cell pressure, back pressure and pore-water pressure in all three triaxial apparatus. Moreover, linear variable differential transformers (LVDT) and load cells were also fitted to measure vertical displacement and the applied axial load respectively.

A 64-channel data logger and tailor-made software (DAQ 32, see Appendix B) were utilised to log the data measured by sensors into a hard disk of a computer for further analysis.

Figure A.3 shows the new equipped triaxial apparatus and Figure A.4 shows the pressure distribution panel and air/water bladder cylinders used in this study.

In the new design, for easy recognising different pressure lines, four different colour codes were used including yellow, red, black, green and blue for applying cell pressure, back pressure, pore-water pressure, filling the chamber and delivering carbon dioxide to the specimens respectively.

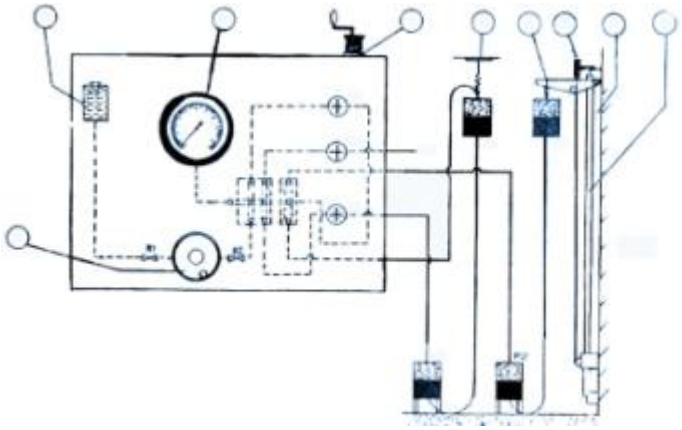

a)

b)

c)

d)

A.1 Equipment for applying water pressure to the triaxial test chamber
a) Mercury/water system[19] b) Oil/water system[20]
c) Air/water system[21] d) Automatic pressure/volume changer controller[22]

[19] http://www.lawrenceandmayoinstruments.com/materialdetails.asp?pID=P1&spID=Sp6
[20] http://www.zealinternational.com/soil/zi3068.asp
[21] http://www.controls-group.com/eng/soil-mechanics-testing-equipment/airwater-pressure-system-and-controls-panels.php
[22] http://www.gdsinstruments.com/products/advdpc.htm

Figure A.2 Former mercury/water pressure controller system at university of Bolton (2008)

Figure A.3 Newly equipped triaxial test apparatus (2009)

Figure A.4 Pressure distribution panel and air/water bladder cylinders

A.3 Manual for use and maintenance of manufactured pressure distribution panel

The frame of pressure distribution panel was made of Perspex sheets. This helps to have a close look through the transparent frame inside the panel to recognise any possible leak. The panel comprises of zero volume change ball valves, pressure regulators and pressure gauges at the front side and inlet/outlet fast release push-in ports on the side.

Front side of the distribution panel is divided into 4 parts. As it is depicted in Figure A.5, the bottom part of the front panel marked as ‘Adjustment’, including 6 air pressure regulators and pressure gauges. This part is used to adjust the main line air pressure to each air/water bladder cylinder. Therefore, the desired air pressure can be adjusted with the help of pressure gauges next to each air pressure regulator.

The second and third parts of the front panel include 6 ball valves for delivering the pressurised water from air/bladder cylinders to back pressure lines and 6 ball valves to deliver the pressurised water from air/water bladder cylinders to cell pressure lines of 6 triaxial chambers on the left/right side of the pressure distribution panel.

The fourth part on the top side of the front panel includes 12 ball valves, three pressure sensors and a digital display read out unit. This part is designed to:

a) Monitor cell pressure, back pressure and pore-water pressure of the six triaxial chambers using mounted digital read out
b) Deaerate the tap water used in the whole system
c) Fill the air/water bladder cylinders with water
d) Deaerate all the water hoses from distribution panel to the triaxial test chambers

For better identification, all ball valves on the panel are coded from V1 to V24. There is an extra panel on the right side of the main panel including two air pressure regulators and 4 ball valves for applying air pressure and vacuum pressure.

The main air supply for the pressure panel is provided by the main air supply of the University in conjunction with an auxiliary portable air compressor which is connected parallel to the main air line using single flow direction fitting. Therefore, this ensures functionality of the whole system at all times.

A.3.1 Adjustment regulators and gauges

Three air pressure regulators and pressure gauges on the left hand side of the panel were designed for regulating the pressure of the air/water bladder cylinders related to back pressure lines. The other three pressure regulators and pressure gauges on the right side of the front panel were designed for adjusting the pressure of the air/water bladder cylinders related to the cell pressure line.

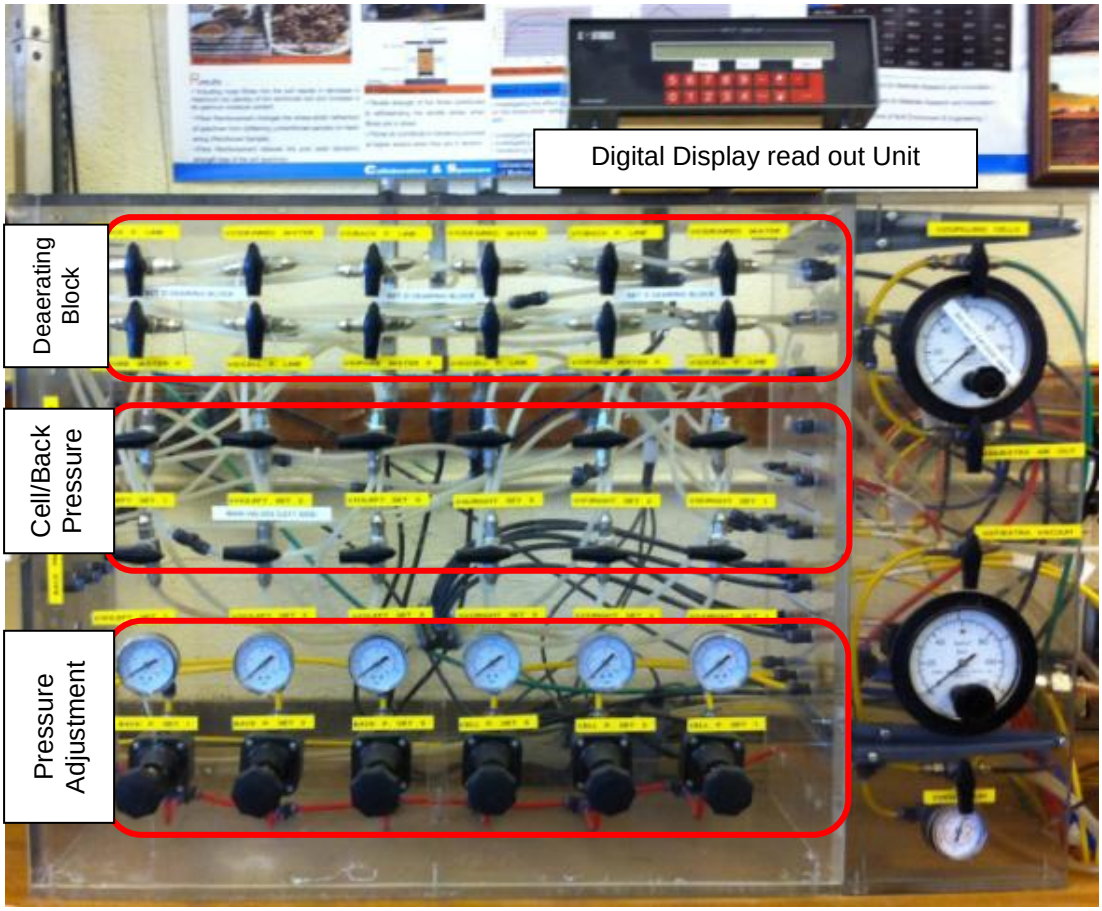

Figure A.5 Main parts of pressure distribution panel

To adjust the required pressure, simply rotate the regulator knob clockwise to increase the pressure. Each pressure regulator is related to one of the triaxial test chambers which are marked with a number. For example, ‘Back P. Set 1’ is the

pressure regulator related to the back pressure of the first set of triaxial test chamber or ‘Cell P. Set 2’ is related to the cell pressure of second test chamber. The approximate applied pressure can be monitored using the supplied pressure gauge on top of the regulator. Moreover, the applied pressure can also be read using the digital display read out unit on the panel or using the software (DAQ 32).

Figure A.6 Adjusting regulators

A.3.2 Applying back pressure and cell pressure

After adjusting the cell pressure and the back pressure using appropriate pressure regulators, the generated pressurised water can be delivered to the triaxial test chambers using the ball valves coded from V13 to V24 on the front panel. Back pressure related ball valves are marked from V19 to V21 for three triaxial chambers on the left side of the pressure distribution panel and from V22 to V24 for the other test chambers on the right side (see Figure A.7).

The same configuration applies to the ball valves related to cell pressure lines with ball valves marked from V13 to V15 for chambers on the left side and from V16 to V18 for the chambers on the right side.

For supplying cell pressure and back pressure, for every single triaxial test chamber, two air/water bladder cylinders are required. In the current setup, there are just 6 air/water bladder cylinders available for supplying the required pressure for six sets of triaxial apparatus. Therefore, each pair of apparatus (one from the left sets and one from the right sets) can receive the same cell pressure and back pressure at a time. However, separate paths and pressure sensors have been used for measuring the induced pore-water pressure. This system can be

developed later by adding six more air/water bladder cylinders for controlling the applied pressures to each test chamber separately.

Figure A.7 Cell pressure and back pressure valves

A.3.3 Digital display read out unit

Ball valves at top of the pressure distribution panel are divided into three parts including 4 ball valves for each triaxial chamber. The main role of these valves is to read the cell pressure, back pressure and pore-water pressure of each set of apparatus on the digital display readout unit.

Each part of top row valves, includes a set of four valves for cell pressure, back pressure, pore-water pressure and one for filling the air/water bladder cylinder with deaerated water. To measure the pressure in the back pressure line, open the back pressure valve related to selected test chamber (V1, V3 or V5). Therefore the measured pressure is displayed on the digital display unit. To measure cell pressure use ball valves coded V8, V10 or V12. Figure A.8 shows the valves at top side of the pressure panel. At the same time for each test apparatus just on of the pressure sources (i.e. cell pressure, back pressure or pore-pressure) can be read from readout unit.

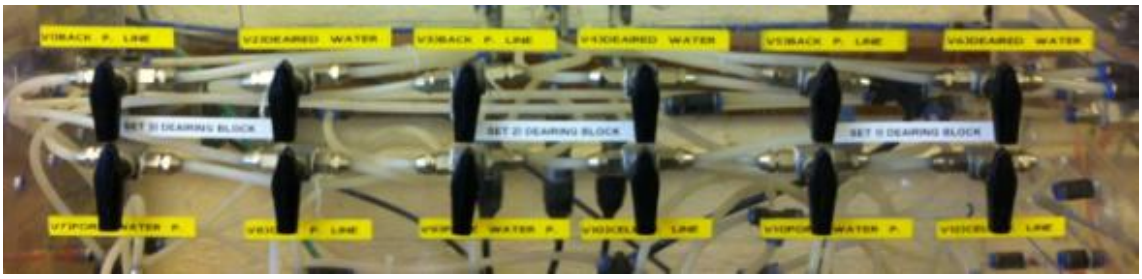

Figure A.8 Deaerating valves

The pore-water pressure of the three soil specimens installed in three separate test chambers can also be read individually using the digital display readout unit. To read the pore-water of a soil specimen in a test chamber during the experiment, the appropriate valve on the side panel and related pore-water pressure valve on the top side of the front panel should be open.

A.3.4 Deaerating pressure lines

For correct measurement of the pressure, all the pressure lines must be deaerated prior to setting up the soil specimen on the triaxial pedestal. To do this, deaerated water must be pushed into the pressure lines using an appropriate method. Before proceeding to deaerate the pressure lines of each test chamber, the pressure blocks at top part of the pressure distribution panel must be deaerated. There are three ball valves on top side of the panel which are connected to the three pressure blocks inside the panel. To deaerated these block, for example the first block on the left side which is related to the third triaxial apparatus, increase either related cell pressure or back pressure to 5 to 10 kPa and then open the ball valve on the panel gently, once air bubbles are seen leave it until there is no sign of air bubble from the bleed valve. This procedure makes the pressure blocks in the panel deaerated. Do the same procedure for the rest of the pressure blocks.

After deaerating pressure blocks of the pressure distribution panel, pressure line circuit from the panel to the triaxial test chambers must be deaerated. Therefore, for example for the first set of triaxial apparatus on the left side, open valves coded with V15 and V19 and open the cell pressure and back pressure deaerating valve on the pressure blocks of the triaxial test chamber to remove air out of the cell pressure and back pressure lines respectively.

To deaerate the pore-water pressure line, connect either cell pressure or back pressure to the pore-water pressure line using the valves on the top part of the panel (V1 to V12).

To do this, for example, for the first set of triaxial apparatus on the left, Increase the cell pressure from 5 to 10 kPa and open the valve V13. Then open valves V11 and V12. Therefore, pressurised water in cell pressure line is ready to be delivered to the pore-water pressure line. Open the valve on the left side of the panel to deliver the pressurised water to the pore-water pressure line of the first set of triaxial test chamber and deaerate the line using pressure block on the apparatus.

A.3.5 Deaerating water

To prepare deaerated water for triaxial tests, a Venturi vacuum generator has been mounted in the pressure distribution panel. Therefore, vacuum pressure can be applied on the water tank mounted on the wall. To do this, increase the vacuum pressure using the vacuum pressure regulator on lower right side of the panel and open valve V28 and leave it for few hours. Deaerating water could take up to 24 hours or more to produce highly deaerated water for triaxial test. Therefore, vacuuming can be left over night to prepare deaerated water for the next test.

There is also an extra vacuum line connected to valve V27 which can be used for making the triaxial chamber empty of water or it may be used for stretching the rubber membranes.

A.3.6 Filling air/water bladder cylinders with deaerated water

To fill the air/water bladder cylinders with deaerated water, open the appropriate ball valve related to each test chamber (i.e. V2, V4 or V6), followed by opening the related cell pressure or back pressure valve (i.e. V13 to V4). Then open the air bleed valve on the air/water bladder cylinder. By doing this, deaerated water flows from the water tank mounted on the wall under gravity to the cylinders

A.3.7 Filling/emptying triaxial cell of water

Before applying the generated pressure to water cylinders, shut any cell pressure valve on the panel (i.e. V13 to V18). To fill the triaxial test chambers with water, increase the air pressure applied to the water cylinders (under the bench) to 1 to 2

bar using pressure regulator on top right side of the panel. Open valve V25, to deliver water to the triaxial test chamber followed by opening related valve on the test chamber (i.e. valve connected to green tube). Therefore, water goes from the water cylinder to the chamber. Figure A.9 (a) shows the air pressure regulator and related valves for filling and making empty of triaxial test chambers.

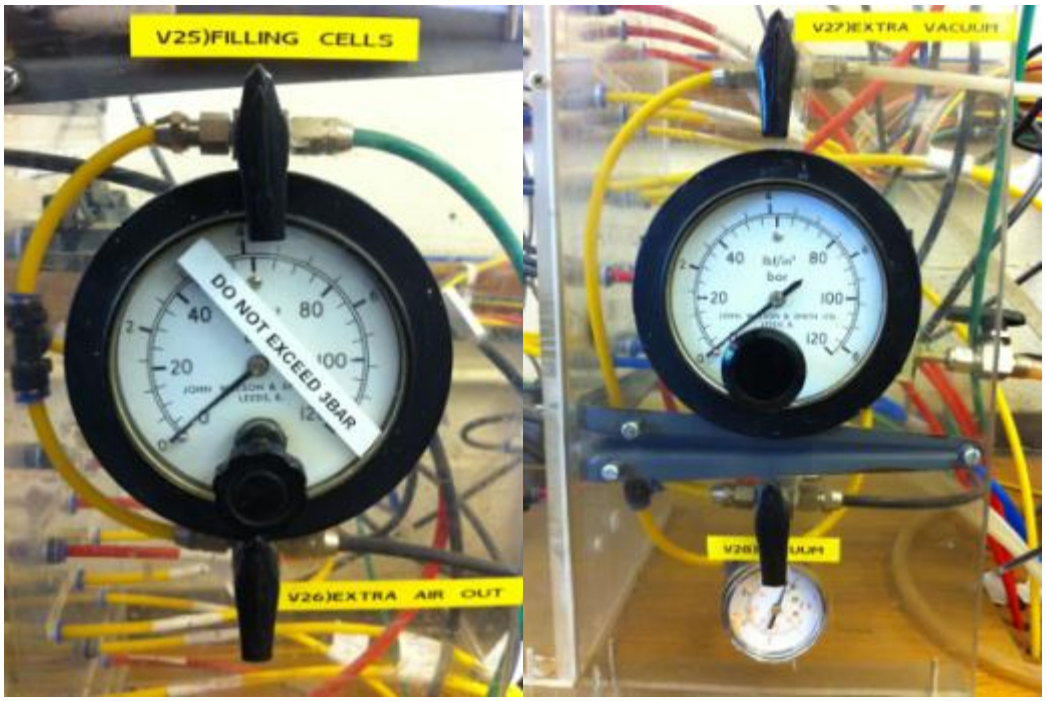

a) b)

Figure A.9 Pressure regulator for a) Filling triaxial cell b) Making triaxial cell empty of water

For emptying the cell after finishing the triaxial test, vacuum pressure can be applied to the cell to remove the water (Figure A.9 (b)). To do this, connect the valve V27 to top of the water cylinder (under the bench) to apply vacuum to the water. Then open valve V25 to deliver vacuum pressure to the triaxial test chambers. On the test chamber, open valve connected to the green tube to return all water from the test chamber to the water cylinder.

A.3.8 Maintenance

On regular bases check all the valves for any possible leakage. If there is any leakage through the valves, remove all the hoses from the panel and repair the leakage using a fresh piece of PTFE tape around the threads of the faulty valve. Algae can produce a green cover on the bladders of air/water bladder cylinders if they are not washed periodically. This might happen due to the nature of the static water inside the cylinders and their location which may not receive enough sun light.

Appendix B User Manual of DAQ

B.1 Introduction

DAQ is a professional data logging software developed by myself in order to acquire data from multiple sensors at varying data sampling rates through 64-channel Agilent series U2300A data logger. DAQ was also developed for logging data from other brands such as Lab Jack, DataQ, eDam, Stack Daq, Pico data loggers and many more.

At the early stage of this research, six old-fashioned sets of stationary triaxial testing apparatus in the geotechnical laboratory of the University of Bolton were converted to computerised modern equipment with automatic data logging capability using different sensors such as LVDTs (Linear Variable Differential Transformer), Load cells and pressure sensors.

Some of the striking features of DAQ include:

- Adding project title, username, date, notes and comments for each logging project
- Defining physical channels with configurations such as name, engineering unit, output range (i.e. mV, V, mA, resistance, frequency, Thermocouple or …), output type (i.e. unipolar or bipolar) and number of decimal places for displaying the value of the channel
- Defining up to 10 engineering units for each channel (i.e. kN, kgf, lbf, … for a load cell)
- Defining unlimited calculated channels by applying math operators on physical channels
- Built-in calibration programme for calibrating sensors using 4 different methods of ‘Logarithmic’, ‘Exponential’, ‘Linear’ and ‘Look up Table’.
- Logging unlimited number of channels simultaneously with the capability of changing over the engineering units during the test
- Activating or deactivating physical channels according to test requirements
- Screen lock feature during logging data

- Five live compound charts with each capable of drawing one parameter as abscissa against up to three parameters as ordinate
- Copy, print or save live charts during logging process
- Manual recording of favourite data before or during data logging process apart from user defined logging intervals (highly useful during getting B-Value in soil triaxial test)
- Defining data logging intervals based on constant number of samples per minute or user defined logging intervals
- Defining chart updating intervals
- Channel resetting feature at all times even during logging process
- Exporting the logged data to Microsoft Excel output file with the capability to define unlimited number of graphs based on logged physical and/or calculated channels
- Highly professional feature to avoid loss of data during electricity cut off with the recovering of logged data on the next start up
- Recording the projects' history for future access
- Multiple calibration feature for calibrating several sensors at the same time

B.2 Introducing windows and menus

B.2.1 Start up screen

On the startup of DAQ, a splash screen containing version of the software and last update details is displayed. In the background, DAQ seeks installed hardware and checks the communication between installed hardware and Microsoft Windows. If DAQ cannot find installed hardware or validated licence, an error message is displayed. Figure B.1 shows splash screen and initialising box after a successful/unsuccessful initialising process.

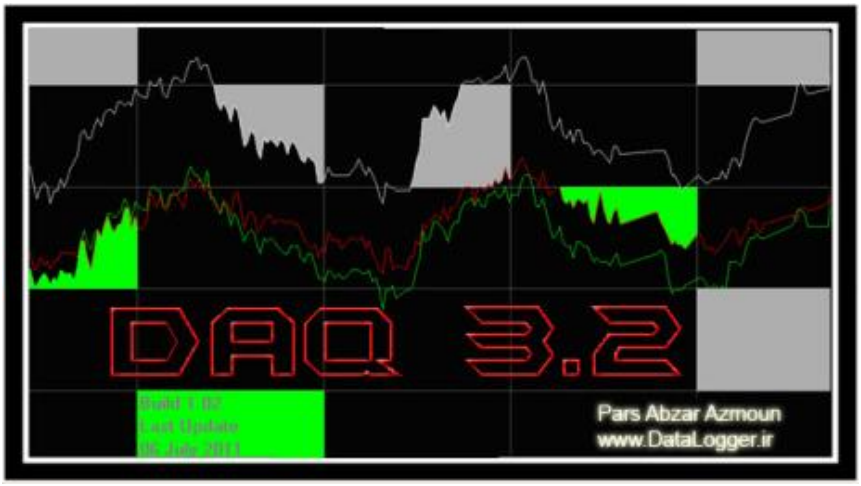

a)

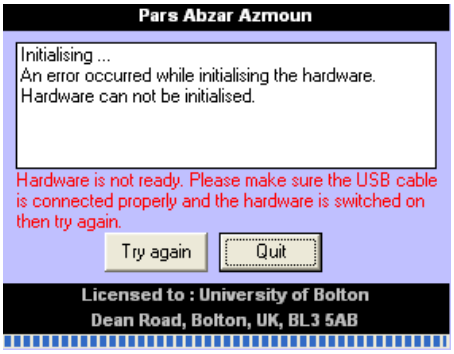

b) c)

Figure B.1 a) splash screen b) successful initialisation c) unsuccessful initialisation

Information such as the manufacturer of the hardware, model number, version of firmware and DAQ version is displayed during initialising process. By clicking on the ‘Start‘ button, main screen of DAQ is displayed. After an unsuccessful initialising ‘Try again‘ button will be displayed instead of ‘Start‘ button.

Once the initialisation process is passed successfully, the user can get access to the software by entering username and password. At the first run of DAQ, the default username and password are ‘superuser’. A New user name and password can be specified from ‘File‘ menu. Once a new username is registered, the default username and password are removed from the database.

B.2.2 Main window

Figure B.2 shows the main window of DAQ. The main window of DAQ consists of three frames including timer, display side bar and data view part. Timer frame is

positioned at the top left side of the main window which includes ‘Absolute timer’, ‘Relative timer’, ‘Timer reset’ button and ‘On the fly record’ button.

‘Absolute timer’ holds the time elapsed from the beginning of the data logging process. ‘Relative timer’ holds the same value however; it can be reset at any time. ‘On the fly record’ button may be used for recording values of all active physical and calculated channels in ‘Recorded Data‘ datasheet any time before or during starting logging project. This is provided for special purposes when user may not wish to run the project and a few readings are enough (such as calculating B-Value in soil triaxial test). Figure B.2 shows main window of DAQ.

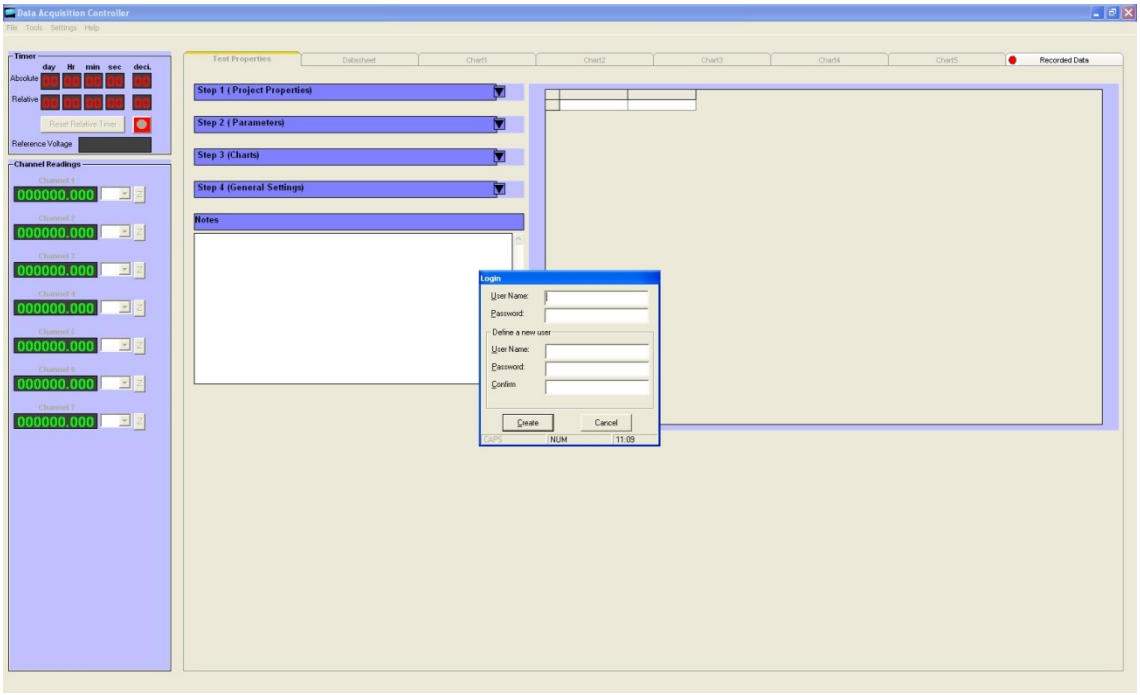

Figure B.2 Main window of DAQ

B.2.3 File menu

File menu contains the following sub menus (Table B.1), which are described briefly here.

Table B.1 File Menu

New Project	To close the current open project and start a new one
Users	To define a new user
Lock Screen	To lock the screen to prevent unauthorised people from interfering in the software settings
Recover Previous Datasheets	To recover and export data of projects which have been carried out in the past
To Do Menu	To show options to save or export results after finishing a project
Print	To print out project information
Exit	To quit software

B.2.4 Tools menu

Tools menu contains the following sub menus (Table B.2), which are described briefly here.

Table B.2 Tools menu

Remote Data Control via Dialup	To manage data logging process remotely using dialup modem
Remote Data Control using GSM modem	To manage data logging process remotely using GSM/GPRS network
Parameter Maker	To Define configuration of physical and calculated channels
Calibration	To calibrate sensors
Auto save Every	To define auto saving property of acquired data during logging
Load frame controller	To control any external equipment such as loading frames which are connected to computer using serial port
Reset Channel	To set the reading of any selected channel to zero
Pause/Resume	To pause/resume process of data logging

B.2.5 Setting menu

Setting menu contains the required settings for the data logging process and cannot be changed by the user.

B.2.6 Help menu

Help menu contains sub menus (Table B.3) for executing help tutorials of software and also updating the main core of the software.

Table B.3 Help menu

Contents	Visual help for using the software
Submit a ticket	To contact technical department with user unique reference number and resolve the possible problems remotely
Check for updates at start up	To allow software to check for new updates every time at start up
Check for updates	For updating the main core of the software
About	Information about software

B.3 How to set up a new project

For defining a new project, first click on ‘New Project‘ from File menu. In order to set the channels and define calculated channels, click on ‘Parameter Maker‘ from ‘Tools’ menu. Parameter Maker window contains a datasheet with a list of all channels and their settings. Default name for all channels is ‘Caption’ and by default, all channels are disabled except time related parameters. Figure B.3 shows the parameter maker window.

Table B.4 shows the editable parameters of physical and calculated channels. The number of rows available in a fresh parameter maker datasheet equals to number of physical channels plus two extra rows for time related parameters. For setting up a new physical channel, double click on an empty row, enter a desired title in ‘Caption‘ text box and enter engineering unit in ‘Unit Caption’ text box. Maximum of 10 engineering units can be defined for a single channel separated by comma.

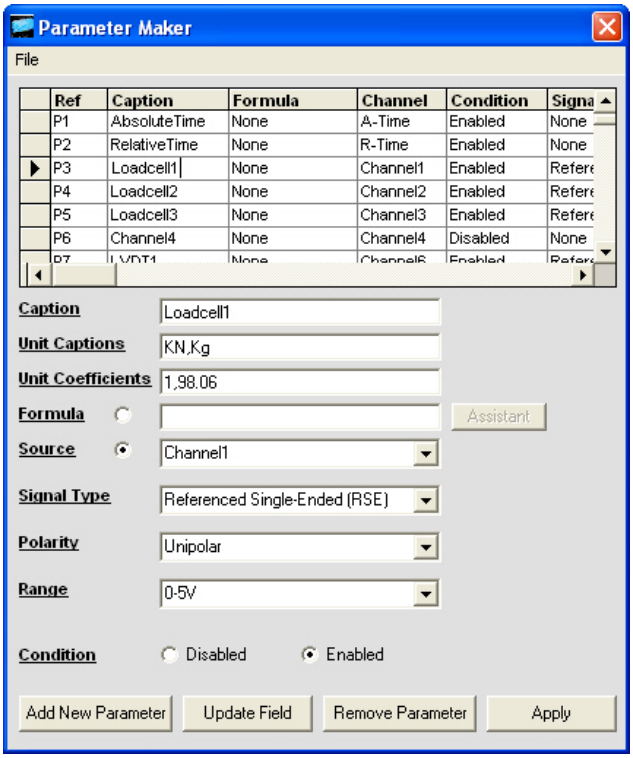

Figure B.3 Parameter maker window

Table B.4 Parameter maker menu

Caption	The desired name for a channel
Unit Caption	Engineering units which may be used for each channel (separated by comma)
Unit Coefficient	Unit conversion coefficients for converting one engineering unit to another
Decimals	Number of decimal places for displaying value of channel
Formula/Source	To specify whether the logged parameter is a physical channel or a calculated channel
Signal Type	Specification attributed to hardware (see hardware technical data)
Polarity	Specification attributed to hardware (see hardware technical data)
Range	Specification attributed to hardware (see hardware technical data)
Condition	To set a channel enabled or disabled during logging

The main engineering unit, which is used for calibrating the sensor, must come first. In order to define the unit conversion coefficients for defined engineering units, enter the relevant coefficients separated by comma in 'Unit Coefficient' text box. The coefficient for the main calibrating unit would be one and others are relative to that. For example to define three engineering units of millimetre,

centimetre and metre for the displacement sensor, unit captions and unit coefficients must be entered as shown in Table B.5.

Table B.5 Defining conversion coefficient of parameters

Unit captions	mm, cm, m
Unit Coefficients	1,0.1,0.001

For each parameter either physical channel or calculated channel, the number of decimal places can be defined between 0 to 6 digits in the ‘Decimals‘ input box.
Select the channel number from the drop-down list. The correct values for ‘Signal Type‘, ‘Polarity‘ and ‘Voltage Range‘ must be selected according to the technical data of the data logger hardware specifications and type of sensor. Once the parameters of a given parameter is set, press ‘Update Field‘ to apply the settings. A physical/calculated channel can also be set as ‘enabled’ or ‘disabled’ from the options available in the parameter maker form.

To define a calculated channel, the same procedure as described above must be followed except choosing ‘Formula‘ option rather than ‘Channels‘. When ‘Formula‘ option is selected, all other data logger parameters such as ‘Signal Type‘, ‘Polarity‘ and ‘Voltage Range‘ are disabled. ‘Formula Builder‘ contains different types of mathematical operators and functions which can be used to define any type of formulae for calculated channels based on the values of the physical channels. Figure B.4 shows the formula builder window.

Each parameter either physical or calculated channel is designated using a reference number which is shown in the first column of the parameters’ datasheet. Therefore, for defining a new formula based on the value of a specific physical channel or other calculated channels, their reference number can be used from the drop-down list in ‘Formula Builder’ form. When the formula is defined, to add the defined formula to the list press ‘Append’ and then press ‘Add New Parameter’.
To update settings of any defined parameter, double click on the row containing the selected reference number and change the relevant settings. To apply the changes click on ‘Update Field’. To remove the settings of a parameter, select it by double clicking and press ‘Remove Parameter’.

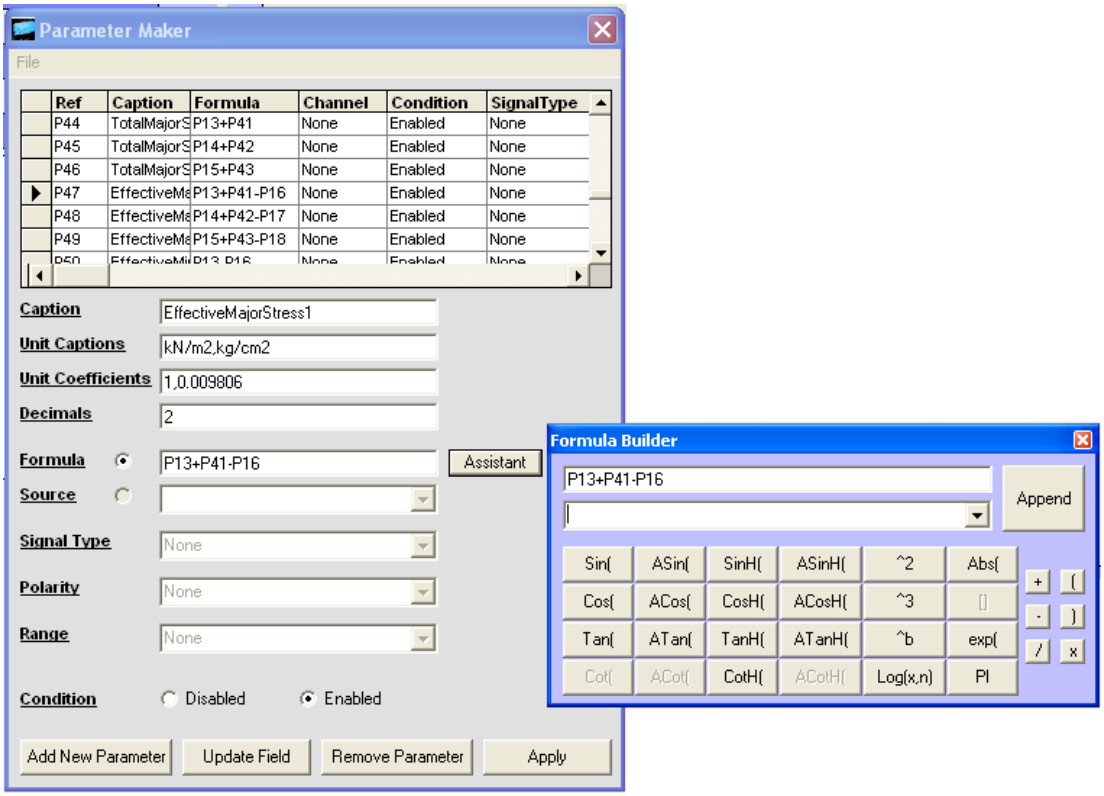

Figure B.4 Formula builder window

The settings for all channels and parameters can be saved in a file for future use. This can be done by choosing ‘Save As’ from the file menu. When all settings are done, press apply all to apply the settings. Figure B.3 shows ‘Parameter Maker’ and ‘Formula Builder’ forms.

B.3.1 Set up the project information

After the successful applying the settings of sensors in ‘Parameters maker’ form, the list of enabled physical channels will be displayed on the left side bar. The pre-defined engineering units for each channel are available from a drop-down list next to display. Project properties including project information, parameters, graphs and general settings can be defined in four steps in separate parts.

B.3.2 Project Properties

To specify information such as name of project, code of project, operator name and date of project, appropriate information can be entered in ‘Project Name’, ‘Project Code’, ‘Operator Name’ and ‘Date of Project’. To set a password on the

output file, fill the ‘Password’ text box otherwise leave it empty. Any extra comments can be entered in ‘Comments’. Figure B.5 shows the project properties page. Once the logging process is started, this information cannot be changed however, there is another text box (i.e. ‘Notes’) which can be used for entering any comments during the logging process.

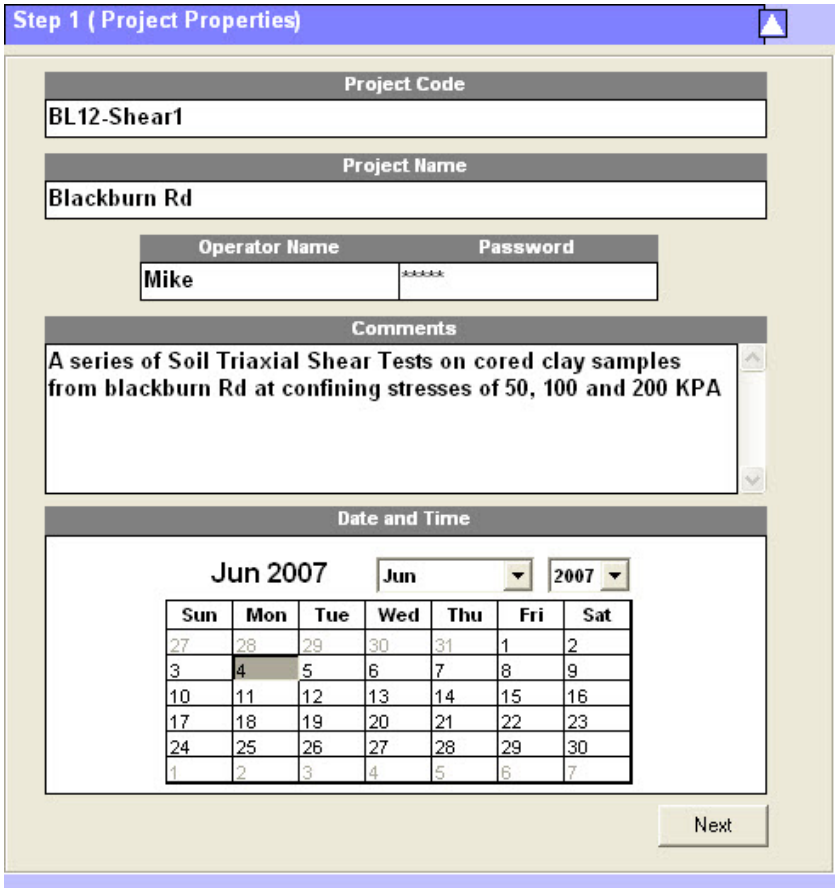

Figure B.5 Project properties

B.3.3 Setting up logging parameters

To create a list of logging parameters, add desired parameters listed in left list of ‘Datasheet Parameters’ to the right list (Figure B.6). Engineering units for using in the live datasheet or live graphs can be defined in ‘Parameters’ Units’.

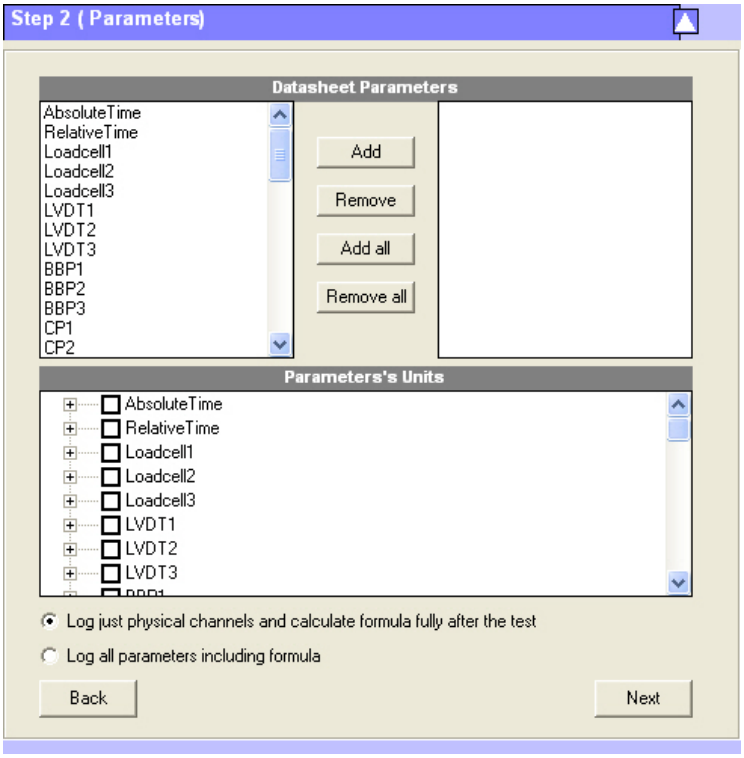

Figure B.6 Datasheet parameters

There are two options for the logging procedure:

1) Logging just physical channels

With this option, just preset physical channels will be logged in to the datasheet and calculated channels are calculated and added to the datasheet after finishing the logging process.

2) Logging all parameters including formula

With this option all parameters either physical channels and/or calculated channels are calculated and logged in to the datasheet instantaneously.

With choosing the second option, although all parameters can be seen lively, the rate of the data logging process will be reduced due to the extra process to calculate the calculated channels. For high sampling rate[23] (i.e. more than 1 sample per second) depending on the number of preset physical and calculated channels, It is recommended to use the first option and once the data logging process is finished, on export to Microsoft Excel; all user-defined formulae will be

[23] Sampling rate is defined as the number of samples per minute or per second which is acquired by data logger and processed in the software.

calculated and saved in the output file. This increases the sampling rate of the software.

B.3.4 Set up live graphs

To monitor the logged data or calculated channels instantly during logging data from sensors, 5 live graphs can be set, each can hold up to three parameters as ordinate against a parameter as abscissa. To add the desired graphs, simply select the graph number and add X-axis and Y-axis parameters from the list of parameters. Figure B.7 shows the chart setup window.

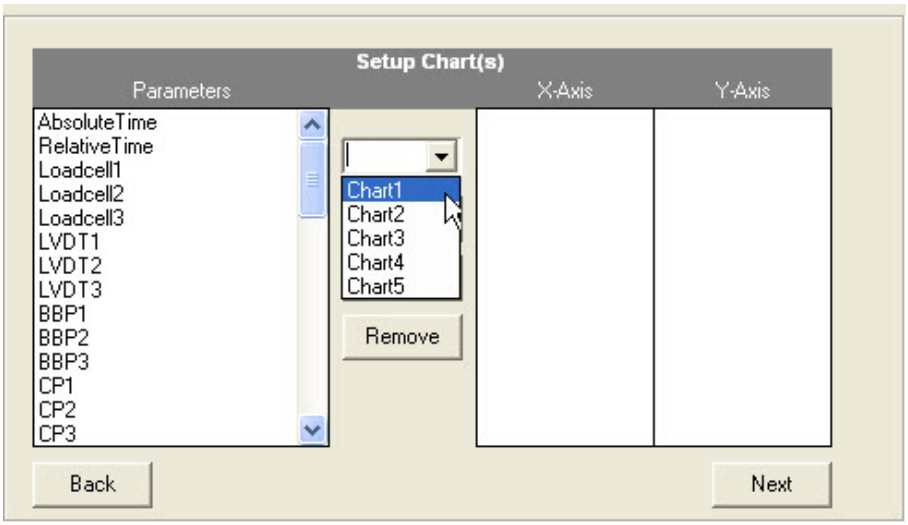

Figure B.7 Chart setup

B.3.5 General settings

Figure B.8 shows the general settings window. To define data sampling rate, the following two approaches can be taken:

1) Defining a constant sampling rate based on number of samples per minute
2) Defining custom intervals for a period of time and constant sampling rate afterwards

Both types of sampling rate options used in DAQ are based on the number of samples per minute per channel. Therefore, the aggregate sampling rate equals to the sampling rate times by number of active channels.

To add user-defined intervals, simply add an appropriate interval and press the green button. Unlimited number of intervals can be defined here. To remove a time interval, select it from the drop down list and press the red button. A constant time interval can be defined in the ‘Then after every’ box. Once the sampling rate is defined and the project is run, it cannot be changed.

Graphs can be updated at a preset time interval by defining a number from 1 to 60 in the general settings window. This can be changed during the data logging process as well.

Once general settings are updated, click on ‘Apply’ to apply all settings. Therefore, previously defined datasheets and graphs are created and all general settings are submitted to the hardware and logging will be initiated. Logged values can be seen from the left side bar. Any physical channel can be set to zero using the ‘Z’ button next to each value in the left bar. To see values of the calculated channels, use ‘Record’ button next to timers.
At this stage logging at preset sampling rate has not yet been started and clicking on ‘Run Now’ starts the logging process.

B.4 Monitoring data

All logged data are saved into a datasheet at preset intervals. Custom data can also be saved apart from the regular logging rate in another datasheet (Recorded Data). ‘Recorded Data’ datasheet shows also a time stamp for determining time and date of recorded data. Defined graphs are updated at preset intervals and can be printed, copied in windows clipboard or saved as a graphic file any time during logging process. Graphs can also be cleared at any time. Figure B.9, Figure B.10 and Figure B.11 show the main datasheet, custom recorded datasheet and graph area respectively.

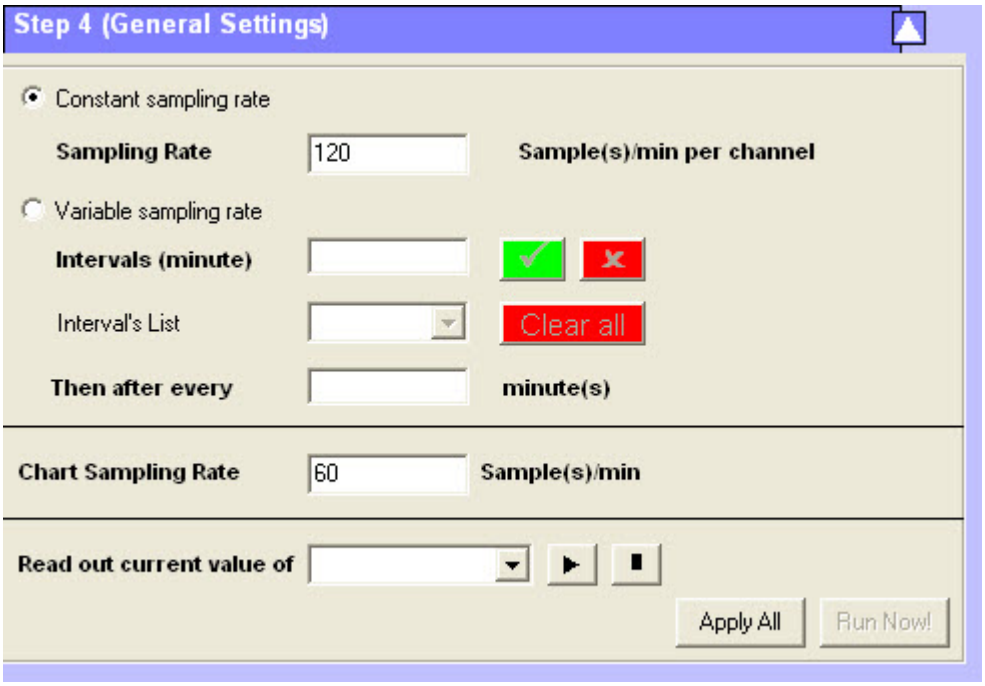

Figure B.8 General settings

To pause/resume data logging choose ‘Tools>Pause/Resume’ and to stop data logging choose ‘Tools>Stop’. Once the data logging process is stopped, a message box is displayed to confirm termination of the data logging process. All project details can be saved in the logging history of DAQ to be accessible later. This option saves a copy of logged data in the installing path of the software for future access. Therefore, even on loss of data by the user, data always can be recovered from the project history.

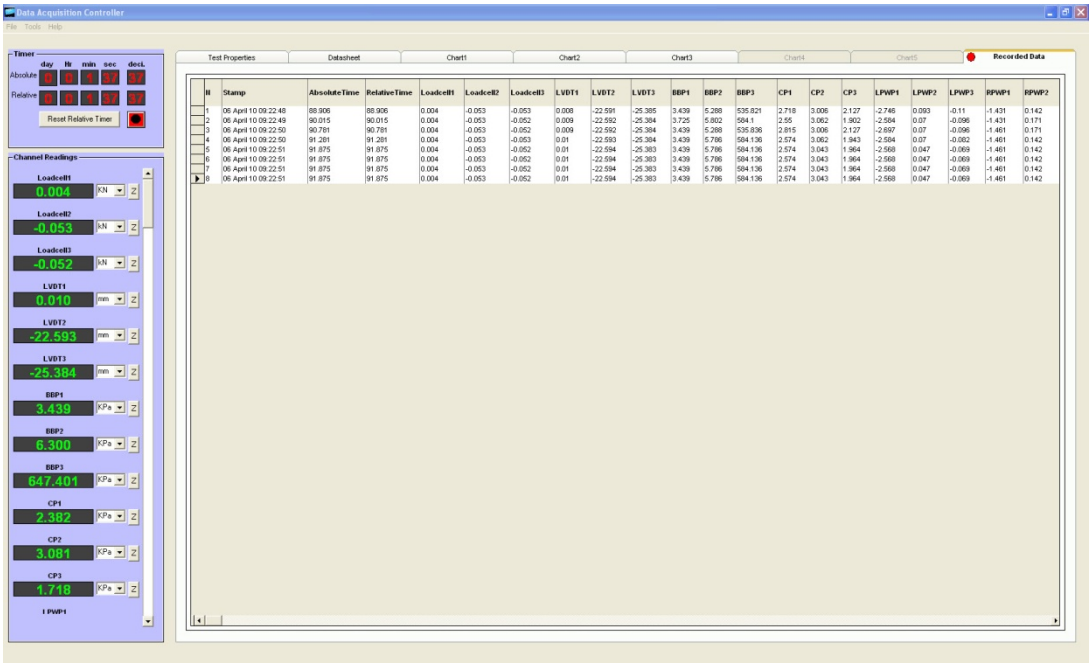

Figure B.9 Main datasheet

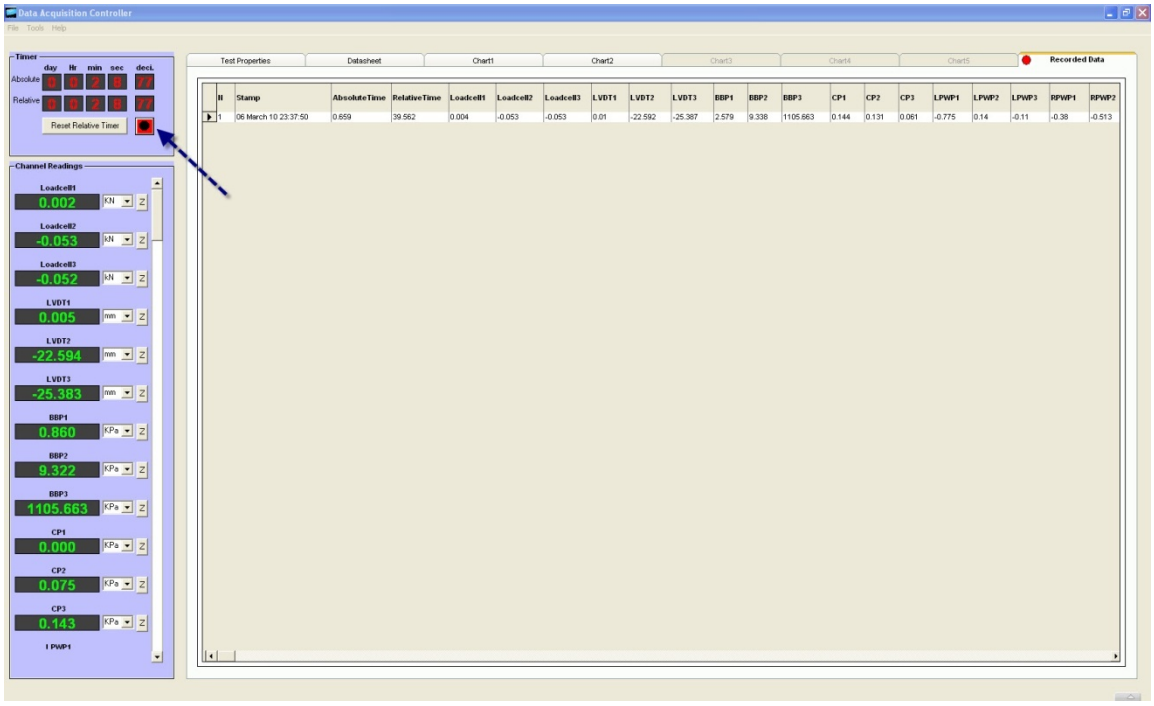

Figure B.10 Custom recorded datasheet

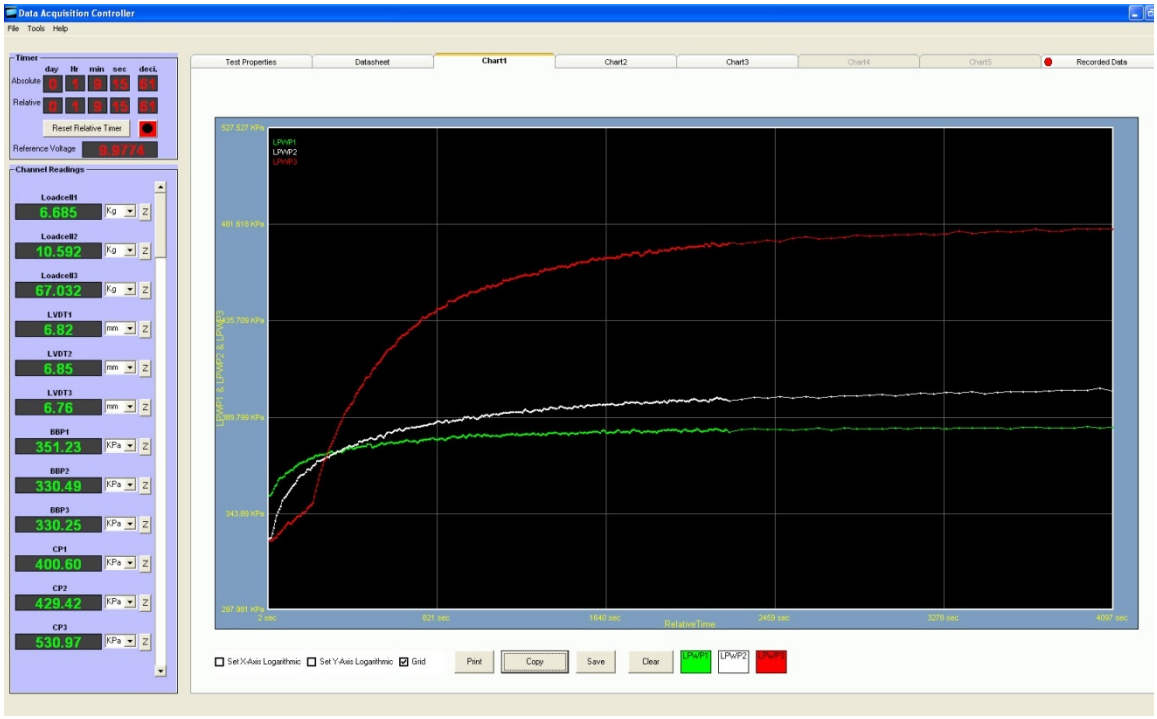

Figure B.11 Graph area

B.5 Export the results

After termination of the logging process, a window pops up to export the results. Results can be exported as Microsoft Excel or DAQ special file (with the extension of ‘pdb’).

Logged data including project information and all datasheets can be exported in a Microsoft Excel file in separate sheets. Furthermore, unlimited number of graphs can also be defined in the Microsoft Excel output file based on all logged data. Figure B.12 shows the export window.

Figure B.12 Export form

B.5.1 Export to Microsoft Excel

Once ‘Export datasheet to Excel’ is selected, an unlimited number of graphs can be defined using available parameters. These parameters include both physical channels and also calculated channels. When required graphs are defined, press ‘Export’ to specify the output file path. All calculated channels will be calculated and saved to the datasheet. This process might take a while depending on the number of the logged data and number of calculated channels. Once this process is completed, a message is displayed. Figure B.13 shows the graph export window.

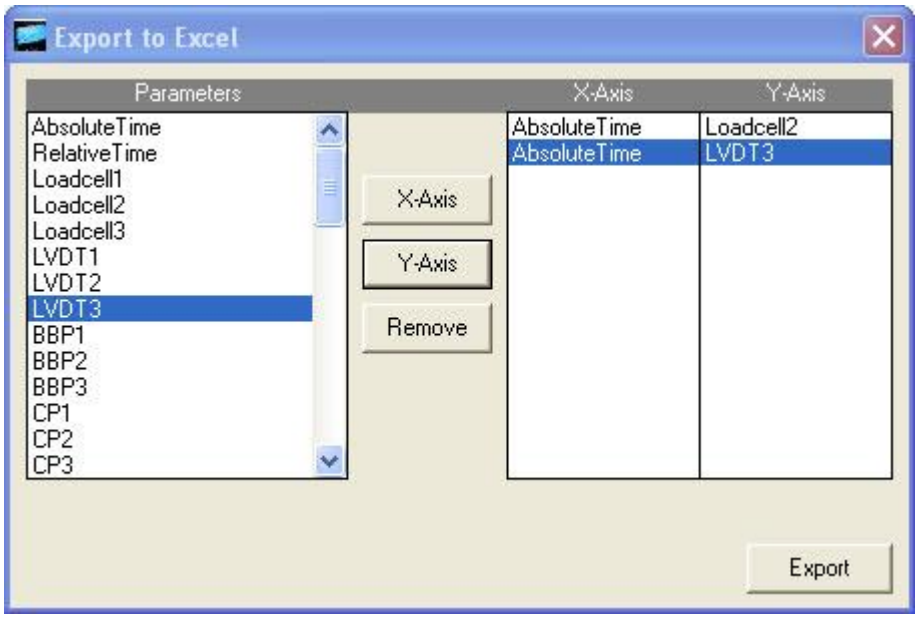

Figure B.13 Export graphs to Microsoft Excel

B.5.2 Export as DAQ ‘pdb’ file

All logged data can also be exported as DAQ ‘pdb’ file. This type of file can be used by complimentary exporter application which is installed with DAQ to export the data to Microsoft Excel at later times.

B.6 Calibration

Sensors can be calibrated using the calibration programme available in DAQ. To calibrate sensors click on ‘Tools>Calibration’ menu. All defined physical channels which had been set earlier as ‘enabled’ in the parameter maker window, are now listed in the calibration list. Figure B.14 shows the calibration window. To calibrate a channel, click on a channel number and then double click on the ‘Calibration path’ to specify a path to save the calibration data. Then enter information such as the serial number, full scale limit, and number of decimals for the selected channel. There are four methods to calibrate the sensors including:

1. Polynomial
2. Logarithmic
3. Linear
4. Look-up table (made up of several linear calibration equations between consecutive points)

Depending on the type of sensor and available data, pick one of the above methods by clicking on the relevant option. ‘Signal’ box shows the current output (bits) of sensor. Fill ‘Value’ box with the current engineering value and on appearance of the green light, press the green button. The green light shows up whenever the output signal is steady and it changes insignificantly. Continue to add more points by changing the current state of physical phenomenon which is sensed by the sensor and enter the relevant value.

Sensors can be calibrated to maximum 200 points. Upon finishing adding calibrating points, press ‘Calibrate’. Therefore, the sensor is calibrated and calibration data is saved in the specified path. Change the state of the sensor to examine the calibration by comparing the real value with the value shown in ‘Predicted Value’. This value is calculated based on the recent regression equation through the calibration span. If there is an undesirable difference between the predicted value and real value, try to increase the number of calibrating points.

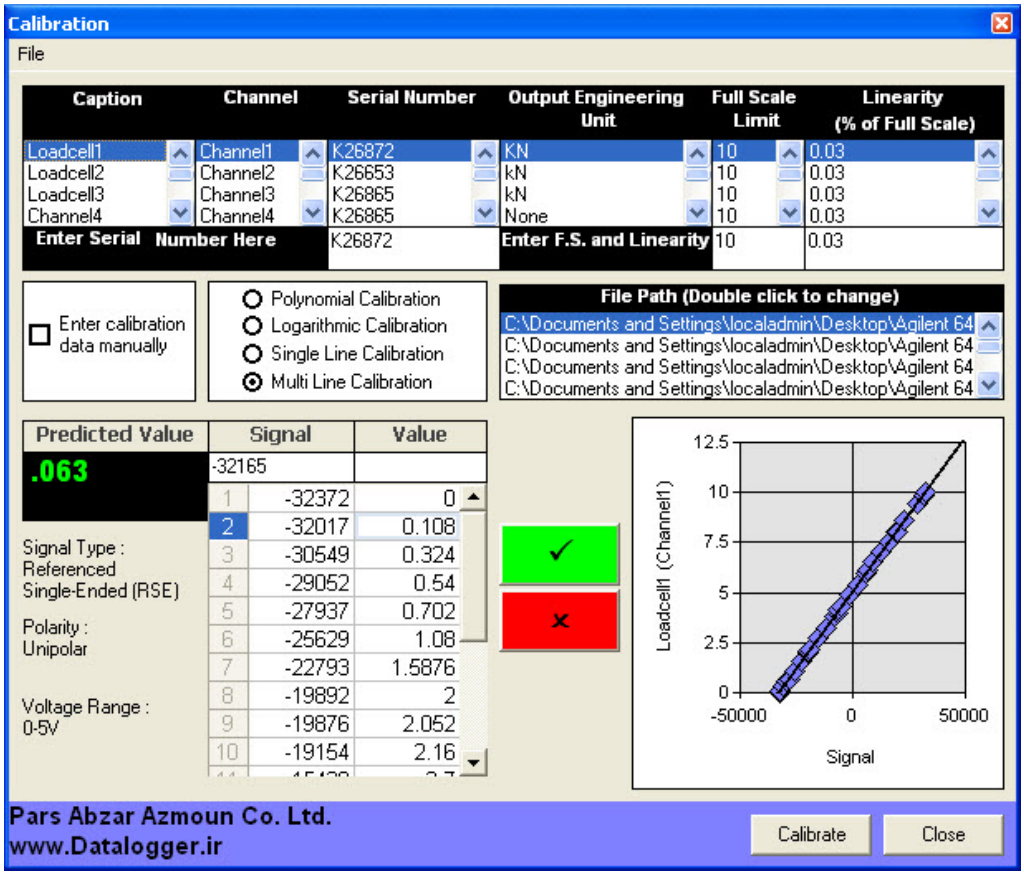

Figure B.14 Calibration window

B.7 Calibration Duplicator

There is an extra feature to calibrate several sensors which are sensing the same physical phenomenon at the same time against a calibrated sensor. An example of this application could be calibrating several pressure sensors which are connected to the same pressure line at the same time against a reference pressure sensor. Therefore, the reference sensor can be used for calibrating several pressure sensors simultaneously when all of them are connected to the same pressure line. Hence, by changing pressure of pressure line the true value which is sensed by the reference pressure sensor is copied to the other pressure sensors corresponding to their individual output signals. Therefore all pressure sensors are calibrated at the same time and under the same pressure steps. This saves time and prevents having to calibrate all sensors one by one.

To do this, select ‘File>Duplicate’ menu. On the new window select the calibrated sensor’s channel number from the left list and select the destiny sensors from the right list. Press ‘Check Data’ and confirm the process. Change the source of the related phenomenon and when the green light is on, press ‘Record’. When the desired quantity of calibrating points is reached, press ‘Apply’ to submit changes. To check the validity of the process select calibrated sensors from the list and check the submitted data. Figure B.15 shows the ‘Duplicate’ window.

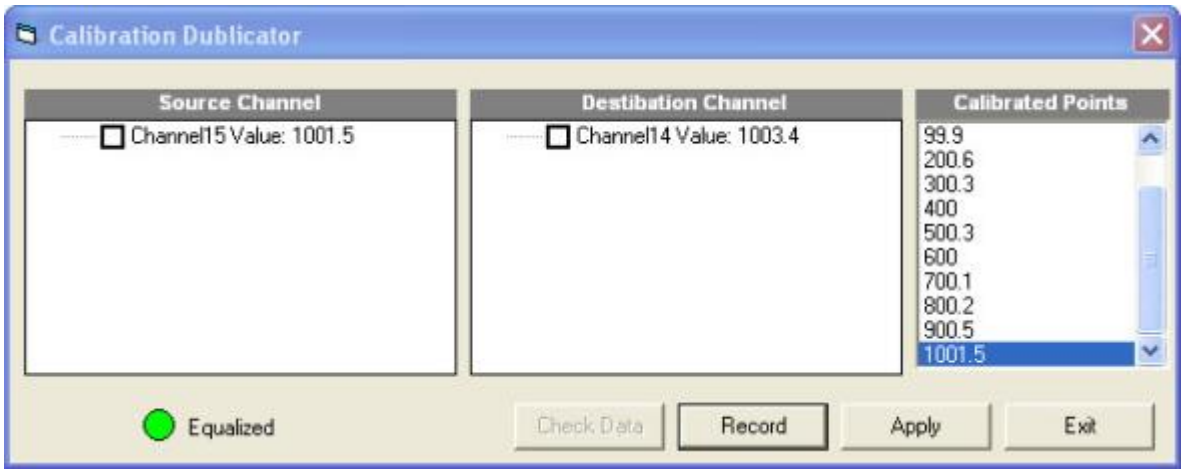

Figure B.15 Calibration duplicator

List of publications

Miraftab, M. and **Mirzababaei, M.** (2009). Carpet waste utilisation, an awakening realisation: A Review, *In: Second International Symposium on Fibre Recycling*, Georgia Institute of Technology, Atlanta, Georgia, USA

Mirzababaei, M., Miraftab, M., McMahon, P. and Mohamed, M. (2009). Undrained behavior of clay reinforced with surplus carpet fibres*, In: Second International Symposium on Fibre Recycling*, Georgia Institute of Technology, Atlanta, Georgia, USA

Mirzababaei, M., Miraftab, M., Mohamed, M. and McMahon, P. (2011). Diverting carpet waste from landfills to reinforce clay soils, *In: Third International Symposium on Fibre Recycling*, University of Bolton, Bolton, UK

Mirzababaei, M., Miraftab, M., Mohamed, M. and McMahon, P. (2012). Unconfined compression strength of clays with waste carpet fibers, Submitted to ASCE Journal of Geotechnical and Geoenvironmental Engineering
(Accepted for publishing)

Mirzababaei, M., Miraftab, M., Mohamed, M. and McMahon, P. (2012) Impact of waste carpet fibres on swelling properties of compacted clays,
Submitted to ASCE Journal of Geotechnical and Geological Engineering
(Accepted with revision)

Saad, S., **Mirzababaei, M.**, Mohamed, M., Miraftab, M. (2012). Uniformity of density of compacted fibre reinforced clay soil samples prepared by static compaction, Submitted to the 5th European Geosynthetics Congress, Valencia, Spain